ABSTRACT

PATEL, NIKUNJ PRAGJIBHAI. Nanostructured Polymeric Membranes for Selective CO_2 Removal from Light Gas Mixtures. (Under the direction of Richard John Spontak)

Two primary materials strategies have been developed to produce nanostructured polymer membranes for selective CO_2 removal from mixed light-gas streams. In one approach, a microphase-ordered poly(styrene-*b*-ethylene oxide-*b*-styrene) (SEOS) triblock copolymer and its miscible blends with poly(ethylene glycol) (PEG) differing in molecular weight have been investigated to establish structure-transport property relationships. These membranes exhibit high CO_2/H_2 selectivity due to the affinity of CO_2 for the ether moiety in the copolymer/homopolymer backbone. Crystalline regions in the EO microphase or introduced by relatively high-molecular-weight PEG serve as impermeable barriers to penetrating gas molecules and therefore compromise membrane performance. This drawback can be overcome through the physical addition of low-molecular-weight PEG, which behaves as a diluent. Upon PEO crystal melting at elevated temperatures, the CO_2/H_2 selectivity undergoes an abrupt increase consistent with the hypothesis that only amorphous regions can participate in penetrant transport.

An alternative approach to near-equilibrium block copolymer/homopolymer blends is the introduction of a B-compatible homopolymer into a swollen ABA triblock or higher-order multiblock copolymer. The resultant "mesoblends" are reproducible, nonequilibrium blends that do not undergo the same morphological transitions induced in the near-equilibrium blend analogues. This procedure has been adopted here to generate novel morphologies in the SEOS triblock copolymer and a poly(amide-*b*-ethylene glycol) (AEG) multiblock copolymer with PEG homopolymers. Solvent quality, solution concentration and

temperature have a profound impact on PEG solubility within the copolymer. Incorporation of amorphous PEG into the AEG copolymer is found to enhance CO_2 permeability, as well as CO_2/H_2 selectivity.

The second approach examined here relies on chemically crosslinked PEG diacrylate (PEGda) oligomers differing in molecular weight, as well as their nanocomposites prepared with up to 10 wt% methacrylate-functionalized fumed silica (FS) or an organically-modified nanoclay. The mechanical, thermal and morphological characteristics of these membranes have been probed by dynamic rheology, thermal gravimetric analysis (TGA) and transmission electron microscopy (TEM), respectively. These PEGda membranes exhibit exceptionally high acid-gas selectivity coupled with high gas permeabilities that tend to increase with increasing oligomer molecular weight. Addition of FS results in improved mechanical properties without deteriorating transport properties. Temperature-dependent permeation studies demonstrate Arrhenius behavior with considerably lower activation energy of permeation for CO_2. The polarity of the matrix, represented by PEGda oligomer molecular weight, and the transmembrane pressure allow systematic tuning of CO_2/H_2 selectivity and CO_2 permeability.

Crosslinked poly(propylene glycol) diacrylate (PPGda) membranes with various additives have also been synthesized due to their reportedly higher CO_2 solubility. Gas transport and rheological properties are extremely sensitive to the molecular weight of oligomer, as in the case of the corresponding PEGda membranes. The major difference between these two membranes is the higher CO_2 permeability, but lower CO_2/H_2 selectivity, in the PPGda membranes. Gas transport properties vary according to the rule of mixtures in PPGda/PEGda membranes blended prior to chemical crosslinking.

NANOSTRUCTURED POLYMERIC MEMBRANES FOR SELECTIVE CO_2 REMOVAL FROM LIGHT GAS MIXTURES

by

NIKUNJ PRAGJIBHAI PATEL

A dissertation submitted to the Graduate Faculty of
North Carolina State University
in partial fulfillment of the
requirements for the Degree of
Doctor of Philosophy

CHEMICAL ENGINEERING

Raleigh
2004

APPROVED BY:

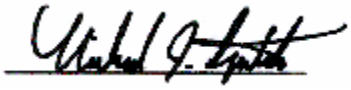

(Chair of Advisory Committee)
(Richard J. Spontak)

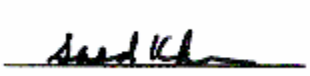

(Saad A. Khan)

(Steve D. Smith)

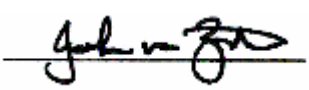

(John H. van Zanten)

PERSONAL BIOGRAPHY

Nikunj Patel, born in Ahmedabad (India) on 13th August, 1978, is the youngest son of Pragjibhai and Lilaben Patel. He completed high-school from Vivekand Vidyalaya and received 5th rank in Gujarat State Board Examination. In 1995, he joined Birla Institute of Technology & Science (Pilani, India) for Bachelor of Engineering (Hons.) in Chemical Engineering. During his undergraduate studies, he worked at Indira Gandhi Center for Atomic Research (IGCAR) as a part of his internship. Following the graduation in 1999, he joined North Carolina State University to pursue a doctoral degree in Chemical Engineering. He has been extremely fortunate to perform research under the able guidance of Dr. Richard Spontak. His thesis topic was to remove carbon dioxide selectively from light gas mixtures by developing nanostructured polymeric membranes. Following the completion, he plans to join an Industry with excellent research and development division in polymer science.

ACKNOWLEDGEMENTS

Doctoral research during my tenure at North Carolina State University was one of the best experiences in my life. It would not have been possible without strong support and encouragement that I received throughout from various people.

I would sincerely like to express my humble gratitude to my academic advisor, Dr. Richard Spontak. He has guided me with extreme zeal in every aspect of my doctoral research. Educational and joyous discussion with him throughout the entire period helped me develop not only as a researcher but also as a creative individual. Dr. Spontak has been more than an adviser to me and I will always regard him as a true friend and an outstanding teacher.

I also wish to acknowledge my committee members, Drs. Saad Khan, John van Zanten, Jeffery L. White and Steve Smith for their time and invaluable suggestions for my thesis and academic career.

I would like to thank group members of polymer morphology group (PMG) for their cooperation in laboratory work and fruitful research discussion. My special thanks go to Liz, Shane, Bin, Angelica, Marcus, Mike and Birgit for experimental help and useful collaboration. I extend my gratitude to Dr. Khan for allowing me to use various rheometers in his lab.

I feel especially grateful to Rajendra for making my graduate life joyful and providing a helping hand whenever needed. Very special thanks to our batchmates, particularly, Changshin, Haiqing for sharing lunch time filled with humor and laughter. The

whole Buiescreek gang, Hiren, Jiten, Teja, Rajesh and Bhavita is acknowledged for a wonderful, joyous time and bringing the most important change in life.

Finally, I thank my family for instilling me the greatest motivation, desire to learn and their deep love and support throughout my life.

TABLE OF CONTENTS

LIST OF TABLES

LIST OF FIGURES

Chapter 1

Introduction

Emerging applications in biotechnology, fuel production and chemical synthesis require industries to seek energy-efficient and environmentally-benign molecular separation strategies. Traditional approaches such as absorption, distillation and adsorption are often complex, and sometimes cumbersome, and they can be economically prohibitive due to the costs associated with materials development, equipment construction and/or process maintenance. Membrane technology has increasingly been utilized in a myriad of separation applications to purify a wide range of species including, but not limited to, relatively large biological organisms and much smaller gas molecules. Besides being inexpensive relative to other unit operations, membrane separations afford energy efficiency, facile processability and mechanical simplicity while remaining a so-called "green" technology. Commercialized technologies currently aimed at gas separation through the use of polymeric membranes include production of high-purity nitrogen from air, recovery of hydrogen from mixtures with larger gas components such as nitrogen, methane and carbon monoxide, and purification of natural gas through the removal of carbon dioxide.

Hydrogen (H_2) is one of the most important commodity chemicals used in industry. Over 5 billion kilograms of H_2 are consumed every year in the U.S. alone.[1] Approximately 96% of the hydrogen is obtained from hydrocarbons in a two-step reaction: steam reforming, $C_nH_m + nH_2O + \text{heat} \leftrightarrow nCO + (m/2+n)\ H_2$, followed by a shift reaction to convert the remaining CO to CO_2 and H_2, $CO + H_2O \leftrightarrow CO_2 + H_2$.[1] Hydrogen produced by this route is utilized in a wide variety of chemical and petrochemical processes. For instance, H_2

generated from synthesis gas ("syngas") is used in the production of ammonia, which is a primary building block for urea. Ammonia and urea ranked as the 6th and 15th most widely produced chemicals in 1995, with worldwide production rates of 16.2 and 7.1 billion kilograms per year, respectively.[2] Thus, even a small improvement in the efficiency of separating CO_2 from its mixture with hydrogen, which is required for use in downstream chemical synthesis, could lead to nontrivial cost and energy savings.

Current technologies employ either amine absorption or zeolitic adsorption to remove CO_2 from the mixture. Amine absorption, however, has severe drawbacks, including corrosion of process equipment, foaming, solution degradation and solution volatilization.[3] These inherent shortcomings result in the release of expensive and toxic amines to the atmosphere, as well as regular replacement of expensive equipment and amine solution. Moreover, amine absorption units are complex and awkward to operate.[3] Zeolitic adsorption requires the use of expensive and fragile nanoporous ceramics that are easily pulverized into powders that can foul pressure-regulated systems. Gas separation using polymer membranes provides an attractive alternative in terms of lower maintenance coupled with economical and reliable operation. Conventional H_2-selective membranes commonly encountered in industry produce the desired hydrogen product at low pressure in the permeate stream of the membrane.[4,5] Hydrogen, however, is typically utilized at pressures equal to or higher than the feed pressure of the mixture. The cost associated with repressurizing H_2 to feed pressure is exorbitant, thereby making membranes less competitive and attractive. The lack of commercially available CO_2-selective membranes exhibiting a high CO_2 flux *and* high CO_2/H_2 selectivity prevents the commercial-scale removal of CO_2 and other acid gases (such as NH_3 and H_2S) from mixtures with light gases (e.g., H_2 and N_2) using membranes.

Polymer membranes used in industrial gas separation can be classified in two categories. In the first category, the membranes are permeable to small penetrants in a gas mixture.[4] Membranes of this nature are typified by stiff-chain, glassy, relatively low-free-volume polymers. The other category of separation involves polymers that selectively allow larger components of the gas mixture to permeate faster than the small ones.[6-8] Membranes in this category are either highly flexible rubbery polymers or a small group of ultrahigh-free-volume, glassy, substituted polyacetylenes. While the second approach constitutes a promising alternative for the separation of CO_2 from light gas mixtures, CO_2 selectivity remains a limiting consideration. Polymers possessing polar linkage, such as poly(ethylene oxide) (PEO), enhance the transport of an acid gas such as CO_2 relative to that of nonpolar gases due to specific interactions between the polymer and the gas molecules.[5] However, such membranes are waxy or rubbery and, as such, are not suitable for the preparation of strong, thin films required in industrial operations due to their poor mechanical properties. Heterophase block copolymers wherein one block (the "soft" block) possesses polar linkages and the other block (the "hard" block) exhibits satisfactory mechanical properties and processability offer a very attractive route by which to purify light gas mixtures and generate a concentrated low-pressure CO_2 stream for further utilization. Such materials can also provide precise control of transport and separation efficacy by tailoring the chemical structure of the soft block or the copolymer chain length/composition (morphology), as well as by physical incorporation of a polar homopolymer into the nanostructured copolymer matrix.

The primary objectives of this study are two-fold: (*i*) to identify viable strategies by which polymer membranes exhibiting high CO_2 permeability and selectivity can be

developed, and (*ii*) to establish molecular design paradigms for the enlightened development of such materials. The remaining parts of this Introduction are divided into two sections. The first addresses the fundamental principles of gas transport through dense polymer membranes, and the second section is intended to provide insight into block copolymer systems and the requirements for preparing miscible block copolymer/homopolymer blends.

1.1. Gas Permeation in Polymeric Membranes

1.1.1. Background

The rate of gas transport through a nonporous polymeric membrane is determined by the permeability coefficient (P_i), which constitutes a measure of the molecular flux of component *i* normalized with respect to pressure difference and membrane thickness. The permeability coefficient of component A is given by[5]

$$P_A = \frac{N_A \times l}{P_{2A} - P_{1A}} \tag{1.1}$$

Here, P_A is the permeability coefficient of A, N_A is the steady-state gas flux through the film and p_{1A} and p_{2A} are the upstream and downstream partial pressures of A, respectively. In 1866, Sir Thomas Graham[9] proposed the "solution-diffusion" mechanism to represent how a penetrating molecule migrates through a dense membrane. According to his vision, penetrants dissolve into the upstream (high pressure) face of the membrane, diffuse across the membrane and finally desorb at the downstream (low pressure) face of the membrane. When the downstream pressure is negligible relative to the upstream pressure and Fickian diffusion constitutes the rate-limiting step in penetrant transport, the permeability can be written as[5]

$$P_A = S_A * D_A \tag{1.2}$$

where S_A is the solubility coefficient of A, expressed as the ratio of penetrant concentration dissolved in the upstream face relative to the upstream partial pressure of A in the gas phase, and D_A is the concentration-averaged diffusion coefficient of A.

Permeabilities vary markedly among penetrants due to differences in diffusivity and solubility. The relative permeability of penetrants A and B in a mixture can be expressed by the ideal selectivity, denoted $\alpha_{A/B}$, so that[4]

$$\alpha_{A/B} = P_A/P_B = \left[\frac{D_A}{D_B}\right] \times \left[\frac{S_A}{S_B}\right] \tag{1.3}$$

where D_A/D_B, the ratio of the concentration-averaged diffusion coefficients of A and B, is designated the diffusivity, or mobility, selectivity. Similarly, S_A/S_B is the ratio of solubility coefficients and is referred to as the solubility selectivity. Gas solubility is a function of operating conditions (pressure, composition and temperature), penetrant condensability, polymer-penetrant interaction and polymer morphology (crystallinity and molecular anisotropy).[10] The diffusion coefficient is sensitive to considerations such as penetrant size, polymer morphology and polymer segmental dynamics.[5]

1.1.2 Membrane Classification

Conventional polymers are classified as glassy or rubbery according to their glass transition temperature (T_g) relative to their application temperature. In general, rubbery polymers are much less effective than glassy polymers at separating gas molecules on the basis of size differences due to their large-scale polymer segmental dynamics.[11] As illustrated in Figure 1.1, the permeability of relatively large penetrants is higher than that of small penetrants in poly(dimethylsiloxane) (PDMS), a well-established example of a

technologically-important rubbery polymer. In marked contrast, permeability decreases strongly with increasing penetrant size in polysulfone (PSF), a typical glassy polymer.[12]

Selective removal of CO_2 from CO_2/H_2 gas mixtures necessitates a high solubility-selective membrane, since H_2 is smaller in size than CO_2 and therefore possesses a higher diffusion coefficient than CO_2. Conversely, CO_2 possesses a higher condensability than H_2, as indicated by a higher normal boiling point and a higher critical temperature (see Table 1.1). For this reason, CO_2 will generally be more soluble in polymers than H_2. Since rubbery polymers are solubility-selective, they will generally exhibit a higher selectivity for CO_2 relative to H_2 in comparison to glassy polymers. Table 1.2 shows relevant permeability data for H_2 and CO_2 in several representative rubbery and glassy polymers. Penetrant solubility increases further if the penetrant is capable of having specific chemical interactions with a given polymer.[5] For example, CO_2/CH_4 solubility selectivity increases with increasing sulfone or carbonyl concentration due to favorable interactions between CO_2 and the two functionalities.[5] A similar trend is observed when other polar groups (such as nitro[13] and hydroxyl[14]) are present in the polymer matrix. In polymers that do not exhibit site-specific interactions, the logarithm of solubility is generally described by a linear function of the normalized Lennard-Jones well depth (ε/k, where k is the Boltzmann constant),[15] or any other measure of penetrant condensability.[16] In PEO-segmented copolymers, all penetrants except CO_2 have been observed[17] to follow a linear relationship between the logarithm of solubility and ε/k. Due to specific interactions between the ether linkages of the PEO backbone and the quadrupolar moment of CO_2, CO_2 is found to exhibit a substantially higher solubility. In Polyethylene (PE), CO_2 obeys the linear relationship anticipated between the logarithm of solubility and condensability.

1.1.3. Transport in Heterogeneous Media

Combining different polymers via physical blending or copolymerization provides an attractive route by which various properties of organic materials can be tuned for a particular application. Gas transport in multicomponent materials has been studied extensively in heterogeneous systems such as polymer blends, copolymers and composites.[18] In numerous gas-separation processes employing polymeric membranes, such materials have been of growing interest because blending or copolymerization of (immiscible) components with different properties could overcome drawbacks (i.e., low selectivity or low permeability) associated with individual homopolymers.[19]

Depending on the degree of mixing achieved, the coexisting phases in an immiscible polymer blend or microphase-separated block copolymer exhibit properties that are similar to those of the parent homopolymers. Thus, the overall transport properties of such multicomponent materials will depend strongly on the inherent transport properties of the constituent species. The average solubility coefficient (<S>) of a composite material containing two species (A and B) in which the phase domains are non-interacting is given by the arithmetic mean of the pure-component solubilities, *viz*.,

$$<S> = S_A * v_A + S_B * v_B \qquad (1.4)$$

where v_A and v_B denote the volume fractions of components A and B, respectively.[20] The overall permeability coefficient depends on the detailed structure of the blend, *i.e.*, the precise topology and spatial arrangement of the phase domains. The composite permeability, however, generally lies between the upper and lower bounds defined by the arithmetic and harmonic mean of P_A and P_B, in which case it immediately follows that[20]

$$P = v_A * P_A + v_B * P_B \qquad (1.5a)$$

$$P^{-1} = v_A * P_A^{-1} + v_B * P_B^{-1} \qquad (1.5b)$$

Equations, 1.5a and 1.5b represent the average permeability in the cases of sheets or lamellae of A and B that are oriented parallel (Eq. 1.5a) or normal (Eq. 1.5b) to the direction of flow.

Determination of transport properties in multicomponent materials is challenging analytically and, hence, a large number of expressions invoking various levels of approximation have been correspondingly developed. For a dilute dispersion of spheres in which the mean interparticle distance is sufficiently large to ensure that the flow-line pattern around any one is effectively undisturbed by the presence of other particles, the following relation is applicable:

$$\frac{P}{P_c} = 1 + 3v_a\left[\left(\frac{\alpha+1}{\alpha-1}\right) - v_a\right]^{-1} \qquad (1.6)$$

Here, P_c corresponds to the permeability of the continuous phase, P_a is the permeability in the discrete phase, and $\alpha = P_a/P_c$. In the case of more concentrated spheres, several independent researchers have proposed more complex expressions that introduce various approximations applicable to random dispersions of spherical particles in a continuous polymer matrix. These expressions are listed below:

$$\left(\alpha - \frac{P}{P_c}\right)\left(\frac{P_c}{P}\right)^{1/3} = (1 - v_a)(\alpha - 1) \qquad \text{(Bruggman)} \qquad (1.7a)$$

$$\left(1 - \frac{P_c}{P}\right)\left(\alpha + \frac{2P}{P_c}\right) = 3v_a(\alpha - 1) \qquad \text{(Bottcher)} \qquad (1.7b)$$

$$\frac{P}{P_c} = 1 + 3v_a\left[\left(\frac{\alpha+2}{\alpha-1}\right) - v_a - K\frac{(1-v_a)(\alpha-1)}{(\alpha+2)}\right]^{-1} \qquad \text{(Higuchi)} \qquad (1.7c)$$

In Eq. 1.7c, K is treated as an empirical structural constant assigned a value of 0.78 on the basis of dielectric data. Petropolous[20] has reviewed many other related expressions and has

endeavored to rationalize them in physically meaningful fashion. He correctly notes that, when the low-permeability component is the continuous phase, the Maxwell model (Eq. 1.6) yields the lower permeability estimated from the Bruggman model (Eq. 1.7a) and vice-versa.

Csernica *et al*.[21] have proposed a "random-column model" to help explain the permeability of gases through microphase-separated block copolymer membranes exhibiting randomly oriented lamellae. While their model, which fits very well with experimental data, has been generalized by Premnath,[22] Miyata et al.[23] have reported percolation behavior in ethanol/water transport studies through poly (dimethylsiloxane-*b*-methyl methacrylate) (PDMS-*b*-PMMA) block copolymers. In this case, permeability and selectivity exhibit a sudden increase or decrease when the siloxane concentration reach 55 and 35 mol% in block and graft copolymers, respectively. This result suggests that continuity of the silicone phase changes at the specific composition that strongly influences the ethanol permselectivity from an aqueous ethanol solution. Similar observations have been noted in poly(phenylene oxide) (PPO)/polyimide (PI) and poly(1-(trimethylsilyl)-1-propyne) (PTMSP)/poly(1-phenyl-1-propyne) (PPP) blends.[24] Hong *et al*.[25] have observed anomalous sorption (divergence from Fickian diffusion) in weakly-segregated poly(styrene-*b*-isoprene) (SI) diblock copolymers and attribute such behavior to solvent-induced disordering of the copolymers.

Semi-crystalline polymers, such as PEO, intrinsically contain impermeable crystallites, which force the gas molecules to diffuse only through constricted amorphous conduits in the intercrystalline regions. As a first approximation, gas transport properties in these polymers are usually modeled by assuming that polymers consist of two distinct phases (crystalline and amorphous) wherein crystals can be envisaged as an impermeable dispersed phase embedded

in an amorphous phase. In a semi-crystalline polymer, penetrant sorption can therefore be described as[15]

$$S = S_a * \varphi_a \tag{1.8}$$

where S is the observed solubility coefficient, S_a is the solubility coefficient in the amorphous polymer, and φ_a is the volume fraction of the amorphous phase. The influence of crystallinity on molecular diffusion can be considered in terms of tortuosity, namely,[26,27]

$$D = \frac{D_a}{\tau\beta} \tag{1.9}$$

where D_a is the penetrant diffusion coefficient in the amorphous phase, τ is a tortuosity factor, and β is a chain immobilization factor. In this case, τ represents the increase in average diffusion distance caused by the crystals. The tortuosity factor is given by[28]

$$\tau = \frac{1}{\varphi_a} \tag{1.10}$$

Likewise, β accounts for restricted segmental mobility in the amorphous phase since crystallites serve as physical crosslinks. In the simplest case, when $\beta = 1$, the gas permeability can be written as

$$P = S \times D = \frac{P_a}{\varphi_a^2} \tag{1.11}$$

Generally speaking, crystallites decrease both gas diffusivity and solubility. By reducing polymer chain mobility in the amorphous phase, crystallites can also increase the activation energy of diffusion, especially for large penetrant molecules.[26] These effects become more pronounced as the crystalline volume fraction increases or as the crystallite size decreases.[15]

Thus, gas transport and sorption properties of semi-crystalline polymers are very sensitive to specimen preparation procedure.

1.2. Morphological Characteristics of Block Copolymer Systems

1.2.1. Phase Behavior of Neat Block Copolymers

As the technological need for lightweight multifunctional materials continues to increase, interest in the design and development of tailored block copolymers likewise increases. Under the right set of conditions, collectively expressed in terms of the thermodynamic incompatibility[29] (χN, where χ denotes the temperature-sensitive Flory-Huggins interaction parameter and N is the number of repeat units along the copolymer backbone), these materials self-organize and, depending on factors such as chemical identity and molecular composition,[29-34] order to form periodic nanoscale morphologies. In the case of block copolymers composed of A and B repeat units, the *classical* equilibrium morphologies observed to date include A(B) spheres positioned on a body-centered cubic (bcc) lattice in a B(A) matrix (Q_{Im3m}), A(B) cylinders arranged on a hexagonal lattice in a B(A) matrix (H) and co-alternating lamellae (bilayers, L). Examples of non-classical, or *complex*, morphologies reported for neat bicomponent (AB or ABA) block copolymers include the gyroid[31,35,36] (Q_{Ia3d}) and perforated lamellar[37-41](or lamellar caternoid) morphologies. Unlike their classical analogs, the complex morphologies, commonly described as bicontinuous channel networks, typically occupy relatively small regions of phase space (*cf*. Fig. 1.2b). Due to their structural intricacy, they are also more prone to form non-equilibrium elements during processing than their classical counterparts. While perforated lamellae, for instance, have been observed in a variety of copolymers, the theoretical analyses of Matsen and Bates,[42,43] coupled with the experimental findings of

Hajduk *et al.*,[44] reveal that this is actually a long-lived metastable, not equilibrium, morphology.

The experimental phase diagrams first reported[32] for the case of poly(styrene-*b*-isoprene) (S-I) diblock copolymers (*cf*. Fig. 1.2a) and later[30] for more complex poly(styrene-*b*-isoprene-*b*-ethylene oxide) (S-I-EO) triblock copolymers demand immediate appreciation for the substantial versatility afforded by block copolymers in terms of morphological development. An important and distinguishing characteristic of block copolymer phase diagrams is that each copolymer composition sampled requires careful synthesis of an entirely new macromolecule, in marked contrast to conventional phase diagrams of polymer blends in which blend composition is easily regulated by the physical addition of one constituent species to another. Although the systematic production of such phase diagrams is vital to the fundamental understanding of block copolymer molecular self-organization (which is more fully described in detail elsewhere[45-48]), the prospect of synthesizing new block copolymer molecules with predetermined compositions and molecular weights for specific applications is not always practically appealing. For this reason, numerous efforts over the past decade or so have sought to tailor block copolymer morphologies through the use of multicomponent systems, which are discussed in this chapter. From the extensive data presently available for such systems, it is possible to develop a set of design paradigms that not only serve to enhance the general versatility of self-organized block copolymers, but also permit fundamental inquiry into the increasingly important issue of macromolecular mixing within molecularly confined environments.

1.2.2. Phase Space in Multicomponent Systems

One can envisage two basic strategies by which to probe the possible spatial arrangements of block copolymer molecules in multicomponent systems. In the first methodology, a block copolymer consisting of A and B moieties is physically added to either (*i*) a single A(B)-selective constituent or a second copolymer to form a binary system or (*ii*) both A- and B-selective species to generate a ternary system. This design motif derives directly from precursor studies of small-molecule surfactant systems[49,50] and is capable of yielding a wealth of phase behavior, which is evidenced in the phase diagram reported by Alexandridis *et al.* [51]for a nearly composition-symmetric poly(ethylene oxide-*b*-propylene oxide-*b*-ethylene oxide) (EO_{19}-PO_{44}-EO_{19}) triblock copolymer in the presence of water and *p*-xylene. The underlying principles responsible for such morphological diversity readily extend to non-aqueous systems wherein an organic solvent is block-selective (*i.e.*, it is more compatible with one block than with the other).[52-54] While many block copolymers of technological relevance are intended for use in solvent-less applications, the general materials design strategy of physically blending a single copolymer with other additives — *e.g.*, one or two block-selective homopolymers or a second copolymer — opens new avenues to nanostructured materials with specific morphologies or dimensions that can be controllably tuned through the rational use of physical parameters. The second methodology to be considered here imparts greater functionality to the copolymer molecule. Thus far, only block copolymers possessing A and B repeat units arranged in different sequence schemes (or architectures) have been explicitly considered. Although tailored synthesis is nonetheless required, the functionality and morphological diversity of linear AB molecules can be greatly increased through the chemical addition of a third block to form linear ABC triblock

copolymers. This approach pioneered by Stadler[55] vastly enlarges the scope of morphologies that can be explored within phase space. Representative examples of some of the morphologies accessible through this design route have been described by Zheng and Wang[56] and Abetz.[57] The possibilities made available through this approach provide a tremendous opportunity for both theoretical and experimental investigation, and require a basic understanding of the factors governing miscibility in these systems.

1.2.3. Factors Regulating Miscibility of Blends

Early studies of commercial block copolymers in the presence of a single block-selective homopolymer for toughening applications often show evidence of macrophase separation,[58] in which the copolymer molecules form a dispersed ordered phase within a homopolymer matrix. In this case, the homopolymer molecules, which tended to be much larger in molecular weight than the corresponding block(s) of the copolymer, could not penetrate the dense brush created by the self-organized copolymer block(s), resulting in the formation of a so-called *dry* brush.[59,60] This conformational entropic penalty ultimately drives the system toward macrophase separation between the copolymer and homopolymer constituents of the blend. The benchmark swelling and transitional studies performed by Thomas and co-workers[61-63] and Hashimoto and co-workers[59,64,65] on binary copolymer/homopolymer blends have established the compositions and molecular-weight ratios required to ensure production of miscible blends wherein the homopolymer molecules penetrate (*wet*) and swell the relevant copolymer brush, ultimately becoming incorporated within the copolymer nanostructure. From such experimental and complementary theoretical[66-69] studies, two general rules regarding the design of miscible copolymer/homopolymer blends are identified:

(*i*) the molecular-weight ratio of the homopolymer (M_{hA}) to that of the corresponding block in the copolymer (M_A) should be less than unity, and (*ii*) the fraction (ϕ) of homopolymer that can be added to a blend increases as M_{hA}/M_A decreases. It immediately follows that block copolymers should not tend to macrophase-separate from selective solvents. While this limit is experimentally observed[51-54,70] and is important in its own right, we restrict the focus of the present work to multicomponent block copolymer systems composed of a copolymer with at least one other macromolecule.

1.2.4. Diblock Copolymer/Homopolymer Binary Blends

Incorporation of parent homopolymer A (hA) to an AB diblock copolymer can result in the formation of either dry or wet copolymer brushes, depending on the magnitude of M_{hA}/M_A, hereafter referred to as α (*not* to be confused with the separation factor). At small values of α, hA molecules are solubilized throughout their host copolymer microphase, indicating that the segmental density distribution of hA across the microphase exhibits is broad. In this case, the increase in translational entropy of the hA molecules exceeds the slight reduction in conformational entropy of the A blocks, which must stretch to permit interpenetration of the hA molecules. As the value of α is increased at constant ϕ_{hA}, however, the hA molecules tend to remain unmixed from the corresponding copolymer blocks due to a high conformational entropic penalty and, thus, localize far from the interface that separates adjacent microphases. This spatial arrangement yields hA segmental density distributions that exhibit a relatively sharp maximum positioned near the center of the host microphase.[66-69,71-73] Eventually, a fraction of hA molecules may separate altogether to form a separate phase, as discussed in the previous section. If the value of ϕ_{hA} is increased at constant α

where α is relatively small, then the hA molecules may ultimately change the packing arrangement of chains along the interface and consequently induce a change in interfacial curvature. By doing so, it is then possible to effect a transition from one morphology to another by varying the homopolymer fraction in the copolymer/homopolymer blend. Careful accounting of the parameters required to promote a desired morphological transition yields the following design variables: the molecular-weight disparity (α), the overall blend composition (ϕ, expressed in terms of hA or AB), the composition of the copolymer (f, given in terms of A or B), and the intrinsic thermodynamic incompatibility of the copolymer (χN).

The experimental phase diagrams reported by Winey *et al.*[61,62] for several series of diblock copolymer/homopolymer blends constitute the first systematic account of tailoring block copolymer morphology via physical blending. Since that time, numerous independent studies have used this approach to investigate the phase behavior of diblock copolymer/homopolymer blends. Of particular interest are the stability and dimensional characteristics of complex bicontinuous morphologies,[74,75]such as the gyroid and perforated lamellar morphologies, which occur naturally over a relatively limited composition range in neat copolymer systems. The experimental phase diagram generated by Bodycomb *et al.*[76] for miscible S-I/hS blends in which $\alpha = 0.55$ reveals that the blend morphology expectedly changes in the following order as the copolymer concentration is reduced: lamellae $\rightarrow$ gyroid $\rightarrow$ cylinders $\rightarrow$ disordered spheres. An interesting feature of their phase diagram is the existence of an order-order transition (OOT) between the gyroid and cylindrical morphologies in this blend series. Upon slow cooling across the order-disorder transition (ODT), the gyroid morphology is produced at all temperatures over the composition range indicated. Rapid cooling, however, results in the formation of a stable cylindrical

morphology at temperatures below the OOT. Heating the blend from the cylindrical morphology promotes a transformation to the gyroid morphology, but cooling the gyroid morphology does not generate cylinders, which suggests the same type of kinetic limitation observed by Hajduk *et al.*[77] in the transition from gyroid to lamellae in unary block copolymer systems. In a related vein, Ahn *et al.*[78] report that the molecular weight of a homopolymer added to a lamellar diblock copolymer strongly influences the formation of the metastable perforated lamellar morphology at compositions intermediate to those yielding the lamellar and gyroid morphologies, thereby confirming that the extent of brush wetting (dictated by α) affects the degree of interfacial chain packing frustration and the complex morphology ultimately stabilized.[42,43]

In a semi-crystalline B-EO/hB blend, thermal calorimetry has been used to detect morphological transitions on the basis of their thermal signatures. According to the data of Chen *et al.*[79] displayed in Fig. 1.3, the neat copolymer exhibits a lamellar morphology and a normal freezing (crystallization) temperature (T_f) of its EO block that is about 5°C below that of a hEO homopolymer of equal molecular weight. The difference in thermal signatures between the homopolymer and matched copolymer is attributed to block confinement within the microphase-ordered morphology. Addition of hB (α = 0.52) to the copolymer initially results in a slight reduction in T_f. As ϕ_{hB} is increased further, however, T_f drops precipitously (by ~55°C) as the blend morphology changes from co-continuous lamellae to dispersed EO cylinders, which serves to more severely constrain the ability of the EO blocks to crystallize. A second discontinuity in T_f is induced at still higher values of ϕ_{hB} where the EO blocks order into spheres on a bcc lattice. The overall confinement-induced reduction in T_f over the range of blend compositions explored is substantial, ~70°C. Similar findings have been

reported by Xu *et al.*[80] for binary blends consisting of a series of poly(ethylene oxide-*b*-butylene oxide) (EO-BO) copolymers and hBO, whereas Liu *et al.*[81] have found that addition of crystallizable polytetrahydrofuran (hTHF) to a (THF-M) diblock copolymer improves the crystallizability of the THF block. These results clearly demonstrate that blend composition and, hence, homopolymer distribution play a prominent role in morphology and property development by regulating the ability of the semi-crystalline copolymer blocks to self-organize and subsequently crystallize. In their related investigation, Chen *et al.*[72] provide direct visualization of how crystallization of the EO block can distort the morphology of miscible B-EO/hB blends. Huang *et al.*[82] and Zhu *et al*[41]. have likewise shown that the morphology of microphase-ordered S-EO/hS blends can be used to direct the growth kinetics, thermodynamic stability and orientation of EO crystals.

1.2.5 ABA Triblock Copolymer Systems

Incorporation of homopolymer A (hA) or an A-compatible homopolymer into a microphase-ordered ABA copolymer to form a miscible blend tends to obey the same design paradigms established for AB/hA blends, since the A endblocks of the triblock copolymer form dense brushes in the same fashion as their diblock analogs. Several recent studies[83-85] have sought to investigate the (dis)ordering and (de)micellization behavior of compositionally asymmetric ABA triblock copolymers in the presence of low-molecular-weight hA and report that the (de)micellization temperature decreases with increasing hA concentration. Addition of S-compatible poly(xylenyl ether) to a poly[styrene-*b*-(ethylene-*co*-butylene)-*b*-styrene] (S-EB-S) copolymer is found[86] to result in improved thermo-mechanical properties and an increase in the ODT, which qualitatively agrees, in principle,

with the predicted phase diagrams. Incorporation of hB into a lamellar ABA copolymer is expected to result in a more complicated segmental distribution.[87] A representative distribution of hB in a lamellar ABA copolymer, predicted from SCF analysis,[88] is provided for illustrative purposes in figure 1.4.a, and the accompanying effect of hB addition on υ_b is displayed as a function of blend composition for several different α ratios in Fig. 1.4b. Since a finite fraction of the B midblocks of the copolymer remain bridged across each B-rich microdomain, the hB molecules must distribute more uniformly within their host microdomain than they would otherwise without bridges (as in AB/hB blends). This constraint, coupled with the physical reduction in the size of the B microdomains (since the B midblocks must either form bridges, in which case they span the entire width of a microdomain, or loops, in which case they effectively behave as single-tethered chains of half molecular weight), therefore requires the value of α to be smaller in ABA/hB blends than in comparable AB/hB blends to retain miscibility. As in comparable AB/hB blends, addition of hB to ordered ABA copolymers can, under the right combination of α and ϕ_{hB}, either swell the B-rich microdomains or induce transitions to other morphologies or macrophase separation.[89] In either case, substantial changes in bulk properties, such as the mechanical and thermal characteristics, are manifested.[88]

1.2.6. Block Copolymer/Homopolymer Mesoblends

As alluded to earlier, an increase in the solvent concentration of a midblock-swollen ABA copolymer promotes morphological changes that are consistent with increasing interfacial curvature, as well as a systematic reduction in modulus. According to the SCF results presented in Fig. 1.4a for ABA/hB blends, the bridging fraction (υ_b) is predicted to

decrease with increasing hB content. Since a midblock-selective solvent establishes the low-molecular-weight limit for a hB homopolymer, it immediately follows that υ_b decreases with increasing solvent concentration in ABA copolymer solutions. Zhulina and Halperin[90] have suggested an alternate design strategy by which to prepare block copolymer gels without sustaining such a reduction in υ_b. In their so-called *mesogels*, the B-selective solvent is diffusively imbibed into a pre-existing microphase-ordered block copolymer with rigid A microdomains to yield non-equilibrium morphologies. Their approach has successfully yielded triblock copolymer gels that exhibit markedly higher moduli than their counterparts prepared by conventional equilibrium protocols.[91] On the basis of this principle, a similar strategy has been introduced[92,93] to produce analogous ABA/hB *mesoblends*, the procedure for which is depicted in Fig.1.5a. In this case, immersion of a microphase-ordered ABA copolymer in a B-selective solvent containing hB molecules results in non-equilibrium ABA/hB blends, such as the one displayed in Fig.1.5b. The solubility of hB within a lamellar ABA matrix at ambient temperature is sensitive to factors such as M_{hB}, M_B and the concentration of hB in solution, in addition to the (in)compatibility of the solvent with the A and B blocks of the copolymer.

1.3. Organization of Dissertation

This dissertation is organized as follows. First, pure-gas permeability and thermal properties of near-equilibrium block copolymer/homopolymer blends containing PEO segments are investigated. These results are subsequently compared with similar properties derived from analogous copolymer/homopolymer mesoblends. A more detailed description of mesoblends is provided elsewhere[92,93] and is not included in this work. We then examine

the logical limit of permeability in PEO-based systems by producing chemically crosslinked membranes from poly(ethylene glycol) diacrylate. Polymer and nanocomposite membranes are then examined and compared with literature data whenever possible to establish the importance of this contribution to the field of gas separations.

1.3. References

(1) Kratz, W. C.; Rarig, D. L.; Pietratonio, J. M. *AIChE Symp. Ser.* **1988**, *84*, 36.

(2) *Chem. Eng. News*, 1996; Vol. 74, p 38.

(3) Kohl, A.; Nielson, R. *Gas Purification*; Gulf Publishing Co.: Houston, TX, 1997.

(4) Stern, S. A. *J. Membr. Sci.* **1994**, *94*, 1.

(5) Ghosal, K.; Freeman, B. D. *Polym. Adv. Technol.* **1994**, *5*, 673.

(6) Freeman, B. D.; Pinnau, I. *Trends Polym. Sci.* **1997**, *5*, 167.

(7) Baker, R. W.; Yoshioka, N.; Mohar, J. M.; Khan, A. J. *J. Membr. Sci.* **1987**, *31*, 259.

(8) Baker, R. W.; Wijmans, J. G. In *Polymeric Gas Separation Membranes,* Paul, D. R., Yampol'skii, Y. P. Eds.; CRC Press: Boca Raton, **1994**, pp.353-398.

(9) Graham, T. *Philos. Mag.* **1866**, *32*, 401.

(10) Weinkauf, D. H.; Paul, D. R. In *Barrier Polymers and Barrier Structures*; Koros, W. J., Ed.; American Chemical Society, 1990.

(11) Koros, W. J.; Hellums, M. W. ; In *Encyclopedia of Polymer Science and Engineering*; Kroschwitz, J. I., Ed.; Wiley: New York, 1989; Supplement volume, pp. 724-802.

(12) Merkel, T. C.; Bondar, V. I.; Nagai, K.; Freeman, B. D.; Pinnau, I. *J. Polym. Sci. B: Polym. Phys.* **2000**, *38*, 415.

(13) Ghosal, K.; Chern, R. T.; Freeman, B. D.; Savariar, R. *J. Polym. Sci. B: Polym. Phys.* **1995**, *33*, 657.

(14) Story, B. J.; Koros, W. J. *J. Membr. Sci.* **1992**, *67*, 191.

(15) Michaels, A. S.; Bixler, H. J. *J. Polym. Sci.* **1961**, *50*, 393.

(16) Amerongen, G. J. V. *Rubber Chem. Tech.* **1964**, *37*, 1065.

(17) Bondar, V. I.; Freeman, B. D.; Pinnau, I. *J. Polym. Sci. B: Polym. Phys.* **2000**, *38*, 2051.

(18) Barrer, R. M. In *Diffusion in Polymers*; Crank, J.; Park, G. S., Eds.; Academic Press: London and New York, 1968; p 165.

(19) Park, C.; Jo, W. H.; Park, H. C.; Kang, Y. S. *Polymer* **2000**, *41*, 1765.

(20) Petropoulos, J. H. *J. Polym. Sci. B: Polym. Phys.* **1985**, *23*, 1309.

(21) Csernica, J.; Baddour, R. F.; Cohen, R. E. *Macromolecules* **1987**, *20*, 2468.

(22) Premnath, V. *J. Membr. Sci.* **1996**, *110*, 133.

(23) Miyata, T.; Obata, S.; Uragami, T. *Macromolecules* **1999**, *32*, 3712.

(24) Toy, L. G.; Freeman, B. D.; Spontak, R. J. *Macromolecules* **1997**, 30, 4766.

(25) Hong, S. U.; Stolken, S.; Zielinski, J. M.; Smith, S. D.; Duda, J. L.; Spontak, R. J. *Macromolecules* **1998**, *31*, 937.

(26) Michaels, A. S.; Bixler, H. J. *J. Polym. Sci.* **1961**, *50*, 413.

(27) Michaels, A. S.; Parker, R. B. *J. Polym. Sci.* **1959**, *61*, 53.

(28) Michaels, A. S.; Vieth, W. R.; Barrie, J. A. *J. Appl. Phys.* **1963**, *34*, 13.

(29) Leibler, L. *Macromolecules* **1980**, *13*, 1602.

(30) Bailey, T. S.; Pham, H. D.; Bates, F. S. *Macromolecules* **2001**, *34*, 6994.

(31) Bates, F. S.; Fredrickson, G. H. *Annu. Rev. Phys. Chem.* **1990**, *41*, 525.

(32) Khandpur, A. K.; Forster, S.; Bates, F. S.; Hamley, I. W.; Bras, W.; Ryan, A. J.; Almadal, K.; Mortensen, K. *Macromolecules* **1995**, *28*, 8796.

(33) Floudas, G.; Vazaiou, B.; Schipper, F.; Ulrich, R.; Wiesner, U.; Iatrou, H.; Hadjichrtistidis, N. *Macromolecules* **2001**, *34*, 2947.

(34) Zhao, J.; Majumdar, B.; Schultz, M. F.; Bates, F. S.; Almdal, K.; Mortensen, K.; Hajduk, D. A.; Gruner, S. M. *Macromolecules* **1996**, *29*, 1204.

(35) Schultz, M. F.; Bates, F. S.; Almdal, K.; Mortensen, K. *Phys. Rev. Lett.* **1994**, *73*, 86.

(36) Laurer, J. H.; Hajduk, D. A.; Dreckotter, S.; Smith, S. D.; Spontak, R. J. *Macromolecules* **1998**, *31*, 7546.

(37) Disko, M. M.; Liang, K. S.; Behal, S. K.; Roe, R. J.; Jeon, K. J. *Macromolecules* **1993**, *26*, 2983.

(38) Förster, S.; Khandpur, A. K.; Zhao, J.; Bates, F. S.; Hamley, I. W.; Ryan, A. J.; Bras, W. *Macromolecules* **1994**, *27*, 6922.

(39) Burger, C.; Micha, M. A.; Förster, S.; Antonietti, M. *Europhys. Lett.* **1998**, *42*, 425.

(40) Spontak, R. J.; Smith, S. D.; Ashraf, A. *Polymer* **1993**, *34*, 2233.

(41) Zhu, L.; Mimnaugh, B. R.; Ge, Q.; Quirk, R. P.; Cheng, S. Z. D.; Thomas, E. L.; Lotz, B.; Hsiao, B. S.; Yeh, F.; Liu, L. *Polymer* **2001**, *42*, 9121.

(42) Matsen, M. W.; Bates, F. S. *Macromolecules* **1996**, *29*, 7641.

(43) Matsen, M. W.; Bates, F. S. *J. Chem. Phys.* **1997**, *106*, 2436.

(44) Hajduk, D. A.; Takenouchi, H.; Hillmyer, M. A.; Bates, F. S.; Vigild, M.; Almdal, K. *Macromolecules* **1997**, *30*, 3788.

(45) Bates, F. S.; Fredrickson, G. H. *Phys. Today* **1999**, *52*, 32.

(46) Hamley, I. W. *The Physics of Block Copolymers*; Oxford University Press: Oxford, 1998.

(47) Hudson, S.D. and Jamieson, A.M. in Polymer Blends Vol. 1: Formulation; Paul, D. R., Bucknall, C. B., eds.; Wiley-Interscience: New York, 2000, Chap. 15.

(48) Hadjichrtistidis, N.; Pispas, S.; Floudas, G. *Block Copolymers: Synthetic Strategies, Physical Properties, and Applications*; Wiley - Interscience: New York, 2003.

(49) Hasegawa, H. *Curr. Opin. Colloid Interface Sci.* **1998**, *3*, 264.

(50) Piirma, I. *Polymeric Surfactants*; Marcel Dekker, Inc.: New York, 1992.

(51) Alexandridis, P.; Olsson, U.; Lindman, B. *Langmuir* **1998**, *14*, 2627.

(52) Lodge, T. P.; Pudil, M.; Hanley, K. J. *Macromolecules* **2002**, *35*, 4707.

(53) Laurer, J. H.; Khan, S. A.; Spontak, R. J.; Satkowski, M. M.; Grothaus, J. T.; Smith, S. D.; Lin, J. S. *Langmuir* **1999**, *15*, 7947.

(54) Hanley, K. J.; Lodge, T. P. *J. Polym. Sci. B: Polym. Phys.* **1998**, *36*, 3101.

(55) Stadler, R.; Auschra, C.; Beckmann, J.; Krappe, U.; Voigt-Martin, I.; Leibler, L. *Macromolecules* **1995**, *28*, 3080.

(56) Zheng, W.; Wang, Z.-G. *Macromolecules* **1995**, *28*, 7215.

(57) Abetz, V., Ed., 3 ed.; John Wiley & Sons, Inc.: Hoboken, New Jersey, 2003.

(58) Holden, G.; Legge, N. R.; Quirk, R. P.; Schroeder, H. E. *Thermoplastic Elastomers*, 2nd ed.; Hanser: Munich, 1996.

(59) Hashimoto, T.; Tanaka, H.; Hasegawa, H. *Macromolecules* **1990**, *23*, 4378.

(60) Leibler, L. *Makromol. Chem. Macromol. Symp.* **1988**, *16*, 1.

(61) Winey, K. I.; Thomas, E. L.; Fetters, L. J. *J. Chem. Phys.* **1991**, *95*, 9367.

(62) Winey, K. I.; Thomas, E. L.; Fetters, L. J. *Macromolecules* **1991**, *24*, 6182.

(63) Winey, K. I.; Thomas, E. L.; Fetters, L. J. *Macromolecules* **1992**, *25*.

(64) Tanaka, H.; Hasegawa, H.; Hashimoto, T. *Macromolecules* **1991**, *24*, 240.

(65) Han, C. D.; Baek, D. M.; Kum, J.; Kimishima, K.; Hashimoto, T. *Macromolecules* **1992**, *25*, 3052.

(66) Banaszyak, M.; Whitmore, M. D. *Macromolecules* **1992**, *25*, 2757.

(67) Matsen, M. W. *Phys. Rev. Lett.* **1995**, *74*, 4225.

(68) Matsen, M. W. *Macromolecules* **1995**, *25*, 5765.

(69) Shull, K. R.; Winey, K. I. *Macromolecules* **1992**, *25*, 2637.

(70) Alexandridis, P.; Spontak, R. J. *Curr. Opin. Colloid Interface Sci.* **1999**, *4*, 130.

(71) Rharbi, Y.; Zhang, J.; Spiro, J. G.; Chen, L.; Winnik, M. A.; Vavasour, J. D.; Whitmore, M. D.; Zhang, J.-X.; Jérôme, R. *Macromolecules* **2003**, *36*, 1241.

(72) Chen, H.-L.; Li, H.-C.; Huang, Y.-Y.; Chiu, F.-C. *Macromolecules* **2002**, *34*, 2417.

(73) Chen, H.-L.; Lin, S.-Y.; Huang, Y.-Y.; Chiu, F.-C.; Liou, W.; Lin, J. S. *Macromolecules* **2002**, *35*, 9434.

(74) Spontak, R. J.; Smith, S. D.; Ashraf, A. *Macromolecules* **1993**, *26*, 956.

(75) Hasegawa, H. *Sen'i Gakkaishi* **1999**, *55*, 82.

(76) Bodycomb, J.; Yamaguchi, D.; Hashimoto, T. *Macromolecules* **2000**, *33*, 5187.

(77) Hajduk, D. A.; Ho, R. M.; Hillmyer, M. A.; Bates, F. S.; Almdal, K. *J. Phys. Chem. B* **1998**, *102*, 1356.

(78) Ahn, J.-H.; Zin, W.-C. *Macromolecules* **2002**, *35*, 10238.

(79) Chen, H.-L.; Hsiao, S.-C.; Lin, T.-L.; Yamauchi, K.; Hasegawa, H.; Hashimoto, T. *Macromolecules* **2001**, *34*, 671.

(80) Xu, J.-T.; Turner, S. C.; Fairclough, J. P. A.; Mai, S.-M.; Ryan, A. J.; Chaibundit, C.; Booth, C. *Macromolecules* **2002**, *35*, 3614.

(81) Liu, L.-Z.; Xu, W.; Li, H.; Su, F.; Zhou, E. *Macromolecules* **1997**, *30*, 1363.

(82) Huang, P.; Zhu, L.; Cheng, S. Z. D.; Ge, Q.; Quirk, R. P.; Thomas, E. L.; Lotz, B.; Hsiao, B. S.; Liu, L.; Yeh, F. *Macromolecules* **2001**, *34*, 6649.

(83) Lee, S.-H.; Char, K. *ACS Symp. Ser.* **2000**, *739*, 496.

(84) Choi, S.; Lee, K. M.; Han, C. D.; Sota, N.; Hashimoto, T. *Macromolecules* **2003**, *36*, 793.

(85) Vaidya, N. Y.; Han, C. D.; Kim, D.; Sakamoto, N.; Hashimoto, T. *Macromolecules* **2001**, *34*, 222.

(86) Baetzold, J. P.; Koberstein, J. T. *Macromolecules* **2001**, *34*, 8986.

(87) Lee, S.-H.; Koberstein, J. T.; Quan, X.; Wignall, G. D.; Wilson, F. C. *Macromolecules* **1994**, *27*, 3199.

(88) Kane, L.; Norman, D. A.; White, S. A.; Matsen, M. W.; Satkowski, M. M.; Smith, S. D.; Spontak, R. J. *Macromol. Rapid Comm.* **2001**, *22*, 281.

(89) Norman, D. A.; Kane, L.; White, S. A.; Smith, S. D.; Spontak, R. J. *J. Mater. Sci. Lett.* **1998**, *17*, 545.

(90) Zhulina, E. B.; Halperin, A. *Macromolecules* **1992**, *25*, 5730.

(91) King, M. R.; White, S. A.; Smith, S. D.; Spontak, R. J. *Langmuir* **1999**, *15*, 7886.

(92) Roberge, R. L.; Patel, N. P.; White, S. A.; Thongruang, W.; Smith, S. D.; Spontak, R. J. *Macromolecules* **2002**, *35*, 2268.

(93) Stevens, J. E.; Thongruang, W.; Patel, N. P.; Smith, S. D.; Spontak, R. J. *Macromolecules* **2003**, *36*, 3206.

(94) Bondar, V. I.; Freeman, B. D.; Pinnau, I. *J. Polym. Sci. B: Polym. Phys.* **1999**, *37*, 2463.

Table 1.1. Physical parameters for H_2 and CO_2[17]

Gas	Size		Condensability	
	Critical Volume (cm^3/mol)	Kinetic diameter (nm)	Normal boiling point (K)	Critical Temperature (K)
H_2	65.1	0.29	20.4	33.2
CO_2	93.9	0.33	194.7	304.1

Table 1.2. Permeability of CO_2 and H_2 in glassy and rubbery polymers.[17]

		Permeability[a] (Barrer)		Selectivity
Type	Polymer	H_2	CO_2	CO_2/H_2
Glassy	Polysulfone (PSF)	14.0	5.6	0.40
	Polycarbonate (PC)	14.0	6.5	0.46
	Poly(4-methyl-1-pentene) (PMP)	97.8	83	0.85
	Poly(2,6-dimethyl phenylene oxide) (PPO)	105	61	0.58
	Cellulose Acetate (CA)	13.6	5.5	0.40
	Polyimide formed from 4,4-hexafluoroisopropylidene diphthalic anhydride and metaphenylenediamine (6FDA-MPD)	50.0	24.2	0.48
Rubbery	*cis*-polyisoprene (PI)	49	134	2.7
	Poly(dimethylsiloxane) (PDMS)	715	3100	4.3

a. 1 Barrer = 10^{-10} cm^3 (STP) cm/(cm^2 s cm Hg)

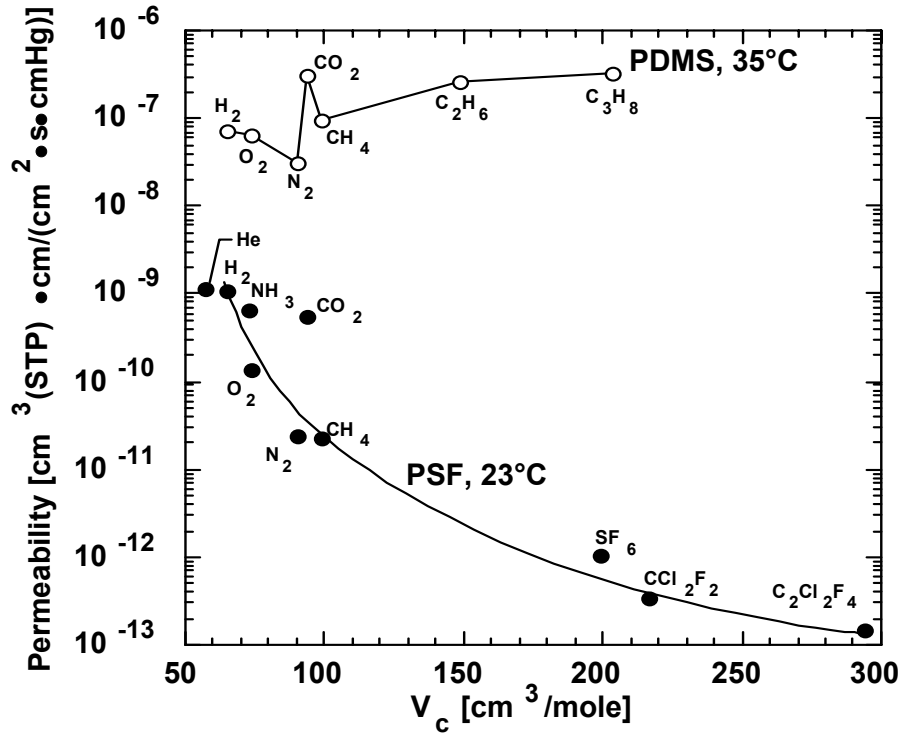

Figure 1.1. Permeability of various penetrants in PDMS and PSF as a function of critical volume (V_c), which provides a systematic measure of penetrant size. (Reprinted with permission from Freeman, B.D. and Pinnau, I., In ACS Symp. Ser.; Freeman, B. D. and Pinnau, I. Eds.; **1999**, 733, pp.1-27. Copyright 1999 American Chemical Society.)

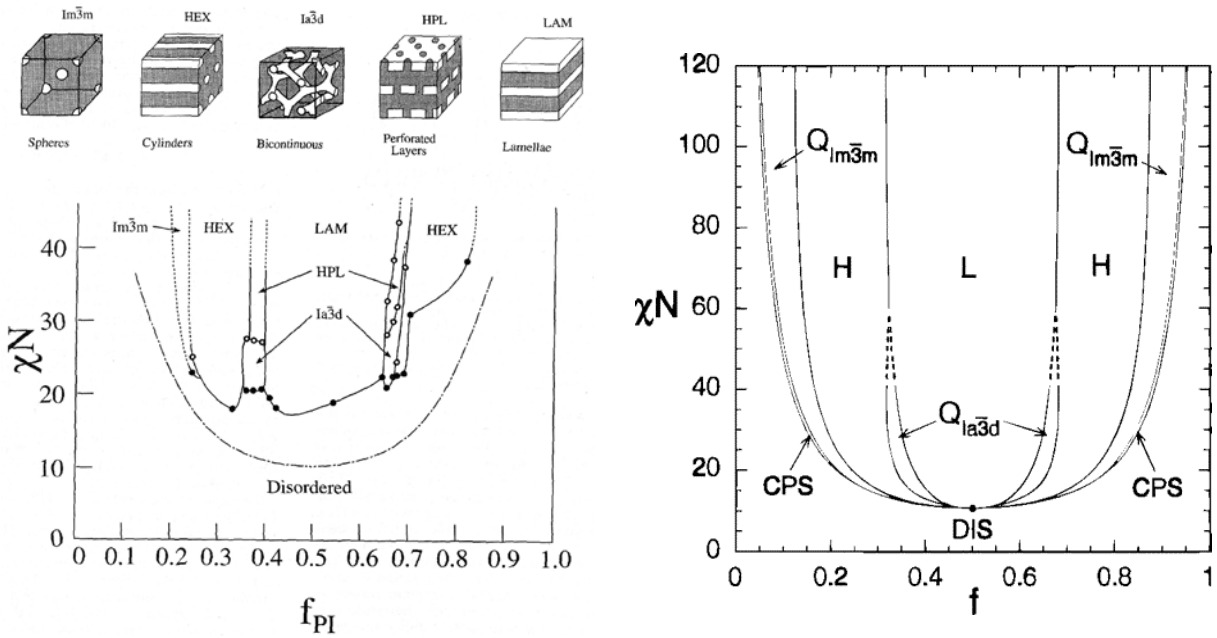

Figure 1.2. (a) Experimentally-determined phase diagram for SI diblock copolymers. (Reprinted with permission from Khandpur, A. K.; Forster, S.; Bates, F. S.; Hamley, I. W.; Bras, W.; Ryan, A. J.; Almadal, K.; Mortensen, K. *Macromolecules* **1995**, *28*, 8796 Copyright 1995 American Chemical Society.) (b) Phase diagram of a conformationally-symmetric diblock copolymer, calculated using self-consistent mean-field theory. (Reprinted with permission from Matsen, M. W.; Bates, F. S. *Macromolecules* **1996**, 29, 1091. Copyright 1996 American Chemical Society).

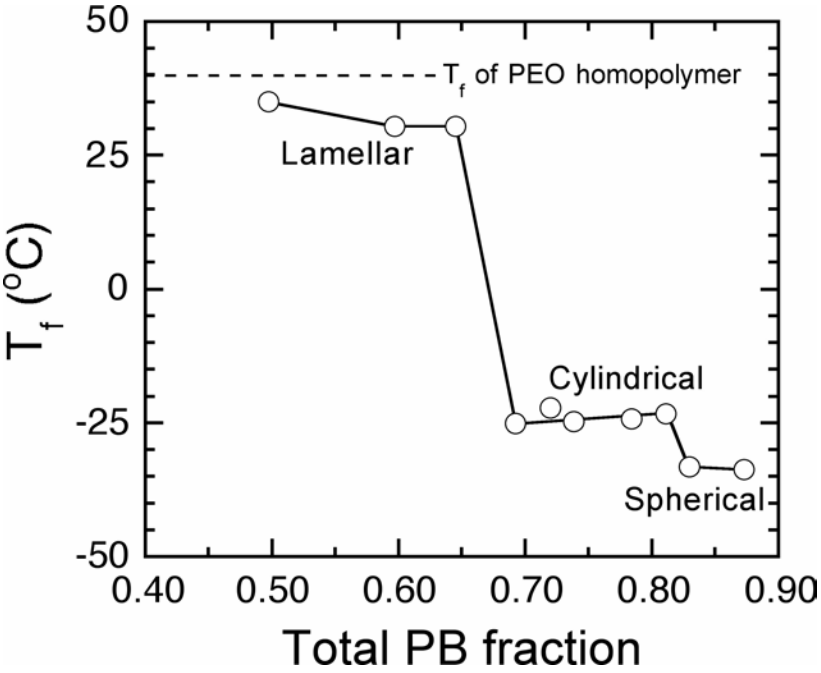

Figure 1.3. Morphology-induced dependence of the crystallization temperature (T_f) of the EO block on total polybutadiene (PB) concentration in binary blends of a polybutadiene homopolymer and an B-EO diblock copolymer. Data obtained from a poly(ethylene oxide) homopolymer are included (dashed line) for reference.(Reprinted with permission from Chen, H.-L.; Hsiao, S.-C.; Lin, T.-L.; Yamauchi, K.; Hasegawa, H.; Hashimoto, T. *Macromolecules* **2001**, *34*, 671. Copyright 2001 American Chemical Society.)

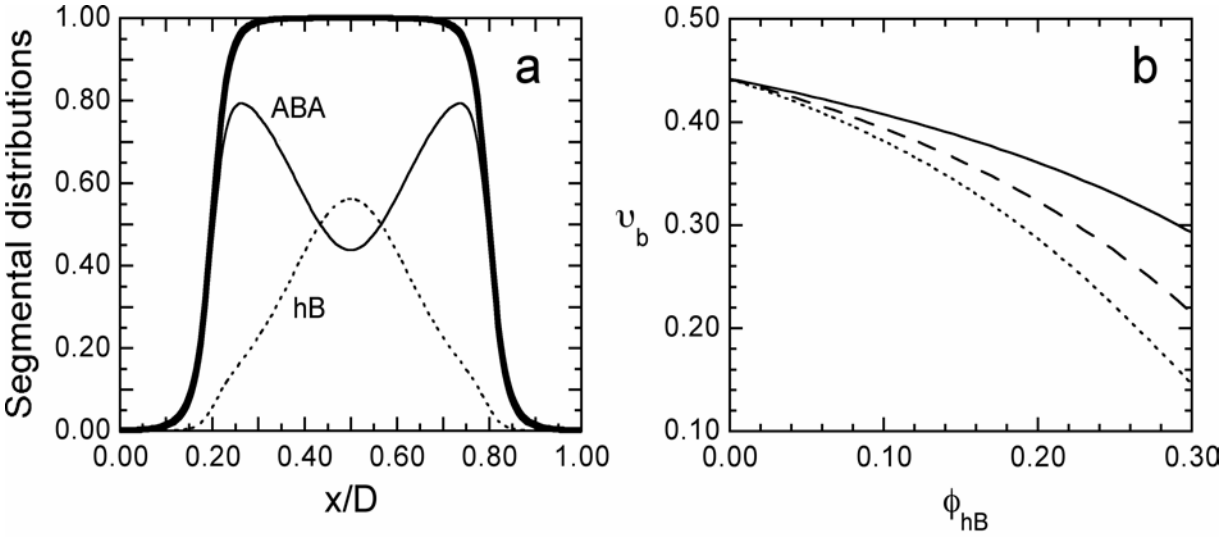

Figure 1.4. Addition of a midblock-selective homopolymer (hB) to a lamellar ABA triblock copolymer: (a) segmental density distributions and (b) effect on bridging fraction (υ_b). In (a), the distributions of B units deposited from the copolymer (solid line) and homopolymer (dotted line) are displayed and labeled. In (b), the dependence of υ_b on hB concentration is shown for three different α (calculated on the basis of half the molecular weight of the B midblock): 0.29 (solid line), 0.59 (dashed line) and 1.18 (dotted line).[88]

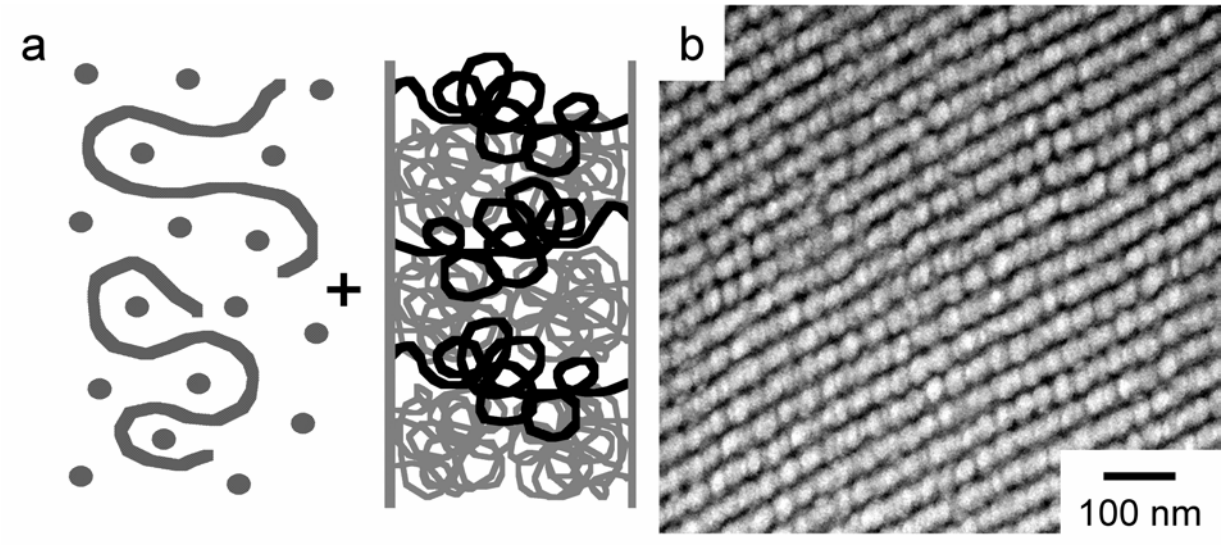

Figure 1.5. Illustration of a block copolymer/homopolymer mesoblend (a) and a TEM image obtained from such a material (b). In (a), a microphase-ordered ABA copolymer is immersed in a B-selective solvent containing a B-compatible homopolymer, which subsequently diffuses into the swollen ABA matrix. In(b), the S-I-S/hI mesoblend displayed has sorbed *ca*. 4.5 wt% hI, for which α (calculated on the basis of half the molecular weight of the B midblock) is 0.59.[92,93]

Chapter 2

Gas-Transport and Thermal Properties of a Microphase-Ordered Poly(styrene-*b*-ethylene oxide-*b*-styrene) Triblock Copolymer and Its Blends with Poly(ethylene glycol)

2.1. Abstract

Block copolymers are under growing consideration as precursor materials for use in a wide variety of emerging nanotechnologies. While these materials can serve as ordered templates in the preparation of nanoporous membranes, they can also be designed for use as dense nanostructured polymer membranes exhibiting chemical specificity. In the present work, we explore the properties of a poly(styrene-*b*-ethylene oxide-*b*-styrene) (SEOS) triblock copolymer and its blends with poly(ethylene glycol) (PEG) as reverse-selective membranes due to their unusually high CO_2 affinity. The permeability of CO_2 measured as a function of blend composition, PEG molecular weight and temperature is consistently found to exceed that of any other gas (H_2, N_2 or O_2) examined here. Addition of PEG eventually results in a composition-dependent transition from an alternating lamellar to polyether-continuous morphology, as evidenced by both gas-transport and thermal properties, and a systematic variation in crystallinity that depend on PEG molecular weight. Since the microphase-ordered copolymer morphology remains intact up to temperatures higher than the polyether melting temperature, the changes in permeability that occur upon polyether melting can be directly measured.

This chapter has been accepted for publication under the same title in Macromolecules.

2.2. Introduction

Due to their highly ordered nanostructures[1-3] and the development of design paradigms[4] to generate nanostructures of particular size and shape, block copolymers and their miscible blends with solvents,[5,6] homopolymers[7,8] and other copolymers[9-12] have become a central component of numerous nanotechnologies, including ultraporous membranes, waveguides and capacitors.[13] Such applications often rely on using ordered block copolymers as templates to which *inorganic* species (*e.g.*, nanoparticles[14] or ceramic precursors[15]) are added. One commercially relevant application of block copolymers and their blends with *organic* additives that has not received much attention is their use in selective gas separations.[16] Polymeric membranes constitute an attractive alternative to conventional separation processes (*e.g.*, cryogenic distillation, absorption and pressure-swing adsorption) in terms of low production cost, as well as economical and reliable operation. While industrial membranes tend to separate gases based on molecular size, allowing smaller molecules to concentrate on the permeate side,[17] the selective removal of acid gases such as CO_2 from mixed gases require larger penetrant molecules to be more permeable than small ones for efficient and competitive membrane function.[18] Such "reverse-selective" membranes may be derived from (*i*) glassy polymers whose free volume is enhanced through the incorporation of nanoparticles[19] or (*ii*) rubbery polymers possessing polar moieties capable of interacting with acid gases. In the case of poly(ethylene glycol) (PEG), which exhibits high CO_2 solubility in its liquid form,[20] the intrinsic mechanical properties are unacceptably low for gas membrane applications, but can be improved substantially via chemical crosslinking.[21,22]

A viable alternative to chemically crosslinking PEG (and introducing covalent linkages to generate a load-bearing network) is to incorporate PEG into a block copolymer that can, upon microphase separation, form a physically crosslinked nanostructure capable of exhibiting satisfactory mechanical properties. This requirement is readily met when low-molecular-weight PEG is copolymerized with a hard block that is either glassy or semicrystalline at application conditions. Indeed, this is the very strategy behind the development of CO_2-selective membranes derived from various polyether segmented copolymers wherein the hard block is either a polyamide or polyimide,[23-25] and the copolymers can best be described as randomly-coupled, in contrast to perfectly-alternating,[26] multiblock copolymers. These materials have been found to exhibit exceptional polar/nonpolar (CO_2/H_2 or CO_2/N_2) gas selectivity. Okamoto *et al.*[23] report that the CO_2 permeability (P_{CO_2}) in poly(ether-*b*-imide) segmented copolymers can be as high as 140 Barrer [1 Barrer = 10^{-10} cm^3 STP)-cm/cm^2-s-cm Hg] with a corresponding CO_2/N_2 selectivity (P_{CO_2}/P_{N_2}), defined as α_{CO_2/N_2}, of up to 70 at 25°C. On the basis of these findings, they propose that such high CO_2 permeability and selectivity reflect an attractive interaction between CO_2 molecules, each with its quadrupolar moment, and the polar ether linkages in the PEG sequences. Bondar *et al.*[24] attribute similar behavior in a limited series of commercial poly(ether-*b*-amide) segmented copolymer to high CO_2/H_2 solubility selectivity, whereas Kim *et al.*[25] have observed that the permeability of nonpolar gases *decreases* with increasing penetrant size, but that of polar gases *increases* with increasing penetrant size, in the same copolymer series.

Although segmented copolymers can, depending on their interblock incompatibility, microphase-separate into a load-bearing nanostructure, they tend not to microphase-order

into periodic morphologies due to their high degree of block connectivity and the corresponding propensity for kinetic entrapment of the chains during self-organization. The pioneering studies by Kinning *et al.*[27] and Cohen and co-workers[28] of non-selective gas transport through model microphase-ordered block copolymers derived from polystyrene (S) and a polydiene confirm that the extent of microphase separation, connectivity and orientation relative to the diffusion axis, collectively expressed here as copolymer morphology, play a critical role in penetrant mobility.[29] Theoretical frameworks developed[28,30-32] to describe molecular transport through microphase-ordered block copolymers must likewise consider the features of the existing morphology. While most studies of gas transport through microphase-ordered block copolymers have focused on the conventional copolymers alluded to above, recent efforts by Arnold *et al.*[33] have sought to employ designer di/triblock copolymers for the selective permeation of particular penetrants. It is in this spirit that this work examines the permeation of polar and nonpolar gases through a microphase-ordered triblock copolymer with a polyether midblock. Miscible blends of this copolymer with PEG are used to ascertain the effect of blend composition and, hence, morphology on these properties, as well as on accompanying thermal characteristics. Because the copolymer endblocks remain glassy over the range of temperatures explored here, the neat copolymer and its blends with PEG behave as physically crosslinked networks, thereby allowing investigation of gas-transport properties above and below the melting point of the polyether.

2.3. Experimental

2.3.1. Materials

A poly(styrene-*b*-ethylene oxide-*b*-styrene) (SEOS) triblock copolymer was obtained from Polymer Source, Inc. (Dorval, Canada). According to ^{1}H NMR and GPC analyses conducted by the manufacturer, the composition, number-average molecular weight and polydispersity of the copolymer were 43 wt% EO, 69000 and 1.03, respectively. Two PEG oligomers with molecular weights of 400 (PEG_{400}, a liquid at 25°C) and 4600 (PEG_{4600}, a semicrystalline powder at 25°C) were purchased from Aldrich (Milwaukee, WI) and used as-received. Solvent-grade chloroform was likewise purchased from Aldrich and used without further purification.

2.3.2. Methods

Bulk films of the copolymer with and without PEG were prepared by dissolving predetermined quantities of the constituent species in chloroform at a polymer concentration of 5-10% w/v. Each solution was stirred at ambient temperature until it became visibly clear and then cast into Teflon molds wherein the solvent was permitted to evaporate over a period of 3-4 days at ambient temperature. The resultant films appeared macroscopically defect-free and were subjected to annealing at 95°C for 24 h to remove residual solvent and promote nanostructural refinement. Following annealing, each film, ranging from 80 to 160 μm in thickness, was sandwiched between Al foil so that a circular area of 0.785 cm^2 was available for gas permeation. Pure-gas permeation properties of the neat SEOS copolymer and its blends were measured by the constant-volume/variable-pressure method described elsewhere.[34] The set-up used here consisted of a downstream vessel of known volume (V), a

permeation cell containing a polymer film and an upstream vessel maintained at a designated temperature. Vacuum was pulled on both sides of the film before exposing the upstream side to a desired gas pressure (p_2). As the gas permeated through the film, the pressure on the downstream side was monitored until the pressure increase rate (dp/dt) remained constant. The permeability of the gas was determined from

$$P_i = (Vl / ARTp_2) \times (dp/dt) \qquad (2.1)$$

where l is the film thickness, A is the exposed film area, R is the gas constant and T denotes absolute temperature. In all the permeation tests discussed here, the highest downstream pressure was 0.007 atm, in which case p_2 effectively corresponds to the transmembrane pressure. All permeation tests were conducted at 35°C unless otherwise specified.

The thermal characteristics of the SEOS copolymer, SEOS/PEG blends and the PEG_{4600} homopolymer were measured by differential scanning calorimetry (DSC) with a Perkin-Elmer DSC-7 unit calibrated with respect to In. Data were collected under a nitrogen blanket in a heat-cool-reheat cycle wherein the specimens were heated to 200°C, cooled to –50°C and then reheated to 200°C. The heating rate in the reheat cycle was held constant at 20°C/min. The normal melting temperatures reported herein correspond to peak temperatures observed during the reheat cycle, and the corresponding percent crystallinity (X_c) is calculated from

$$X_c = 100\% \times \Delta H_m / (W_{EO}\, \Delta H_m^{o}) \qquad (2.2)$$

where ΔH_m is the latent heat of melting approximated by the area under the melting endotherm, and ΔH_m^{o} is the latent heat of melting for 100% crystalline poly(ethylene oxide) (186.188 J/g, as reported elsewhere[35]). The composition W_{EO} denotes the weight fraction of crystallizable polyether and is given by $w_{EO}(1-w_{PEG}/100) + w_{PEG}/100$, where w_{EO} is the

weight fraction of the EO block in the copolymer (0.43) and w_{PEG} is the weight percentage of added PEG. Optical micrographs of the neat copolymer and several blends were acquired under crossed polars at 25°C with an Olympus BX60 microscope. Images were collected digitally with a CCD camera.

2.4. Results and Discussion

2.4.1. Factors Governing Gas Transport

The permeability of penetrant *i* (P_i) through a dense polymer film is generally given by

$$P_i = Ni \times l / \Delta p_i \tag{2.3}$$

where N_i is the steady-state gas flux of species *i* through the film, and $\Delta p_i = p_{2i} - p_{1i,}$ with p_{2i} and p_{1i} being the upstream and downstream partial pressures of *i*, respectively. When p_{1i} is negligible relative to p_{2i} and Fickian diffusion constitutes the rate-limiting step in penetrant transport, the permeability can be conveniently written in terms of the solution-diffusion model for nonporous (dense) polymer membranes[36] as

$$P_i = D_i \times S_i \tag{2.4}$$

Here, D_i is the concentration-averaged effective diffusion coefficient, and S_i is the solubility defined as the ratio of penetrant concentration dissolved in the upstream face relative to the upstream partial pressure in the gas phase. According to the solution-diffusion model, penetrant molecules dissolve into the upstream (high pressure) face of the film, diffuse across the film and ultimately desorb at the downstream (low pressure) face. Thus, depending on their diffusivity and solubility within a given polymer, different penetrants exhibit different permeabilities. The permeability of penetrant A relative to that of penetrant B is commonly expressed by the ideal selectivity ($\alpha_{A/B}$), which is defined as

$$\alpha_{A/B} = (P_A / P_B) = (D_A / D_B) \times (S_A / S_B) \quad (2.5)$$

The ratio D_A/ D_B is termed the diffusivity, or mobility, selectivity, whereas S_A/ S_B is known as the solubility selectivity.[37] Gas solubility is sensitive to factors such as operating conditions, penetrant condensability, polymer-penetrant interaction and polymer morphology (crystallinity and molecular orientation). The diffusion coefficient also depends on penetrant size, polymer morphology and polymer segmental dynamics.[38]

With these considerations in mind, we now turn our attention to the strategy adopted here for controllably altering the composition and, hence, morphology and, ultimately, the gas-transport properties of a microphase-ordered SEOS copolymer (illustrated in Fig.2.1). The neat copolymer exhibits a lamellar morphology, as evidenced by its composition and transmission electron microscopy (TEM) images.[39] While the S microphases (colored black in Fig.2.1) are glassy at ambient temperature, the EO microphases (speckled in the top of Fig.2.1) are semicrystalline due to the relatively high molecular weight of the copolymer midblock (~30,000). Addition of PEG_{4600}, a semicrystalline homopolymer, to the SEOS copolymer should promote lamellar swelling and, eventually, a transition to a polyether-continuous morphology wherein the polyether microphase remains semicrystalline, which is unfavorable for molecular transport. If, on the other hand, PEG_{400}, an amorphous liquid at ambient temperature, is used in analogous fashion, the degree of midblock crystallinity is expected to decrease with increasing PEG_{400} concentration. A reduction in polyether crystallinity will improve penetrant solubility, which is crucial to the design of CO_2-selective membranes, and diffusivity (through the removal of obstacles impeding molecular mobility). Thus, by judicious selection of blend composition and PEG homopolymer, an amorphous, polyether-continuous morphology with improved CO_2 permeability and selectivity relative to

nonpolar gases should be achievable through physical modification of the semicrystalline SEOS copolymer. The viability of this strategy is supported by results recently obtained[40] by sorbing PEG of different molecular weights from selective solvents (*e.g.*, water and ethanol) into the same microphase-ordered SEOS copolymer, as well as into the poly(ether-*b*-amide) multiblock copolymer discussed earlier, to form "mesoblends."

2.4.2. Gas Transport in SEOS/PEG Blends

The permeability data presented as a function of upstream (or, equivalently, transmembrane) pressure in Fig.2.2 for the neat SEOS copolymer indicate that the copolymer, despite its intrinsic crystallinity, behaves as a CO_2-selective membrane. Over the entire pressure range examined at ambient temperature, the permeability of CO_2 is clearly the highest of all the gases investigated, followed by H_2, O_2 and then N_2. Since this order is comparable to that observed with regard to rubbery polymers such as poly(dimethylsiloxane)[41] and *cis*-polyisoprene,[42] permeation through the SEOS copolymer is expected to occur primarily through the amorphous (rubbery) region of the EO lamellae. Another feature of the data shown in Fig.2.2 is that only the CO_2 permeability appears to be pressure-dependent. This characteristic behavior has likewise been observed in polyether-containing segmented copolymers[24] and crosslinked PEG.[22] Selectivity ranges based on Eq.2.5 and extracted from the data in Fig.2.2 are as follows: 2.1-2.4 for CO_2/H_2, 8.1-8.5 for CO_2/O_2 and 17-22 for CO_2/N_2. While these selectivity ranges are low relative to, for instance, those measured from chemically crosslinked PEG diacrylate with a molecular weight of 700 (9.5-11 for CO_2/H_2, 26-30 for CO_2/O_2 and 68 to 84 for CO_2/N_2),[22] Fig.2.2 confirms that the presence of a polyether block within the copolymer promotes CO_2 specificity. The apparent

reduction in chemical specificity compared to pure (crosslinked) PEG can be attributed to a combination of (*i*) the crystallinity of the polyether midblock and (*ii*) the non-specificity of the S microdomains. Systematic variation of polyether crystallinity through physical incorporation of PEG is the topic of further discussion in subsequent sections. The permeability of each gas used in Fig.2.2 through homopolystyrene can be determined from its temperature dependence since Arrhenius behavior is observed.[43] In this case the permeability is given by

$$P = P_0 \exp(-E_P / RT) \tag{2.6}$$

where P_0 is the frequency factor and E_P is the apparent activation energy for permeation. Values of P_0 and E_P reported by Yamada and Nakagawa[43] are listed in Table 2.1 and yield the following permeabilities at 35°C (in Barrer): 14 for CO_2, 27 for H_2, 2.9 for O_2 and 0.51 for N_2. For completeness, the corresponding CO_2/H_2, CO_2/O_2 and CO_2/N_2 selectivities are calculated to be 0.54, 4.9 and 28, respectively, confirming that the CO_2/H_2 selectivity of this SEOS triblock copolymer membrane is regrettably compromised by the presence of the non-selective S microdomains.

The permeation results displayed in Fig.2.2 can also be used as a probe of the copolymer morphology. Since both microphases of the copolymer are permeable to the gases investigated here, we employ the permeability relationships proposed by Robeson *et al.*[44] as extensions to the model originally developed by Maxwell[45] to describe the dielectric properties of a suspension of solid spheres. For a lamellar morphology in which the lamellae lie normal to the direction of flow (the series orientation), the net permeability can be expressed as

$$P = P_S P_{EO} / (\phi_S P_S + \phi_{EO,a} P_{EO}) \tag{2.7a}$$

where ϕ_i (i = S or EO) is the volume fraction of i, and the designation a signifies the amorphous fraction. In the parallel orientation with the lamellae lying along the direction of penetrant flow, the net permeability is written as

$$P = \phi_S P_S + \phi_{EO,a} P_{EO} \quad (2.7b)$$

While the block copolymer possesses a lamellar morphology in which the lamellae are oriented within a single grain, grains will exhibit different orientations with respect to the direction of penetrant flow. Thus, the copolymer can be considered microscopically anisotropic but macroscopically isotropic,[28] in which case Eqs. 2.7a and 7b are used to determine the permeability limits corresponding to each orientation. Alternative approaches such as those discussed by Subramanian and Plotzker[46] could likewise be applied to discern, for example, the crystallinity of the neat copolymer, but thermal calorimetry can be used with greater accuracy for this purpose.

The permeabilities of CO_2, H_2, O_2 and N_2 in the SEOS triblock copolymer and a low-density polyethylene,[47] which resembles PEG in terms of chemical structure, are presented as a function of penetrant normal boiling point (T_b), an established[48] measure of condensability (solubility), in Fig.2.3a. In both cases, CO_2 is observed to be more permeable than any of the other gases investigated. The corresponding selectivity of each gas relative to H_2 is included in Fig.2.3b and reveals that the N_2/H_2 and O_2/H_2 selectivities are virtually identical for the SEOS copolymer and the polyethylene. Once again, however, the CO_2/H_2 selectivity is noticeably higher in the copolymer. This apparent trend can be explained in terms of the physical properties[49,50] of CO_2 and H_2, which are provided in Table 2.2. While the normal boiling point (or critical temperature) can be considered a good measure of gas solubility, the critical volume is a indicator of penetrant diffusivity.[37] Since H_2 is smaller than CO_2, H_2

possesses a higher diffusion coefficient than CO_2, in which case $D_{CO_2}/D_{H_2} < 1$. Conversely, CO_2 is more soluble than H_2 due to its higher condensability. This thermodynamic aspect, coupled with specific interactions between CO_2 molecules and the polar linkages of amorphous PEG, increases the CO_2/H_2 solubility selectivity sufficiently to not only overcome the effect of reduced CO_2/H_2 mobility selectivity (see Eq.2.5), but also yield an overall CO_2/H_2 selectivity that is markedly greater than unity (~2.3). Thus, it immediately follows that, due to its enhanced solubility in the amorphous regions of the EO lamellae, CO_2 is more permeable in the SEOS copolymer membrane than H_2.

Addition of PEG_{4600} to the SEOS copolymer at concentrations of 20 and 40 wt% yields the results included in Fig.2.3. At both PEG_{4600} concentrations, the permeability of each gas decreases (see Fig.2.3a), as does the CO_2/H_2 selectivity (see Fig.2.3b). If PEG_{400} is added at a concentration of 22 wt%, neither the CO_2 permeability nor the CO_2/H_2 selectivity changes significantly from that of the neat copolymer. At a concentration of 45 wt% PEG_{400}, however, P_{CO_2} increases markedly (from ~33 for the neat copolymer to ~86 in the blend) in conjunction with a substantial increase in α_{CO_2/H_2} (from 2.3 to 4.3). To put this increase in perspective, the CO_2/H_2 selectivity of poly(dimethylsiloxane) is reported[41] to be ~3.6 at 35°C. The effects of PEG concentration and molecular weight on CO_2 permeability and CO_2/H_2 selectivity are shown for two series of SEOS/PEG blends in Fig.2.4. For blends prepared with either PEG_{400} or PEG_{4600}, an upper limit of *ca*. 45 wt% PEG is dictated by the mechanical stability of the films used in the permeation analysis. As first observed in Fig.2.3, addition of PEG_{4600} to the SEOS copolymer promotes a general reduction in (Fig.2.4a), as well as a decrease in CO_2/H_2 selectivity over most of the blend composition range explored (Fig.2.4b). Only at high PEG_{4600} concentrations (> 45 wt%) is a CO_2/H_2 selectivity

comparable to that of the neat copolymer recovered. If PEG_{400} is added to the copolymer, very different results are obtained. At PEG_{400} concentrations typically less than ~20 wt%, the CO_2 permeability decreases slightly, whereas the corresponding CO_2/H_2 selectivity is only marginally affected (ranging from 2.1 to 2.5 in Fig.2.4b). At higher PEG_{400} concentrations (> 37 wt%), however, P_{CO_2} and α_{CO_2/H_2} both increase dramatically (by ~160% and 87%, respectively, at 45 wt% PEG_{400} relative to the neat SEOS copolymer) due most likely to a morphological transition to a continuous polyether microphase. Note that a blend with 37 wt% PEG_{400} corresponds to about 65 wt% polyether, which would be a reasonable composition to expect a cylindrical morphology composed of S cylinders in an EO matrix. These pronounced increases in CO_2 permeability and selectivity due to the addition of PEG_{400} testify to the high CO_2 solubility afforded by amorphous PEG solubilized within the SEOS nanostructure. The difference in gas-transport properties between PEG_{400} and PEG_{4600} is directly attributable to their disparate crystallinities, as discussed in the following section.

2.4.3. Thermal Characteristics of SEOS/PEG Blends

To ascertain if the copolymer/homopolymer blend strategy depicted in Fig.2.1 is accurate, optical images of the neat SEOS copolymer and blends with PEG_{4600} and PEG_{400} at a concentration of 45 wt% PEG have been collected under crossed polars at ambient temperature. These images are displayed in Fig.2.5 and confirm that the neat copolymer is semicrystalline due to its high degree of birefringence (Fig.2.5a). Regions of strong birefringence increase substantially upon addition of PEG_{4600} to the copolymer (Fig.2.5b). [The inset included in Fig.2.5b is obtained from the neat PEG_{4600} homopolymer.] In marked contrast, the SEOS/PEG blend composed of PEG_{400} (Fig.2.5c) exhibits almost no

birefringence, indicating that the polyether constituents of this blend are, for the most part, amorphous. Corresponding DSC thermograms acquired from the neat SEOS copolymer and the two blends pictured in Fig.2.5 are presented in Fig.2.6. Addition of PEG_{4600} to the SEOS copolymer yields both a shift in normal melting temperature (T_m) to higher temperature and a concurrent increase in ΔH_m, signifying a higher degree of crystallinity relative to the neat copolymer. In the case of PEG_{400}, however, the primary melting peak is shifted to a lower temperature and ΔH_m is reduced considerably. Included in the inset of Fig.2.6 is an enlargement of the thermogram collected from the neat SEOS copolymer showing the existence of the S glass transition temperature ($T_{g,S}$). Values of T_m and $T_{g,S}$ gleaned from DSC thermograms of the neat copolymer and several SEOS/PEG blends such as those displayed in Fig.2.6 are provided as a function of PEG concentration for PEG_{400} and PEG_{4600} in Fig.2.7a, whereas corresponding crystallinities (X_c) computed from values of ΔH_m in conjunction with Eq.2.2 are shown in Fig.2.7b.

Since the S block of the copolymer and PEG homopolymer are strongly incompatible and therefore remain largely unmixed, it is not surprising that $T_{g,S}$ is virtually independent of PEG addition up to *ca*. 40 wt% PEG_{4600} in Fig.2.7a. The sharp drop in $T_{g,S}$ (by ~10°C) in the vicinity of 50 wt% PEG_{4600} suggests that the copolymer undergoes a PEG_{4600}-induced transition to a morphology that precludes the same degree of chain packing available to the S blocks in an alternating lamellar arrangement. A highly defective layered morphology or a dispersed morphology composed of S cylinders or spheres in an polyether-continuous matrix would be consistent with such a confinement effect. In the case of the lower molecular weight PEG, a reduction of ~5°C is achieved with only 10 wt% PEG_{400}, thereby indicating limited incorporation of PEG_{400} into the S lamellae. A further decrease in $T_{g,S}$ (of ~8°C)

similar to the one observed via addition of PEG_{4600} also occurs in the SEOS/PEG_{400} blend series, but at a lower PEG concentration (30-40 wt% for PEG_{400}, in contrast to 40-50 wt% PEG_{4600}). This shift in transition concentration is consistent with prior reports[4-7] of solvent- and homopolymer-induced morphological (order-order) transitions in block copolymer blends, and reflects the ability of PEG_{400} to more uniformly distribute within the EO microphases and consequently promote an increase in interfacial chain packing and an accompanying change in interfacial curvature at a lower concentration relative to PEG_{4600}. Values of T_m shown in Fig.2.7a likewise display a difference for blends prepared with PEG_{4600} and PEG_{400}. Upon addition of PEG_{4600} (T_m = 60°C), T_m of the resultant SEOS/PEG copolymer blends (initially at 50°C for the neat copolymer) increases up to 63°C at 40 wt% PEG_{4600} and then decreases to 48°C at 70 wt%. This same trend is echoed in terms of X_c for the SEOS/PEG_{4600} blends in Fig.2.7b, suggesting that PEG_{4600} not only swells the EO lamellae but also serves as a nucleating agent for the EO copolymer blocks. Concurrent reductions in $T_{g,S}$, T_m and X_c at *ca*. 50 wt% PEG_{4600} in this SEOS/PEG blend series further support the existence of an order-order transition in the vicinity of this blend composition. The thermal signatures of the SEOS/PEG_{400} blends in Fig.2.7, on the other hand, indicate that (*i*) T_m and X_c generally decrease with increasing PEG_{400} content up to about 50 wt% and (*ii*) these reductions are relatively gradual. At PEG_{400} concentrations greater than 50 wt%, both T_m and X_c become independent of blend composition.

The variation in X_c promoted by the incorporation of either PEG_{4600} or PEG_{400} is expected to have a profound effect on the gas-transport properties of the resultant SEOS/PEG blends. Crystallites generally behave as impermeable obstacles that force penetrant molecules to diffuse through irregular, molecularly-constricted conduits within accessible

intercrystalline regions. The segmental mobility of the chains in the neighborhood of discrete crystallites is also affected, resulting in lower gas diffusivity, since these chains are covalently connected to the chains comprising the crystallites. Both factors decrease the penetrant diffusivity according to[51]

$$D = D_a / \tau\beta \tag{2.8}$$

where D_a represents the diffusion coefficient of a penetrant molecule through a completely amorphous phase, τ is a tortuosity factor and β is the chain immobilization factor. Another way to describe the diffusion coefficient is as[38]

$$D = D_a \phi_a^{\,m} \tag{2.9}$$

where ϕ_a denotes the volume fraction of the amorphous phase, and m (in the same fashion as τ) provides an empirical measure of the effective diffusive path length (an increase in the value of m signifies greater tortuosity). Since a diffusing penetrant species is virtually insoluble within crystalline regions, crystallites likewise hinder penetrant solubility, in which case the solubility can be expressed in analogous fashion as Eq.2.9:

$$S = S_a \phi_a \tag{2.10}$$

where S_a is the solubility of a species in a purely amorphous polymer. Substitution of Eqs. 2.9 and 2.10 into Eq.2.4 yields the permeability of a penetrant through a semicrystalline homopolymer, *viz*.,

$$P = P_a \phi_a^{\,m+1} \tag{2.11}$$

Although the exponent m can be calculated directly from measured values of P and calculated values of ϕ_a (via X_c), its physical meaning is obscured due to the biphasic nature of the SEOS nanostructure. Generally speaking, the effective reduction in diffusivity arising from restricted molecular motion of polymer chains in the neighborhood of crystallites tends

to increase with increasing penetrant size and is therefore expected to be more pronounced for CO_2 relative to H_2.[38] In this case, m for CO_2 is expected to be larger than that for H_2 under identical conditions of crystal-induced tortuosity. A relative value of Δm (= m_{CO_2}-m_{H_2}) can be computed from the CO_2/H_2 selectivity according to

$$\alpha_{CO_2/H_2} = \left(\alpha_{CO_2/H_2}\right)_a \phi_a^{\Delta m} \qquad (2.12)$$

Here, $(\alpha_{CO_2/H_2})_a$ is the CO_2/H_2 selectivity of the completely amorphous material. Since the mass densities of glassy homopolystyrene and amorphous/crystalline EO are not far removed from unity, ϕ_a can be reasonably approximated by $100 - X_c$ (where X_c is expressed as a percentage). Figure 2.8 shows the dependence of α_{CO_2/H_2} on $100 - X_c$ and reveals that the data are favorably represented by Eq.2.12 with $\Delta m > 0$ (~ 4) and $(\alpha_{CO_2/H_2})_a$ 6.0. While the value of Δm is in agreement with intuitive expectation, it must be recognized, however, that the regressed value of $(\alpha_{CO_2/H_2})_a$ is not physically meaningful, since it reflects gas transport through the amorphous S *and* EO microphases (the morphology and fraction of which depend on blend composition).

2.4.4. Temperature Effect on Gas Transport

The permeabilities of CO_2 and H_2 are presented on semi-logarithmic coordinates as functions of reciprocal temperature for the semicrystalline SEOS copolymer and 55/45 w/w SEOS/PEG_{4600} blend in Figs. 9a and 9b, respectively. The linearity of the data at high and low temperature confirms that gas transport through these membranes is temperature-activated and can therefore be described by Eq.2.6. In both semicrystalline materials, the permeabilities at low temperature (below T_m) are lower, and exhibit a distinctly different

temperature dependence, than those at high temperature (above T_m, but below $T_{g,S}$). Comparison of results obtained from the analogous 55/45 SEOS/PEG_{400} blend (see Fig.2.10), which does not exhibit such variation, indicates that the change in permeability temperature-dependence observed in Fig.2.9 can be unambiguously attributed to the existence of crystals within the polyether microphase. It is important to note that, in all these variable-temperature permeation measurements (which traverse T_m of the polyether), a microphase-ordered nanostructure remains intact to provide the SEOS/PEG blends with sufficient mechanical integrity. Thus, we extend the previous studies of Hirayama *et al.*[21] and Okamoto *et al.*[23] by discerning the effect of polyether melting on gas-transport properties as a function of composition in blends of the SEOS copolymer with PEG_{4600}. This analysis cannot be conducted for the SEOS/PEG_{400} blends due to their apparently low crystallinity (see Fig.2.7b).

One way to characterize the change in permeability upon melting is through a permeability switch (P^*), which is defined as

$$P^* = P_a(T_m) / P_c(T_m) \tag{2.13}$$

Here, P_c is the permeability of the semicrystalline membrane. Since the permeability cannot be measured at T_m, values of $P_a(T_m)$ and $P_c(T_m)$ are computed by using Eq.2.7a to extrapolate the temperature-dependent P_a and P_c to T_m evaluated from Fig.2.6, in which case

$$P^* = (P_{0a} / P_{0c}) \exp (-\Delta E_{P,m} / RT_m) \tag{2.14}$$

where P_{0a} and P_{0c} are the frequency factors of the amorphous and semicrystalline membranes, and $\Delta E_{P,m}$ is the change in the apparent activation energy for permeation upon melting (= $E_{P,a} - E_{P,c}$, where the subscripted *a* and *c* have the same meaning as above). Values of $E_{P,a}$, $E_{P,c}$ and $\Delta E_{P,m}$ determined for CO_2 and H_2 in the SEOS copolymer and three

SEOS/PEG_{4600} blends are provided in Table 2.3. The dependence of P^* on PEG_{4600} content is displayed in Fig.2.11, which reveals that P^* is (*i*) consistently larger for CO_2 relative to H_2 and (*ii*) weakly dependent on w_{PEG} up to 30 wt% PEG_{4600}. Increasing the PEG_{4600} concentration to 45 wt%, however, promotes a sharp increase in P^* for CO_2, as well as a less pronounced increase in P^* for H_2, which is again consistent with a morphological transition to a polyether-continuous nanostructure in the vicinity of 40 wt% PEG_{4600} (see Fig.2.7a).

It is interesting that $\Delta E_{P,m}$ for CO_2 tends to decrease substantially (from –16.8 to –49.6 kJ/mol), while that for H_2 exhibits less composition dependence, with increasing PEG_{4600} concentration up to 30 wt%. Following the same trend displayed by $P^*(w_{PEG})$ in Fig.2.11, $\Delta E_{P,m}$ for both CO_2 and H_2 likewise shows a dramatic increase at 45 wt% PEG_{4600}. Since E_P constitutes the summation of activation energies arising from diffusion (E_D) and sorption (E_S),[52] we can qualitatively describe how these contributions differ for CO_2 and H_2. Since H_2 is physically smaller than CO_2, E_D is generally expected (and has been shown[53]) to be smaller for H_2 relative to CO_2. Conversely, since CO_2 is more condensable in and can interact specifically with the polar linkages of the polyether microphase, it should have a smaller E_S compared to H_2. Combining these contributions yields comparable magnitudes of E_P for both CO_2 and H_2, which, for the most part, are observed for the semicrystalline SEOS copolymer and its blends with PEG_{4600} at temperatures below T_m (see Table 2.3). Only the blend with 30 wt% PEG_{4600} deviates substantially (and reproducibly) from this expectation and warrants further investigation. Comparison of the results listed in Table 2.3 reveals that E_P is generally in excess of 20 kJ/mol. At temperatures above T_m, however, the values of E_P for CO_2 and H_2 are observed to differ significantly, indicating that another aspect of E_P must be considered. Under these conditions, E_P for CO_2 and H_2 permeation through the glassy S microphase is of

the same magnitude as that for CO_2 and H_2 through the amorphous EO microphase (see Table 2.1), confirming that this contribution to the overall gas-transport process cannot be neglected. Over the temperature range illustrated in Fig.2.9, the changes in permeability of CO_2 and H_2 through polystyrene, calculated from the frequency factors and activation energies provided in Table 2.1, are 7.8 and 31 Barrer, respectively.

With this apparent limitation of the present membranes notwithstanding, the CO_2/H_2 selectivities of the neat SEOS copolymer and the 55/45 SEOS/PEG blends with PEG_{4600} and PEG_{400} are presented as a function of temperature in Fig.2.12 and confirm that α_{CO_2/H_2} for the SEOS/PEG_{400} blend remains relatively constant across its polyether melting transition. In this case, the reduction in solubility selectivity promoted by an increase in temperature is offset by enhanced CO_2 diffusivity (relative to H_2 diffusivity) so that the overall CO_2/H_2 selectivity shows very little dependence on temperature. Both semicrystalline membranes, however, undergo an abrupt increase in α_{CO_2/H_2} upon melting, with the magnitude of this change in selectivity increasing with increasing blend crystallinity. The melting of EO crystals in the neat SEOS copolymer and the SEOS/PEG_{4600} blend promotes a relatively sharp increase in CO_2 solubility selectivity that dominates the overall selectivity due to the increased availability of ether linkages accessible for interaction with diffusing CO_2 molecules.

2.5. Conclusions

The gas-permeation properties of CO_2, H_2, N_2 and O_2 have been measured as a function of composition in a microphase-ordered (lamellar) SEOS triblock copolymer with a polyether midblock, as well as in its miscible blends with PEG differing in molecular weight.

If the added PEG is semicrystalline, blends with the SEOS copolymer are observed to exhibit elevated melting temperatures and enhanced crystallinity due to nucleation of the EO blocks residing within the confined polyether lamellae. Incorporation of amorphous PEG into the SEOS copolymer results in reduced S glass transition and EO melting temperatures, as well as a decrease in the overall crystallinity. All the membranes consistently exhibit higher CO_2 permeability than H_2 due to the unusually high solubility of CO_2 in the polyether, thereby confirming that the polyether microphase constitutes the main locus of gas transport within these biphasic materials at temperatures below the polyether melting temperature. Under these conditions, the presence of EO crystals lowers CO_2/H_2 selectivity because crystalline regions serve as impermeable obstacles to molecular diffusion and likewise reduce solubility due to inaccessibility of the polymer chains. In this regard, an increase in blend crystallinity (as in the case of the SEOS/PEG_{4600} blends) promotes an overall reduction in CO_2/H_2 selectivity. At sufficiently high PEG concentrations, the gas-transport and thermal properties indicate the existence of a morphological transition to a polyether-continuous nanostructure. Details of this transition and of the corresponding morphologies in PEG- and S-rich SEOS/PEG blends are forthcoming.[39] Abrupt increases in CO_2 and H_2 permeability are observed upon heating the neat SEOS copolymer and the SEOS/PEG_{4600} blends due to polyether crystal melting within copolymer-stabilized nanostructured membranes. A permeation switch determined at the composition-dependent melting point and the temperature-dependent CO_2/H_2 selectivity together reveal that CO_2 permeation is more strongly influenced than H_2 permeation by such crystal melting, especially in light of an apparent morphological transition at relatively high PEG_{4600} concentrations. The results reported herein confirm that microphase-ordered block copolymers containing a polyether

block can serve as reverse-selective membranes exhibiting high CO_2 specificity. We have shown that, through judicious choice of PEG molecular weight and blend composition, the gas-transport and thermal properties of near-equilibrium SEOS/PEG blends can be systematically tailored using the design paradigms[4] established for block copolymer/ homopolymer (or solvent) blends.

2.6. Acknowledgements

This work was supported by the U. S. Department of Energy under Contract No. DE-FG02-99ER14991.

2.7. References

1. Bates, F. S.; Fredrickson, G. H. *Phys. Today* **1999**, *52*, 32.
2. Hamley, I. W. *The Physics of Block Copolymers*; Oxford University Press: Oxford, 1998.
3. Hadjichristidis, N.; Pispas, S.; Floudas, G. A *Block Copolymers: Synthetic Strategies, Physical Properties, and Applications*; Wiley-Interscience: New York, 2003.
4. Spontak, R. J.; Patel, N. P. In *Developments in Block Copolymer Science and Technology*; Hamley, I. W., Ed.; Wiley: New York, 2004, pp. 159-212.
5. Hanley, K. J.; Lodge, T. P. *J. Polym. Sci. B: Polym. Phys.* **1998**, *36*, 3101. Lodge, T. P.; Pudil, B.; Hanley, K. J. *Macromolecules* **2002**, *35*, 4707.
6. Laurer, J. H.; Khan, S. A.; Spontak, R. J.; Satkowski, M. M.; Grothaus, J. T.; Smith, S. D.; Lin, J. S. *Langmuir* **1999**, *15*, 7947.
7. Winey, K. I.; Thomas, E. L.; Fetters, L. J. *J. Chem. Phys.* **1991**, *95*, 9367. Winey, K. I.; Thomas, E. L.; Fetters, L. J. *Macromolecules* **1991**, *24*, 6182; **1992**, *25*, 2645. Urbas, A.; Sharp, R.; Fink, Y.; Thomas, E. L.; Xenidou, M.; Fetters, L. J. *Adv. Mater.* **2000**, *12*, 812.
8. Tanaka, H.; Hashimoto, T. *Macromolecules* **1991**, *24*, 5713. Kimishima, K.; Hashimoto, T.; Han, C. D. *Macromolecules* **1995**, *28*, 3842. Bodycomb, J.; Yamaguchi, D.; Hashimoto, T. *Macromolecules* **2000**, *33*, 5187.
9. Schulz, M. F.; Bates, F. S.; Almdal, K.; Mortensen, K. *Phys. Rev. Lett.* **1994**, *73*, 86. Zhao, J.; Majumdar, B.; Schulz, M. F.; Bates, F. S.; Almdal, K.; Mortensen, K.; Hajduk, D. A.; Gruner, S. M. *Macromolecules* **1996**, *29*, 1204.

10. Kane, L.; Satkowski, M. M.; Smith, S. D.; Spontak, R. J. *Macromolecules* **1996**, *29*, 8862. Spontak, R. J.; Fung, J. C.; Braunfeld, M. B.; Sedat, J. W.; Agard, D. A.; Kane, L.; Smith, S. D.; Satkowski, M. M.; Ashraf, A.; Hajduk, D. A.; Gruner, S. M. *Macromolecules* **1996**, *29*, 4494. Kane, L.; Norman, D. A.; White, S. A.; Matsen, M. W.; Satkowski, M. M.; Smith, S. D.; Spontak, R. J. *Macromol. Rapid Commun.* **2001**, *22*, 281.

11. Abetz, V.; Goldacker, T. *Macromol. Rapid Commun.* **2000**, *21*, 16.

12. Yamaguchi, D.; Shiratake, S.; Hashimoto, T. *Macromolecules* **2000**, *33*, 8258. Yamaguchi, D.; Hashimoto, T. *Macromolecules* **2001**, *34*, 6495. Yamaguchi, D.; Hasegawa, H.; Hashimoto, T. *Macromolecules* **2001**, *34*, 6506. Yamaguchi, D.; Takenaka, M.; Hasegawa, H.; Hashimoto, T. *Macromolecules* **2001**, *34*, 1707. Court, F.; Hashimoto, T. *Macromolecules* **2001**, *34*, 2536. Court, F.; Hashimoto, T. *Macromolecules* **2002**, *35*, 2566.

13. Park, C.; Yoon, J.; Thomas, E. L. *Polymer* **2003**, *44*, 6725.

14. Bronstein, L. M. *Top. Curr. Chem*. **2003**, 226, 55.

15. Simon, P. F. W.; Ulrich, R.; Spiess, H. W.; Wiesner, U. *Chem. Mater.* **2001**, *13*, 3464.

16. Jonquières, A.; Clément, R.; Lochon, P. *Prog. Polym. Sci.* **2002**, *27*, 1803 and the references provided therein.

17. Stern, S. A. *J. Membr. Sci.* **1994**, *94*, 1. Ghosal, K.; Freeman, B. D. *Polym. Adv. Technol.* **1994**, *5*, 673.

18. Bhide, B. D. Stern, S. A. *J. Membr. Sci.* **1993**, *81*, 209; **1993**, *93*, 239.

19. Merkel, T. C.; He, Z. J.; Pinnau, I.; Freeman, B. D.; Meakin, P.; Hill, A. J. *Macromolecules* **2003**, *36*, 8406. Merkel, T. C.; Freeman, B. D.; Spontak, R. J.; He, Z.;

Pinnau, I.; Meakin, P.; Hill, A. J. *Chem. Mater.* **2003**, *15*, 109. Merkel, T. C.; Freeman, B. D., Spontak, R. J.; He, Z.; Pinnau, I.; Meakin, P.; Hill, A. J. *Science* **2002**, *296*, 519.

20. Saha, S.; Chakma, A. *Energy Conversion Management* **1992**, *33*, 413. Davis, R. A.; Sandall, O. C. *AIChE J.* **1993**, *39*, 1135.
21. Hirayama, Y.; Kase, Y.; Tanihara, N.; Sumiyama, Y.; Kusuki, Y.; Haraya, K. *J. Membr. Sci.* **1999**, *160*, 87.
22. Patel, N. P.; Miller, A. C.; Spontak, R. J. *Adv. Mater.* **2003**, *15*, 729.
23. Okamoto, K. -I.; Fujii, M.; Okamyo, S.; Suzuki, H.; Tanaka, K.; Kita, H. *Macromolecules* **1995**, *28*, 6950.
24. Bondar, V. I.; Freeman, B. D.; Pinnau, I. *J. Polym. Sci. B: Polym. Phys.* **1999**, *37*, 2463; **2000**, *38*, 2051.
25. Kim, J. H.; Seong, Y. H.; Lee, Y. M. *J. Membr. Sci.* **2001**, *190*, 179.
26. Spontak, R. J.; Smith, S. D. *J. Polym. Sci. B: Polym. Phys*. **2001**, *39*, 947.
27. Kinning, D. J.; Thomas, E. L.; Ottino, J. M., *Macromolecules* **1987**, *20*, 1129.
28. Csernica, J.; Baddour, R. F.; Cohen, R. E., *Macromolecules* **1987**, *20*, 2468; **1989**, *22*, 1493. Rein, D. H.; Csernica, J.; Baddour, R. F.; Cohen, R. E. *Macromolecules* **1990**, *23*, 4456. Csernica, J.; Rein, D. H.; Baddour, R. F.; Cohen, R. E. *Macromolecules* **1991**, *24*, 3612. Rein, D. H.; Baddour, R. F.; Cohen, R. E. *J. Appl. Polym. Sci.* **1992**, *45*, 1223.
29. Zielinski, J. M. In *Encyclopedia of Materials: Science and Technology*; Buschow, K. H. J., Cahn, R. W., Flemings, M. C., Ilschner, B., Kramer, E. J., Mahajan, S., Eds.; Elsevier: Oxford, 2001; Vol. 1.

30. Sax, J.; Ottino, J. M. *Polym. Eng. Sci.* **1983**, *23*, 165. Sax, J.; Ottino, J. M. *Polymer* **1985**, *26*, 1073.

31. Faridi, N.; Duda, J. L.; Hadj Romdhane, I. *Ind. Eng. Chem. Res.* **1995**, *34*, 3556.

32. Vrentas, J. S.; Vrentas, C. M. *Chem. Eng. Sci.* **1997**, *52*, 985.

33. Arnold, M. E.; Nagai, K.; Freeman, B. D.; Spontak, R. J.; Leroux, D.; Betts, D. E.; DeSimone, J. M.; DiGiano, F. A.; Stebbins, C. K.; Linton, R. W. *Macromolecules* **2002**, *35*, 3697. Arnold, M. E.; Nagai, K.; Freeman, B. D.; Spontak, R. J.; Betts, D. E.; DeSimone, J. M.; Pinnau, I. *Macromolecules* **2001**, *34*, 5611.

34. Felder, R. M.; Huvard, G. S. *Permeation, Diffusion and Sorption of Gases and Vapors*; Fava, R., Ed.; Academic Press: New York, 1978; Vol. 16C, p. 315.

35. Geng, H. Z.; Rosen, R.; Zheng, B.; Shimoda, H.; Fleming, L.; Liu, J.; Zhou, O. *Adv. Mater.* **2002**, *14*, 1387.

36. Wijmans, J. G.; Baker, R. W. *J. Membr. Sci.* **1995**, *107*, 1.

37. Freeman, B. D.; Pinnau, I. *Trends Polym. Sci.* **1997**, *5*, 167.

38. Weinkauf, D. H.; Paul, D. R. In *Barrier Polymers and Barrier Structures*; Koros, W. J., Ed.; American Chemical Society: Washington, D.C., 1990, pp. 60-91. Petropoulos, J. H. In *Polymeric Gas Separation Membranes*; Paul, D. R., Yampol'skii, Y. P., Eds.; CRC Press: Boca Raton, LA, 1994, p. 17.

39. Patel, N. P.; Spontak, R. J. manuscript in preparation.

40. Patel, N. P.; Spontak, R. J. *Macromolecules* (in press).

41. Merkel, T. C.; Bondar, V. I.; Nagai, K.; Freeman, B. D.; Pinnau, I. *J. Polym. Sci. B: Polym. Phys*. **2000**, *38*, 415.

42. Zolandz, R. R.; Fleming, G. K. In Membrane Handbook; Ho, W. S. W., Sirkar, K. K., Eds.; Van Nostrand Reinhold: New York, 1992; pp. 17-101.

43. Yamada, S.; Nakagawa, T. *Kobunshi Ronbunshu* **1982**, *39*, 391.

44. Robeson, L. M.; Noshay, A.; Matzner, M.; Merriam, C. N. *Angew. Makromol. Chem*. **1973**, *29/30*, 47.

45. Maxwell, C. *Treatise on Electricity and Magnetism*; Oxford University Press: London, 1873; Vol. 1.

46. Subramanian, P. M.; Plotzker, I. G. In *Polymer Blends, Vol. 2*; Paul, D. R., Bucknall, C. B., Eds.; Wiley: New York, 2000; Chap. 30.

47. Michaels, A. S.; Bixler, H. J. *J. Polym. Sci.* **1961**, *50*, 413.

48. Amerongen, G. J. V. *Rubber Chem. Technol.* **1964**, *37*, 1065.

49. Reid, R. C.; Prausnitz, J. M.; Poling, B. E. *The Properties of Gases and Liquids*; McGraw-Hill: New York, 1987, p. 741.

50. Breck, D. W. *Zeolite Molecular Sieves*; Wiley-Interscience: New York, 1974; p. 65.

51. Michaels, A. S.; Bixler, H. J. *J. Polym. Sci.* **1961**, *50*, 393.

52. Kim, J. H.; Seong, Y. H.; Lee, Y. M. *J. Membr. Sci.* **2001**, *193*, 209.

53. Petropoulos, J. H. *J. Membr. Sci.* **1990**, 53, 229.

Table 2.1. Frequency factors and apparent activation energies for several gases in glassy polystyrene.[a]

Gas	P_0 (10^3 Barrer)	E_P (kJ/mol)
H_2	9.67	15.1
N_2	6.99	24.4
O_2	2.91	17.7
CO_2	0.38	8.41

[a] Data from Yamada and Nakagawa.[43]

Table 2.2. Pertinent physical characteristics of CO_2 and H_2.

Gas	Penetrant size		Condensability	
	Critical volume[a] (cm^3/mol)	Kinetic diameter[b] (nm)	Normal boiling point[a] (K)	Critical temperature[b] (K)
H_2	65.1	0.29	20.4	33.2
CO_2	93.9	0.33	194.7	304.1

[a] Data from Reid *et al*.[51]

[b] Data from Breck[50]

Table 2.3. Apparent activation energies for CO_2 and H_2 permeation in the SEOS copolymer and its blends with PEG.[a]

Membrane	w_{PEG} (wt%)	$E_{P,c}$ (kJ/mol)		$E_{P,a}$ (kJ/mol)		$\Delta E_{P,m}$ (kJ/mol)	
		CO_2	H_2	CO_2	H_2	CO_2	H_2
SEOS	0	22.8	29.5	5.97	11.3	–16.8	–18.2
SEOS + PEG_{4600}	10	48.3	51.1	12.4	22.8	–35.9	–28.3
	30	51.4	31.0	1.84	6.09	–49.6	–24.9
	45	26.5	20.4	15.9	21.8	–10.6	+1.38
SEOS + PEG_{400}	45	21.7	24.9	21.7	24.9	—	—

[a] Values are extracted from data such as those presented in Fig.2.9 in conjunction with Eq.2.6.

List of symbols:

E = open circle

J = filled circle

C = open triangle

H = filled triangle

G = open square

B = filled square

A = open diamond

S = open inverted triangle

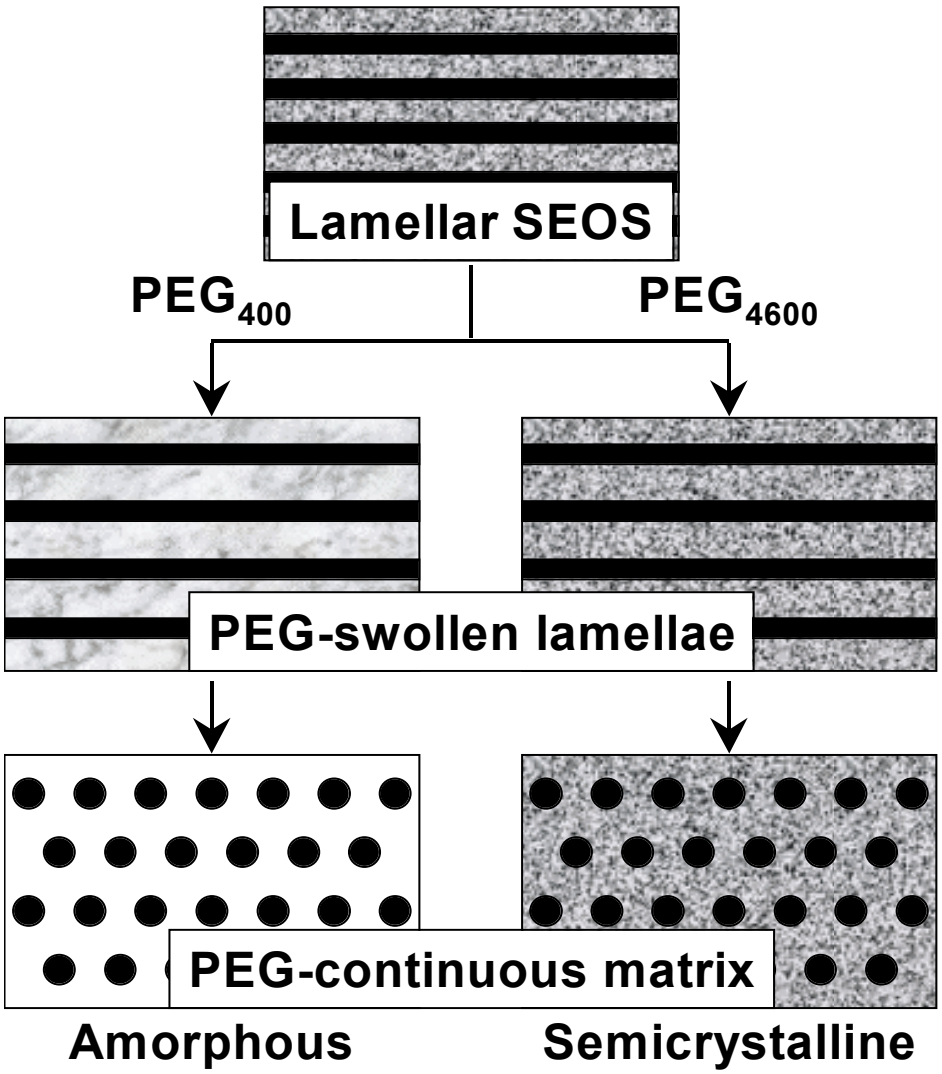

Figure 2.1. Schematic illustration of the blending strategy proposed here to probe the effects of blend composition (morphology) and crystallinity on the gas-permeation properties of a microphase-ordered SEOS triblock copolymer that exhibits the lamellar morphology. Addition of either PEG_{400} (amorphous) or PEG_{4600} (semicrystalline) initially swells, as well as alters the crystallinity of, the host EO lamellae. Further addition of either PEG is anticipated to promote an order-order transition to a polyether-continuous morphology wherein the PEG-rich matrix is either principally amorphous (PEG_{400}) or semicrystalline (PEG_{4600}).

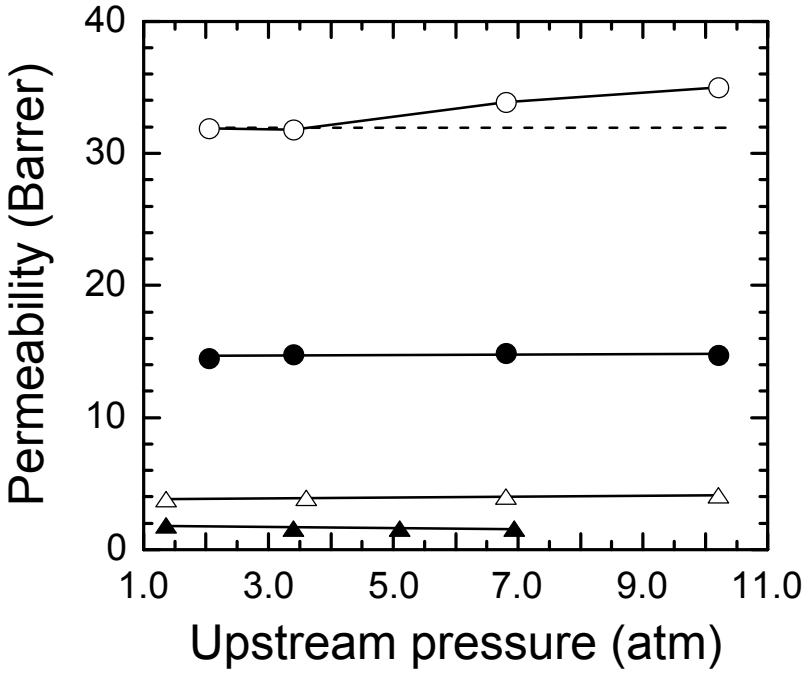

Figure 2.2. Dependence of permeability on upstream (transmembrane) pressure for four gases – CO_2 (E), H_2 (J), O_2 (C) and N_2 (H) – through the neat SEOS triblock copolymer at 35°C. The solid lines connect the data, whereas the dashed line corresponds to constant permeability for CO_2.

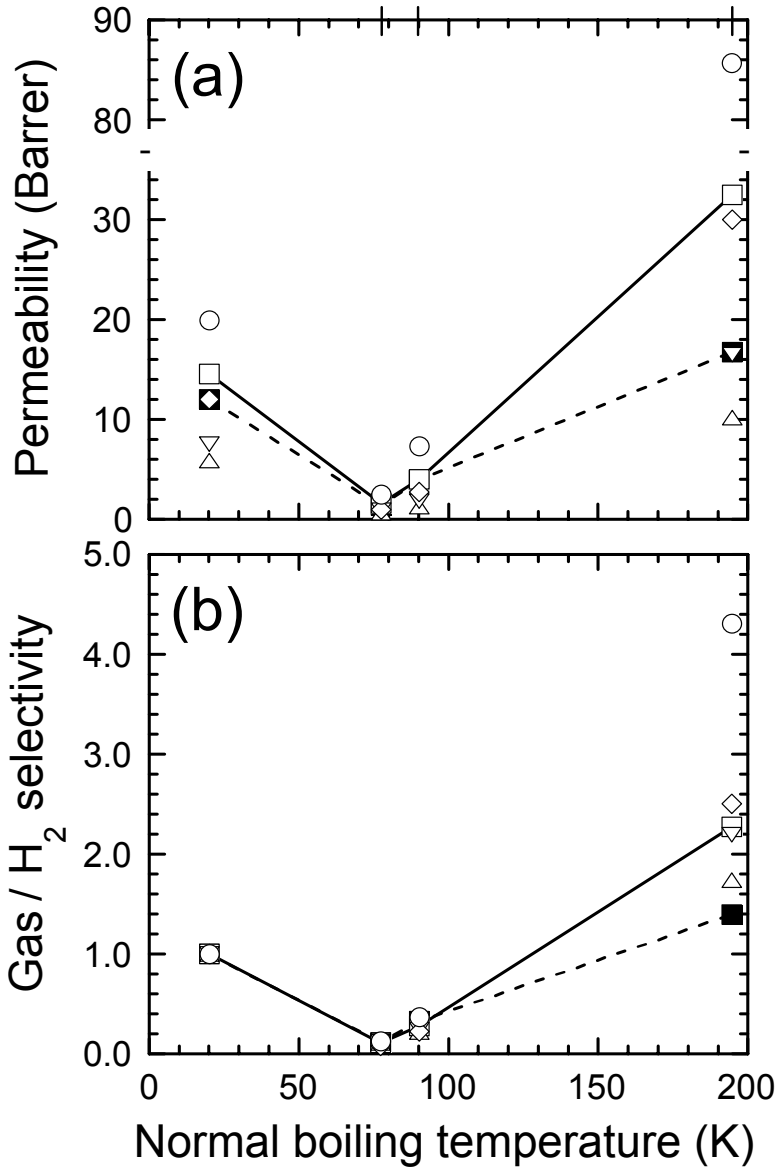

Figure 2.3. Variation of (a) permeability and (b) selectivity relative to H_2 with normal boiling temperature, a measure of gas condensability within a dense polymer membrane, for the neat SEOS copolymer (G, connected by a solid line) and four SEOS/PEG blends: 20 wt% PEG_{4600} (C), 45 wt% PEG_{4600} (S), 22 wt% PEG_{400} (A) and 45 wt% PEG_{400} (E). Results obtained for a low-density polyethylene (B, connected by a dashed line) are included for comparison.

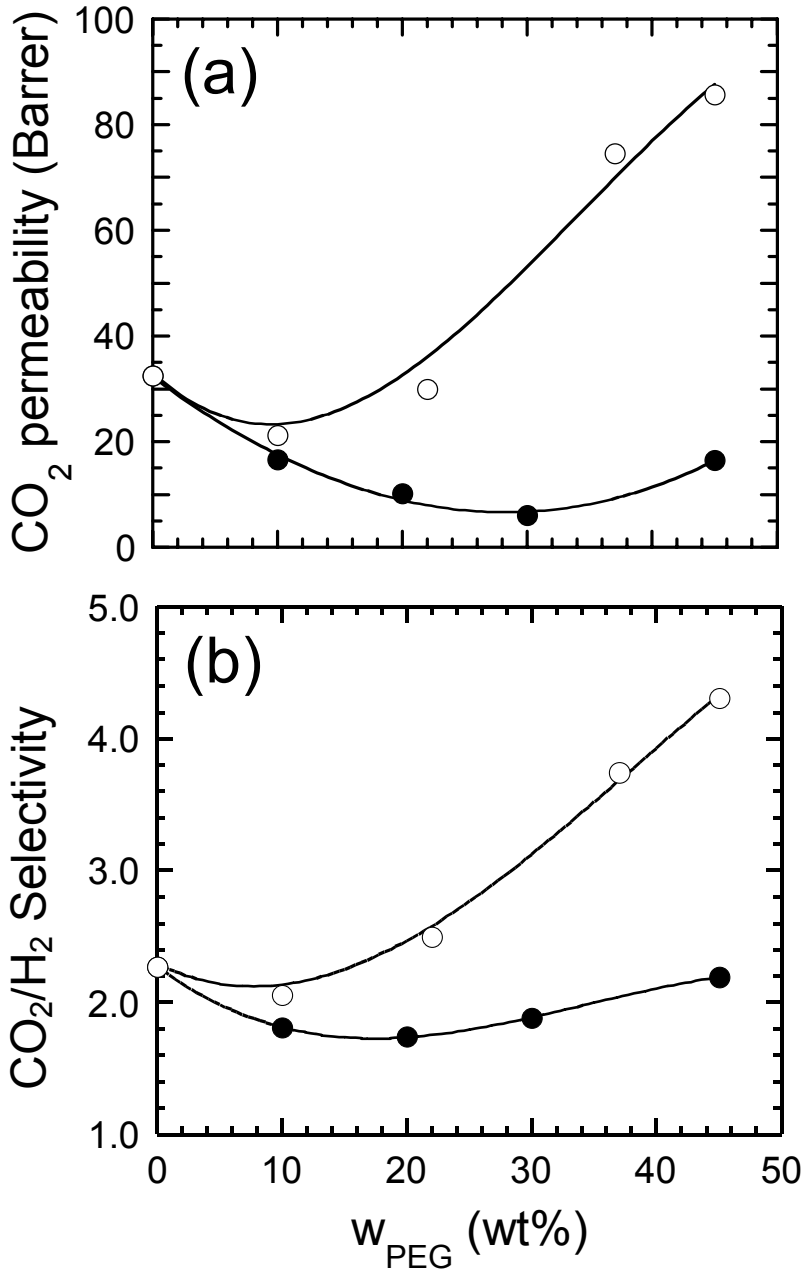

Figure 2.4. Dependence of (a) CO_2 permeability and (b) CO_2/H_2 selectivity on blend composition for SEOS/PEG blends containing PEG_{400} (E) and PEG_{4600} (J). The solid lines serve as guides for the eye.

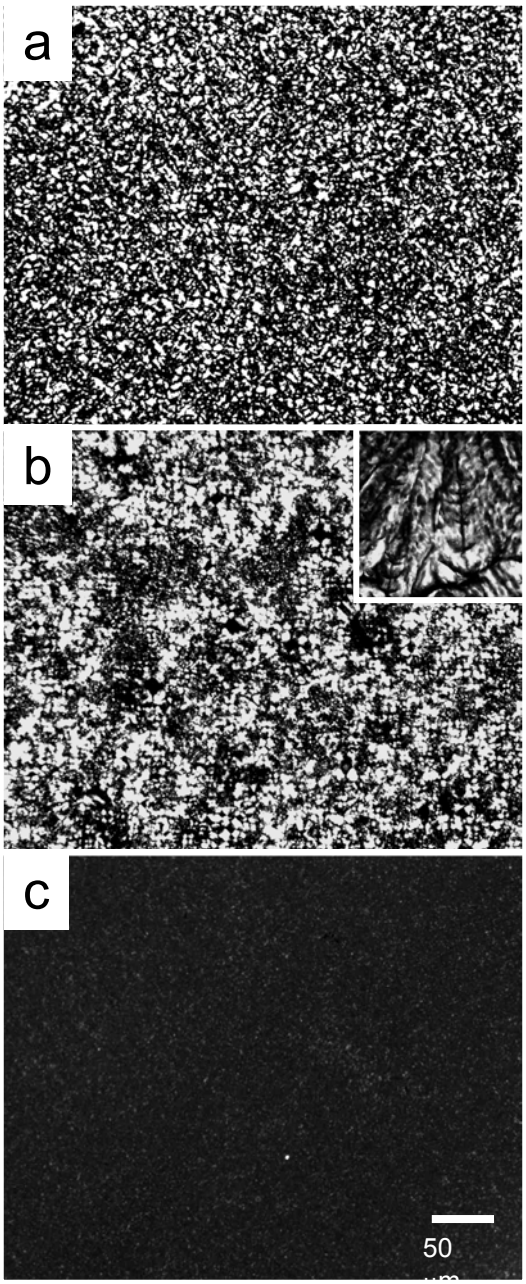

Figure 2.5. Polarized light micrographs of (a) the neat SEOS triblock copolymer, (b) a 55/45 SEOS/PEG_{4600} blend and (c) a 55/45 SEOS/PEG_{400} blend at 23°C. The inset in (b) shows the semicrystalline PEG_{4600} homopolymer under crossed polars at the same magnification.

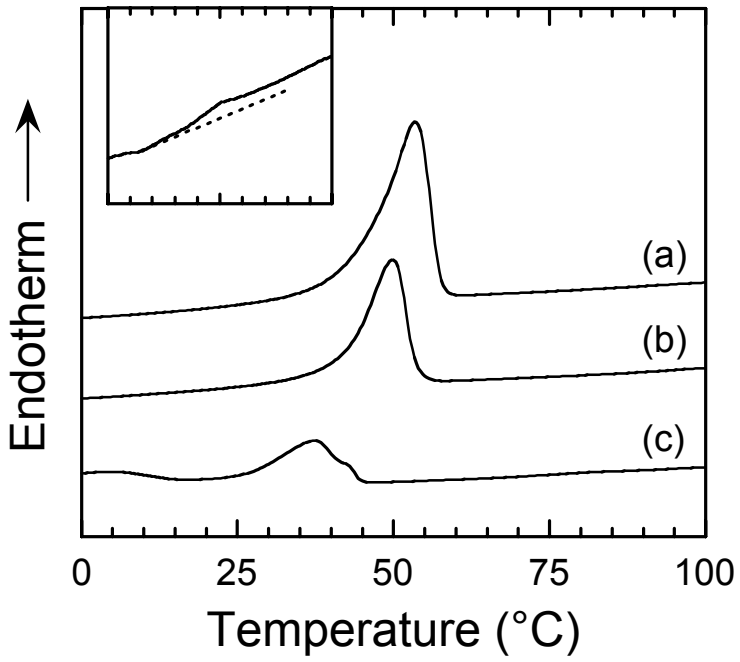

Figure 2.6. DSC thermograms acquired during the second heating cycle from (a) a 55/45 SEOS/PEG_{4600} blend, (b) the neat SEOS triblock copolymer and (c) a 55/45 SEOS/PEG_{400} blend at a heating rate of 20°C/min. The inset shows the upper (S) glass transition of the SEOS copolymer.

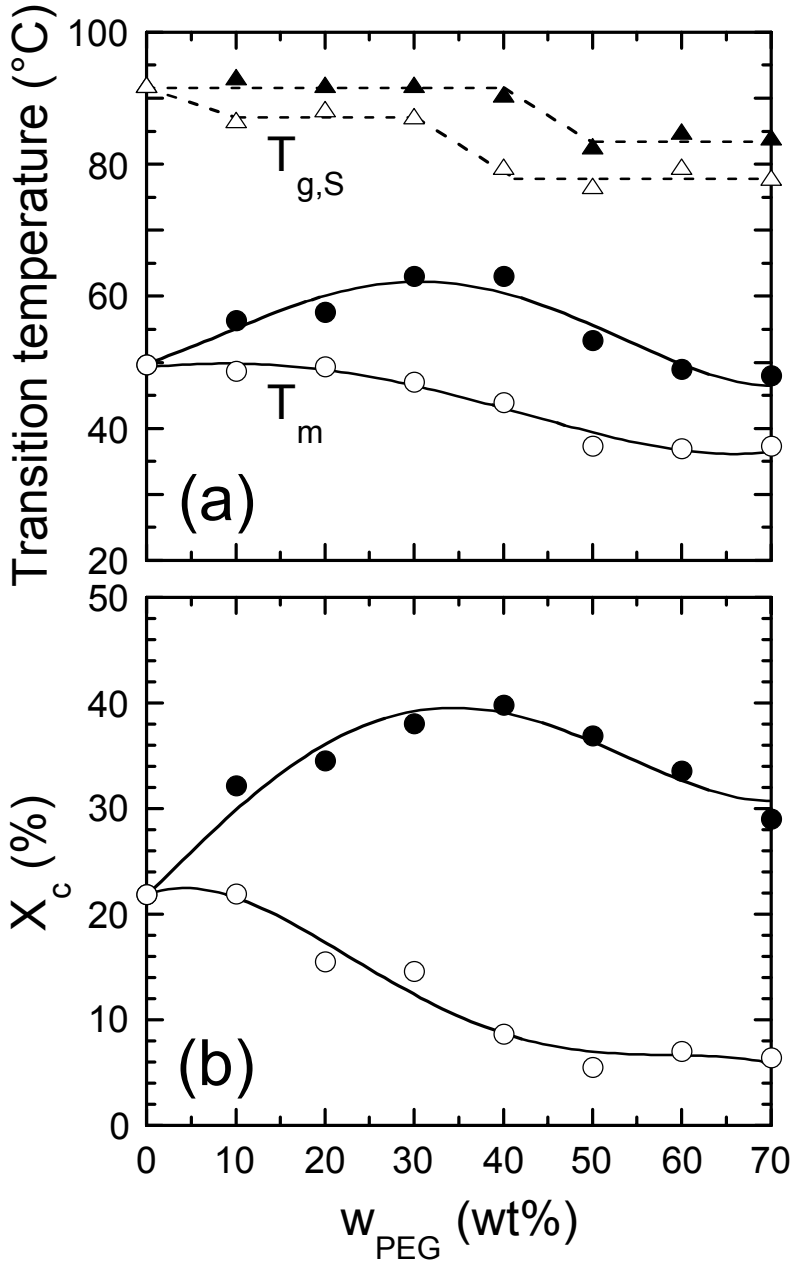

Figure 2.7. Dependence of (a) the EO normal melting temperature (T_m, circles) and S glass transition temperature ($T_{g,}S$, triangles) and (b) crystallinity (X_c) on blend composition in SEOS/PEG blends containing PEG_{400} (open symbols) and PEG_{4600} (filled symbols). The solid and dashed lines serve as guides for the eye.

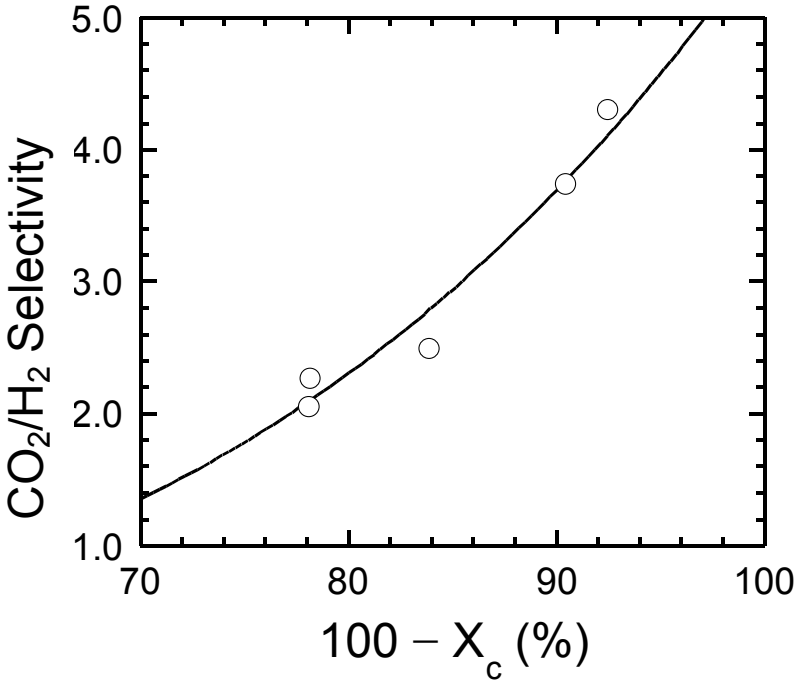

Figure 2.8. CO_2/H_2 selectivity at 35°C as a function of the amorphous percentage ($100 - X_c$) for SEOS/PEG_{400} blends varying in PEG concentration. The solid line is a linear regression of Eq.2.12 to the data.

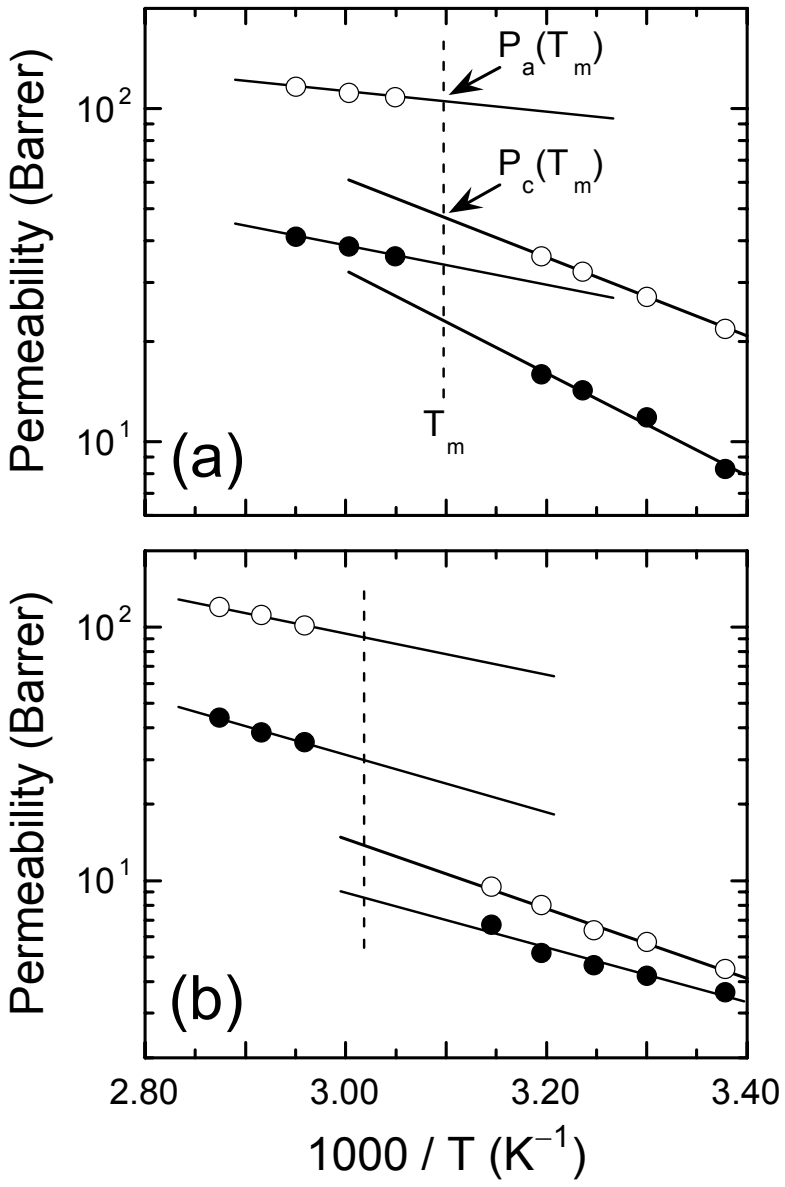

Figure 2.9. Variation of permeability with respect to reciprocal temperature for CO_2 (E) and H_2 (J) in (a) the neat SEOS triblock copolymer and (b) a 55/45 SEOS/PEG_{4600} blend. The solid lines denote regressed fits of Eq.2.6 to the data at low and high temperatures, whereas the dashed vertical lines identify the composition-dependent polyether melting temperature obtained from Fig.2.7a. The positions of $P_a(T_m)$ and $P_c(T_m)$ for CO_2 are labeled for illustrative purposes in (a).

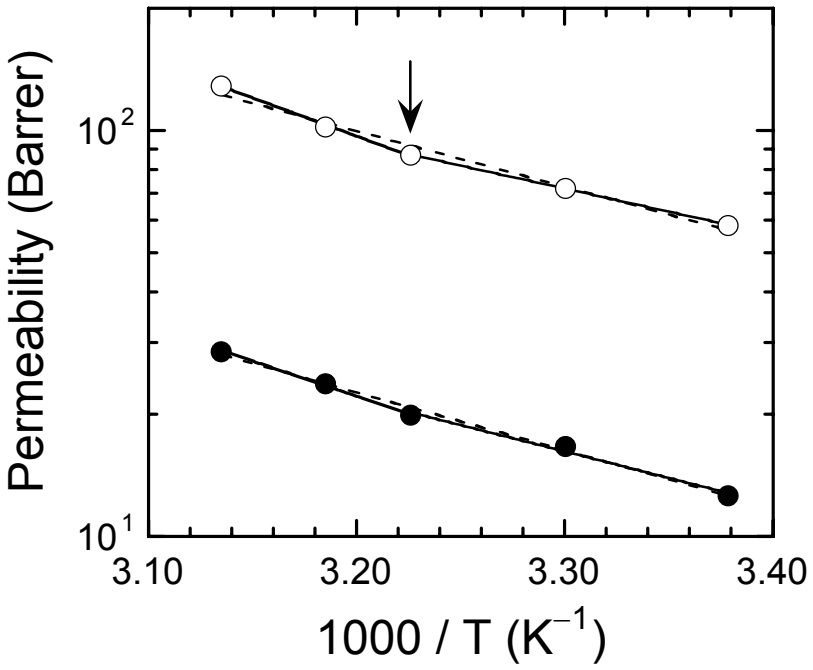

Figure 2.10. Permeability as a function of reciprocal temperature for CO_2 (E) and H_2 (J) in a 55/45 SEOS/PEG_{400} blend. The solid lines are regressed fits of Eq.2.6 to the data at low and high temperatures, the dashed line is a single regression to all the data and the arrow identifies T_m.

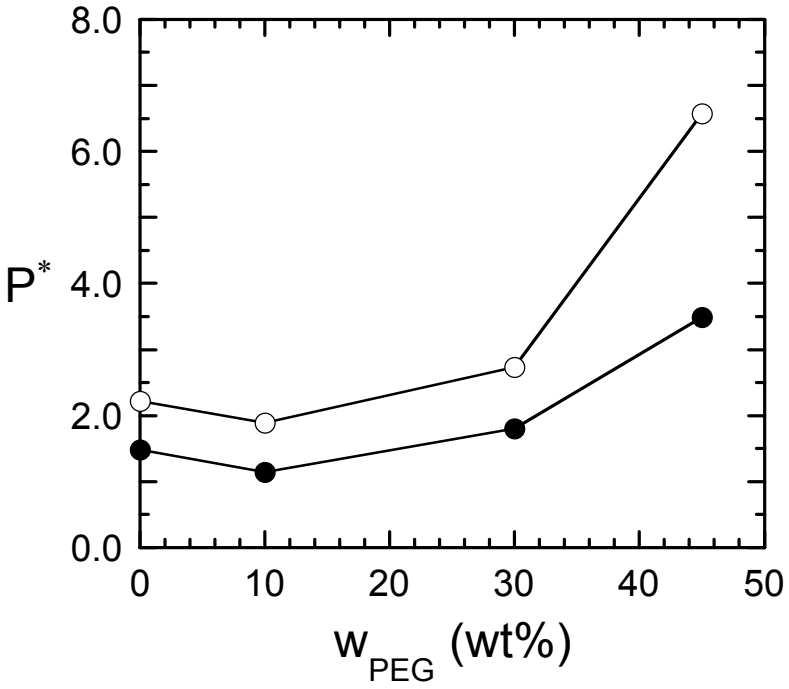

Figure 2.11. Dependence of the permeability switch (P^*) on blend composition for CO_2 (E) and H_2 (J) in SEOS/PEG_{4600} blends. The solid lines connect the data.

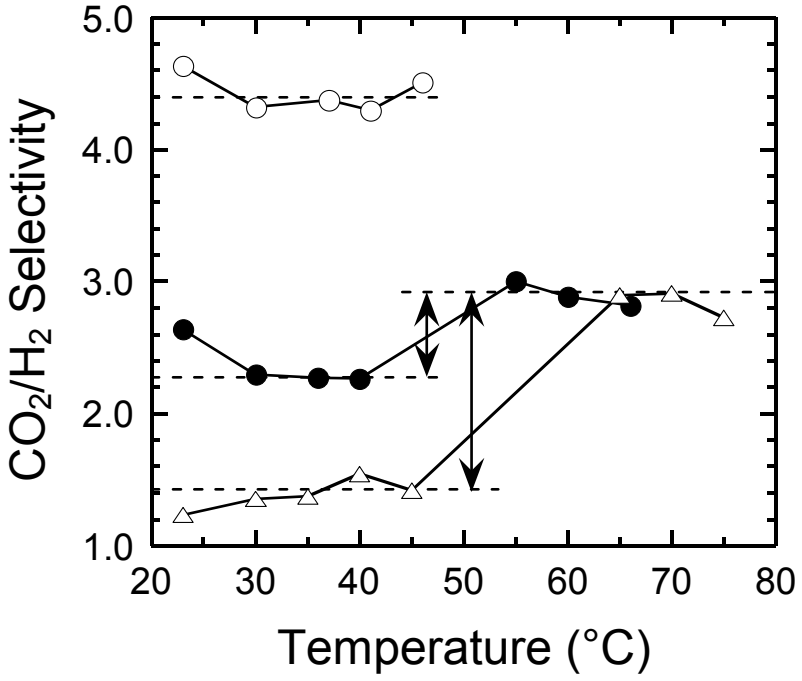

Figure 2.12. CO_2/H_2 selectivity as a function of temperature for the neat SEOS copolymer (J), a 55/45 SEOS/PEG_{400} blend (E) and a 55/45 SEOS/PEG_{4600} blend (C). The solid lines connect the data, and the dashed horizontal lines represent guides to show relevant trends. The arrows identify the change in CO_2/H_2 selectivity upon polyether melting.

Chapter 3

Mesoblends of Polyether Block Copolymers with Poly(ethylene glycol)

3.1. Abstract

Mesoblends are conveniently generated by sorbing a parent homopolymer into a microphase-separated triblock or higher-order multiblock copolymer swollen by a block-selective solvent. These nonequilibrium systems afford a viable route by which to produce, in systematic fashion, novel copolymer/homopolymer blends, as well as explore homopolymer transport and solubility within a molecularly-confined polymer environment. In the present work, we have imbibed poly(ethylene glycol) (PEG) differing in molecular weight into a model poly(styrene-*b*-ethylene oxide-*b*-styrene) (SEOS) triblock copolymer and a commercial poly(amide-*b*-ethylene glycol) (AEG) multiblock copolymer. Solvent quality and solution concentration are found to have a profound effect on PEG solubility in both copolymers, whereas PEG molecular weight over the range 100 to 4600 is generally less influential. Transmission electron microscopy reveals the spatial distribution of amorphous PEG within the SEOS copolymer matrix, and complementary differential scanning calorimetry establishes the role of added PEG on the thermal behavior of the copolymer midblock. Incorporation of PEG into the AEG copolymer serves to improve the CO_2/H_2 selectivity of this material at ambient temperature and low pressure.

This chapter has been published in *Macromolecules*, **2004**, 37, 1394.

3.2. Introduction

The current generation of polymeric materials is being designed to meet the needs of contemporary technologies by employing multicomponent systems in which a homopolymer or copolymer is controllably modified through the addition of (*i*) one or more macromolecules to form a blend/alloy[1-3] or (*ii*) an inorganic species to form a nanocomposite.[4-6] Such systems exhibit the multifunctionality required for either improved processing or ultimate application, and permit tremendous versatility in terms of materials design. In this work, we consider the modification of microphase-separated block copolymers through the incorporation of a parent homopolymer. Block copolymers, macromolecules composed of long, contiguous sequences arranged in a variety of architectures, can microphase-order if the sequences are sufficiently incompatible.[7,8] For linear molecules, the thermodynamic incompatibility is conveniently expressed by χN, where χ denotes the temperature-dependent Flory-Huggins interaction parameter and N is the number of statistical units along the copolymer backbone.[9] Microphase-ordering promotes self-organization of binary block copolymer molecules composed of A and B units into several periodic nanostructures predominantly regulated by composition and described as A(B) spheres positioned on a body-centered cubic lattice in a B(A) matrix, hexagonally-packed A(B) cylinders in a B(A) matrix, bicontinuous channels or alternating lamellae. While only binary (AB) copolymers are explicitly considered here, a greatly expanded list of accessible morphologies is available with ternary (ABC) block copolymers.[8,10] Higher-order multiblock copolymers may, however, organize into nanoscale domains without long-range (periodic) order due to greater block connectivity and the accompanying propensity for kinetic entrapment.[11]

In neat block copolymers, production of a specific nanostructure for a given application requires tailored molecular synthesis, which can be pragmatically undesirable. An alternative approach to nanostructure design in block copolymers involves blending a copolymer capable of microphase-ordering with a parent homopolymer[12-14] or a second copolymer.[15-18] Under the right set of composition and molecular-weight conditions,[19] the two macromolecules remain miscible and form a single new morphology, which may be unobtainable in the neat copolymer alone.[20] Traditional efforts designed to introduce a parent homopolymer into a microphase-ordered block copolymer via "equilibrium" routes (*e.g.*, co-dissolution in and co-casting from a common solvent) have established that, at low concentrations, the homopolymer molecules swell the host microphases of the copolymer. At higher concentrations, an added homopolymer that adequately interpenetrates (*wets*) the brush of the compatible copolymer block can alter interfacial curvature and thereby induce a morphological transition. The nonequilibrium analogs to such blends are block copolymer/homopolymer *mesoblends*, in which a parent homopolymer is sorbed into a microphase-separated block copolymer via a selective carrier solvent (see Fig.3.1). This idea originates from the concept of block copolymer/solvent *mesogels* introduced by Zhulina and Halperin[21] and later verified by King et al.[22] Our recent studies[23,24] of block copolymer/ homopolymer mesoblends have explored lamellar poly(styrene-*b*-isoprene-*b*-styrene) (SIS) copolymers to which polyisoprene (PI) is imbibed from *n*-hexane. Results from those studies indicate that (*i*) PI uptake is sensitive to homopolymer molecular weight and solution concentration, and (*ii*) the resultant mesoblend morphologies differ considerably from those realized by equilibrium routes.

Previous endeavors to elucidate homopolymer sorption and accompanying structure-

property development in block copolymer/homopolymer mesoblends have been complicated by the use of a carrier solvent that has low, but non-negligible, solubility in the microphases formed by the incompatible styrenic blocks. Such limited solubility sufficiently softens the glassy lamellae to permit molecular rearrangement into non-lamellar morphologies due to the high osmotic pressure induced by the hexane-swollen I microphases. In the present work, this complication is alleviated by employing polyether-containing block copolymers to which poly(ethylene glycol) (PEG) is imbibed into the copolymers from highly polar solvents (*e.g.*, water and short-chain alcohols), which do not permit the hard (mechanically-stabilizing) microphases of the copolymers to rearrange to a discernible extent. This is the same general strategy adopted by Wiesner and co-workers[25] in their preparation of nanoscale objects from water-soluble ceramic precursors sorbed into polyether-containing block copolymer templates. Another reason for examining mesoblends of these particular copolymer-homopolymer pairs is the ongoing interest in developing highly CO_2-selective membranes to be used in gas-separation applications.[26] Bondar et al.[27] and Kim et al.[28] have previously demonstrated that randomly-coupled multiblock copolymers composed of polyamide hard blocks and PEG soft blocks exhibit very high CO_2/H_2 selectivity (α), which is defined hereafter as

$$\alpha \equiv P_{CO_2} / P_{H_2} \tag{3.1}$$

If molecular transport is accurately described by a solution-diffusion process,[29] the permeability of each gas through the membrane (P_i, where *i* is either CO_2 or H_2) is given by the following:

$$P_i = D_i \times S_i \tag{3.2}$$

Here, D_i and S_i denote the diffusivity and solubility of penetrant species *i* in the membrane.

We have shown[30] that α of a polyether block copolymer can be improved substantially upon addition of PEG via co-dissolution/casting, and now seek to discern if comparable property enhancement can be likewise achieved with block copolymer/homopolymer mesoblends.

3.3. Experimental

3.3.1. Materials

A model poly(styrene-*b*-ethylene oxide-*b*-styrene) (SEOS) triblock copolymer was obtained in powder form from Polymer Source, Inc. (Dorval, Canada). According to ^{1}H NMR and GPC analyses conducted by the manufacturer, the composition, number-average molecular weight and polydispersity index of the copolymer were 57 wt%, 69000 and 1.03, respectively. A commercial poly(amide-*b*-ethylene glycol) (AEG) multiblock copolymer known as PEBAX® 1074 was supplied by Elf Atochem (Philadelphia, PA) in pellet form. The hard amide block is composed of nylon-12, poly[imino(1-oxododecamethylene)], and accounts for 45 wt% of the copolymer, according to the manufacturer. While information regarding molecular weight and average block lengths in this randomly-coupled multiblock copolymer is unavailable, previous studies have reported[27] that the amide block is semicrystalline and that the polyether blocks are sufficiently short to remain liquid. Several PEG oligomers with molecular weights ranging from 100 to 4600 were purchased from Aldrich (Milwaukee, WI) and used as-received. Each oligomer is hereafter designated as PEG_M, where the subscripted M denotes the molecular weight. With the exception of the highest-molecular-weight grade (PEG_{4600}, which exists as a semicrystalline powder), all the remaining PEG oligomers were received in liquid form. Chloroform, methanol, ethanol and *n*-butanol were likewise purchased from Aldrich and used without further purification.

3. 3. 2. Methods

Bulk films of the SEOS copolymer were produced from 5-10% (w/v) copolymer solutions in chloroform. After ample dissolution time, the solutions were cast in Teflon molds, and the solvent was permitted to evaporate over the course of 2 weeks at ambient temperature. Resultant films measuring 100-300 μm in thickness were annealed for 24 h at 100°C to remove residual solvent and promote nanostructural refinement prior to removal from the mold in liquid nitrogen. The AEG copolymer possesses greater solvent resistance and was consequently dissolved in *n*-butanol at 80°C to form a 4% solution. To avoid premature precipitation of the copolymer during film formation, the solution was cast and the solvent was evaporated over the course of 2 weeks at the dissolution temperature. The AEG films produced in this fashion measured 50-200 μm thick and were subsequently annealed for 24 h at 60°C for the same purposes as above.

In the sorption tests, dried copolymer films were cut into sheets measuring *ca*. 0.5 cm x 0.5 cm and weighed. Each PEG was dissolved at a predetermined concentration in a specific solvent. Copolymer sheets were immersed in each chosen solution within an isolated beaker. After a given sorption time, each film was removed from the solution, and excess solvent on the film surface was blotted with filter paper. Swollen films were initially dried under ambient conditions, followed by vacuum-drying at 60°C) overnight to remove residual solvent. The mass of sorbed PEG was determined directly from gravimetric analysis. Copolymer films were also suspended in pure solvent and measured in the same fashion to ensure that no solvent remained in the film after vacuum-drying and that the results were free of solvent artifacts. Any measurable increase in weight after vacuum-drying was attributed solely to sorbed PEG.

The location of the sorbed PEG within the SEOS copolymer matrix was determined by transmission electron microscopy (TEM). Films of the neat copolymer and several of its PEG-modified mesoblends were sectioned at –100°C in a Leica Ultracut-S cryoultramicrotome to yield ~100 nm specimens, which were subsequently subjected to the vapor of a 4% OsO_4(aq) solution for 90 min at ambient temperature. The stained specimens were imaged with a Zeiss EM902 electron spectroscopic microscope operated at 80 kV and energy-loss (ΔE) settings of 60-110 eV. Negative plates were scanned at 1000 dpi and enlarged for analysis and presentation purposes. The thermal characteristics of the pure and PEG-swollen SEOS block copolymer were measured by differential scanning calorimetry (DSC) with a Perkin-Elmer DSC-7 unit. Data were collected under a nitrogen blanket in a heat-cool-heat cycle to ascertain the effect of thermal treatment on mesoblend stability. Heating and cooling rates were held constant at 20 and -20°C/min, respectively. The normal melting (T_m) and freezing (T_f) temperatures reported herein correspond to peak temperatures, and the degree of crystallinity (X_c) is calculated from

$$X_c = \Delta H_m / (W_{EO}\, \Delta H_m^{o}) \tag{3.3}$$

where ΔH_m is the latent heat of melting approximated by the area under the melting endotherm, ΔH_m^{o} is the latent heat of melting for 100% crystalline poly(ethylene oxide) (186.188 J/g, as reported elsewhere[31]), and W_{EO} is the weight fraction of the crystallizable midblock of the SEOS copolymer. In SEOS/PEG_{4600} mesoblends, W_{EO} is set equal to unity since both contributing polyether constituents (the PEG_{4600} in addition to the copolymer midblock) can crystallize.

Pure-gas permeation properties of the neat AEG copolymer and its PEG mesoblends were measured by the constant-volume/variable-pressure method.[32] The set-up used here consisted

of a downstream vessel of known volume (V), a permeation cell containing a polymer film and an upstream vessel maintained at a designated temperature. Vacuum was pulled on both sides of the film before exposing the upstream side to a desired gas pressure (P_2). As the gas permeated through the film, the pressure on the downstream side was monitored until the pressure increase rate (dP/dt) remained constant. The permeability of the gas was determined from

$$P_i = (Vl / ARTP_2) \times (dP/dt) \quad (3.4)$$

where l is the film thickness, A is the exposed film area, R is the gas constant and T denotes absolute temperature. In all the permeation tests discussed here, the highest downstream pressure was 0.007 atm, in which case P_2 effectively corresponds to the transmembrane pressure.

3. 4. Results and Discussion

3. 4. 1. Mesoblends derived from the SEOS triblock copolymer

Sorption of PEG into the SEOS copolymer is complicated by two considerations. The first obstacle in this endeavor is the inherent crystallinity of the relatively high-molecular-weight EO midblock of the copolymer. The value of T_m associated with the EO midblock is, according to DSC analysis,[30] 50°C, which, due to molecular-level confinement within a microphase-separated (lamellar) morphology, deviates substantially from the normal melting point of pure poly(ethylene oxide) (PEO) of comparable molecular weight (72°C, according to ref. 31). Chen et al.[33] have reported that such confinement effects not only tend to reduce T_m in EO-containing block copolymers, but also become more pronounced as the EO block is more highly constrained in dispersed morphologies (i.e., cylinders and spheres). The

complication afforded by impermeable EO crystals in the present work is readily overcome by sorbing PEG into the copolymer at a temperature that is higher than T_m. In this same vein, an upper sorption temperature associated with the styrenic blocks of the copolymer likewise exists. Since the hard (glassy) blocks must remain relatively impervious to solvent-induced swelling and alteration so that the copolymer remains microphase-ordered during PEG sorption, the sorption temperature cannot exceed the glass transition temperature (T_g) of the styrenic block, which is measured[30] to be 92°C in the neat copolymer. Thus, to preclude the possibility of softening the glassy styrenic microdomains during PEG sorption into amorphous EO-rich microdomains, the sorption temperature is held constant at 60°C unless otherwise specified.

The second obstacle to be considered is the choice of carrier solvent from which PEG sorption into the copolymer will take place. While PEG with a solubility parameter (δ) ranging from 19.2 to 30.6 $MPa^{1/2}$ depending on molecular weight according to group-contribution methods[34] is soluble in a wide variety of common solvents (including water), the solvent must be selected so that it does not interact substantially with the ordered styrenic microdomains (with δ = 18.7 $MPa^{1/2}$ from ref. 35) for the same reasons discussed above. Roberge et al.[23] have shown that even low solvent solubility within the styrenic microdomains is sufficient to permit spectacular morphological changes within the ordered copolymer. Water, assigned[35] δ = 47.9 $MPa^{1/2}$, is therefore the obvious choice for PEG sorption, since it constitutes a nonsolvent for polystyrene. As the uptake kinetic data presented in Fig.3.2a demonstrate, however, use of water results in little sorption of PEG_{400} into the copolymer. In this and subsequent figures, each datum point represents a fresh sample, and W_{PEG} refers to the mass fraction of sorbed PEG. According to Fig.3.2a, W_{PEG} is

only 0.06 after ~100 h of immersion time (t) in a 20% w/v PEG_{400} solution. This problem arises due to the inherent hydrophobicity of the styrenic microdomains and can be overcome by using a polar organic solvent, such as a short-chain alcohol. As the data displayed in Fig.3.2a attest, use of ethanol (δ = 26.0 $MPa^{1/2}$ from ref. 35) instead of water as the carrier solvent promotes a substantial increase in sorbed PEG_{400} (W_{PEG} = 0.58 at t ~ 100 h) under identical temperature and solution concentration conditions. At long immersion times in both solvents, the concentration of sorbed PEG becomes constant and corresponds to the solubility (S) under the conditions identified.

The data presented in Fig.3.2a are replotted in Fig.3.2b in the more familiar form of m_t/m_∞, where m_t denotes the mass uptake of PEG sorbed at time t and m_∞ is the mass uptake at long t (at the solubility limit), as a function of $t^{1/2}$ to confirm that the mechanism of molecular mobility is Fickian diffusion. Moreover, the PEG_{400} uptake data collected from both solvents are observed to superimpose, indicating that, although the two solvents promote drastically different PEG_{400} solubilities (see Fig.3.2a), the mobility of PEG_{400} molecules into the solvent-swollen copolymer matrices is essentially independent of carrier solvent. Values of an effective diffusion coefficient (D_{eff}) can be extracted from the data provided in Fig.3.2b using a variety of protocols (most of which rely on the initial slope of the sorption curve).[36] For consistency with our previous study,[24] we elect to use the Balik[37] model for fitting the entire sorption curve with a single expression:

$$\frac{m_t}{m_\infty} = \phi(x)\, f(x) + [1 - \phi(x)]\, g(x) \tag{3.5}$$

where $x = D_{eff}t/L^2$ and L is the thickness of the film. The short- and long-time contributions to Eq.3.5 are given by

$$f(x) = 4(x/\pi)^{1/2} \tag{3.6a}$$

and

$$g(x) = 1 - (8/\pi^2)e^{-\pi^2/x}, \tag{3.6b}$$

respectively, and the weighting factor $\phi(x)$ is derived on the basis of the Fermi function, namely,

$$\phi(x) = \left(1 + e^{(x-a)/b}\right)^{-1} \tag{3.7}$$

Here, the parameters a and b are set[37] equal to 0.05326 and 0.001, respectively. The value of D_{eff} determined by fitting Eq.3.5 to all the data in Fig.3.2b is $1.1(\pm 0.1)\times 10^{-9}$ cm^2/s irrespective of solvent. For comparison, the value of D_{eff} deduced[24] for PI sorbed into a lamellar SIS copolymer swollen by *n*-hexane is just under an order of magnitude larger, $3.3(\pm 0.7)\times 10^{-8}$ cm^2/s (independent of midblock molecular weight), which indicates that the PI has greater mobility in the swollen SIS copolymer than PEG_{400} in the SEOS copolymer despite its larger size (M_{PI} = 7500) and a pendant methyl group in its repeat unit. Possible explanations for this disparity include a more tortuous (less interconnected) lamellar morphology or the presence of physical obstacles (*e.g.*, incompletely dissolved EO crystals) in the SEOS copolymer matrix. Alternatively, since *n*-hexane has been reported[23] to modify the inherent morphology of the SIS copolymer by introducing perforations into the styrenic lamellae, it is conceivable that additional diffusive pathways may have become accessible through which the PI molecules could diffuse.

The data displayed in Fig.3.2 have been collected from solutions in which the concentration of PEG_{400} was maintained at 20% w/v. Figure 3.3 shows the effect of solution concentration (C) in both water and ethanol on PEG_{400} solubility (S) in the SEOS copolymer

after 100 h at 60°C. Increasing C under isothermal conditions renders a larger chemical potential difference, which ultimately leads to enhanced solubility, as Fig.3.3 confirms. In water, S increases almost linearly with increasing C up to 70% w/v PEG_{400}. A qualitatively similar trend has been reported by Stevens et al.[24] for PI in swollen SIS copolymers differing in midblock molecular weight. According to Fig.3.3, the slope $(\partial S/\partial C)_T$ ascertained for PEG_{400} sorbed from water into the SEOS copolymer is about 0.31, which is much lower in magnitude than comparable slopes measured for PI sorbed from *n*-hexane into SIS copolymers (3.9 to 9.0, depending on midblock molecular weight). In marked contrast, the solubility of PEG_{400} sorbed from ethanol is observed to increase abruptly at low C and reach a limiting value in the range 0.7-0.8 at high C. Thus, use of ethanol as the carrier solvent greatly increases the propensity for PEG_{400} molecules to enter the swollen EO lamellae of the SEOS copolymer relative to water at a fixed solution concentration. The explicit effect of solvent quality on S is discussed further in a later section. Another design issue to be considered is the molecular weight of the sorbed PEG (M_{PEG}). In Fig.3.4, S is presented as a function of M_{PEG} after immersion of the SEOS copolymer for 24 h in a 25% w/v PEG/methanol solution (δ = 29.6 $MPa^{1/2}$ for methanol[35]) maintained at ambient temperature. Note that the temperature is below the melting point of the EO block, which strongly suggests that residual EO crystals reside in the copolymer matrix. This variation in temperature (and, to a much lesser extent, solvent) provides a clear indication of how the presence of EO crystals negatively impacts the extent to which PEG can be sorbed. At 60°C, for instance, the solubility of PEG_{400} in the SEOS copolymer swollen under the same solvent/concentration/time conditions in Fig.3.4 is about 0.37, which is considerably larger than the ~0.08 measured at 23°C. In addition, the data shown in this figure provide evidence

that an increase in M_{PEG} promotes an almost linear decrease in S, which is contrary to the $S \sim M_{PI}^{-1/2}$ dependence reported[23] for the sorption of PI varying in molecular weight into a SIS copolymer swollen by *n*-hexane. While such a reduction in S is to be qualitatively expected *a priori* on the basis of the increased incompatibility and entropic penalty (brush dewetting) encountered with increasing M_{PEG}, the difference in the dependence of S on M_{PEG} is not so obvious. We return later to discuss these relationships.

Factors governing the sorption of PEG into a solvent-swollen SEOS copolymer have thus far been identified and discussed. In this section, we explore the effect of sorbed PEG on the morphology and thermal properties of SEOS/PEG mesoblends. The TEM images displayed in Fig.3.5 have been acquired from the neat SEOS copolymer (Fig.3.5a), as well as the copolymer immersed at 60°C for 100 h in 25% w/v solutions of PEG_{4600} in ethanol (Fig.3.5b), PEG_{400} in water (Fig.3.5c) and PEG_{400} in ethanol (Fig.3.5d). In all cases, only the amorphous PEG present is stained by the OsO_4(aq) treatment described in the Experimental section and consequently appears electron-opaque (dark). In Fig.3.5a, the two features visible in the image correspond to contaminants used for focusing purposes. It is interesting to note that none of the EO units within the copolymer are stained and, by inference, amorphous. According to thermal calorimetry, the EO microdomains of this copolymer are only about 22% crystalline, which appears sufficiently high to preclude staining of the amorphous segments of the EO blocks to any discernible extent. The image in Fig.3.5b, on the other hand, clearly confirms the presence of amorphous (stained) PEG throughout the mesoblend. Faint features and the discrete black dots, attributed to amorphous PEG residing at the surface of the microtomed section and measuring *ca*. 3-9 nm in diameter, show no evidence of spatial regularity, which suggests that sorption of PEG_{4600} into the copolymer may not be

uniform throughout the lamellar matrix. The effect of added PEG_{4600} on mesoblend crystallinity will be addressed further in a subsequent section.

Sorption of PEG_{400} into the SEOS copolymer from water and ethanol solutions (Figs. 3.5c and 3.5d, respectively) results in very different mesoblend morphologies. The image presented in Fig.3.5c shows the presence of numerous elongated "dispersions" measuring as long as ~40 nm and as wide as ~4 nm, as well as several large features measuring more than 80 nm long and about 8 nm wide. Close examination of this and related images reveals that many of these "dispersions" are often oriented along a common direction. This spatial distribution strongly suggests that the amorphous PEG_{400} molecules sorb into the EO lamellae and, due to the low level of sorbed PEG_{400} (S = 0.07 from Fig.3.3), form discrete, amorphous aggregates within the lamellae upon crystallization of the EO blocks. In a few instances, these isolated aggregates appear to be sufficiently numerous to converge into continuous amorphous channels in the otherwise semicrystalline EO lamellae. By changing the solvent to ethanol and thereby increasing the solubility of PEG_{400} within the swollen SEOS copolymer (S = 0.59), this tendency is markedly improved, resulting in numerous lamellae that exhibit evidence of stained PEG. The thickness and period of these long, amorphous channels, which consist of pure PEG_{400} or, more likely, a mixture of PEG_{400} and noncrystalline EO segments, measure 2.8(±0.6) and 13.7(±0.6) nm, respectively. In light of these dimensions, it is comforting to note that the unperturbed gyration diameter of a PEO coil with M = 400 is estimated[34] to be 1.4(±0.2) nm. Moreover, the period extracted from Fig.3.5d is slightly larger than that discerned from the neat copolymer,[38] which confirms that the EO lamellae are swollen due to the presence of sorbed PEG_{400}. The intensely dark features are again attributed to amorphous PEG lying on (or, in the case of PEG_{400}, possibly

migrating to) the surface of the microtomed section.

The thermal characteristics of the three mesoblends featured in Fig.3.5 are provided in Figs. 3.6 and 3.7. In Fig.3.6, first- and second-heat cycles of the mesoblends prepared with PEG_{4600}/ethanol (Fig.3.6a), PEG_{400}/water (Fig.3.6b) and PEG_{400}/ethanol (Fig.3.6c) are compared with the first-heat cycle of the neat SEOS copolymer. Initial sorption of PEG_{4600} into the copolymer induces a shift in T_m from 50 to 56°C. During the second heating cycle, the mesoblend is closer to an "equilibrium" blend in which nonequilibrium characteristics have been thermally erased to a relatively large extent. In this case, T_m of the SEOS/PEG_{4600} blend is only slightly lower than T_m of the initial mesoblend (54°C), and the corresponding crystallinity of the blend calculated from Eq.3.3 is about 35% higher than that of the neat copolymer. Corresponding values of ΔH_m and X_c measured from each of the systems and heating cycles portrayed in Fig.3.6 are listed in Table 3.1. The thermograms provided in Fig.3.6b show that the addition of PEG_{400} from water have an insignificant effect on T_m and X_c during the first- and second-heat cycles, which is consistent with the very low level of PEG_{400} sorbed from water. Several intriguing features are evident, however, in the SEOS/PEG_{400} mesoblends prepared from ethanol. The first-heat cycle indicates that T_m is lowered slightly upon incorporation of PEG_{400}. While this feature is not very interesting, a second feature absent in thermograms of the other two mesoblends is a large exothermic process that begins at the T_g of the styrenic blocks comprising the copolymer. This process is attributed to the immense stress placed on the glassy lamellae by the presence of imbibed PEG_{400} molecules. At a comparable PEG_{400} concentration in equilibrium SEOS/PEG_{400} blends equal to the solubility of PEG_{400} in the present mesoblend, the morphology transforms from alternating lamellar to a continuous matrix, according to thermal calorimetry and

permeation measurements.[30]

Thus, we propose that the exothermic process visible in the first-heat thermogram of Fig.3.6c reflects the release of stress built up in the mesoblend due to constrained swelling via morphological alteration once the styrenic microdomains soften and become pliable at and above their T_g. This hypothesis is consistent with the results from the second-heat cycle of Fig.3.6c in which residual PEG/EO segregation can be gleaned. The first endotherm in the vicinity of –4°C can most likely be assigned to PEG_{400} (which possesses a softening point of –6°C, according to the manufacturer), whereas the second, broad endotherm centered at about 12°C is attributed to co-crystallization of the PEG_{400} molecules and the EO blocks of the copolymer. The third, sharp endotherm corresponds to crystallization of the EO blocks and is shifted to lower temperature (41°C) due to PEG_{400} dilution. Similar results are apparent in the cooling curves displayed in Fig.3.7 for all three mesoblends. In the case of the SEOS/PEG_{4600} system, the principal freezing exotherm lies at 31°C, whereas a significantly smaller freezing process occurs at about –19°C. Upon sorption of PEG_{400} from water, the resultant mesoblend exhibits a reduced primary freezing point (15°C) and a slightly more pronounced peak in the vicinity of –19°C. Substitution of ethanol for water as the carrier solvent for PEG_{400} yields a broad freezing exotherm at ~11°C, a shoulder at –7°C and a principal peak at –16°C. Recall that, while the two mesoblends prepared from PEG_{4600}/ethanol and PEG_{400}/water display only a single melting peak upon re-heating, the one imbibed with PEG_{400} from ethanol similarly exhibits several melting events, indicative of PEG_{400} segregation within the EO-rich microdomains. This result is consistent with the amorphous PEG channels visible in Fig.3.5d.

3.4.2. Mesoblends derived from the AEG multiblock copolymer

Unlike the SEOS copolymer the AEG copolymer consists of semicrystalline hard (nylon-12) blocks and liquid soft (PEG) blocks arranged in a randomly-coupled multiblock architecture. While the polyamide block is subject to imbibing polar solvents due to its hydrogen-bonding nature, the moisture content in nylon-12 immersed in liquid water at 23°C is reported[39] to be only 1.5%. Thus, it is sensible to expect that the polyamide blocks and their corresponding microdomain structure will be virtually unaffected by the carrier solvent or sorbed PEG during AEG/PEG mesoblend preparation. Since the PEG blocks are intrinsically molten at ambient temperature (T_m is measured[27] to be 11°C), it is unnecessary to heat the specimens to promote sorption of PEG from solution. Mass uptake curves obtained at 23°C for PEG_{400} sorbed into the AEG copolymer from 20 and 60% w/v solutions in ethanol are displayed for comparison in Fig.3.8. As with the SEOS/PEG_{400} mesoblends (see Fig.3.3), an increase in solution concentration (C) is accompanied by an increase in PEG_{400} solubility (S) according to Fig.3.8a. Normalization of the mass uptake curves in the form required for analysis by Eq.3.5 yields the superimposed curves provided in Fig.3.8b and an effective diffusion coefficient of $8.6(\pm 0.5)\times 10^{-7}$ cm^2/s irrespective of solution concentration. Note that this value is significantly higher (by almost two orders of magnitude) than that discerned for PEG_{400} in the swollen SEOS copolymer, but is closer in magnitude to that measured[40] for PEG_{290} in water at 20°C ($D_{eff} = 3.7\times 10^{-6}$ cm^2/s) and determined[24] for PI in swollen SIS copolymers. This latter similarity may reflect homopolymer diffusion through a highly defective lamellar morphology, which is, in fact, observed[23] in the SIS/PI mesoblends and anticipated[11] for the AEG copolymer due to its molecular architecture.

The influence of C on S for PEG_{400} sorbed from water and ethanol solutions into the AEG copolymer for 100 h at 60°C is presented in Fig.3.9 and closely resembles the analogous S(C) trend exhibited by the SEOS copolymer in Fig.3.3. In both cases, the solubility of PEG_{400} imbibed from ethanol appears to reach a limiting value, whereas S increases monotonically when the carrier solvent is water. An important difference between the data shown in Figs. 3.3 and 3.9 is that the solubility of PEG_{400} in the AEG copolymer is much less sensitive to solvent quality than that of PEG_{400} in the SEOS copolymer. Another intriguing feature of the data in these two figures is that the solubilities measured from both SEOS/PEG_{400} and AEG/PEG_{400} mesoblends prepared from PEG_{400}/water solutions are almost identical, which confirms our earlier conclusion that water is not a suitable carrier solvent for PEG sorption into an organic nanostructured matrix. The effect of M_{PEG} on the solubility of PEG sorbed from methanol (25% w/v solutions) at 23°C in the swollen AEG copolymer is evident in Fig.3.10. As with the SEOS/PEG mesoblends (see Fig.3.4), an increase in M_{PEG} promotes a systematic reduction in S. Comparison of the two figures immediately reveals a striking difference in the dependence of S on M_{PEG}: S decreases nearly linearly with increasing M_{PEG} in Fig.3.4, but non-linearly in Fig.3.10. Regressed scaling relationships of the form $S \sim M_{PEG}^{-\beta}$ are included for two values of β in Fig.3.10. The first (β = 1/2) corresponds to the scaling exponent deduced[24] from SIS/PI mesoblends, but does not adequately fit the data as well as the second (β = 1). Thus, the dependence of S on M_{PEG} in AEG/PEG mesoblends is closer (but not identical) to that previously reported for SIS/PI mesoblends. This observation further supports our earlier contention based on effective diffusion coefficients that the defect-riddled SIS and AEG microdomains may provide similar nanostructured environments into which the relatively low-molar-mass

homopolymers (PI or PEG) sorb from solution.

Since the nanostructure of the AEG copolymer is not expected[11] to possess the degree of long-range (periodic) order exhibited by the model SEOS copolymer and since the incorporation of PEG into the AEG copolymer is not anticipated to have a discernible effect on the thermal characteristics of the semicrystalline microdomains, we do not provide any morphological or thermal analyses of the AEG/PEG mesoblends produced here. Instead, we explore a property that has become closely associated[27,28] with the PEBAX® copolymers, namely, CO_2 separation. Pure-gas permeabilities of CO_2 and H_2 have been measured from two AEG/PEG_{400} mesoblends after different exposure times to PEG_{400} (60% w/v in ethanol) at 23°C. The CO_2/H_2 selectivity (α) calculated from Eq.3.1 is displayed as a function of sorbed PEG (W_{PEG}) in Fig.3.11 and provides evidence that an increase in the PEG content of the AEG copolymer markedly improves the gas-separation efficacy of the mesoblend. To put these results in perspective, the maximum value of α obtained from the AEG/PEG mesoblend with 17 wt% sorbed PEG_{400} at ambient temperature and a transmembrane pressure of 6.8 atm is 9.4. Bondar et al.[27] report a CO_2/H_2 selectivity of 9.8 for the neat copolymer at 35°C and a pressure of 10 atm. Even after taking into account the effect of gas pressure, the reason for the considerable difference in the measured value of α for the neat copolymer is not known, but incorporation of PEG certainly improves α in the present study. It should be noted that attempts to introduce PEG into the AEG copolymer by conventional co-dissolution/co-casting methods typically yields heterogeneous membranes due to the propensity of the AEG molecules to self-organize into highly interconnected nanoscale aggregates.[41]

3.4.3. Effects of solvent quality and temperature on both mesoblend series

The previous sections have examined the sorption kinetics and resultant property changes of PEG imbibed into two chemically-dissimilar linear multiblock copolymers. Throughout these analyses, comparisons between the two mesoblend series have been made whenever possible. In this section, we present a direct comparison between the two series with regard to two environmental conditions: solvent quality and temperature. In Fig.3.12a, the solubility of PEG_{400} in the SEOS and AEG copolymers at 23°C is provided as a function of solubility parameter (δ) for three pure solvents (water, ethanol and methanol) and one miscible solvent mixture (50/50 v/v methanol/water) at a PEG_{400} concentration of 25% w/v. The dependence of S on increasing δ (solvent polarity) is slight in the case of the AEG copolymer, but much more pronounced (especially at relatively low δ) for the SEOS copolymer. In highly polar solvents containing water, the solubility of PEG_{400} in each copolymer is surprisingly comparable. Recall, however, that the sorption temperature is below T_m in the SEOS copolymer. Figure 3.12b shows the dependence of PEG_{400} solubility on temperature in both copolymers immersed in methanol under similar sorption conditions. As the temperature is increased, S increases systematically in both mesoblend series. This can be generally attributed to accompanying increases in (*i*) the molecular mobility of PEG_{400} and (*ii*) the configurational entropy within the polyether microdomains of the copolymers. Once the EO crystals in the SEOS copolymer are melted at 60°C, the solubility of PEG_{400} is observed to increase sharply, as anticipated from a comparison of Figs. 3.3 and 3.4.

3.5. Conclusions

The uptake kinetics, morphological characteristics and property changes associated with

PEG sorption into two polyether-containing block copolymers to form nonequilibrium mesoblends have been investigated. The effective diffusion coefficient of PEG of a single molecular weight discerned from uptake kinetics is found to be independent of solvent quality and solution concentration, whereas the equilibrium solubility is sensitive to both considerations, as well as PEG molecular weight. The mobility of PEG into the host microdomains of the copolymer matrix from solution is faster in the AEG multiblock copolymer than in the lamellar SEOS triblock copolymer due presumably to the lower degree of structural order in the former (more diffusive pathways) and the possibility of residual crystals (more diffusive obstacles) in the latter. The solubility of PEG sorbed from a polar organic solvent, on the other hand, is generally higher in the SEOS copolymer, which is less molecularly constrained than the multiblock copolymer and is capable of greater swelling. If the carrier is or contains water, the solubility of PEG in both copolymers is unexpectedly comparable. Incorporation of amorphous PEG into the SEOS copolymer can be spatially monitored by TEM, whereas the effect of imbibed PEG on the thermal characteristics of the resultant mesoblends is amenable to DSC analysis, which reveals the existence of a strong exothermic process suggestive of stress release at the polystyrene T_g in SEOS/PEG mesoblends containing a large fraction of sorbed PEG. Addition of PEG to the AEG copolymer likewise has a pronounced effect on gas transport properties. This work is part of a series that demonstrates the utility of mesoblends in (*i*) probing the thermodynamic and transport properties of homopolymer molecules in a swollen, molecularly-confined environment and (*ii*) producing novel nonequilibrium materials with new properties in systematic fashion.

3.6. Acknowledgements

This work was supported by the U. S. Department of Energy under Contract No. DE-FG02-99ER14991.

3.7. References

1. Paul, D. R.; Bucknall, C. B. In *Polymer Blends*; Paul, D. R., Bucknall, C. B., Eds.; Wiley: New York, 2000; Vol. 1, pp. 1-14.
2. Araki, T.; Tran-Cong, Q.; Shibayama, M. (Eds.) *Structure and Properties of Multiphase Polymeric Materials*; Marcel-Dekker: New York, 1998.
3. Utracki, L. A. *Polymer Alloys and Blends: Thermodynamic and Rheology*; Oxford University Press: New York, 1990.
4. Krishnamoorthi, R.; Vaia, R. A. (Eds.) *Polymer Nanocomposites: Synthesis, Characterization and Modeling*; American Chemical Society: Washington, D. C., 2002; Vol. 804.
5. Bronstein, L. M. *Top. Curr. Chem*. **2003**, 226, 55.
6. Walls, H. J.; Riley, M. W.; Gupta, R. R.; Spontak, R. J.; Fedkiw, P. S.; Khan, S. A. *Adv. Funct. Mater.* **2003**, *13*, 710.
7. Hamley, I. W. *The Physics of Block Copolymers*; Oxford University Press: Oxford, 1998.
8. Bates, F. S.; Fredrickson, G. H. *Phys. Today* **1999**, *52*, 32.
9. Leibler, L. *Macromolecules* **1980**, *13*, 1602.
10. Stadler, R.; Auschra, C.; Beckmann, J.; Krappe, U.; Voigt-Martin, I.; Leibler, L. *Macromolecules* **1995**, *28*, 3080.
11. Spontak, R. J.; Smith, S. D. *J. Polym. Sci. B: Polym. Phys.* **2001**, *39*, 947.
12. Winey, K. I.; Thomas, E. L.; Fetters, L. J. *J. Chem. Phys.* **1991**, *95*, 9367. Winey, K. I.; Thomas, E. L.; Fetters, L. J. *Macromolecules* **1991**, *24*, 6182; **1992**, *25*, 2645. Urbas,

A.; Sharp, R.; Fink, Y.; Thomas, E. L.; Xenidou, M.; Fetters, L. J. *Adv. Mater.* **2000**, *12*, 812.

13. Tanaka, H.; Hashimoto, T. *Macromolecules* **1991**, *24*, 5713. Kimishima, K.; Hashimoto, T.; Han, C. D. *Macromolecules* **1995**, *28*, 3842. Bodycomb, J.; Yamaguchi, D.; Hashimoto, T. *Macromolecules* **2000**, *33*, 5187.

14. Spontak, R. J.; Smith, S. D.; Ashraf, A. *Macromolecules* **1993**, *26*, 956.

15. Schulz, M. F.; Bates, F. S.; Almdal, K.; Mortensen, K. *Phys. Rev. Lett.* **1994**, *73*, 86. Zhao, J.; Majumdar, B.; Schulz, M. F.; Bates, F. S.; Almdal, K.; Mortensen, K.; Hajduk, D. A.; Gruner, S. M. *Macromolecules* **1996**, *29*, 1204.

16. Kane, L.; Satkowski, M. M.; Smith, S. D.; Spontak, R. J. *Macromolecules* **1996**, *29*, 8862. Spontak, R. J.; Fung, J. C.; Braunfeld, M. B.; Sedat, J. W.; Agard, D. A.; Kane, L.; Smith, S. D.; Satkowski, M. M.; Ashraf, A.; Hajduk, D. A.; Gruner, S. M. *Macromolecules* **1996**, *29*, 4494. Kane, L.; Norman, D. A.; White, S. A.; Matsen, M. W.; Satkowski, M. M.; Smith, S. D.; Spontak, R. J. *Macromol. Rapid Commun.* **2001**, *22*, 281.

17. Abetz, V.; Goldacker, T. *Macromol. Rapid Commun.* **2000**, *21*, 16.

18. Yamaguchi, D.; Shiratake, S.; Hashimoto, T. *Macromolecules* **2000**, *33*, 8258. Yamaguchi, D.; Hashimoto, T. *Macromolecules* **2001**, *34*, 6495. Yamaguchi, D.; Hasegawa, H.; Hashimoto, T. *Macromolecules* **2001**, *34*, 6506. Yamaguchi, D.; Takenaka, M.; Hasegawa, H.; Hashimoto, T. *Macromolecules* **2001**, *34*, 1707. Court, F.; Hashimoto, T. *Macromolecules* **2001**, *34*, 2536. Court, F.; Hashimoto, T. *Macromolecules* **2002**, *35*, 2566.

19. Spontak, R. J.; Patel, N. P. In *Developments in Block Copolymer Science and Technology*; Hamley, I. W., Ed.; Wiley: New York (in press).

20. Abetz, V. In *Encyclopedia of Polymer Science and Technology, 3rd ed.*; Kroschwitz, J. I., Ed.; Wiley: Hoboken, NJ, 2003, Vol. 1, pp. 482-523.

21. Zhulina, E. B.; Halperin, A. *Macromolecules* **1992**, *25*, 5730.

22. King, M. R.; White, S. A.; Smith, S. D.; Spontak, R. J. *Langmuir* **1999**, *15*, 7886.

23. Roberge, R. L.; Patel, N. P.; White, S. A.; Thongruang, W.; Smith, S. D.; Spontak, R. J. *Macromolecules* **2001**, *35*, 2268.

24. Stevens, J. E.; Thongruang, W.; Patel, N. P.; Smith, S. D.; Spontak, R. J. *Macromolecules* **2003**, *36*, 3206.

25. Simon, P. F. W.; Ulrich, R.; Spiess, H. W.; Wiesner, U. *Chem. Mater.* **2001**, *13*, 3464.

26. Patel, N. P.; Miller, A. C.; Spontak, R. J. *Adv. Mater.* **2003**, *15*, 729.

27. Bondar, V. I.; Freeman, B. D.; Pinnau, I. *J. Polym. Sci. B: Polym. Phys.* **1999**, *37*, 2463; **2000**, *38*, 2051.

28. Kim, J.-H.; Seong, Y. H.; Lee, Y. M. *J. Membr. Sci.* **2001**, *190*, 179.

29. Graham, T. *Philos. Mag*. **1866**, *32*, 401.

30. Patel, N. P.; Spontak, R. J. *Macromolecules* (submitted).

31. Geng, H. Z.; Rosen, R.; Zheng, B.; Shimoda, H.; Fleming, L.; Liu, J.; Zhou, O. *Adv. Mater.* **2002**, *14*, 1387.

32. Felder, R. M.; Huvard, G. S. *Permeation, Diffusion and Sorption of Gases and Vapors* (Fava, R., Ed.); Academic Press: New York, 1978; Vol. 16C, p. 315.

33. Chen, H.-L.; Hsiao, S.-C.; Lin, T.-L.; Yamauchi, K.; Hasegawa, H.; Hashimoto, T. *Macromolecules* **2001**, *34*, 671.

34. van Krevelen, D. W. *Properties of Polymers*; Elsevier Science B. V.: Amsterdam, 1997; pp. 196-197, 572.

35. Du, Y.; Xue, Y.; Frisch, H. L. In *Physical Properties of Polymers Handbook*; Mark, J. E., Ed.; AIP Press: New York, 1996; Chapter 16.

36. Jonquières, A.; Clément, R.; Lochon, P. *Prog. Polym. Sci.* **2002**, *27*, 1803 and the references cited therein.

37. Balik, C. M. *Macromolecules* **1996**, *29*, 3025.

38. Patel, N. P. *Ph. D. Dissertation*, North Carolina State University, Raleigh, NC (in progress).

39. Rohde-Liebenau, H. U. W. In *Polymer Data Handbook*; Mark, J. E., Ed.; Oxford University Press: New York, 1999; p. 225.

40. Yuan, Q. W. In *Polymer Data Handbook*; Mark, J. E., Ed.; Oxford University Press: New York, 1999; p. 549.

41. Borisov, O. V.; Halperin, A. *Macromolecules*, **1996**, *29*, 2612; *Curr. Opin. Colloid Interface Sci.* **1998**, *3*, 415.

Table 3.1. Thermal Properties of the SEOS copolymer and its Mesoblends with PEG.[a]

System	W_{PEG}	Heating cycle	ΔH_m (J/g)	X_c
SEOS	0.00	1	17.2	0.21
		2	17.7	0.22
SEOS/PEG_{4600}/ethanol	0.18	1	35.5	0.36
		2	38.2	0.39
SEOS/PEG_{400}/water	0.07	1	16.9	0.19
		2	17.9	0.21
SEOS/PEG_{400}/ethanol	0.59	1	13.6	0.10
		2	9.6	0.07

[a] Determined from the DSC thermograms displayed in Fig.3.6.

List of symbols:

E = open circle

J = filled circle

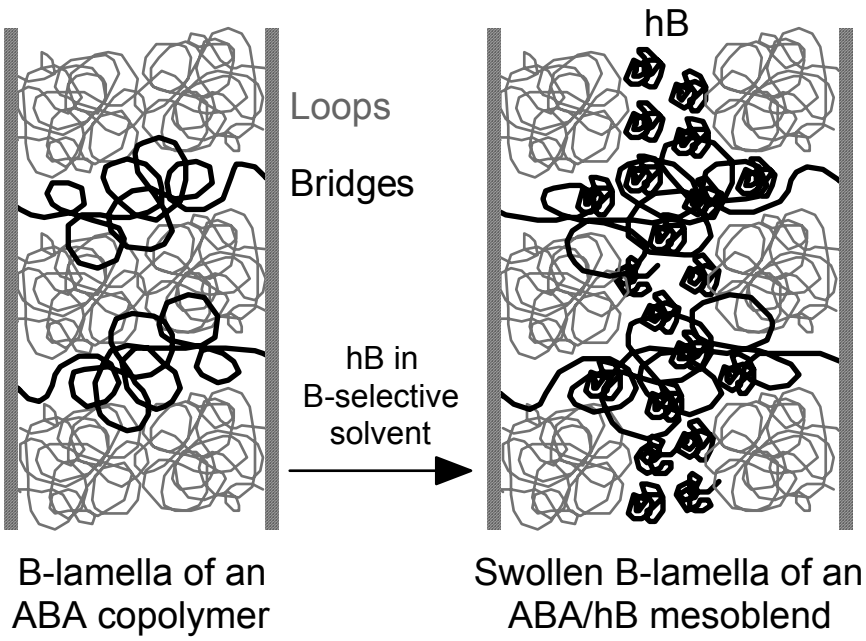

Figure 3.1. Schematic illustration of the general approach to preparing a block copolymer/ homopolymer mesoblend with a microphase-ordered ABA triblock copolymer. The copolymer molecules spontaneously order into A and B lamellae, the latter of which are composed of looped and bridged copolymer midblocks. Immersion of the copolymer into a B-selective solvent into which homopolymer B (hB) is dissolved results in sorption of hB molecules into, and subsequent swelling of, the B lamellae. If the carrier solvent is a nonsolvent for the A lamellae, they are expected to remain intact, despite the stress build-up due to copolymer swelling.

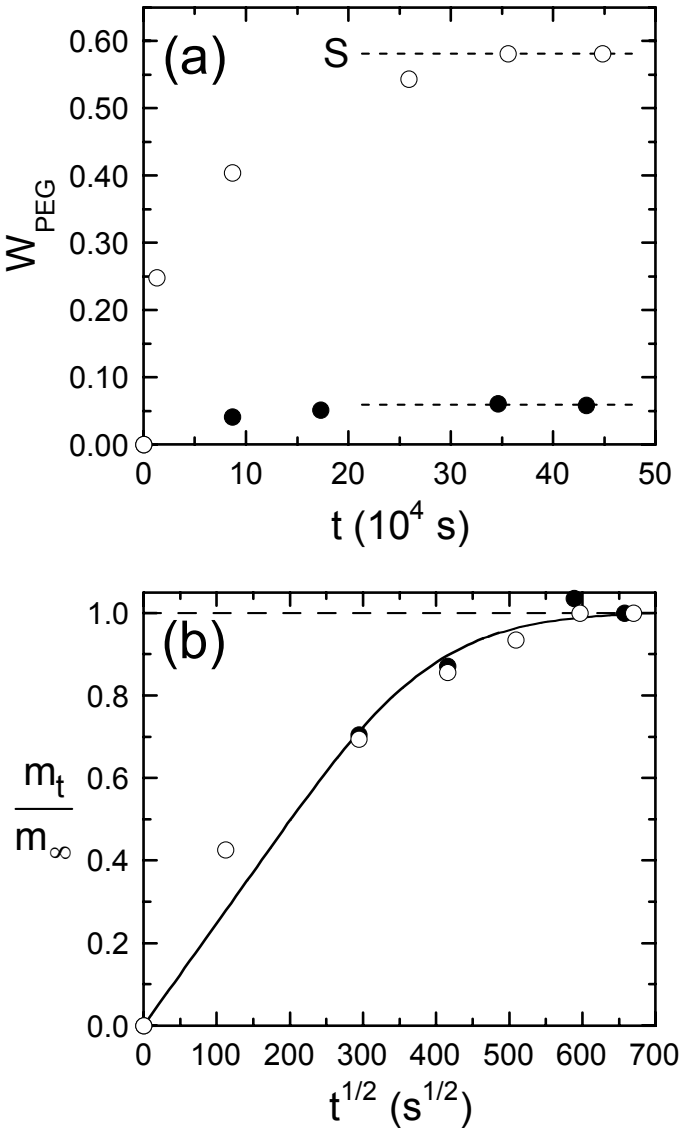

Figure 3.2. Mass uptake kinetics of PEG_{400} in the SEOS triblock copolymer after immersion in a 20% w/v solutions in ethanol (E) and water (J) at 60°C. In (a), the fraction of PEG_{400} in the resultant mesoblend (W_{PEG}) is displayed as a function of time (t), and the equilibrium solubility (S, dashed horizontal lines) is defined. In (b), the mass of sorbed PEG_{400} at time t relative to that at long time is shown as a function of $t^{1/2}$ and the regressed curve corresponds to Eq.3.5 in the text.

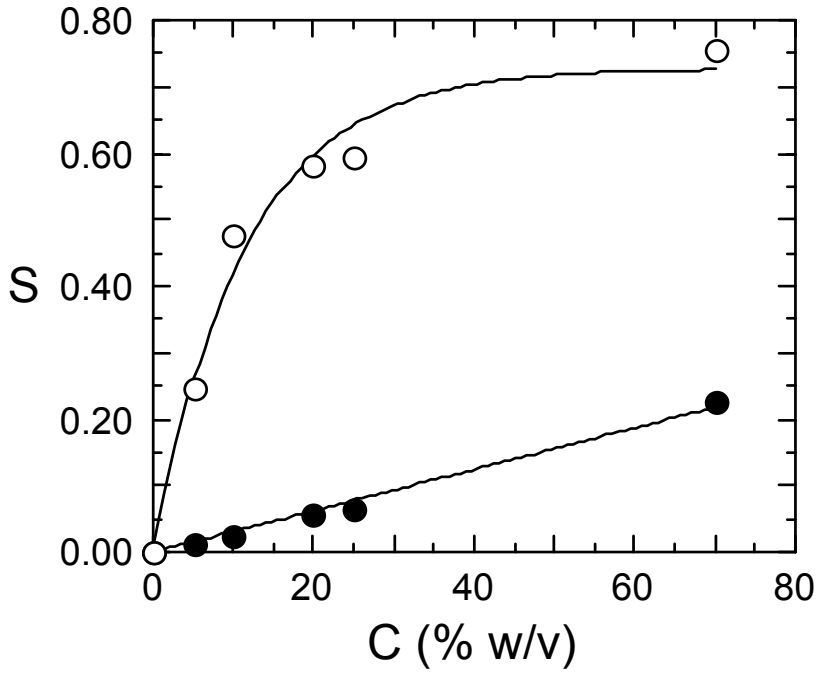

Figure 3.3. The effect of solution concentration (C) on PEG_{400} solubility (S) in the SEOS copolymer swollen by ethanol (E) and water (J) for 100 h at 60°C. The solid lines serve as guides for the eye.

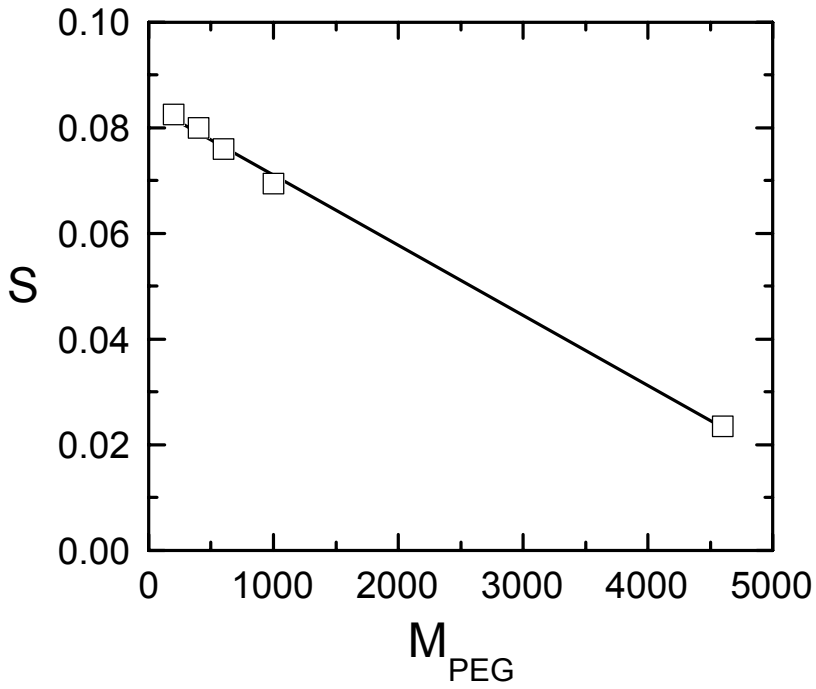

Figure 3.4. The dependence of PEG solubility in the SEOS copolymer on PEG molecular weight (M_{PEG}) in 25% w/v solutions in methanol at 23°C. The solid line is a linear regression of the data.

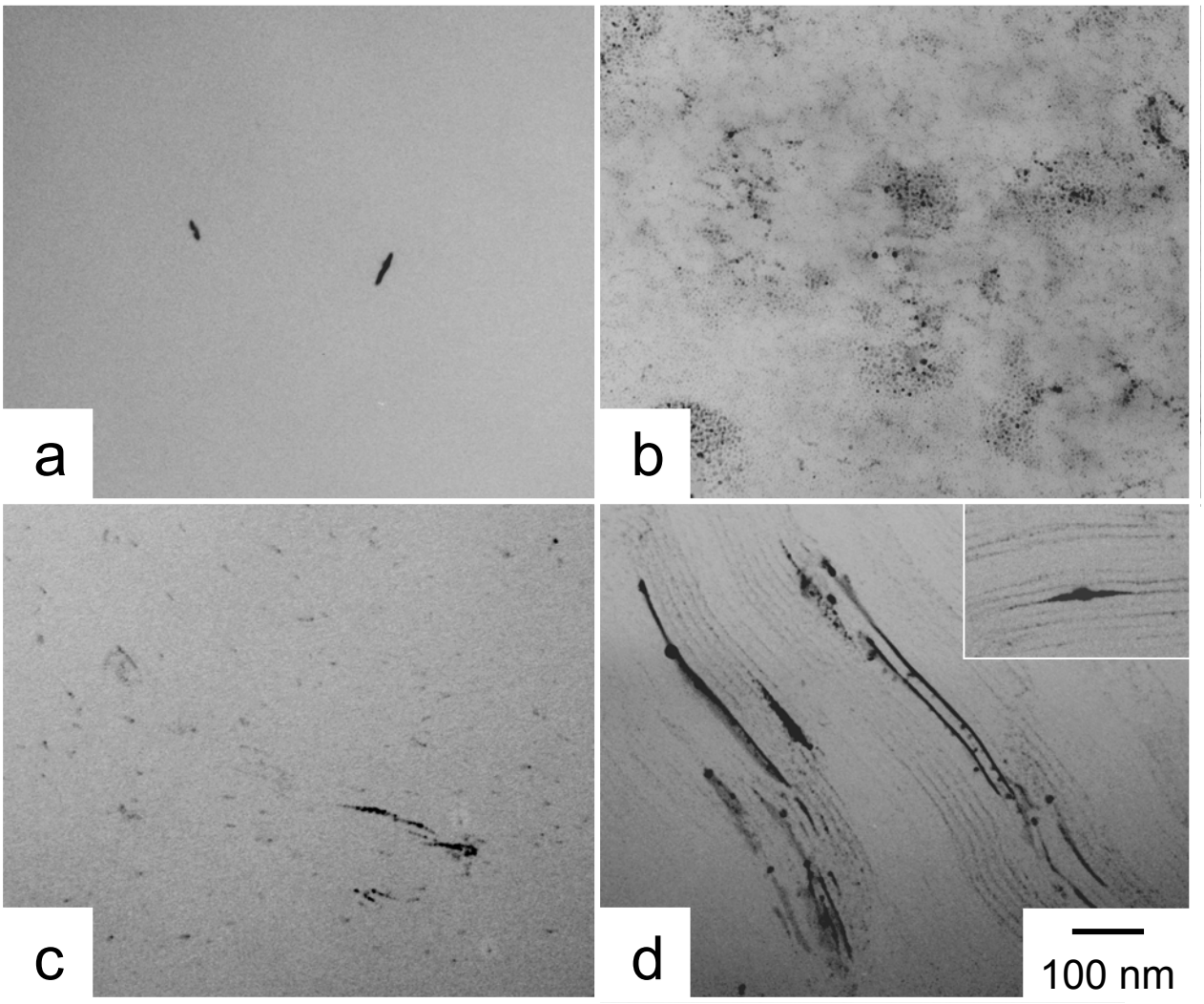

Figure 3.5. Series of TEM images obtained from (a) the neat SEOS triblock copolymer and three SEOS/PEG mesoblends composed of (b) PEG_{4600} from ethanol, (c) PEG_{400} from water and (d) PEG_{400} from ethanol. Mesoblend preparation conditions include a 100 h immersion time at 60°C in 25% w/v solutions. The electron-opaque (dark) features identify amorphous PEG that has been selectively stained by OsO_4. The inset in (d) is at the same magnification as the primary images.

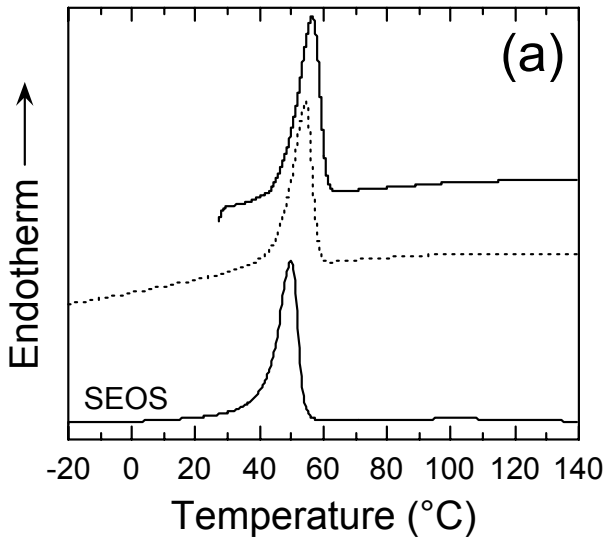
(a)
Endotherm
SEOS
-20 0 20 40 60 80 100 120 140
Temperature (°C)

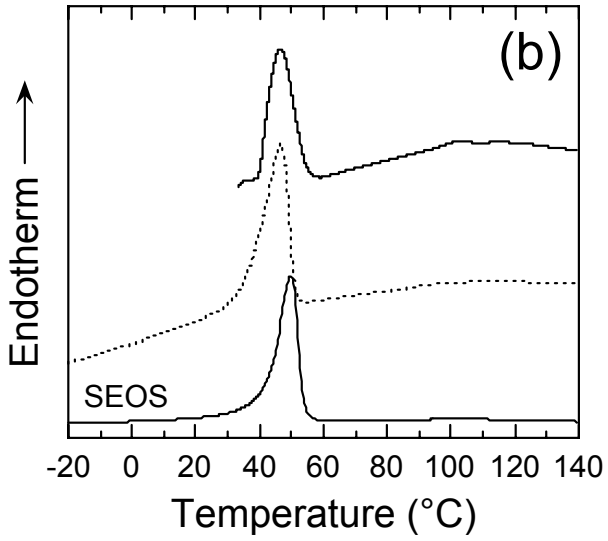
(b)
Endotherm
SEOS
-20 0 20 40 60 80 100 120 140
Temperature (°C)

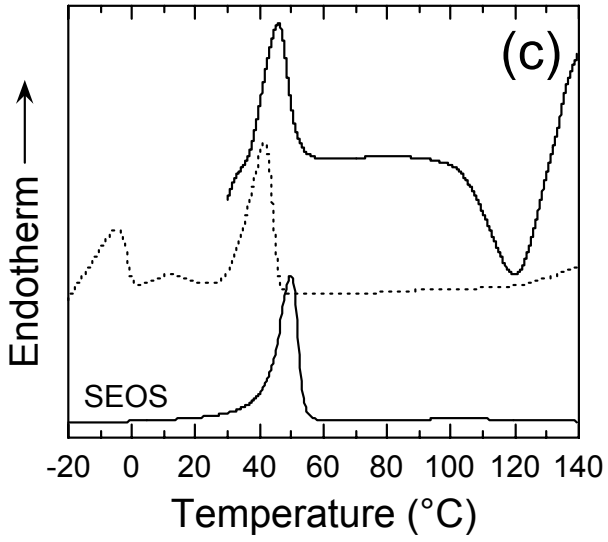
(c)
Endotherm
SEOS
-20 0 20 40 60 80 100 120 140
Temperature (°C)

Figure 3.6. DSC thermograms of the three mesoblends described in Fig.3.5: (a) PEG_{4600} from ethanol, (b) PEG_{400} from water and (c) PEG_{400} from ethanol. Shown here are the first-heat cycle (solid line) and the second-heat cycle (dashed line). Included for comparison in each part is the thermogram of the neat SEOS copolymer to facilitate direct comparison.

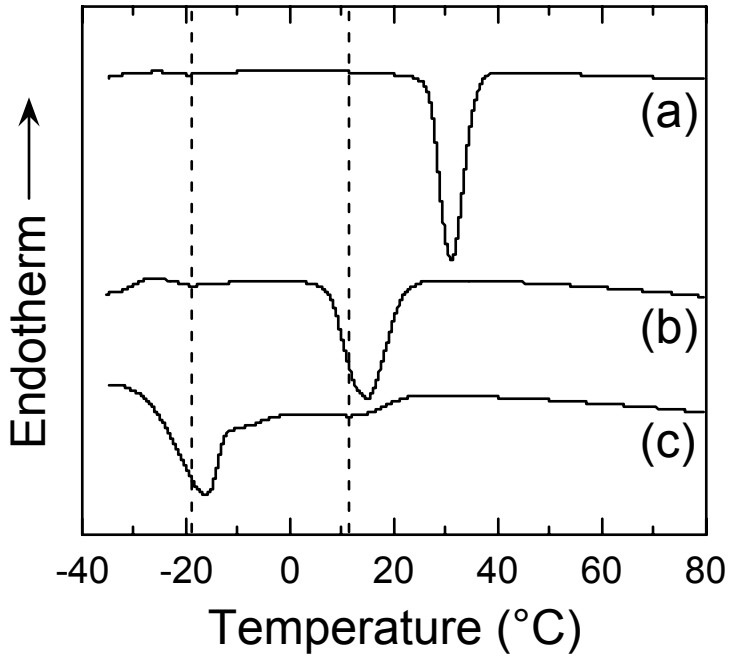

Figure 3.7. DSC thermograms of the three mesoblends discussed with regard to Fig.3.6: (a) PEG_{4600} from ethanol, (b) PEG_{400} from water and (c) PEG_{400} from ethanol. The vertical dashed lines identify the temperatures of relatively weak exothermic transitions to allow comparison.

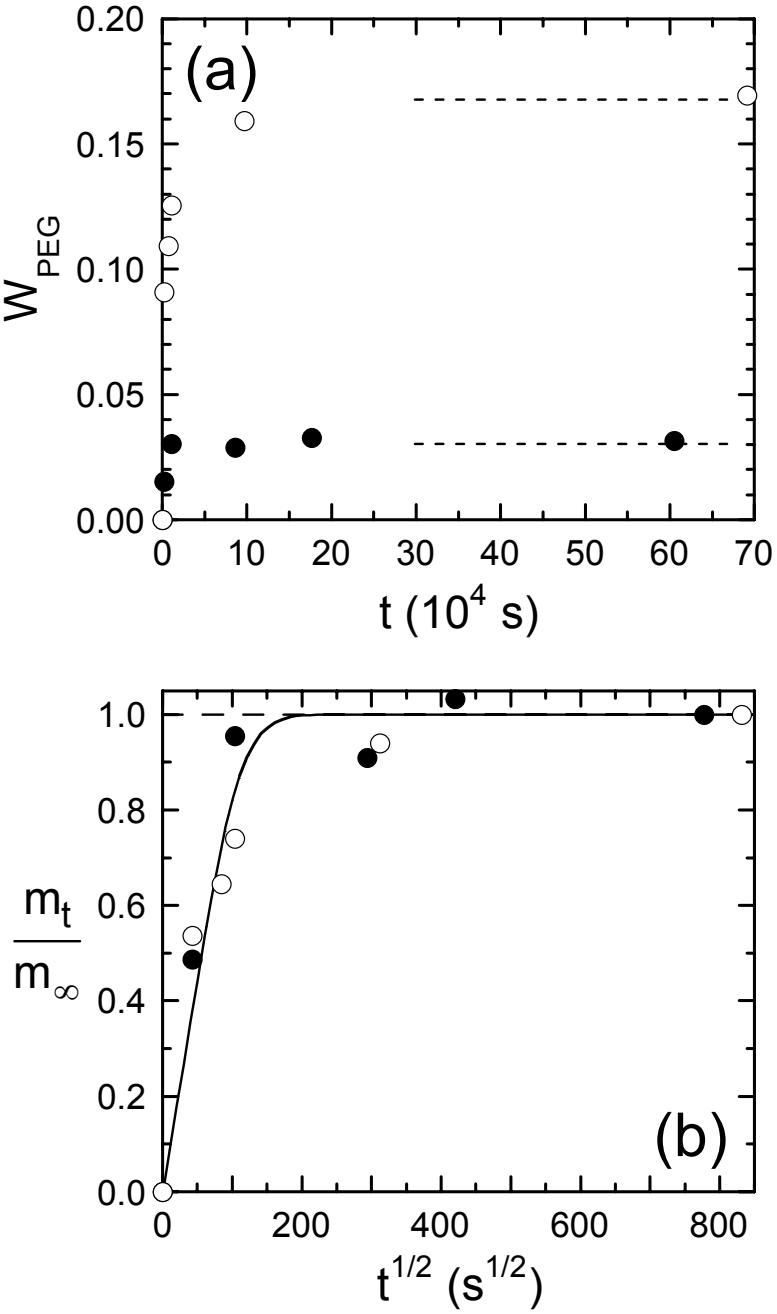

Figure 3.8. Mass uptake kinetics of PEG_{400} in the AEG multiblock copolymer at 23°C after immersion in ethanol solutions at two different concentrations (in % w/v PEG_{400}): 20 (J) and 60 (E). The format of parts (a) and (b) is identical to that described in Fig.3.2 regarding PEG_{400} sorption into the SEOS triblock copolymer.

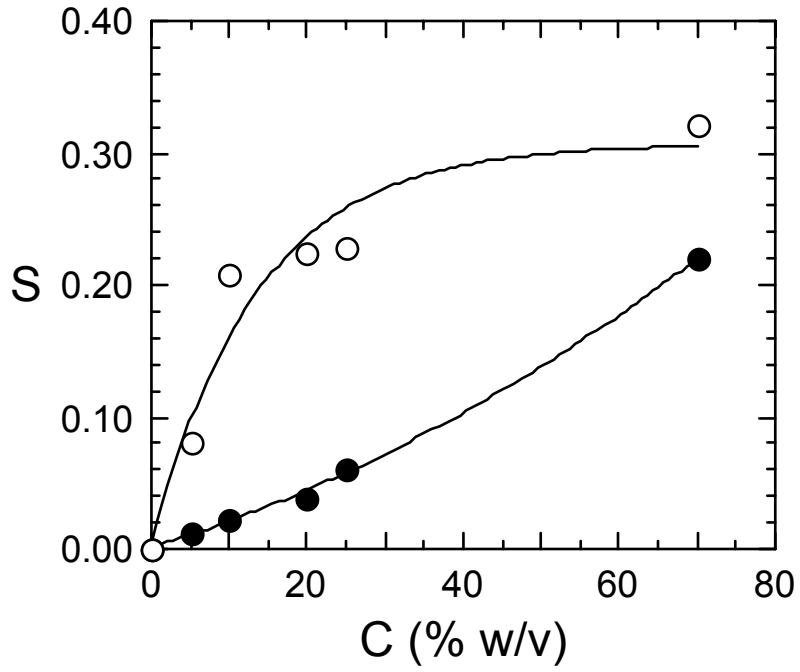

Figure 3.9. The effect of solution concentration on PEG_{400} solubility in the AEG copolymer swollen by ethanol (E) and water (J) for 100 h at 60°C. The solid lines are guides for the eye.

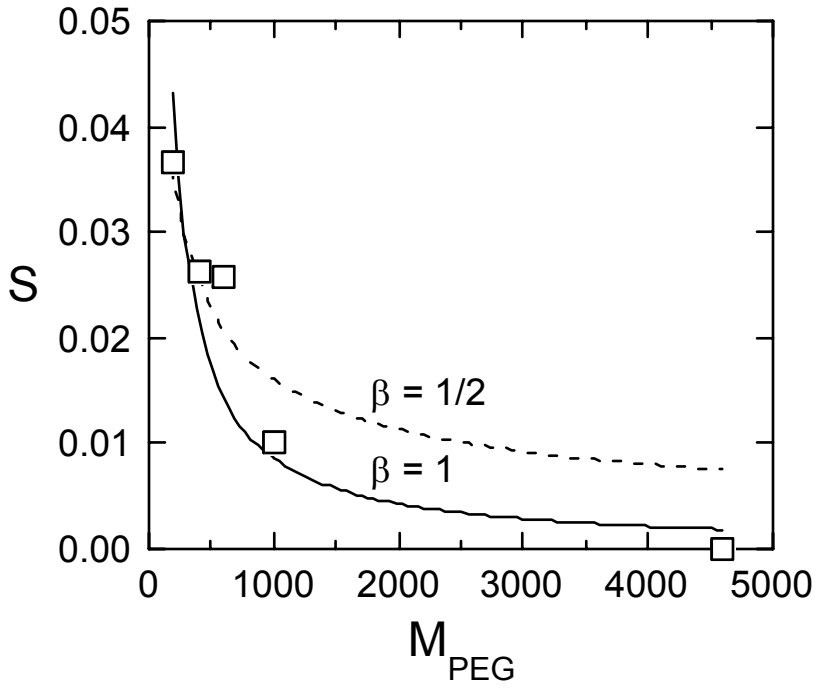

Figure 3.10. The dependence of PEG solubility in the AEG copolymer on PEG molecular weight (M_{PEG}) in 25% w/v solutions in methanol at 23°C. The lines are fits of the expression $S \sim M_{PEG}^{-\beta}$ to the data in which β is set equal to 1 (solid line) or 1/2 (dashed line).

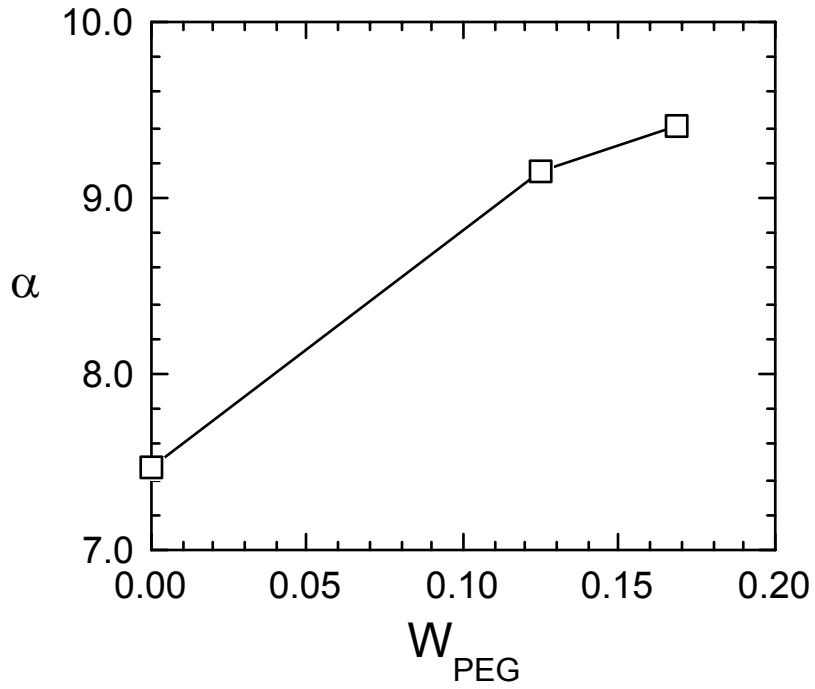

Figure 3.11. The CO_2/H_2 selectivity (α) presented as a function of PEG concentration in AEG mesoblends immersed in 60% w/v PEG_{400} solutions in ethanol at 23°C. The permeation tests used to calculate α have been performed at 23°C and a transmembrane pressure of 6.8 atm. The solid line serves to connect the data.

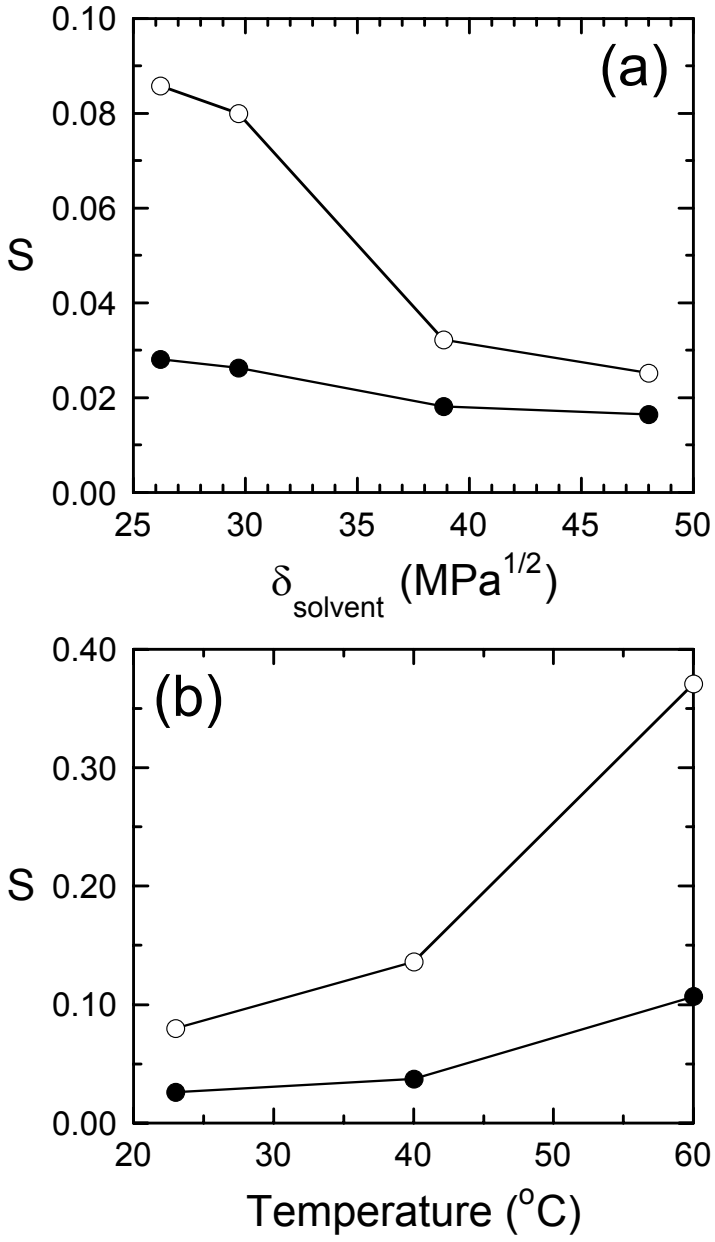

Figure 3.12. Variation of PEG_{400} solubility with (a) the solubility parameter (δ) of the carrier solvent and (b) temperature in the SEOS triblock copolymer (E) and the AEG multiblock copolymer (J) after an immersion time of 24 h in solutions containing 25% w/v PEG_{400}. The temperature in (a) is 23°C for the AEG copolymer and 60°C for the SEOS copolymer, and the solvent in (b) is methanol. The solid lines serve to connect the data.

Chapter 4

Highly CO_2-Permeable and Selective Polymer Nanocomposite Membranes

4.1. Abstract

Efficient purification of mixed light gas streams containing polar gases such as CO_2 remains an ongoing challenge for (petro)chemical industries that use, generate or recycle products containing such gases. One of the most commercially important processes that requires CO_2 removal is the large-scale production of H_2 feedstock from hydrocarbons via the water-gas shift reaction.[1] Current efforts designed to achieve cost-effective removal of CO_2 employ technologies based on amine,[2] mesopore[3] or zeolite[4] absorption. A viable alternate strategy is the use of multifunctional polymer membranes that exhibit high CO_2 permeability and selectivity, as well as the necessary mechanical properties to withstand typical application conditions.[5,6] In this work, we show that both CO_2 permeability and CO_2/H_2 selectivity in chemically-crosslinked amorphous poly(ethylene glycol) diacrylate are attractively high, and that their magnitudes can be judiciously controlled by adjusting polymer polarity or operating pressure. Incorporation of nanoscale fumed silica modified with methacrylate surface groups to permit covalent coupling with the acrylate-terminated polymer chains, thereby forming tough organic-inorganic hybrid nanocomposite membranes, is found to improve the bulk modulus without adversely affecting CO_2/H_2 selectivity or optical clarity.

This chapter was published in Advanced Materials, 15, 729, **2003**.

4.2. Introduction

Hydrogen is one of the most important commodity chemicals used in industry, with about $5x10^8$ kg produced annually in the U.S. alone.[7] This consumption rate is anticipated to increase as conventional fuel resources continue to dwindle and the need for clean, H_2-based, energy becomes increasingly urgent.[8,9] Over 90% of the H_2 produced worldwide is generated by the two-step water-gas shift reaction[1] in which hydrocarbons of the general type C_nH_m are first subjected to steam to yield CO and H_2 according to $C_nH_m+H_2O\leftrightarrow nCO+(m/2+n)H_2$. Additional H_2 is obtained through the conversion of CO to CO_2 by $CO+H_2O\leftrightarrow CO_2+H_2$. Hydrogen produced in this fashion is frequently used in the commercial synthesis of many other commodity and specialty chemicals such as ammonia[1] (ranked[7] 6^{th} in U.S. chemical volume production in 2001), which likewise serves as the reactant feedstock for other chemicals including urea, a primary constituent of fertilizer. Thus, cost-effective removal of CO_2 from H_2 is of paramount importance in chemical operations requiring relatively pure H_2. Since these processes are conducted in very large volumes, a small improvement in H_2 purification could render huge cost, energy and environmental savings.

Carbon dioxide is presently removed from H_2 by amine absorption, a solvent-based separations strategy that suffers from limitations associated with reaction heat, equipment corrosion and material degradation.[2] Together, these shortcomings can, for instance, promote the release of expensive and toxic volatile organic compounds (VOCs) to the atmosphere, thereby necessitating regular replacement of the amine solution and reclamation of discharged VOCs.[10] Membrane-based separation constitutes an alternative, green

technology to CO_2 removal from H_2, since less maintenance is often required and greater reliability is routinely achieved. While tremendous advances have been realized in the development of mesoporous inorganic membranes[3] and zeolites[4] for CO_2 removal, we turn our attention to organic (polymer) membranes for this purpose due to their versatility, processability and generally low cost. Membranes consisting of stiff-chain, glassy polymers with relatively low free volume (the volume unoccupied by polymer chains) can be used to sieve molecules in a gas mixture according to size.[11] Alternatively, highly flexible rubbery polymers and a small family of glassy substituted polyacetylenes possessing ultrahigh free volume are reverse-selective and facilitate permeation of larger molecules in a gas mixture.[12] While the latter approach appears promising as a means by which to remove CO_2 from light gases such as H_2, N_2 and O_2, the nonpolar polymer membranes routinely employed in this endeavor are not sufficiently CO_2-selective to favor commercialization.

Molecular transport of light gases in dense polymer membranes typically occurs by a solution-diffusion mechanism[13] in which the permeability (P) is given by SxD, where S and D denote the solubility and diffusivity, respectively, of the permeating species. The solubility provides a measure of interactions between the polymer matrix and penetrant molecules, whereas the diffusivity describes molecular mobility, which is normally governed by the size of the penetrant molecules as they wind their way through the permanent and transient voids afforded by the free volume of the membrane.[11,14] The selectivity of a polymer for one penetrant (A) over another (B) is given by

$$\alpha_{A/B} = \frac{P_A}{P_B} = \left(\frac{S_A}{S_B}\right) \times \left(\frac{D_A}{D_B}\right) \tag{4.1}$$

where S_A/S_B identifies the solubility selectivity and D_A/D_B is the mobility selectivity. For a

polymer membrane to be seriously considered for the removal of CO_2 from H_2, the values of P_{CO_2} and α_{CO_2/H_2} must both be competitively high. Since H_2 is physically smaller than CO_2 and diffuses more rapidly through polymer membranes than CO_2, it follows that $D_{CO_2}/D_{H_2}<1$. Thus, the only way to increase P_{CO_2} and α_{CO_2/H_2} simultaneously is to increase S_{CO_2}, which can be achieved by introducing chemical moieties into the polymer membrane to promote specific chemical interactions with the permeating CO_2 molecules and thereby facilitate molecular transport.

Independent studies[5,6] confirm that block copolymers composed of polyamide (PA) and poly(ethylene glycol) (PEG) sequences, the latter of which possess regularly-spaced polar ether linkages along the backbone, exhibit unusually high CO_2 selectivity due to specific interactions between the ether moieties and CO_2 molecules. Such interactions promote facilitated CO_2 transport through the membrane and should, in similar fashion, benefit separations designed to remove other acid gases, *e.g.*, ammonia and hydrogen sulfide, from mixed gas streams.[15] In the case of PA-PEG copolymers, the microphase-separated[16] semicrystalline PA blocks ensure structural integrity, since PEG, at sufficiently low-molecular-weight, exists as a liquid at ambient temperature and above. Mechanically strong, free-standing films are necessary to avoid the expensive equipment and hazards currently encountered in the amine absorption process.[2] To overcome the need for a hard (glassy or semicrystalline) block in designer PEG-containing copolymers, high-molecular-weight PEG can be used to form stable, but mechanically weak, membranes. An increase in PEG molecular weight is, however, ultimately accompanied by crystallization, and the formation of crystals in polymer membranes is generally deleterious, since they act as impermeable

obstacles to molecular transport and reduce the permeability of diffusing species.[17] Recent evidence[18] suggests that chemically crosslinked low-molecular-weight PEG may afford a viable route to the preparation of stable films with high CO_2 selectivity. In this work, we demonstrate that high CO_2 permeability and CO_2/H_2 selectivity can be achieved in crosslinked PEG, as well as in mechanically robust nanocomposites derived there from, and can be tuned by adjusting PEG polarity and operating pressure.

4.3. Experimental

4.3.1. Membrane Preparation

Two grades of diacrylate-terminated PEG, with molecular weights of 575 (PEGda575) and 700 (PEGda700), and 2,2'-azobisisobutyronitrile (AIBN) crosslinking agent were purchased from Aldrich Chemicals (Milwaukee, WI) and used as-received. Nonporous fumed silica modified with methacrylate surface groups (Aerosil R711) and having a primary particle size of 12 nm was obtained from Degussa Corp. (Parsippany, NJ). Each membrane, containing 0.5 wt% AIBN and up to 10 wt% FS, was prepared by first mixing its components thoroughly at 23°C in a Teflon vial until the specimen appeared clear and homogeneous. The liquid mixture was placed under vacuum at ambient temperature to remove air bubbles, carefully poured onto a glass plate and covered with a second glass plate before being placed in an oven maintained at 80°C. Crosslinking proceeded for 18-20 h, after which time the resultant film was removed and analyzed. A specimen for transmission electron microscopy (TEM) was prepared by sectioning a hybrid nanocomposite containing 10 wt% FS at -100°C in a Reichert-Jung cryoultramicrotome. Electron-transparent sections measuring *ca*. 80 nm thick were imaged with a Zeiss EM902 electron spectroscopic microscope operated at an

accelerating voltage of 80 kV and an energy loss of 0 eV.

4.3.2. Permeation

Defect-free films ranged from 40 to 200 μm in thickness, and permeation tests were typically conducted at 23°C and *ca*. 6.8 atm upstream pressure, unless otherwise indicated, on Al-masked films designed to provide a 1 cm^2 exposure area. Pure gas permeation properties were measured by the constant-volume/variable-pressure method, in which a specimen is held under vacuum until it is exposed to a gas at a specific pressure. The value of P measured in this fashion is determined from

$$P = \frac{Vl}{ART\Delta p}\left(\frac{dp}{dt}\right) \tag{4.2}$$

Here, V is the downstream volume, *l* is the membrane thickness, A is the membrane area, R is the universal gas constant, T denotes absolute temperature, Δp is the transmembrane pressure (= $p_2 - p_1$, where p_2 and p_1 are the upstream and downstream pressures, respectively), and dp/dt is the steady rate at which the pressure increases on the downstream side.

4.4. Results and Discussions

4.4.1. Effect of Ether Linkages

A cross-correlation analysis[19] of CO_2/H_2 selectivity as a function of CO_2 permeability is presented in Fig.4.1a for various polymer membranes under diverse experimental conditions. This compilation clearly reveals that CO_2/H_2 selectivity generally increases with increasing permeability. Included for comparison in this figure is a datum point (at a CO_2/H_2 selectivity of 9.5) corresponding to the crosslinked PEGda700 membrane

(with no FS) evaluated here at 23°C and 6.8 atm, indicating that this material exhibits superior separation performance under these experimental conditions. To put this improvement in perspective, the PA-PEG block copolymer membranes reported[5] earlier exhibit CO_2/H_2 selectivities ranging between 7.8 and 9.8 at 35°C and 10 atm. This concurrent improvement in CO_2 permeability and CO_2/H_2 selectivity, attributed to specific interactions between permeating CO_2 molecules and the polar linkages of the polyether matrix,[5] is more clearly seen in Fig.4.1b. In this figure, permeability and selectivity relative to H_2 are displayed as functions of penetrant species for H_2, N_2, O_2 and CO_2, which can be conveniently distinguished according to their normal boiling temperatures, for three polymers differing in polarity. In nonpolar low-density polyethylene, the permeabilities of all four gases are low (<17 Barrers), and their selectivities relative to H_2 are on the order of unity or less. Both observations are consistent with the molecular transport of light gases in a passive polymer membrane.

Figure 4.1b also shows that the permeabilities and selectivities of H_2, N_2 and O_2 do not change appreciably in the presence of the two crosslinked polyethers examined here. According to dynamic mechanical analysis performed on a Rheometrics Solids Analyzer (RSA-II) at ambient temperature, values of the elastic modulus (E') extracted from frequency spectra in the linear viscoelastic limit are 44.9 and 30.8 MPa for PEGda575 and PEGda700, respectively. While the precise topology of these (free-radical) crosslinked networks is not known, we estimate their crosslink densities (N, in nm^{-3}) from $E' = 3NkT$, where k is Boltzmann's constant, to be 3.6 (PEGda575) and 2.5 (PEGda700). Since the polyether molecular weight dictates the number density of polar bonds available for interaction with permeating CO_2 molecules, PEGda575 affords a less polar matrix than PEGda700. We

therefore conclude from the data presented in Fig.4.1b that H_2, N_2 and O_2 do not chemically interact to any significant extent with the polar bonds in PEG. In the case of CO_2, however, the permeability and selectivity relative to H_2 both increase substantially as the polarity of the polymer matrix increases. Relative to the transport of CO_2 in PE, the CO_2/H_2 selectivity is found to increase by a factor of ~4x in PEGda575 and ~7x in PEGda700. Another important result can be gleaned from the permeabilities of CO_2 and N_2 in Fig.4.1b. Besides removing CO_2 from H_2, we propose that our polymer membranes are likewise suitable for the removal of CO_2 from N_2/O_2 mixtures and, therefore, the purification of air in recirculation systems.[20] In such applications, the CO_2/N_2 selectivity provides a sensible measure of efficacy. Values of CO_2/N_2 selectivity derived from the data in Fig.4.1b are 12 (PE), 54 (PEGda575) and 70 (PEGda700).

4.4.2. Effect of Pressure

While membrane polarity has little effect on the transport properties of H_2, N_2 and O_2, it profoundly impacts the molecular transport of CO_2. Similar behavior is observed when the operating pressure is varied. The dependence of permeability on upstream pressure (which approximates the transmembrane pressure due to the low, <0.013 atm, downstream pressure) is displayed in Fig.4.2 for each of these light gases in PEGda575 and PEGda700. Note that the permeabilities of H_2, N_2 and O_2 are all very low (<8 Barrers) and virtually independent of both pressure and polymer polarity over the pressure range explored, providing further evidence that these gases do not undergo specific interactions to any significant extent with the polar linkages of the polyether. However, increasing pressure has a substantial effect on the permeability of CO_2. An increase in pressure from 4.8 to 13 atm

increases CO_2 permeability in PEGda575 by 32%, whereas an analogous pressure increase from 5.7 to 12 atm increases CO_2 permeability in PEGda700 by 24%. If these variations vary linearly with respect to pressure (as suggested by the data in Fig.4.2), then the CO_2 permeability and CO_2/H_2 selectivity in PEGda700 at 10 atm are estimated to be ~79 Barrers and just under 11, respectively. At the highest pressure examined (12 atm), the CO_2/H_2 selectivity in PEGda700 slightly exceeds 11, and the corresponding CO_2 permeability increases to ~83 Barrers.

4.4.3. Effect of Fumed Silica Addition

Although the crosslinked polyethers investigated here form stable films, their mechanical properties require improvement for practical implementation. Mechanically strong films can be readily achieved through the incorporation of inorganic nanoscale fillers.[21] Addition of nonporous (nano)particles to polymer membranes unfortunately tends to reduce penetrant permeability in the same manner as polymer crystals. This effect can be accurately modeled by the Maxwell[22] relationship originally derived to describe the dielectric properties of a suspension of spheres, *viz*.,

$$P_c = P_m \left(\frac{1 - \phi_f}{1 + \frac{\phi_f}{2}} \right) \tag{4.3}$$

Here, ϕ_f is the volume fraction of filler, and the subscripts c and m denote composite and matrix, respectively. In certain cases involving rigid, glassy polymers possessing ultrahigh free volume, however, the particles may actually increase available free volume and, hence, penetrant permeability by disrupting chain packing.[23] To retain the optical clarity of CO_2-

selective PEGda membranes and incorporate the particles within the crosslinked network, we have produced polymer nanocomposites containing fumed silica (FS) surface-modified with methacrylate groups that can participate in the crosslinking reaction. Addition of up to 10 wt% FS has no discernible effect on optical clarity, but increases E' of the membranes by over 60% in the PEGda700 series. A typical TEM image of a nanocomposite with 10 wt% FS is shown in Fig.4.3a and confirms that the FS is uniformly distributed throughout the polymer matrix with little evidence of gross aggregation.

The permeabilities of H_2 and CO_2 in PEGda575 and PEGda700 are presented as functions of FS concentration in Fig.4.3b and generally decrease, in accord with the Maxwell[22] relationship (Eq.4.3), with increasing FS content over the composition range explored. The corresponding selectivities included in the figure are, within experimental scatter, nearly independent of FS concentration. This result, which is consistent with electrical conductivity measurements of Li-doped PEG/FS nanocomposite electrolytes,[24] is a direct consequence of Eq.4.2. The CO_2/H_2 selectivity in the hybrid nanocomposite ($\alpha_{c,CO_2/H_2}$) is given by $P_{c,CO_2}/P_{c,H_2}$, which is equal to P_{CO_2}/P_{H_2} for a given ϕ_f.

4.5. Conclusions

Thus, the present organic-inorganic nanocomposite membranes can be made mechanically robust without adversely affecting their CO_2/H_2 separation effectiveness. From the data reported in Figs.4.1b and 4.2, we anticipate that this observation likewise applies to CO_2/N_2 selectivity. Since these materials are chemically crosslinked, they can be easily produced in a wide variety of shapes and sizes to satisfy application requirements. Moreover, their optical clarity can facilitate on-line diagnostic testing and multilayer fabrication (as, for

example, a CO_2-selective coating on porous hollow fiber membranes). Lastly, because other acid gases exhibit similar affinity for the polar ether linkages of PEG as CO_2,[15] the polymer nanocomposite membranes developed here are expected to be generally useful in molecular separations directed at purifying light gases such as H_2 and air.[25]

4.6. Acknowledgments

This work was supported by the U.S. Department of Energy and the National Science Foundation.

4.7. References

1. W. C. Kratz, D. L .Rarig, J. M. Pietratonio, AIChE Symp. Ser. 1988, 84, 36.
2. A. Kohl and R. Nielson, Gas Purification, Gulf Publishing Co., Houston, TX 1997.
3. R. M. de Vos, H. Verweij, Science 1998, 279, 1710.
4. A. Tavolaro, E. Drioli, Adv. Mater. 1999, 11, 975.
5. V. I. Bondar, B. D. Freeman, I. Pinnau, J. Polym. Sci. B: Polym. Phys. 2000, 38, 2051.
6. J. H. Kim, S. Y. Ha, Y. M. Lee, J. Membr. Sci. 2001, 190, 179.
7. Chemical & Engineering News, June 24, 2002, pp. 61-62.
8. S. Young, Nature 2001, 414, 487.
9. J. M. Ogden, Phys. Today 2002, 55, 69.
10. S. H. Lin, C. T. Shyu, Environ. Technol. 2000, 21, 1245.
11. B. D. Freeman, I. Pinnau, Trends Polym. Sci. 1997, 5, 167.
12. A. Morisato, I. Pinnau, J. Membr. Sci. 1996, 121, 243.
13. T. Graham, Philos. Mag. 1866, 32, 401.
14. V. P. Shantarovich, I. B. Kevdina, Y. P. Yampolskii, A. Y. Alentiev, Macromolecules 2000, 33, 7453.
15. B. D. Bhide, S. A. Stern, J. Membr. Sci. 1993, 81, 209.
16. I. W. Hamley, The Physics of Block Copolymers, Oxford Univ. Press, NY 1998.
17. R. M. Barrer, in Diffusion and Permeation in Heterogeneous Media (Eds: J. Crank, G. S. Park), Academic Press, London and New York 1968, p. 165.
18. Y. Hirayama, Y. Kase, N. Tanihara, Y. Sumiyama, Y. Kusuki, K. Haraya, J. Membr. Sci. 1999, 160, 87.
19. L. M. Robeson, J. Membr. Sci. 1991, 62, 165.

20. L. van de Beld, K. R. Westerterp, AIChE J. 1996, 42, 1139.

21. T. J. Pinnavaia, Science 1983, 220, 365.

22. C. Maxwell, Treatise on Electricity and Magnetism, Oxford Univ. Press, London 1873, vol. 1.

23. T. C. Merkel, B. D. Freeman, R. J. Spontak, Z. He, A. Morisato, I. Pinnau, P. Meakin, A. J. Hill, Science 2002, 296, 519.

24. H. J. Walls, J. Zhou, J. A. Yerian, P. S. Fedkiw, S. A. Khan, M. K. Stowe, G. L. Baker, J. Power Sources 2000, 89, 156.

25. M. B. Shiflett, H. C. Foley, Science 1999, 285, 1902.

List of symbols:

E = open circle

J = filled circle

C = open triangle

H = filled triangle

G = open square

A = open diamond

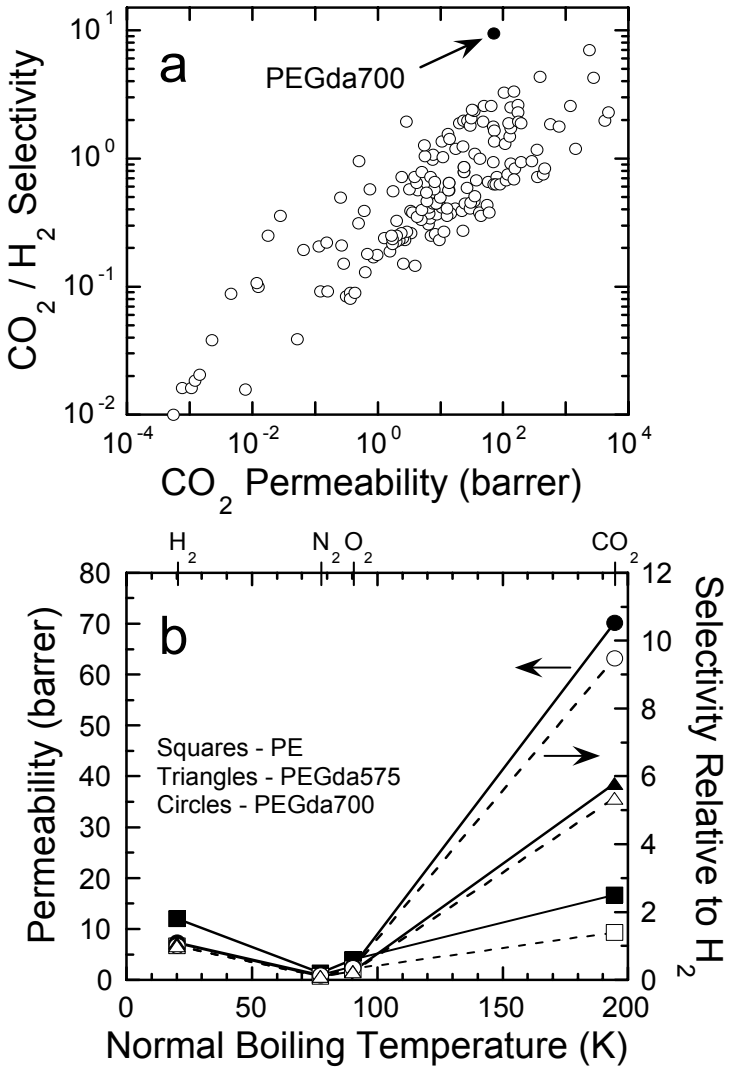

Figure 4.1. (a) Double-logarithmic cross-correlation analysis[19] of CO_2/H_2 selectivity *versus* CO_2 permeability (1 Barrer = 10^{-10} cm^3(STP)-cm/cm^2-s-cm Hg) for diverse polymer membranes under various experimental conditions (E). A datum point obtained from chemically-crosslinked PEGda700 (J) at 23°C and *ca*. 6.8 atm is included for comparison. (b) Permeability (filled symbols, solid lines) and selectivity relative to H_2 (open symbols, dashed lines) presented as functions of gas species, designated by their normal boiling temperature, in three polymer media differing in polarity: PE (squares), PEGda575 (triangles) and PEGda700 (circles). The solid and dashed lines serve to connect the data.

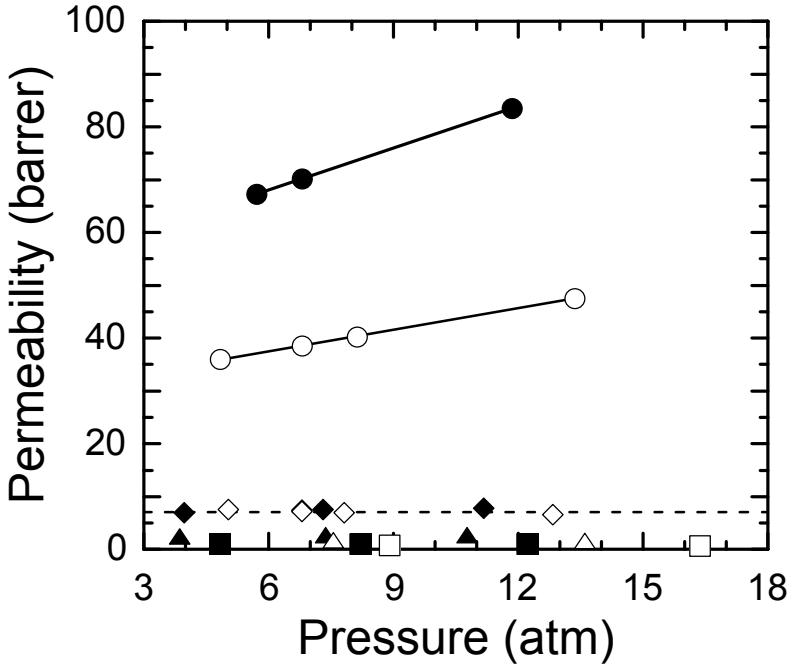

Figure 4.2. Dependence of permeability for H_2 (diamonds), O_2 (triangles), N_2 (squares) and CO_2 (circles) on pressure in two polyethers differing in polarity: PEGda575 (open symbols) and PEGda700 (filled symbols). The matrix polarity is related to the number of ether linkages per unit volume (ε) given by $n_e N_A \rho_p / M$, where n_e is the number of ether linkages per molecule, N_A is Avogadro's number, ρ_p is the mass density of the polymer (1.12 g/cm^3 for both PEGda575 and PEGda700, according to the manufacturer) and M denotes molecular weight. Calculated values of ε are 12.9 and 13.5 ether linkages/nm^3 for PEGda575 and PEGda700, respectively. The solid and dashed lines in the figure are linear regressions to the CO_2 and H_2 permeability data, respectively.

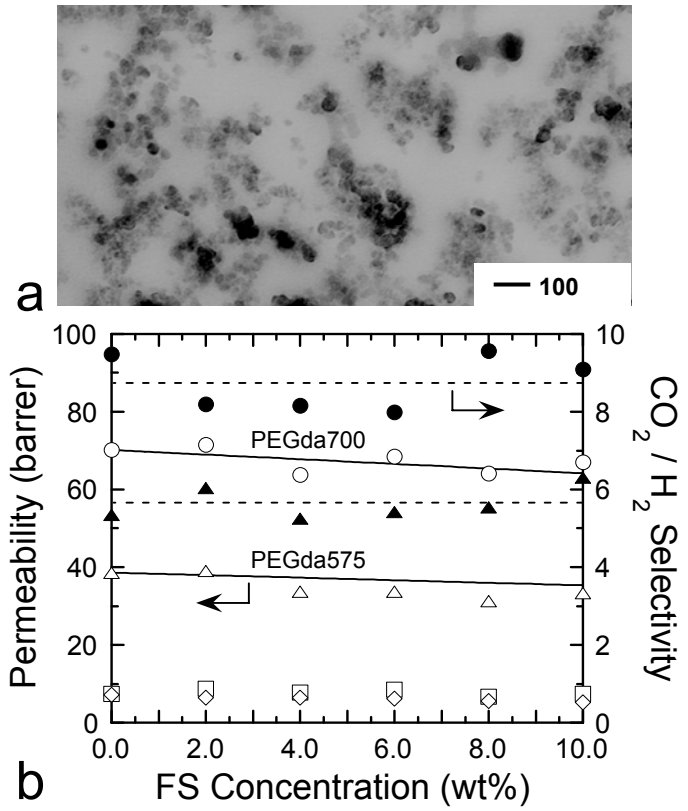

Figure 4.3. (a) Energy-filtered TEM image of a polymer nanocomposite membrane containing 10 wt% FS particles, which appear dark due to their electron density. The primary particle size is about 12 nm. (b) Effect of FS concentration on the permeabilities of H_2 and CO_2 in two polyethers differing in polarity: PEGda575 (A, H_2; C, CO_2) and PEGda700 (G, H_2; E, CO_2). The solid lines represent permeability predictions from the Maxwell relationship (Eq.4.2) in which ϕ_f is calculated from $w_f/(w_f+w_p\rho_f/\rho_p)$, where w represents weight fraction and the subscripts f and p denote filler and polymer, respectively. According to the manufacturer, $\rho_f \approx 2$ g/cm^3. Included here are corresponding values of the CO_2/H_2 selectivity in PEGda575 (H) and PEGda700 (J). The dashed lines represent the averages of the selectivity data.

Chapter 5

Highly CO_2-Permeable and Selective Membranes Derived from Cross-linked Poly(ethylene glycol) and Its Nanocomposites

5.1. Abstract

Cross-linked polyethylene glycol diacrylate (PEGda) oligomers differing in molecular weight, as well as their nanocomposites prepared with up to 10 wt% methacrylate-functionalized fumed silica (FS) or an organically-modified nanoclay, have been examined as amorphous CO_2-selective membranes. These novel materials have been characterized by dynamic rheology before and after cross-linking to ascertain the effect of incorporated FS on mechanical properties. The permeabilities of CO_2, H_2, N_2 and O_2 have been measured as functions of PEGda molecular weight, nanofiller content and temperature. In all cases, CO_2 displays very high permeability, coupled with high CO_2 selectivity, due to the specific interaction between quadrupolar CO_2 and the ether linkages along the PEG backbone, and the accompanying enhancement in CO_2 solubility. Variable-temperature permeation exhibits Arrhenius behavior, and the activation energy for CO_2 permeation is found to be markedly lower than that of any of the other gases examined.

This chapter has been accepted for publication under the same title in Adv.Funct.Mater..

5.2. Introduction

Current research trends in the energy and transportation industries are feverishly pursuing the development of hydrogen-based fuel cells as viable alternatives to conventional petroleum-based fuel resources, which continue to dwindle rapidly.[1-3] One of the primary commercialization challenges in this endeavor is to procure large volumes of purified hydrogen. Over 95% of H_2 production in the U.S. is achieved[4] through the use of synthesis gas ("syngas"), a mixture of H_2 with various light hydrocarbons. Following the two-step water-gas shift reaction,[4] H_2 is generated along with CO_2, in which case expedient CO_2 removal becomes essential for further utilization of H_2. Since H_2 is also required in the industrial production of many other important chemicals such as ammonia (the building block of urea), methods designed to facilitate CO_2 removal from H_2 are expected to result in significant energy and cost minimization. One such strategy that is currently employed for this purpose is based on amine absorption,[5] which is compromised by a number of serious operational drawbacks, including equipment corrosion, complicated use, material loss, personnel safety, and environmental impact.[6] For this reason, polymer membranes designed to remove CO_2 from H_2 afford an attractive alternative due to their versatile properties, processing ease, low maintenance and reduced cost.

While current CO_2/H_2 separation technology also relies on pressure-swing zeolite[7,8] or mesoporous[9] adsorption, we only consider the use of polymer membranes further in this work. In particular, recent advances[10,11] in the development of reverse-selective polymer membranes, *i.e.*, membranes that preferentially remove large permeating molecules from small ones in a mixture, serve to broaden the spectrum of applications suitable for polymer membranes. In the present case, such a membrane would be required to remove CO_2 from the

low-pressure downstream side of a permeating CO_2/H_2 gas mixture so that costly H_2 repressurization can be avoided. Previously, we have demonstrated[12] the function and efficacy of CO_2-selective polymer membranes derived from cross-linked polyethylene glycol diacrylate (PEGda) oligomers, along with their hybrid nanocomposites fabricated with methacrylate-functionalized fumed silica (FS). These amorphous membranes, illustrated in Fig.5.1, exhibit remarkably high CO_2/H_2 selectivity, coupled with high CO_2 permeability. Free-standing films of the cross-linked PEGda alone are relatively easy and inexpensive to produce, and they are mechanically strong, optically clear and typically defect-free. Addition of FS nanoparticles is found to increase the elastic modulus of the membrane without deleteriously affecting CO_2/H_2 selectivity. Incorporation of an inorganic nanofiller such as FS into cross-linked PEGda to form a nanocomposite is preferable over the use of high-molecular-weight PEG alone[13] (which crystallizes to form a physically cross-linked molecular network) for several reasons: (*i*) only those ether linkages residing in an amorphous PEG-rich matrix can interact with, and improve the solubility of, permeating CO_2 molecules; (*ii*) precise control over the kinetics and extent of polymer crystallization is non-trivial; and (*iii*) macroscopic spherulites adversely affect the diffusion of small-molecule penetrants,[14] as well as the optical clarity of the membrane, by serving as impermeable obstacles and diffracting entities.

To avoid the need for crystallization or cross-linking altogether and yet retain mechanically strong membranes, several research efforts have actively sought to develop CO_2-selective membranes from PEG-containing randomly-coupled block (segmented) copolymers that undergo microphase separation into PEG-rich microdomains.[15] Okamoto *et al.*[16] have reported that poly(ether-*b*-imide) copolymer membranes can exhibit CO_2

permeabilities as high as 140 Barrer (1 Barrer = 10^{-10} cm^3(STP)-cm/(cm^2-S-cm Hg) and CO_2/N_2 selectivities up to 70 at ambient temperature. Bondar *et al.*[17] have examined the gas sorption of several commercial poly(ether-*b*-amide)s, and their findings confirm that these materials likewise possess exceptionally high CO_2 solubility relative to nonpolar gases. Kim *et al.*[18] have extended this design paradigm for highly CO_2-selective membranes by grafting acrylate-terminated PEG oligomers onto polyacrylonitrile to form defect-free, mechanically strong membranes. However, two complications that arise in such studies are material availability and morphological development. In the first case, a very limited number of PEG-containing thermoplastic elastomers are commercially available, which therefore requires tailored copolymer synthesis for systematic analysis.[19] The second impediment refers to the reproducibility of the morphology formed by the copolymer upon microphase separation. Unlike their model diblock and triblock analogs, multiblock copolymers form highly interconnected networks[20] and, if their sequences are polydisperse, will not microphase-order into periodic morphologies,[21] which further thwarts systematic analysis. To overcome this complication, we are currently establishing structure-property relationships in miscible blends of a model PEG-containing triblock copolymer in the presence of low-molecular-weight PEG.[22]

In this work, we seek to provide a more detailed account of our efforts to produce cross-linked PEGda polymer and PEGda/FS nanocomposite membranes exhibiting high CO_2 selectivity. In addition to probing the effects of FS concentration and temperature on CO_2 permselectivity, the mechanical properties of the membranes before and after cross-linking are investigated by dynamic rheology.

5.3. Experimental

5.3.1. Materials

Three PEGda oligomers with number-average molecular weights of 258, 575 and 700, as well as 2,2'-azobisisobutyronitrile (AIBN) used as the cross-linking agent, were purchased from Aldrich Chemicals (Milwaukee, WI) and used without further purification. According to the manufacturer, the density of all three PEGda oligomers, hereafter designated as PEGdaM (M is the molecular weight), was constant at 1.12 g/cm^3. A methacrylate-functionalized nonporous FS with a mean primary diameter of 12 nm and a reported density of ~2 g/cm^3 (Aerosil R711) was obtained from Degussa Corp. (Parsippany, NJ). Two organically-modified montmorillonite clays (OCs) were provided by Southern Clay Products, Inc.(Gonsalez, TX): one (Cloisite 30B, OC1) was modified with methyl, tallow, bis-2-hydroxy ethyl, quaternary ammonium, and the other (Cloisite 93A, OC2) was modified with methyl, dihydrogenated tallow ammonium. The aspect ratio of these disk-shaped OC nanoparticles ranged from 75 to 100. Unless explicitly stated otherwise, the PEGda nanocomposites contained FS.

5.3.2 Methods

Free-radical cross-linking of the PEGda oligomers with and without inorganic nanofiller by AIBN was performed at 80°C, as described in detail elsewhere.[12] Resultant membranes generally measured between 40 and 200 μm in thickness, and their measured permeabilities exhibited no dependence on film thickness over this range. Pure-gas permeation tests were performed at 23°C and *ca*. 6.8 atm upstream pressure using the constant-volume, variable pressure technique,[23] in which a specimen is held under vacuum until it is exposed to a gas

at a specific pressure. The value of P thus measured is determined from

$$P = \frac{Vl}{ART\Delta p}\left(\frac{dp}{dt}\right) \tag{5.1}$$

where V is the downstream volume, l is the membrane thickness, A is the membrane area, R is the universal gas constant, T denotes absolute temperature, Δp is the transmembrane pressure ($= p_2 - p_1$, where p_2 and p_1 are the upstream and downstream pressures, respectively), and dp/dt is the steady rate at which pressure increases on the downstream side. Temperature was controlled to within ±1°C with a thermal regulator connected to a heater in the permeation cell wall.

Dynamic rheology was performed on materials with and without FS before and after cross-linking. The dependence of the dynamic elastic and viscous shear moduli (G' and G", respectively) on strain amplitude (γ_o) and oscillatory frequency (ω) was measured with a TA Instruments AR2000 rheometer with 40 mm parallel plates. The analogous tensile moduli (E' and E", respectively) were determined as functions of strain amplitude (ε_o) and ω on a Rheometrics Solids Analyzer (RSA-II).

5.4. Results and Discussion

5.4.1. Rheological Analysis

Addition of inorganic nanoscale fillers such as FS can, at certain concentration and temperature conditions, result in the formation of physically cross-linked colloidal networks, as described in detail by Raghavan *et al.*[28] and, more recently, Walls *et al.*[29] in their rheological studies of polymer-based electrolyte gels. The requirements for a physical network in this regard are two-fold:[30] (*i*) G' must be consistently greater than G", and (*ii*) G'

must be independent of ω, especially in the terminal zone at low ω (which correspond to long relaxation times). Figure 5.2a shows the dependence of G' and G" on strain amplitude (γ_o) for the uncross-linked PEGda575 and PEGda700 oligomers containing 10 wt% FS. In both cases, G" exceeds G' over two decades in γ_o, indicating that, despite the presence of inorganic fillers, these precursor suspensions behave as liquids and the FS nanoparticle aggregates exist as discrete flocks. While the moduli for the PEGda700 suspension are larger in magnitude than those of the PEGda575 suspension, it is interesting that the strain identifying their linear viscoelasticity limit (γ_{LVE}) appears virtually independent of n. At $\gamma_o < \gamma_{LVE}$, the moduli are independent of the extent of deformation and can be quantitatively compared as material properties.[30]

The moduli of the specimens analyzed in Fig.5.2b are presented as a function of ω in the LVE regime and confirm that G" is consistently larger than G', and that the suspensions exhibit a liquid-like rheological signature, over the range of ω displayed. This behavior is also shown in terms of tan δ (= G"/G'), where δ represents the phase angle, in the inset of Fig.5.2b. In this case, tan δ is always greater than unity, although a minimum in each ω spectrum of tan δ is clearly discernible. The physical origin of such a minimum is beyond the scope of the present work. In the terminal zone, a linear polymer melt exhibits two distinguishing characteristics:[30] $G' \sim \omega^a$ and $G'' \sim \omega^b$, where a=2 and b=1. These limiting slopes are included in Fig.5.2b. While the data shown in Fig.5.2b yield slightly smaller scaling exponents (a=1.2-1.3 for G' and b=0.75-0.85 for G"), we recognize that these measured exponents may increase to their expected values at lower ω.

The dynamic shear rheology described in conjunction with Fig.5.2 demonstrates that, at the highest FS loading used here, the uncross-linked materials do not exhibit a FS network.

This characteristic constitutes an important design consideration, since a contiguous diffusive pathway along the FS nanoparticles might have a deleterious effect on the selectivity of the membranes.[31] Since these materials form a molecular network and behave solid-like upon cross-linking, the dependence of only E' on strain amplitude (ε_o) for cross-linked PEGda575 and PEGda700 with 10 wt% FS is displayed in Fig.5.3 (corresponding values of E" are at least two orders of magnitude smaller than E' and are not shown for that reason). Three features of the data in Fig.5.3 warrant mention. The first is that the magnitude of E' is about seven orders of magnitude greater than that of G' upon cross-linking. Secondly, E' of the PEGda575 specimen is marginally larger in magnitude than that of the PEGda700 nanocomposite, which suggests that the molecular network comprising the PEGda575 material is somewhat stiffer. Moreover, the LVE limit is seen to extend to larger strain amplitudes (ε_{LVE}) in the PEGda700 system. Taken together, these latter two results provide additional evidence to suggest that the cross-link density and network rigidity both increase with decreasing PEGda chain length (n), in qualitative agreement with the chloroform sorption analyses described in the previous section.

A value of the cross-link density (N) can be estimated from E' by the theory of rubber elasticity, which states that

$$E' = 3NkT \tag{5.2}$$

where k is the Boltzmann constant. Values of N (in cross-links/nm^3) determined from Eq.5.2 are 3.6 for PEGda575 and 2.5 for PEGda700. The effect of FS concentration, expressed in weight percent (ϕ), on E' for cross-linked PEGda575 and PEGda700 from ω spectra (not shown due to their uninteresting behavior with E' > E" and E' invariant with respect to ω) is included in the inset of Fig.5.3. These measurements indicate that (*i*) E' generally increases

with increasing ϕ, (*ii*) E' of cross-linked PEGda575 is always larger than that of PEGda700, and (*iii*) E' increases more noticeably with increasing ϕ in the PEGda575 system than in the PEGda700 material. While values of N for these PEGda/FS nanocomposites cannot be estimated from Eq.5.2, it is apparent from Eq.5.2 that N effectively increases with increasing E' and that incorporation of FS into cross-linked PEGda yields a stiffer and, by inference, stronger material[29]

5.4.2. Permeation Analysis

Figure 5.4 shows the relationship between CO_2/H_2 selectivity and CO_2 permeability for a variety of different polymers under different experimental conditions. This trade-off, first identified by Robeson[33] and later expounded upon by Freeman,[34] indicates the upper limit placed on nonporous (dense) polymer membranes through which gas transport occurs by the solution-diffusion mechanism proposed by Graham.[35] According to this model, a penetrant molecule absorbs on the high-pressure (upstream) side of the membrane, diffuses through the membrane due to an applied pressure gradient and ultimately desorbs on the low-pressure (downstream) side of the membrane. In this view of molecular transport, permeability represents a pressure-induced flux of penetrant that is normalized with respect to membrane thickness. When the downstream pressure can be neglected and Fickian diffusion constitutes the rate-limiting step of this mechanism, the permeability of species i is given by[36]

$$P_i = D_i \times S_i \tag{5.3}$$

where D_i and S_i represent the diffusion coefficient and solubility, respectively, of i. The selectivity of penetrant A with respect to penetrant B ($\alpha_{A/B}$) is given by their permeability ratio, *viz*.,

$$\alpha_{A/B} = \frac{P_A}{P_B} = \left(\frac{D_A}{D_B}\right) \times \left(\frac{S_A}{S_B}\right) \tag{5.4}$$

Here, the ratio of diffusion coefficients is referred to as the mobility selectivity, and the ratio of solubility coefficients is the solubility selectivity. Generally speaking, rubbery polymers with low glass transition temperatures (T_gs) and flexible chains separate penetrant molecules on the basis of solubility, whereas glassy polymers with rigid chains sieve molecules on the basis of size. Rational design of CO_2-selective polymer membranes therefore requires a low-T_g polymer with an intrinsically high CO_2 solubility so that the solubility selectivity dominates Eq.5.4, as well as the overall selectivity of CO_2 with regard to nonpolar gases such as H_2. Application of this design paradigm to the cross-linked PEGda575 and PEGda700 polymers under current investigation at 23°C and an upstream pressure of 100 Pa results in high CO_2/H_2 selectivities and CO_2 permeabilities that lie well above the Robeson trade-off indicated in Fig.5.4.

Figure 5.4 also reveals that the CO_2 permeability and selectivity of PEGda575 are measurably less than those of PEGda700, which implies that these metrics are sensitive to PEGda chain length (n). This effect is more closely examined in Fig.5.5. In Fig.5.5a, the permeabilities of CO_2, H_2, N_2 and O_2 are examined as functions of n for three different PEGda membranes at 23°C. While the permeabilities of the nonpolar gases increase with increasing n, the magnitude of their permeabilities remains not far removed from unity (H_2 exhibits the highest permeability, 7.4 Barrer, in PEGda700). In marked contrast, the permeability of CO_2 increases sharply with increasing n due to the increase in CO_2 solubility dictated by the number density of ether linkages available for specific interaction. Corresponding selectivities of CO_2 relative to each of the nonpolar gases listed in Fig.5.5a

are provided in Fig.5.5b and suggest that there exists a gas- and temperature-specific limiting selectivity at some value of n not far above that of PEGda700.

This type of trend would not be surprising, since a wide variety of polymer properties (*e.g.*, T_g and surface energy) exhibit limiting behavior at large n where end-group effects become vanishingly small. It is interesting, and it may just be fortuitous, that this limiting selectivity appears to coincide with the chain length of PEG needed to induce interchain registry and, hence, crystallization. At the other extreme, low gas permeability and CO_2/gas selectivity in PEGda258 are the results of a highly rigid and dense network. Since there are only 3 repeat units between the cross-link sites, segmental mobility is extremely low, which induces a tremendous reduction in both penetrant diffusivity and solubility. Since the permeability of N_2 through PEGda258 in Fig.5.5a is very low (which would result in a very high CO_2/N_2 selectivity), the CO_2/N_2 selectivity in PEGda258 is not included in Fig.5.5b due to its experimental uncertainty.

The nonpolar gases investigated in conjunction with Fig.5 have been selected due to their technological importance. The need for facilitated removal of CO_2 from mixed CO_2/H_2 streams has already been established, whereas stripping CO_2 from mixed CO_2/N_2 streams may be critical for air purification in confined environments such as underwater/space vehicles or habitats. Table 5.1 lists the physical properties of the penetrant molecules studied in this work. Penetrant size and solubility can be accurately described[36] by the kinetic diameter and normal boiling temperature (T_b), respectively, and penetrant diffusivity relates inversely to size. Since CO_2 is larger in size than H_2, it possesses a smaller diffusion coefficient. Conversely, H_2 has a lower T_b than CO_2 and is consequently less soluble in dense polymers. Since PEG is a rubbery polymer with an infinite-molecular-weight T_g on the order

of –53 °C, the PEG segments of PEGda are highly flexible and offer little resistance to penetrant diffusion. It immediately follows that the mobility selectivity (D_{CO_2}/D_{H_2}) in Eq.5.4 is ~1, despite the large molecular size difference between CO_2 and H_2. The high CO_2/H_2 selectivity evident in Fig.5.5b is attributed to the high solubility selectivity of CO_2 relative to H_2 (S_{CO_2}/S_{H_2}) in Eq.5.4. To further test this hypothesis in Fig.5.6, we explore the permeability and corresponding CO_2/gas selectivity of several gases as a function of T_b (*i.e.*, gas solubility) in PEGda700 and polyethylene (PE). The PE differs from the PEGda700 in that it is semi-crystalline (with physical cross-link sites) and does not possess ether linkages along the backbone nor acrylate termination.

Figure 5.6a confirms that the permeabilities of the nonpolar gases are comparably low in PE and PEGda700, whereas the permeability of CO_2, while equally low in PE, increases sharply in PEGda700. As surmised from the results presented in Fig.5.5, the polar environment provided by the ether linkages in PEGda700 has a profound effect on CO_2 transport, promoting favorable intermolecular interactions (recall that CO_2 possesses a quadrupolar moment) and, thus, enhanced solubility. Similar solubility disparity attributed to specific interactions has been previously reported with regard to PEG-containing copolymers, in which all penetrants except for CO_2 obey a linear relationship between solubility and the Lennard-Jones well depth, another measure of penetrant condensability. Specific interactions such as those apparently induced by the polar ether linkages of PEG and its chemical derivatives are known to influence molecular transport in polymer systems containing nitro[37] and hydroxyl[38] groups. The CO_2/gas selectivities deduced from the data shown in Fig.5.6a are displayed in Fig.5.6b and reveal two consistent trends between PE and PEGda700. The first is that the CO_2/gas selectivities are always higher in PEGda700, and the

second is that $\alpha_{CO_2/N_2} > \alpha_{CO_2/CH_4} \sim \alpha_{CO_2/O_2} > \alpha_{CO_2/H_2}$. These results acquired at ambient temperature and an upstream pressure of 100 Psi demonstrate that, while the PEGda700 polymer membrane may suffice in removing CO_2 from N_2 ($\alpha_{CO_2/N_2} \sim 70$), CH_4 ($\alpha_{CO_2/CH_4} \sim 33$) and H_2 ($\alpha_{CO_2/H_2} \sim 9.5$), it is not yet sufficiently competitive with existing technologies. We return to address this point later.

The dynamic rheological results provided in Fig.5.3 indicate that the mechanical properties of the PEGda membranes can be systematically improved through the chemical incorporation of nonporous FS nanoparticles. As evidenced by the data reported in Fig.5.7, the effect of FS loading level on the permeability of CO_2, H_2, O_2 and N_2 in PEGda575 and PEGda700 nanocomposites is not very substantial over the range of ϕ examined in this work. As anticipated from Figs. 5.5 and 5.6, the order of permeability is given by $CO_2 > H_2 > O_2 > N_2$, with PEGda700 consistently exhibiting higher gas permeability than PEGda575. Addition of a nonporous inorganic filler to a polymer membrane generally reduces gas permeability due to the increased tortuosity of the diffusive pathway a penetrant must take to traverse the membrane.[31] An exception to this rule occurs when nanoscale filler particles disrupt the packing of relatively rigid polymer chains, thereby effecting an increase in local free volume. This unusual behavior has been observed[10] in substituted polyacetylenes and is not expected in the present work due to the flexibility of the PEGda chains even upon cross-linking. The reduction in permeability commonly encountered upon increasing the concentration of discrete nanoparticles has been accurately predicted[14] by the formalism originally proposed by Maxwell[39] to describe the dielectric properties of a suspension of spheres, namely,

$$P_c = P_m \left(\frac{1 - \Phi_f}{1 + \frac{\Phi_f}{2}} \right) \tag{5.5}$$

Here, P_c and P_m are the composite and matrix permeabilities, respectively, and Φ_f is the volume fraction of filler. Predictions based on Eq.5.5 are included in Fig.5.7 and appear to be in favorable agreement with the data since the FS nanoparticles can, to a rudimentary approximation, be considered spheroidal in shape.

Incorporation of the plate-like OC nanoparticles into PEGda700 yields markedly different permeation results. Figure 5.8a confirms that the permeability of CO_2 in the PEGda700/FS nanocomposite decreases, while the CO_2/H_2 selectivity remains relatively invariant, with increasing ϕ according to Eq.5.5. When either of the OC species investigated here is incorporated into PEGda700, however, the permeability of CO_2 drops sharply with only 2 wt% filler and then remains surprisingly constant, in stark contrast to the composition dependence predicted by Eq.5.5. Since the H_2 permeability is nearly independent of OC concentration, the dependence of CO_2/H_2 selectivity on ϕ (Fig.5.8b) in PEGda700/OC nanocomposites exhibits the same trend as the CO_2 permeability (Fig.5.8a). This distinct difference between the effect of FS and OC on gas permeability and CO_2/H_2 selectivity is attributed to the shape and dispersion of the plate-like OC nanoparticles. While individual FS nanoparticles may form aggregates or clusters (see Fig.5.1), each OC nanoparticle may exfoliate into its individual layers that can, if properly oriented, impact molecular transport of penetrant gases. In a related comparative study of FS and nanoclays, Walls *et al*. have found that, even at reduced loading levels, Na-hectorite nanoclays have a more pronounced influence on the rheology of PEG dimethyl ether than FS[40].

All the permeation results presented thus far have been acquired at ambient temperature. Figure 5.9a clearly illustrates that the permeability of CO_2, H_2, O_2 and N_2 in PEGda700 increases with increasing temperature and exhibits Arrhenius behavior over the temperature range explored. In this case, the permeability of each penetrant gas may be expressed as[41]

$$P = P_o \exp(-E_P / RT) \tag{5.6}$$

where P_o is a gas-specific constant and E_P denotes the activation energy of permeation. Similar results are obtained for the permeabilities of these gases in PEGda575, as well as in PEGda575 and PEGda700 nanocomposites with up to 10 wt% FS, and are not included here for that reason. Hirayama *et al.*[42] have studied gas transport in PEG-containing polymer membranes and report that their measured gas permeabilities display an abrupt increase at a specific temperature. Similarly, Kim *et al.*[43] have likewise identified discrete breakpoints in the temperature-dependent permeability of gases in a segmented poly(ether-*b*-amide) copolymer. An abrupt increase in gas permeability can be attributed to PEG melting, which is accompanied by the elimination of physical obstacles that impede molecular transport and, specifically in the case of CO_2, improved accessibility to individual PEG chains (and their polar ether linkages). Through physical blending of a model poly(styrene-*b*-ethylene oxide-*b*-styrene) (SEOS) triblock copolymer with low-molecular-weight PEG, we have controllably shifted the polyether melting point (T_m) and have confirmed that the transition temperature at which gas permeation changes markedly in these miscible blends corresponds to T_m.

In the present study, there is no such transition because the PEGda oligomers possess sufficiently low molecular weight to remain completely amorphous at temperatures above ambient. Corresponding CO_2/gas selectivities derived from the permeabilities in Fig.5.9a are provided as a function of temperature in Fig.5.9b. These data are presented to indicate that

vastly improved CO_2/H_2 and CO_2/N_2 selectivities can be easily achieved by operating at sub-ambient temperatures, insofar as PEG crystallization is avoided. On the basis of the relationships portrayed in this figure, we estimate that commercially-competitive CO_2/H_2 and CO_2/N_2 selectivities of, for instance, 20 and 100 can be realized at the reasonable operating temperatures of –9 and 11°C, respectively. While temperature-dependent selectivity data, such as those provided in Fig.5.9b, can help to guide the future design and commercial development of PEGda polymer and nanocomposite membranes, we now turn our attention back to the results shown in Fig.5.9a to elucidate the fundamental characteristics of molecular transport in these membranes. Table 5.2 lists the values of E_P extracted from the data included in this figure, as well as from additional data not shown. It is interesting to note that the magnitude of E_P generally obeys the following order: $CO_2 < H_2 < O_2 < N_2$.

Since diffusivity and solubility also tend to exhibit Arrhenius-type behavior, E_P can be written as the summation of energy contributions arising from penetrant diffusion (with an activation energy, E_d) and solubilization (with a heat of sorption, ΔH_s) so that

$$E_P = E_d + \Delta H_s \tag{5.7}$$

Sorption of a penetrant molecule is envisaged[36] to occur by a two-step process: a gas molecule condenses to a densified phase and subsequently mixes in a molecule-size gap created within the polymer. Therefore, enthalpy of sorption can be expressed as

$$\Delta H_s = \Delta H_{cond} + \Delta H_{mix} \tag{5.8}$$

where ΔH_{cond} and ΔH_{mix} denote the enthalpy changes associated with the two steps described above. For nonpolar, permanent gases, ΔH_{cond} is usually negligibly small, in which case ΔH_s is governed by ΔH_{mix}. For penetrant gases that do not interact with the polymer matrix, $\Delta H_{mix} > 0$, and their solubility tends to increase with increasing temperature. Diffusivity generally

display a stronger temperature dependence than solubility, increasing significantly with temperature. In a rubbery polymer, E_d is often related[41] to the energy required to open a cylindrical cavity having a length comparable to the mean diffusive jump length (λ) and a diameter equal to that of the diffusing gas molecule (d). It immediately follows from these size requirements that $E_d \sim d^2$. Figure 5.10 provides E_P for four penetrants in PEGda575 containing 0 and 10 wt% FS. In the cases of H_2, O_2 and N_2, E_P increases slightly due to the presence of FS, but clearly scales with d^2 at both FS concentrations. The marginal increase evident in E_P upon addition of FS reflects the impediment to molecular transport caused by the addition of physical obstacles, whereas the scaling relationship is consistent with the general observation that E_d dominates E_P for nonpolar gases. Since CO_2 is a polar molecule and possesses a quadrupolar moment that can specifically interact with the polar ether linkages of the PEG backbone, it possesses a negative ΔH_{mix}. Moreover, CO_2 is more condensable than the other penetrants examined here, in which case ΔH_{cond} is both negative and non-negligible. Kim *et al.*[43] have calculated ΔH_s for CO_2 in a poly(ether-*b*-amide) copolymer and report that it is more negative than in other rubbery polymers. For these reasons, E_P for CO_2 is expected to deviate markedly from E_d and, hence, d^2, as seen in Fig.5.10. It is interesting to note in this figure that the addition of FS has no discernible effect on E_P for CO_2.

5.5. Conclusions

Development of highly CO_2-permeable and selective polymer membranes that can be easily and inexpensively produced affords an attractive alternative to the facile removal of CO_2 from mixed gas streams, such as syngas and contaminated air. The rigidity of the cross-

linked PEGda network investigated in this work dictates both the mechanical and transport properties of these polymers and can be tailored through judicious choice of polymer chain length insofar crystallization of the chains is avoided. In this work, we have further demonstrated that incorporation of FS into the PEGda membranes serves to improve the mechanical properties without adversely affecting gas transport properties. Figure 5.11 shows the relative property enhancement/retention achieved upon addition of FS. The elastic modulus (E') and CO_2/H_2 selectivity (α_{CO_2/H_2}), normalized with regard to their respective values for the pure polymers, are provided as functions of FS concentration in this figure and reveal that the relative modulus increases systematically, while the relative CO_2/H_2 selectivity remains effectively constant, with increasing ϕ. Another membrane property unaffected by the use of low-molecular-weight (amorphous) PEGda oligomers or the addition of FS is optical clarity, which may play an important role in applications requiring on-line diagnostics.

Due to the amorphous nature of the PEGda oligomers, CO_2 molecules can interact specifically with the polar ether linkages along the PEG backbone, thereby yielding a consistently high CO_2/H_2 selectivity. While increasing the chain length of PEGda promotes a substantial increase in CO_2/H_2 selectivity, our results suggest that a limiting selectivity value will be ultimately reached, indicating that other operational parameters must be explored to improve the commercial competitiveness of this approach. We have shown, for instance, that both CO_2/H_2 and CO_2/N_2 selectivity can be increased to competitive performance levels at accessible sub-ambient temperatures. Moreover, our previous study[12] indicates that an isothermal increase in CO_2 pressure can likewise augment membrane performance due to enhanced CO_2 solubility. The robust and tunable transport, mechanical and optical attributes

of these membranes, which can be readily formed to any size or shape, make them ideally suited for a wide variety of technologies aimed at the removal of CO_2 from mixed gas streams for the expedient recovery of important gases such as H_2 and air. Since the principles upon which these polymer and nanocomposite membranes function are fundamentally general, we anticipate that the membranes should be of comparable success in the removal of other acid gases (*e.g.*, hydrogen sulfide and ammonia) from mixed gas streams.

5.6 . Acknowledgements

This work was supported by the U.S. Department of Energy under Contract No. DE-FG02-99ER14991 and the National Science Foundation.

5.7. References

1) Hefner, R. A. *Inter. J. Hydrogen Energ.* 2002, *27*, 1.

2) Guy, K. W. A. *Process Saf. Environ.* 2000, *78*, 324.

3) Winebrake, J. J.; Creswick, B. P. *Technol. Forecast. Soc.* 2003, *70*, 359.

4) Kratz, W. C.; Rarig, D. L.; Pietratonio, J. M. *AIChE Symposium Series* 1988, *84*, 36.

5) Yeh, J. T.; Pennline, H. W.; Resnik, K. P. *Energ. Fuel.* 2001, *15*, 274.

6) Kohl, A.; Nielson, R. *Gas Purification*; Gulf Publishing Co.: Houston, TX, 1997.

7) Tavolaro, A.; Drioli, E. *Adv. Mater.* 1999, *11*, 975.

8) Chatterjee, A.; Iwasaki, T. *J. Phys. Chem. A* 1999, *103*, 9857.

9) de Vos, R. M.; Verweij, H. *Science* 2002, *279*, 1710.

10) Merkel, T. C.; Freeman, B. D.; Spontak, R. J.; He, Z.; Pinnau, I.; Meakin, P.; Hill, A. J. *Science* 2002, *296*, 519.

11) Merkel, T. C.; Freeman, B. D.; Spontak, R. J.; He, Z.; Pinnau, I.; Meakin, P.; Hill, A. J. *Chem. Mater.* 2003, *15*, 109.

12) Patel, N. P.; Miller, A. C.; Spontak, R. J. *Adv. Mater.* 2003, *15*, 729.

13) Li, J.; Wang, S.; Nagai, K.; Nakagawa, T.; Mau, A. W.-H. *J. Membrane Sci.* 1998, *138*, 143.

14) Barrer, R. M. *Diffusion and permeation in heterogeneous media*; Crank, J. and Park, G. S., Ed.; Academic Press: London and New York, 1968, pp 165.

15) Bondar, V. I.; Freeman, B. D.; Pinnau, I. *J. Polym. Sci. Polym. Phys.* 2000, *38*, 2051.

16) Okamoto, K.-I.; Fujii, M.; Okamiyo, S.; Suzuki, H.; Tanaka, K.; Kita, H. *Macromolecules* 1995, *28*, 6950.

17) Bondar, V. I.; Freeman, B. D.; Pinnau, I *J. Polym. Sci. Polym. Phys.* 1999, *37*, 2463.

18) Kim, J. H.; Ha, S. Y.; Nam, S. Y.; Rhim, J. W.; Baek, K. H.; Lee, Y. M. *J. Membrane Sci.* 2001, *186*, 97.

19) Holden, G.; Legge, N. R.; Quirk, R. P.; Schroeder, H. E. *Thermoplastic Elastomer*; 2nd ed.; Hanser: Munich, 1996.

20) Glotzer, S. C.; Bansil, R.; Gallagher, P. D.; Sciortino, F.; Stanley, E. *Physica A,* 1993, *201*, 482.

21) Hamley, I. W. *The Physics of Block Copolymers*; Oxford University Press: Oxford, 1998.

22) Patel, N. P.; Spontak, R. J. *in preparation*.

23) Felder, R. M.; Huvard, G. S. *Permeation, diffusion and sorption of gases and vapors.*; Fava, R., Ed.; Academic Press: New York, 1978; Vol. 16C, pp 315.

24) Patras, G.; Qiao, G. G.; Solomon, D. H. *Electrophoresis* 2000, *21*, 384.

25) Balik, C. M. *Macromolecules* 1996, *29*, 3025.

26) Stevens, J. E.; Thongruang, W.; Patel, N. P.; Smith, S. D.; Spontak, R. J. *Macromolecules* 2003, *36*, 3206.

27) Nugay, N.; Erman, B. *Macromol. Symp.* 2001, *169*, 269.

28) Raghavan, S. R.; Riley, M. W.; Fedkiw, P. S.; Khan, S. A. *Chem. Mater.* 1998, *10*, 244.

29) Walls, H. J.; Zhou, J.; Yerian, J. A.; Fedkiw, P. S.; Khan, S. A.; Stowe, M. K.; Baker, G. L. *J. Power Sources* 2000, *89*, 156.

30) Macosko, C. W. *Rheology: Principles, Measurements and Applications*; VCH Publisher: New York, 1994.

31) Petropoulos, J. H. *J. Polym. Sci. Polym. Phys*. 1985, *23*, 1309.

32) Zilg, C.; Dietsche, C.; Hoffmann, B.; Dietrich, C.; Mulhaupt, R. *Macromol. Symp.* 2001, *169 (Fillers and filler polymers)*, 65.

33) Robeson, L. M. *J. Membrane Sci.* 1991, *62*, 165.

34) Freeman, B. D. *Macromolecules* 1999, *32*, 375.

35) Graham, T. *Philos. Mag.* 1866, *32*, 401.

36) Ghosal, K.; Freeman, B. D. *Polym. Advan. Technol.* 1994, *5*, 673.

37) Ghosal, K.; Chern, R. T.; Freeman, B. D.; Savariar, R. *J. Polym. Sci. Polym. Phys.* 1995, *33*, 657.

38) Story, B. J.; Koros, W. J. *J. Membrane Sci.* 1992, *67*, 191-210.

39) Maxwell, C. *Treatise on Electricity and Magnetism*; Oxford University Press.: London, 1873; Vol. 1.

40) Walls, H. J.; Riley, M. W.; Gupta, R. R.; Spontak, R. J.; Fedkiw, P. S.; Khan, S. A. *Adv. Functional Mater.* 2003, *13*, 710.

41) Petropoulos, J. H. *Mechanisms and Theories for Sorption and Diffusion of Gases in Polymers*; CRS Press: Boca Raton, 1994.

42) Hirayama, Y.; Kase, Y.; Tanihara, N.; Sumiyama, Y.; Kusuki, Y.; Haraya, K. *J. Membrane Sci.* 1999, *160*, 87.

43) Kim, J. H.; Seong, Y. H.; Lee, Y. M. *J. Membrane Sci.* 2001, *190*, 179.

Table 5.1. Properties of the gases used in this study

Gas	Kinetic diameter[a] (A^o)	T_b [b] (K)
H_2	2.89	20.1
N_2	3.64	77.4
O_2	3.46	90.2
CH_4	3.80	111.4
CO_2	3.30	194.7

[a]Smith, J. M.; Van Ness, H. C.; Abbott, M. M. *Introduction to Chemical Engineering Thermodynamics*, 5th Ed.;McGraw-Hill: New York; 1996, pp. 653-656.

[b]Mulder, M. *Basic Principles of Membrane Technology*; Kluwer Academic: Dordrecht, Netherlands; 1991, p. 226.

Table 5.2. Activation energy of permeation (E_P, in kJ/mol) for several gases in two cross-linked PEGda polymers and their FS nanocomposites

Membrane	CO_2	H_2	O_2	N_2
PEGda575	18.6	24.0	34.9	32.5
PEGda575 + 10 wt% FS	18.2	25.3	38.6	36.8
PEGda700	17.7	30.0	40.7	32.8
PEGda700 + 10 wt% FS	17.8	31.9	41.2	34.1

List of symbols:

E = open circle

J = filled circle

C = open triangle

H = filled triangle

G = open square

A = open diamond

D = filled diamond

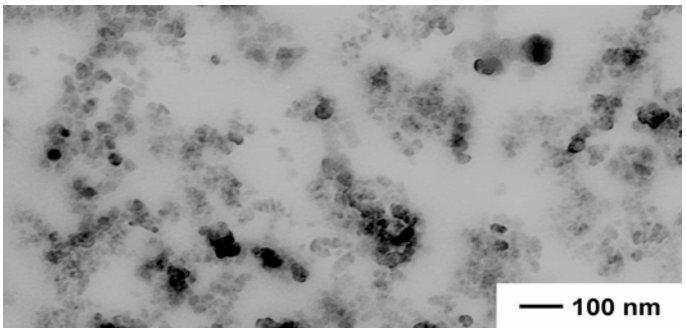
100 nm

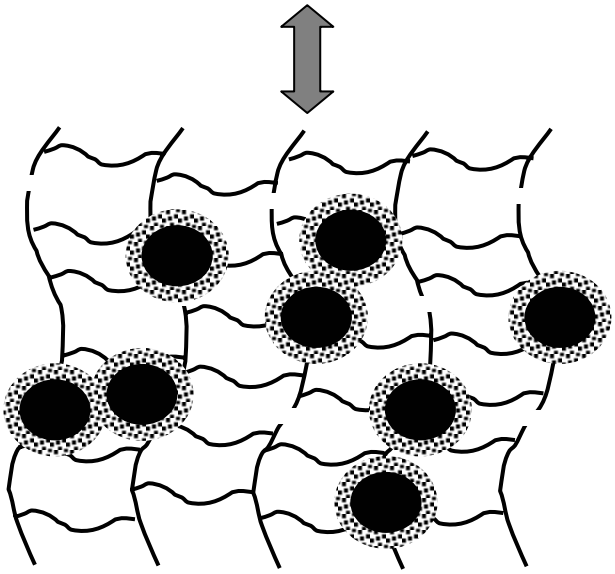

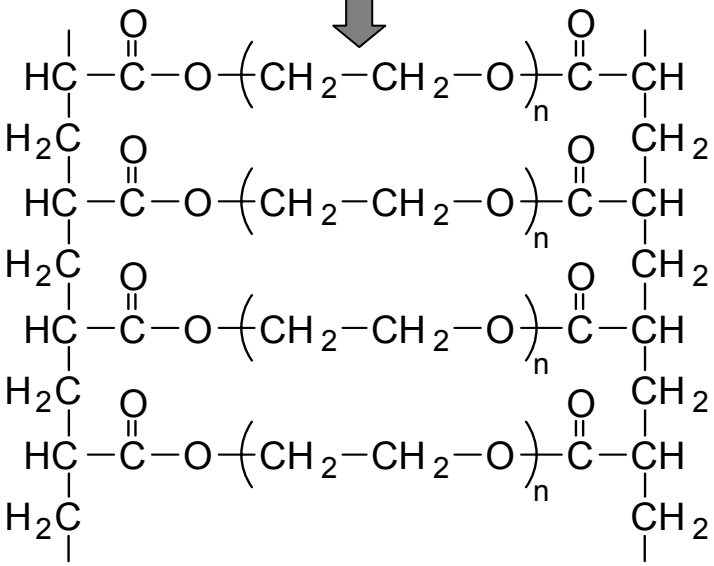

Figure 5.1. Morphological features of cross-linked PEGda/FS nanocomposite membranes at different size scales. The transmission electron micrograph (top) displays the electron-opaque (dark) FS particles and their aggregates.12 The schematic of the molecular network (middle) shows discrete FS particles (black) possessing a methacrylate-functionalized surface (speckles). The chemical structure of the PEGda molecules (bottom) illustrates their ideal arrangement upon cross-linking (the actual network is more highly interconnected due to the stochastic nature of the free-radical polymerization).

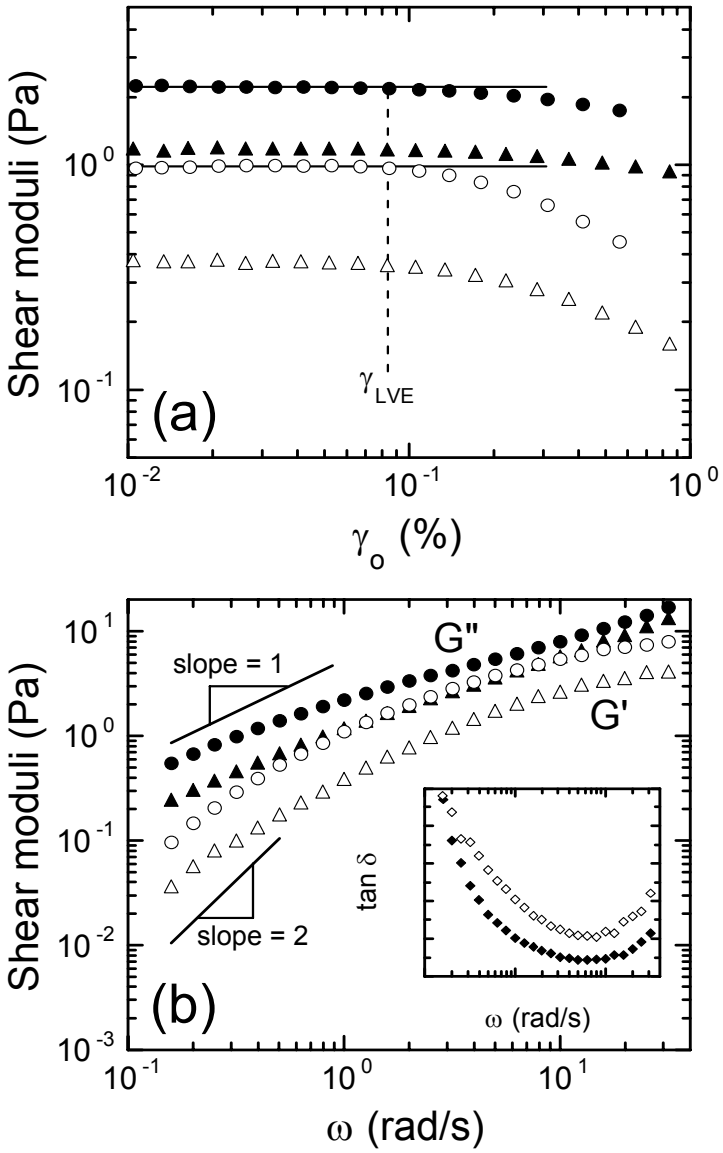

Figure 5.2. Dynamic shear moduli (G', open symbols; G", filled symbols) presented as functions of (a) strain amplitude (γ_o) and (b) oscillatory frequency (ω) in uncross-linked PEGda with 10 wt% FS. Circles and triangles correspond to PEGda700 and PEGda575, respectively. The ω spectra of tan δ (= G"/G') corresponding to the moduli displayed in (b) are provided in the inset and confirm that these materials exhibit liquid-like rheological behavior.

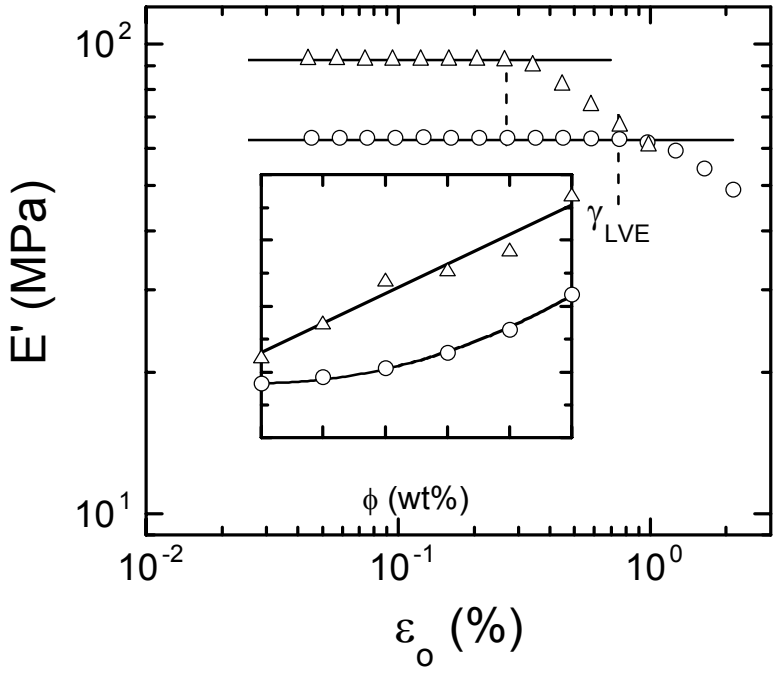

Figure 5.3. Dependence of the dynamic elastic tensile modulus (E') on strain amplitude (ε_o) for cross-linked PEGda575 (C) and PEGda700 (E), each with 10 wt% FS. The variation in E' with FS concentration in PEGda575 and PEGda700 is included in the inset (in which the solid lines serve as guides for the eye).

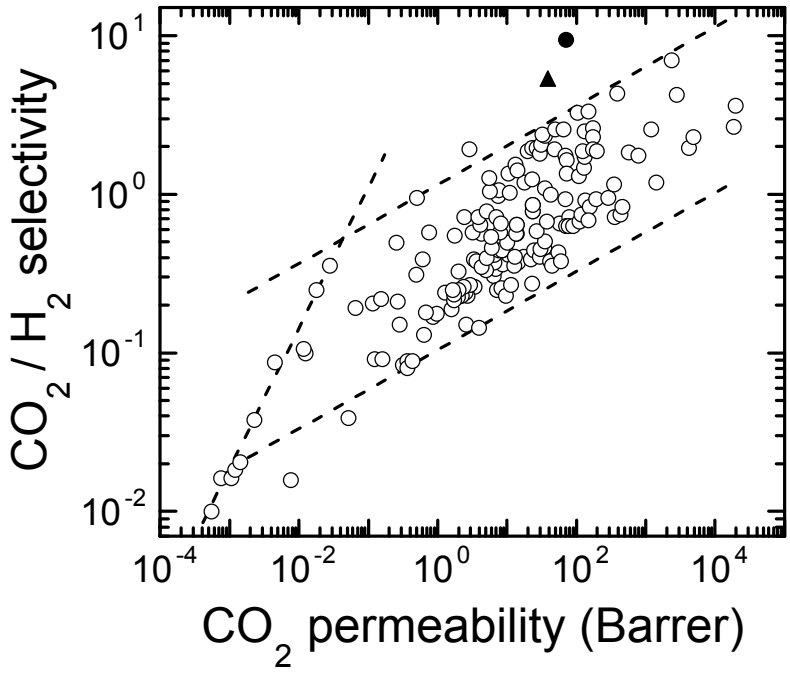

Figure 5.4. CO_2/H_2 selectivity presented as a function of CO_2 permeability for a wide variety of polymers under different conditions (E) showing the Robeson[33] trade-off relationship. Data acquired from the cross-linked PEGda575 and PEGda700 membranes examined here are included as (H) and (J), respectively, for comparison.

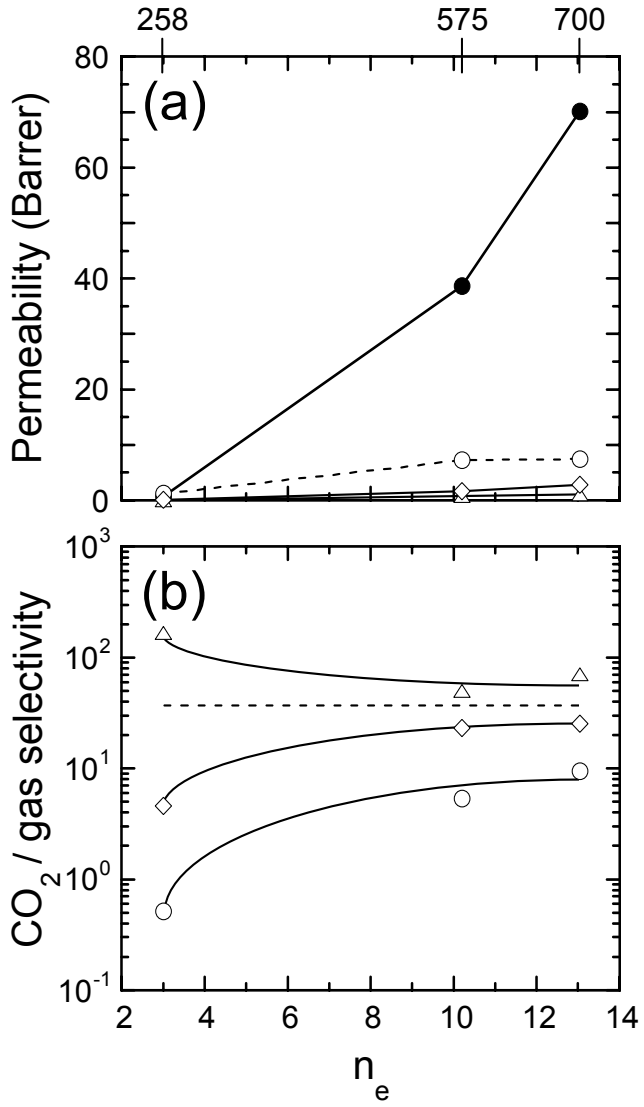

Figure 5.5. Dependence of (a) permeability and (b) CO_2/gas selectivity on cross-linked PEGda chain length (expressed in terms of the repeat number, n, shown in Fig.1) for several gases: CO_2 (J), H_2 (E), O_2 (A) and N_2 (C). The solid and dashed lines in (a) connect the data, whereas those in (b) serve as guides for the eye.

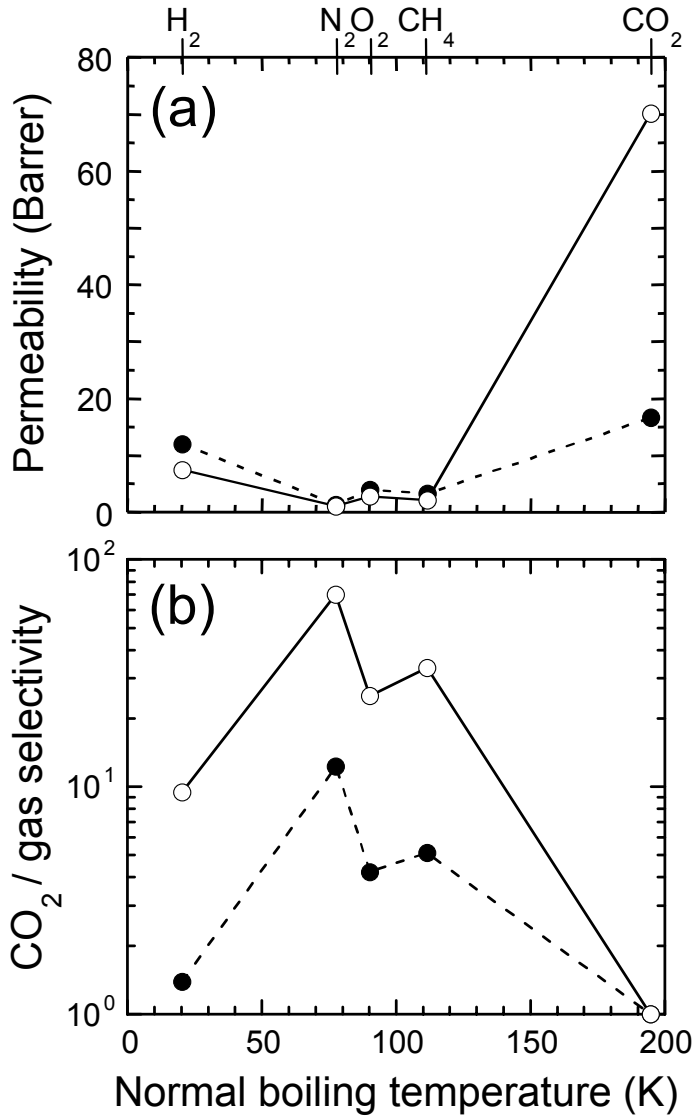

Figure 5.6. Variation of (a) permeability and (b) CO_2/gas selectivity with the normal boiling temperature (T_b) of several gases (labeled) in PE (J) and cross-linked PEGda700 (E) matrices. The solid and dashed lines connect the data.

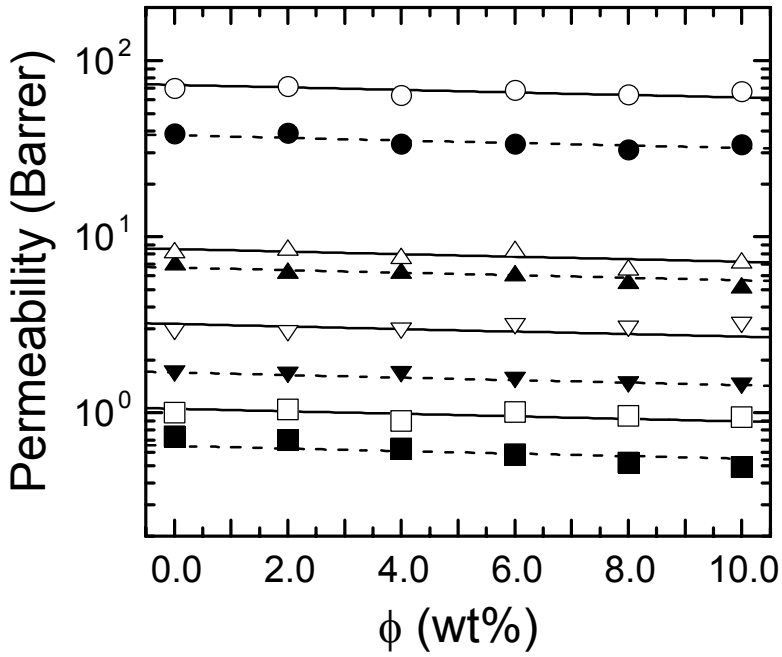

Figure 5.7. CO_2 (circles), H_2 (triangles), O_2 (inverted triangles) and N_2 (squares) permeabilities presented as functions of FS concentration (Φ) in cross-linked PEGda575 (filled symbols, dashed lines) and PEGda700 (open symbols, solid lines) nanocomposites. The lines displayed in this figure are regressed fits of Eq.5.5 to the data.

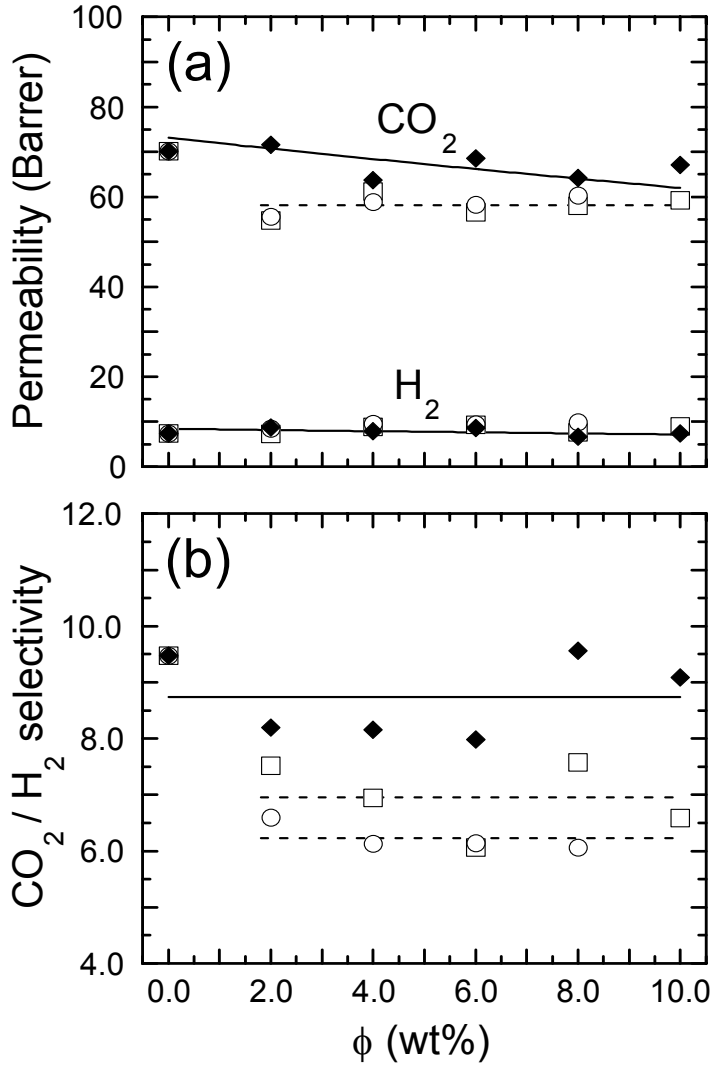

Figure 5.8. Dependence of (a) CO_2 and H_2 permeability and (b) CO_2/H_2 selectivity on filler concentration (Φ) for three nanoscale additives in cross-linked PEGda700: methacrylate functionalized FS (D), hydroxy-functionalized OC1 (G) and alkane-functionalized OC2 (E) (see the Experimental Section for organoclay designations). The solid lines are regressed fits of Eq.5.9 to the data corresponding to the PEGda700/FS nanocomposites, whereas the dashed lines denote averages in the data collected from the PEGda700/organoclay nanocomposites.

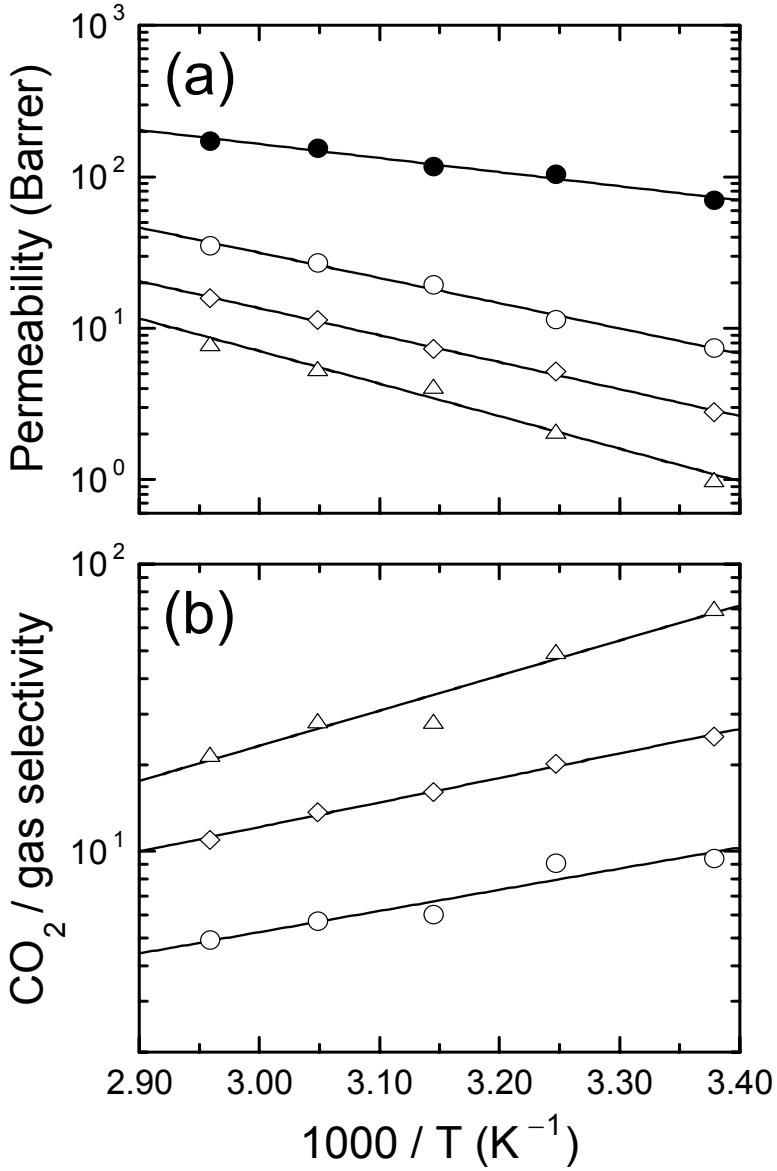

Figure 5.9. Variation of (a) permeability and (b) CO_2/gas selectivity with reciprocal temperature for several gases in cross-linked PEGda700: CO_2 (J), H_2 (E), O_2 (A) and N_2 (C). The solid lines are regressed fits of Arrhenius-type expressions (see Eq.5.10) to the data.

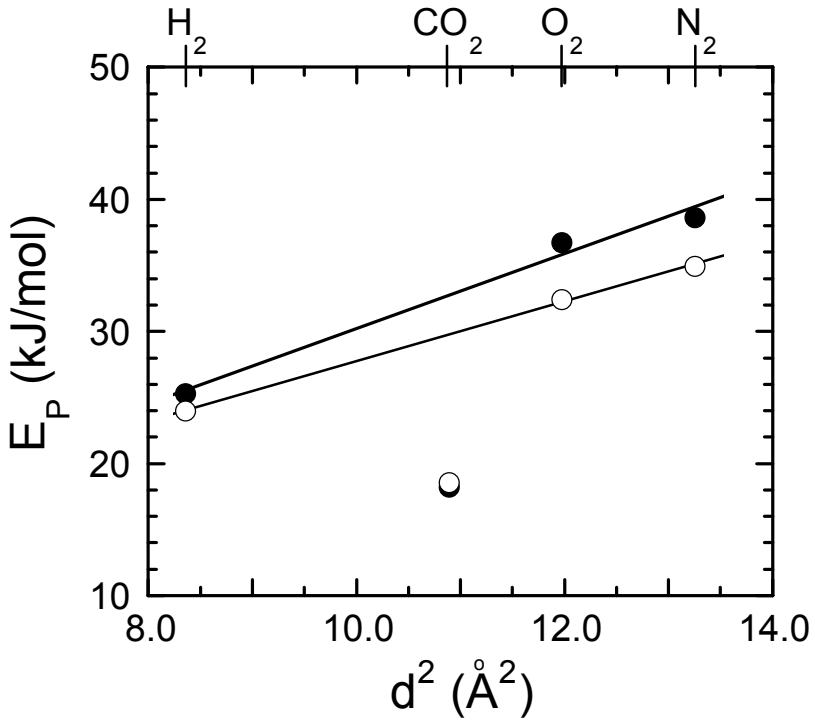

Figure 5.10. The activation energy of permeation (E_P) presented as a function of d^2, where d denotes the kinetic diameter of the gases labeled in the figure, in the cross-linked PEGda575 polymer (E) and PEGda575 nanocomposite with 10 wt% FS (J). The solid lines represent linear regressions to the data acquired from the nonpolar gases.

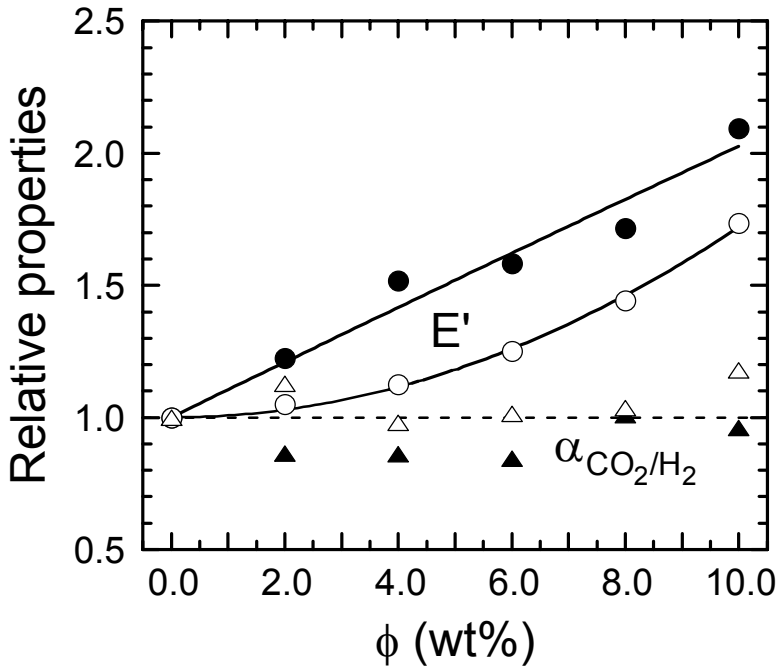

Figure 5.11. Effect of FS concentration (Φ) on the dynamic elastic tensile modulus (E', circles) and CO_2/H_2 selectivity (α_{CO_2/H_2}, triangles) normalized with respect to their values at Φ = 0 in cross-linked PEGda575 (filled symbols) and PEGda700 (open symbols). The solid lines serve as guides for the eye.

Chapter 6

Morphological, Mechanical and Gas-Transport Characteristics of Crosslinked Poly(propylene glycol): Homopolymers, Nanocomposites and Blends

6.1. Abstract

Linear polyethers possess unusually high CO_2 solubility and, hence, selectivity due to the presence of accessible ether linkages that can interact with the quadrupolar moment of CO_2 molecules. In this work, membranes derived from crosslinked poly(propylene glycol) diacrylate (PPGda) oligomers differing in molecular weight (M), as well as PPGda nanocomposites containing either an organically-modified montmorillonite clay or a methacrylate-terminated fumed silica, are investigated and compared with highly CO_2-selective poly(ethylene glycol) diacrylate (PEGda) homopolymer and nanocomposite membranes previously reported. The rheological and permeation properties of PPGda depend sensitively on M, with the elastic modulus decreasing, but CO_2 permeability and CO_2/H_2 selectivity increasing, with increasing M. Incorporation of either nanofiller into PPGda enhances the elastic modulus and reduces the gas permeability in the resultant nanocomposites without affecting CO_2/H_2 selectivity. Blending PPGda and PEGda prior to chemical crosslinking yields binary membranes that exhibit intermediate gas-transport properties accurately described by a linear rule of mixtures.

This chapter has been submitted for publication in Polymer.

6.2. Introduction

In an era of dwindling petroleum reserves, attention must be drawn to technologies based on new fuel feedstocks that are plentiful, sustainable, economical and environmentally benign. As a manufacturer of products that require enormous fuel consumption worldwide, the automotive industry has identified H_2 as its choice of fuel replacement, with H_2-powered automobiles already in production.[1] The development of H_2 fuel cells, a topic of increasing technological interest,[2-4] requires a relatively pure and abundant source of H_2, which is also used in the large-scale[5] synthesis of ammonia, fertilizer and synthetic polymers. One of the most important commercial routes to hydrogen starts with synthesis gas ("syngas"), a mixture of CO_2 and H_2 produced in the petrochemical industry from the two-step water-gas shift reaction, which accounts for over 96% of H_2 generated worldwide:[6]

$$C_nH_m + nH_2O \Leftrightarrow nCO + (m/2 + n)H_2$$

$$CO + H_2O \Leftrightarrow CO_2 + H_2$$

It is immediately apparent that H_2 must be purified from its mixture with CO_2, thereby requiring a cost-effective gas-separation strategy. Current technologies employ liquid amine absorption[7] or pressure-swing zeolitic adsorption[8] that suffer from operational drawbacks (*e.g.*, high reaction heat, chemical migration/toxicity, equipment corrosion and membrane frailty). Polymeric membranes, on the other hand, are, in general, mechanically robust, environmentally benign and easily processable, and therefore constitute an attractive option for CO_2 removal.

Due to the high diffusivity of H_2 relative to other gases through dense polymer matrices, commercially available polymer membranes tend to sieve CO_2 on the basis of molecular size and generate purified H_2 at the low-pressure permeate side of the membrane.[9,10] The cost

associated with H_2 repressurization is, however, prohibitive and presents a significant challenge to develop so-called "reverse-selective" membranes that are capable of removing CO_2 through to the low-pressure permeate side of the membrane while permitting H_2 to remain at (nearly) initial pressure. Reverse selectivity can be achieved by improving either the diffusivity or solubility (or both) of one penetrant relative to another in a gas mixture. Addition of nonporous nanoscale fillers such as fumed silica (FS) to glassy polymers that possess rigid backbones — *e.g.*, poly(4-methyl-2-pentyne)[11,12] and poly(2,2-bis(trifluoromethyl)-4,5-difluoro-1,3-dioxole-*co*-tetrafluoroethylene)[13] — increases free volume due to frustrated chain packing and, consequently, enhances organic vapor permeability and selectivity. Alternatively, reverse selectivity can be realized through judicious choice of a polymer possessing an intrinsically high solubility for a particular penetrant in a gas mixture. It is in this spirit that microphase-separated multiblock copolymers,[14-17] as well as microphase-ordered triblock copolymers,[18-20] containing linear polyether sequences (with accessible polar linkages that interact with CO_2 molecules) have been successfully used to achieve high CO_2 permeability and selectivity relative to other light gases (*e.g.*, H_2, N_2 and O_2). While such copolymer membranes consist of physically crosslinked networks that impart requisite mechanical integrity, permanent polyether-based networks can also be readily produced.

Our recent efforts[21,22] have focused on the feasibility of chemically-crosslinked poly(ethylene glycol) diacrylate (PEGda) and its nanocomposites with fumed silica (FS) and organically-modified clays (OCs) for use in selective acid-gas removal. These prior results have established that PEGda nanocomposites, despite their more tortuous permeation pathway,[23] exhibit excellent CO_2/H_2 selectivity, coupled with high CO_2 permeability and

superior mechanical properties, thereby adding a new benefit to the diverse attributes already afforded by polymer nanocomposites.[24,25] While the reverse-selective nature of crosslinked PEGda membranes for CO_2 removal has been examined in detail,[21,22] O'Neill *et al*.[26] report that the solubility of CO_2 is higher in poly(propylene glycol) (PPG) than in PEG due to the lower cohesive energy density of PPG. Motivated by these results, we now turn our attention to crosslinked poly(propylene glycol) diacrylate (PPGda) membranes with and without added nanofillers or a second polymer for selective CO_2 removal from mixtures with nonpolar gases. Since the efficacy of gas-separation membranes is largely governed by morphology[11,27-29] and the utility of such membranes is dependent on mechanical stability,[27,30] these essential design considerations are also addressed in this work. Direct comparisons with analogous PEGda membranes are made whenever possible.

6.3. Experimental

6.3.1. Materials

Two PPGda oligomers [CH_2=CH-COO-(CH_2-CH-CH_3O)$_n$-CO-CH=CH_2, where n is hereafter the integral number of repeat units per molecule] with number-average molecular weights (M) of 540 and 900 g mol^{-1}, as well as one PEGda oligomer [CH_2=CH-COO-(CH_2-CH_2-O)$_n$-CO-CH=CH_2] with M = 700 g mol^{-1} and 2,2'-azobisisobutyronitrile (AIBN) as the crosslinking agent, were purchased in liquid form from Aldrich Chemicals (Milwaukee, WI) and used without further purification. According to the manufacturer, the densities of the PPGda and PEGda oligomers used here, designated as PPGdaM and PEGdaM, respectively, were (in g cm^{-3}) 1.02 (PPGda540),1.01 (PPGda900) and 1.12 (PEGda700). A nonporous methacrylate-terminated FS with a mean primary diameter of 12 nm and a reported density of

~2 g cm^{-3} (Aerosil R711) was obtained from Degussa Corp. (Parsippany, NJ). The OC employed in this study was a montmorillonite clay modified with an alkane-functionalized quaternary ammonium (Cloisite® 93A) and was kindly provided by Southern Clay Products, Inc. (Gonsalez, TX). The aspect ratio of the OC platelets ranged from *ca*. 75 to 100, and the reported density of the OC was 1.88 g cm^{-3}.

6.3.2. Methods

The crosslinked PPGda homopolymer, nanocomposite and blend membranes investigated here were prepared by adding 0.5 wt% AIBN and up to 10 wt% nanofiller or up to 100 wt% PEGda to either PPGda540 or PPGda900 to form a visibly clear mixture upon stirring. After bubbles were removed under vacuum, each liquid was transferred to a flat glass plate onto which a second flat glass plate was placed to produce a film of uniform thickness. Following crosslinking for ~18 h at 80°C, films ranging in thickness from 30 to 300 μm were carefully removed from the glass plates for analysis. Transmission electron microscopy (TEM) was performed on thin sections of the 90/10 w/w PPGda900/FS nanocomposite produced by microtoming the film after it had been coated on each surface (to ensure isolation) with 20 nm Au/Pd and subsequently embedded in epoxy. Zero-loss TEM images were acquired on a Zeiss EM902 electron spectroscopic microscope operated at 80 kV. X-ray diffractometry (XRD) was performed on the pure OC, as well as on 90/10 w/w PPGda900/OC and PEGda700/OC nanocomposites, with an Inel XRG 3000 diffractometer operated at 35 kV and 30 mA using monochromated Cu K_α radiation over the 2θ range 2-120° to discern the extent to which the OC platelets are intercalated.

Pure-gas permeability measurements were performed using the constant-volume, variable-pressure approach described by Felder and Huvard.[31] Once vacuum was pulled on

both sides of a membrane of thickness *l* positioned within the permeation cell, the pressure of a gas (either CO_2, H_2, N_2 or O_2) was increased to a predetermined value on the upstream side of the membrane, resulting in permeation of the gas through the membrane into a vessel of known volume (V) on the downstream side. The downstream pressure was constantly monitored with a transducer connected to a computer. The permeability of each gas (P) was calculated from

$$P = \frac{Vl}{ART\Delta p}\left(\frac{dp}{dt}\right) \tag{6.1}$$

where A is the membrane area, R is the universal gas constant and T denotes absolute temperature. The transmembrane pressure (Δp) is equal to $p_2 - p_1$, where p_2 and p_1 are the upstream and downstream pressures, respectively, and dp/dt is the steady rate at which pressure increases on the downstream side. Unless otherwise stated, the permeability values reported herein were measured at 23°C and an upstream pressure of 6.8 atm. The downstream pressure was held constant at 0.007 atm, in which case $\Delta p \approx p_2$ and p_2 can furthermore be regarded as the transmembrane pressure The dynamic elastic and viscous tensile moduli (E' and E", respectively) were measured as functions of strain amplitude at ambient temperature and a frequency of 10 Hz on a Rheometrics Solids Analyzer (RSA-II). Values of E' reported here were obtained under conditions of linear viscoelasticity wherein E' is independent of strain amplitude.[27,32]

6.4. Results and Discussion

6.4.1. Crosslinked PPGda Homopolymers

Values of E' acquired from the crosslinked PPGda540 and PPGda900 membranes are (*i*) consistently greater in magnitude than the corresponding values of E" and (*ii*) independent of

frequency (data not shown). These signatures satisfy the conditions required[33] to establish the existence of a polymer network that exhibits an elastic response to an imposed deformation. Figure 1a shows the average E' extracted from strain sweeps as a function of M and reveals that E' decreases substantially with increasing PPGda chain length. This observation indicates that the network becomes more open and flexible within increasing M, in agreement with intuitive expectation. Included for comparison in Fig.6.1a are elastic modulus values recorded from two PEGda membranes, demonstrating that E' values measured from both series of crosslinked polyethers exhibit a similar dependence on M. The solid line displayed in Fig.6.1a is a power-law fit to the two data sets and yields a scaling relationship of the form $E' \sim M^{\gamma}$, where $\gamma = -1.6$. In a crosslinked polymer network, the plateau modulus (E), approximated by E', can be expressed as

$$E = \rho_x RT/M_c \qquad (6.2)$$

where ρ_x constitutes a measure of the crosslink density and M_c is the molecular weight between crosslink sites. If M_c is taken as M, the crosslink density can be discerned as an explicit function of M from the E'(M) data provided in Fig.6.1a. Computed values of ρ_x are presented in Fig.6.1b for the PPGda and PEGda membranes and show that the crosslink density generally decreases, and the networks tend to become less constrained, with increasing M in each membrane series.

Since the membranes are molecularly homogeneous and virtually featureless, we next turn our attention to their gas-transport properties. Permeation of a molecule across a dense polymer membrane generally occurs when a pressure gradient exists between the upstream and downstream faces of the membrane. Here, the permeability of penetrant *i* (P_i) is defined[34] as

$$\mathbf{P_i = \frac{N_i \times l}{\Delta p_i}} \tag{6.3}$$

where N_i is the steady-state gas flux of species *i* through the film, and Δp_i is the difference between the upstream and downstream partial pressures of *i*. When the downstream pressure is negligible and Fickian diffusion serves as the rate-limiting step by which molecular transport proceeds, the permeability can be expressed in terms of the solution-diffusion model[35] as

$$P_i = D_i \times S_i \tag{6.4}$$

Here, D_i is the concentration-averaged diffusion coefficient, and S_i is the solubility defined as the ratio of penetrant concentration dissolved in the upstream face relative to the upstream partial pressure in the gas phase. According to the solution-diffusion model, penetrant molecules (*i*) first dissolve into the upstream (high pressure) face of the film, (*ii*) then diffuse across the film and (*iii*) ultimately desorb at the downstream face. Thus, the permeability of a penetrant depends on both its diffusivity and solubility within a particular homopolymer, and these properties can be systematically varied through judicious choice of molecular design (*e.g.*, chemical structure and molecular weight) and environmental factors (*e.g.*, pressure and temperature).

The permeability of penetrant species A relative to that of species B provides an established measure of molecular separation efficacy and is given by the ideal selectivity ($\alpha_{A/B}$), *viz.*,

$$\mathbf{\alpha_{A/B} = \frac{P_A}{P_B} = \left[\frac{D_A}{D_B}\right] \times \left[\frac{S_A}{S_B}\right]} \tag{6.5}$$

The ratio D_A/ D_B is referred to as the diffusivity, or mobility, selectivity, whereas S_A/ S_B is the solubility selectivity. These contributions to the overall selectivity can be used to describe the mechanism of gas separation in dense polymer membranes, which are classified as either rubbery or glassy. As the name implies, rubbery membranes possess a relatively low glass transition temperature (T_g) and, hence, flexible chains that readily accommodate penetrant species differing in size. Due to their weak size-sieving capability, membranes in this genre are typically used to separate penetrants on the basis of solubility. Glassy membranes, on the other hand, consist of rigid chains that generally separate penetrants on the basis of size, allowing smaller penetrants to permeate faster than larger ones. The linear polyether (PPGda and PEGda) materials under current investigation can be considered rubbery membranes due to their low T_gs, in which case preferential separation of CO_2 relative to other light gases demands high CO_2 solubility in these polyethers. Thus, a reverse-selective polymer membrane exhibiting high CO_2/H_2 selectivity for use in hydrogen purification can only be achieved when the solubility selectivity dominates over the diffusivity selectivity in eq.6. 5. As alluded to above, the solubility and, hence, permeability of CO_2 may be controlled by varying environmental factors such as upstream pressure. Pressure-dependent molecular transport is apparent in Fig.6.2, which displays the permeability of CO_2 and H_2 in the PPGda900 membrane (Fig.6.2a) and the corresponding CO_2/H_2 selectivity (Fig.6.2b).

While the permeability of H_2 is virtually unaffected by a pressure increase of ~7 atm, the surprisingly high CO_2 permeability increases monotonically with increasing pressure in Fig.6.2a. An increase in pressure typically reduces (slightly) the free volume available for molecular transport and, consequently, penetrant permeability,[36] but rubbery polymers are capable of swelling under identical conditions. Thus, the larger, more soluble CO_2 molecules

swell the PPGda900 membrane more than the H_2 molecules as the available gas reservoir (pressure) is increased. This explanation accounts for the linear increase in CO_2 permeability, as well as the negligible change in H_2 permeability, with increasing pressure. Similar behavior is observed for a PEGda700 membrane, which is included for comparison in Fig.6.2, and PEG-containing block copolymers,[14,15,19] implying that CO_2 generally possesses an inherently high affinity for linear polyethers. Since the permeability of CO_2 is considerably higher in PPGda900 than in PEGda700 (both have ~14 ether linkages per molecule), we deduce that the solubility of CO_2 is higher in PPG relative to PEG, in accord with previous findings.[26] Due primarily to the pressure dependence of CO_2 permeability, the CO_2/H_2 selectivity presented in Fig.6.2b is likewise linearly dependent on pressure. It is important to recognize, however, that, while the PPGda900 membrane is more permeable to CO_2, the PEGda700 membrane is more CO_2-selective. This difference can be attributed to the higher permeability of H_2 in PPGda900 (see Fig.6.2a) that accompanies incorporation of a bulky pendant methyl group along the polymer backbone. This subtle structural difference between the two polyethers appears sufficient to alter chain packing/ cohesion in such fashion as to enhance the sorptive capacity of both CO_2 and H_2.

The CO_2 permeability and selectivity data provided in Fig.6.2 establish that the PPGda900 membrane is reverse-selective, although less so than its PEGda700 counterpart. This observation is attributed to the high CO_2 solubility afforded by the presence of polar ether linkages along the polymer backbone. The effect of the number of ether linkages/molecule ($n_e = n + 1$) on CO_2 permeability and selectivity relative to H_2 is displayed for semicrystalline polypropylene[37] (PP, $n_e = 0$), PPGda540 ($n_e \approx 8$) and PPGda900 ($n_e \approx 14$) in Figs. 3a and 3b, respectively. An increase in n_e promotes a sharp increase in CO_2

permeability, but a less pronounced increase in CO_2/H_2 selectivity. In fact, Fig.6.3b confirms that, while PP is H_2-selective, both PPGda membranes are clearly CO_2-selective. While the permeability of each gas included in Fig.6.3a tends to increase with increasing n_e, the corresponding gas/H_2 selectivity (with the exception of CO_2) exhibits very little variation among the three rubbery polymers wherein permeability is governed principally by penetrant solubility, signified, for instance, by the normal boiling temperature. Penetrant sorption into a dense polymer is envisaged[34] to proceed by two thermodynamically-driven steps. In the first, the gaseous penetrant condenses on the upstream face of the membrane, whereas the second step requires generation of voids within the polymer matrix to accommodate the denser penetrant and permit subsequent diffusion. Although the sorption of nonpolar penetrants is generally dictated by the first step, the existence of attractive interactions between the penetrant and polymer may favor the second step by enhancing mixing and, hence, penetrant solubility within the polymer.[38,39] This is indeed the case for CO_2, with its quadrupolar moment that arises from the difference in electronegativity between the constituent C and O atoms,[40] and PEG-based polymers, wherein CO_2 solubility is higher than that predicted from established metrics of penetrant condensability (*e.g.*, the normal boiling temperature in Fig.6.3).

The permeability of CO_2 in the PPGda and PEGda membranes investigated here, as well as two other PEGda membranes described elsewhere,[22] is presented as a function of M in Fig.6.4a, and the data suggest a common (systematic) trend for both polyether series. The substantial increase in CO_2 permeability promoted by M coincides with an increase in the number of ether linkages per unit volume (data not shown) and reductions in the stiffness (E') and crosslink density (ρ_x) of the molecular network (see Fig.6.1). Both considerations,

corresponding to a greater density of sites for CO_2/ether interaction and a greater ability on the part of the polymer matrix to accommodate more CO_2 molecules (by swelling), are expected to enhance the overall solubility and, hence, permeability of CO_2. To probe the influence of the first consideration in more detail, an ether linkage density (ε) is defined[21] as

$$\varepsilon = \frac{n_e N_A \rho}{M} \tag{6.6}$$

where N_A is Avogadro's number and ρ denotes the mass density of each polyether (1.12 g cm^{-3} according to the manufacturer). Figure 4b shows the dependence of CO_2/H_2 selectivity on ε for all the PPGda and PEGda membranes included in Fig.6.4a. Although the data are somewhat scattered, an increase in ε generally tends to promote an increase (which appears nearly linear) in selectivity for both polyether series. While it would be desirable to extend this correlation to higher values of M, the onset of crystallization in PPGda and PEGda at ambient temperature effectively precludes such analysis, since polymer crystals generally serve as large, impermeable obstacles that lower penetrant permeability.[41] In the next section, however, the utility of adding impermeable nanoscale objects (*e.g.*, FS and OC) to the PPGda membranes is explored.

6.4.2. Crosslinked PPGda Nanocomposites

A TEM image of the PPGda900 membrane containing 10 wt% FS is presented in Fig.6.5 and confirms that the FS nanoparticles are uniformly distributed much in the same fashion as the analogous PEGda700/FS nanocomposite membranes previously reported.[21] While nanocomposites consisting of crosslinked PEGda and a different clay (hectorite) have been successfully imaged by TEM,[27] attempts to do so with the present PPGda900/OC membrane have repeatedly failed due to the relatively soft nature of the crosslinked material (see

Fig.6.1a). To ascertain the aggregate morphology of the OC platelets alone and in the polyether membranes, we turn our attention to XRD analysis. A series of XRD patterns acquired from the neat OC, as well as the 90/10 PPGda900/OC and PEGda700/OC nanocomposites, is displayed in Fig.6.6 and reveals that the characteristic spacing of the OC (Fig.6.6a) is 2.46 nm, which is slightly larger than that reported by the manufacturer (2.36 nm). The spacing of the PPGda900/OC nanocomposite extracted from Fig.6.6b is 3.22 nm, indicating that the hydrophobic platelets are marginally intercalated by the hydrophobic polyether. In contrast, the spacing of the PEGda700/OC membrane (Fig.6.6c) is only 2.46 nm, in which case the OC platelets are unaffected by the hydrophilic PEGda700. This is contrary to results obtained from a comparable PEGda700 nanocomposite prepared with a different OC (Cloisite® 30B, a montmorillonite clay modified with an alcohol-functionalized quaternary ammonium).[42] In this case, XRD patterns collected from the OC and a 90/10 PEGda700/OC nanocomposite yield spacings of 1.83 (1.85 according to the manufacturer) and 3.15 nm, respectively, confirming that the hydrophilic OC platelets are, in fact, intercalated by PEGda700 molecules. Thus, the degree of OC intercalation in the two polyethers is sensitive to the degree to which the surface functionalities on the platelets interact with the surrounding polyether medium. This consideration is of general importance, since the extent of nanofiller aggregation will affect the mechanical properties of,[43] as well as penetrant transport in,[28] the polyether membranes under investigation in this work.

Representative strain sweeps collected from the neat PPGda900 membrane and its nanocomposites with 10 wt% FS and OC are shown for comparison in Fig.6.7 and demonstrate that (*i*) the PPGda900 and PPGda900/FS membranes exhibit linear viscoelasticity beyond 100% strain, and (*ii*) the OC is more effective than the FS at

increasing the magnitude of the dynamic elastic modulus (E'). The reduction in the range of linear viscoelasticity and the precipitous drop in E' for the PPGda900/OC membrane have been previously reported by Walls *et al*.[27] and are attributed to slippage of neighboring OC platelets during deformation. The superior efficacy of the OC nanofiller relative to FS is observed over the entire range of nanocomposite compositions examined here. Figure 8a shows E' as a function of nanofiller content (ϕ, expressed as a weight percentage) for both PPGda900 and PEGda700 with FS and OC nanofillers. Whereas the OC promotes the greatest increase in E' for the PPGda900 membrane series, the FS is generally more effective at increasing E' in the PEGda700 series. This difference in mechanical performance reflects the degree of OC intercalation and, hence, OC/matrix interaction discussed above. A normalized E' enhancement, defined as $E'(\phi) / E'(\phi = 0)$, is displayed in Fig.6.8b and provides a more accurate assessment of nanofiller benefit. In this representation, data from the PPGda900/FS and PEGda700/FS nanocomposites are comparable, suggesting that the FS nanoparticles function equally well in both polyether matrices, in qualitative agreement with morphological results obtained by TEM (see Fig.6.5 and ref. 21).

The permeabilities of CO_2, H_2, O_2 and N_2 are presented as functions of ϕ in PPGda900 nanocomposites containing either FS or OC in Fig.6.9. As in Fig.6.3 for the neat PPGda540 and PPGda900 membranes, the order of gas permeability in these nanocomposite membranes is given by $CO_2 > H_2 > O_2 > N_2$. Two interesting features of this figure are that (*i*) the permeability of CO_2 in the PPGda900/OC nanocomposites tends to be marginally higher than in the corresponding PPGda900/FS membranes, and (*ii*) the permeability data collected for H_2, O_2 and N_2 are virtually independent of nanofiller type over the entire composition range explored. In the same vein as the mechanical properties discussed in regard to Fig.6.8, the

difference in permeation behavior evident in Fig.6.9 is again attributed to the extent of nanofiller aggregation. The solid lines included in Fig.6.9 are predictions obtained for obstructed gas permeation from the model originally proposed by Maxwell[44] to describe the effect of dispersed spheres in a dielectric medium. This model, which accounts for the tortuosity introduced by impermeable (nonporous) particulates in a dense polymer matrix, can be expressed as

$$\mathbf{P_{c,i} = P_{m,i}\left[\frac{1-\Phi}{1+\Phi/2}\right]} \tag{6.7}$$

where $P_{c,i}$ and $P_{m,i}$ represent the permeabilities of penetrant *i* in the composite and matrix media, and Φ is the volume fraction of the nanofiller. Close examination of Fig.6.9 immediately reveals that the predictions from eq.6.7 differ markedly from the CO_2 permeability data collected from the PPGda900/FS nanocomposites. It is interesting to note that this discrepancy does not exist for PEGda700/FS nanocomposites.[21] A measure of the predictive accuracy of eq.6.7 can be written as

$$\mathbf{\xi_i = \frac{1}{k}\sum_{j=1}^{k}\sqrt{\left\{P_{e,i} - P_{p,i}\right\}^2}} \tag{6.8}$$

Here, $P_{e,i}$ and $P_{p,i}$ are the experimental and predicted permeabilities of penetrant *i*, and *k* is the number of data points sampled. Values of ξ_i are listed in Table 6.1 for each penetrant in each nanocomposite portrayed in Fig.6.9 and confirm that, despite the generally spherical nature of FS, the permeability of CO_2 in the PPGda900/FS series deviates the most from predicted behavior. It is somewhat surprising that the Maxwell[44] model predicts the permeation behavior of all four penetrants in the PPGda900/OC series with such accuracy. Nielsen[45] has modified eq.6.7 to account for the anisotropy introduced by nonspherical particulates (*e.g.*, platelets) to yield

$$P_{c,i} = P_{m,i}\left[\frac{1-\Phi}{1+\beta\Phi/2}\right] \tag{6.9}$$

where β is the aspect ratio of the platelets. Values of β regressed from the data shown in Fig.6.9 are 5.94 for CO_2 and 5.10 for H_2. Experimental scatter in the data precludes assessment of physically meaningful values of β for O_2 and N_2. As indicated by the values of ξ_I listed in Table 6.1 for CO_2 and H_2 permeability in the PPGda900/OC nanocomposites, predictions generated from eq.6.9 are in better overall agreement with the data than those from eq.6.7. Corresponding values of β ascertained for CO_2 in PEGda700/OC nanocomposites prepared with either Cloisite® 93A or Cloisite® 30B could not be accurately determined, since the data are not well-represented by eq.6.9. More complex expressions proposed[28] for $P_{c,I}$ are apparently required to describe the data.

The corresponding CO_2/H_2 selectivities determined from the data presented in Fig.6.9 are displayed as a function of ϕ for the PPGda900/FS and PPGda900/OC nanocomposites in Fig.6.10a, and reveal that CO_2/H_2 selectivity in these membranes is, for the most part, independent of both nanofiller concentration (ϕ) and nanofiller type (FS *versus* OC). This feature is contrary to results obtained from PEGda700/FS and PEGda700/OC nanocomposites (included for comparison in Fig.6.10a). In these membranes, the CO_2/H_2 selectivity of the PEGda700/FS nanocomposites fluctuates near the value corresponding to the neat PEGda700 membrane, whereas the CO_2/H_2 selectivity of the PEGda700/OC nanocomposites drops sharply and then levels off to a constant value. If the permeabilities of CO_2 and H_2 in these polyether nanocomposites are accurately represented by Eqs.6.7 or 6.9, then by 6.5 the CO_2/H_2 selectivity should be independent of ϕ, which is only observed for the nanocomposites derived from PEGda700. Figure 10b shows another technologically relevant

quantity — the CO_2/N_2 selectivity (an important metric for air-purification purposes) — discerned from the data provided in Fig.6.9, and confirms that this selectivity is likewise independent of ϕ for both PPGda900 and PEGda700 nanocomposites containing FS. As anticipated from Figs. 2 and 3, the CO_2/H_2 and CO_2/N_2 selectivities in Fig.6.10 are profoundly greater for the PEGda700 (nanocomposite) membranes relative to the PPGda900 (nanocomposite) membranes. In the next section, we explore the feasibility of preparing membranes with intermediate properties from crosslinked homogeneous blends of the two parent polyethers.

6.4.3. Crosslinked PPGda/PEGda Blends

For certain specialty applications, the CO_2 permeability and/or selectivity relative to another gas should be maximized to achieve satisfactory gas separation. In the particular case of membranes based on PEGda, this can be achieved through judicious choice of M, nanofiller type/content, pressure and temperature.[21,22] Alternatively, some applications require that a full set of optimized mechanical and gas-transport properties be designed into a material, thereby requiring control over property development in multicomponent polymer systems. It is in this spirit that we now examine crosslinked blends of hydrophobic PPGda900 and hydrophilic PEGda700 to ascertain if homogeneous membranes exhibiting intermediate gas-transport properties can be produced in straightforward fashion. It must be recognized, however, that binary blends of relatively low-molecular-weight PPG and PEG homopolymers can exhibit surprisingly complex phase behavior arising from, for instance, hydrogen-bond clusters.[46] Through careful selection of homopolymer molecular weight, such complications can be minimized, if not altogether avoided. Since no evidence of gross phase

separation has been detected in the present work (although we do not discount the possibility of such), the blends used to produce binary PPGda900/PEGda700 membranes are presumed to be miscible under the conditions of preparation and analysis. Figure 11 illustrates the dependence of CO_2 and H_2 permeability (Fig.6.11a) and CO_2/H_2 selectivity (Fig.6.11b) on PEGda700 concentration (denoted by the mass fraction ω) in a series of crosslinked PPGda900/PEGda700 blends. As ω is increased, the permeabilities of CO_2 and H_2 decrease, but the CO_2/H_2 selectivity increases, monotonically. The dashed lines included in Fig.6.11a represent predictions computed for the permeability of each penetrant in the crosslinked blend ($P_{blend,i}$) from the linear rule of mixtures:

$$P_{blend,i} = P_{PPG,i}(1 - \omega) + P_{PEG,i}(\omega) \qquad (6.10)$$

Here, $P_{PPG,i}$ and $P_{PEG,i}$ are the permeabilities of penetrant *i* in the neat PPGda900 and PEGda700 membranes, respectively. Corresponding values of the CO_2/H_2 selectivity are obtained as a function of ω from eq.6.10 in conjunction with eq.6.5. As Fig.6.11 attests, these predictions are in favorable agreement with the data, indicating that this design strategy can be used to generate, in systematic fashion, polyether blends possessing intermediate gas-transport properties.

6.5. Conclusions

Crosslinked polyethers, as well as their nanocomposites and blends, show tremendous promise as reverse-selective membranes for targeted acid-gas (*e.g.*, CO_2) removal. Membranes derived from PEGda are highly effective for this purpose,[21,22] but analogous membranes prepared from PPGda also exhibit CO_2 selectivity. While the permeability of CO_2 in PPGda membranes is consistently and considerably higher than that measured in

PEGda systems, the corresponding CO_2/H_2 and CO_2/N_2 selectivities, which constitute good indicators for H_2 and air purification, are significantly higher in the PEGda membranes. In both polyether series, an increase in oligomer molecular weight promotes systematic reductions in elastic modulus and crosslink density, but increases in CO_2 permeability and CO_2/H_2 selectivity. Addition of an inorganic nanofiller such as a fumed silica or an organically-modified clay improves the elastic modulus to an extent that is commensurate with the degree of nanofiller dispersion, which, in turn, reflects the level of compatibility between the surface functionalities on the nanofiller and the polymer matrix.[43] This factor is likewise observed to affect the permeation and relative selectivity of penetrants in PPGda and PEGda. We have furthermore demonstrated that binary polyether membranes with intermediate gas-transport properties can be controllably achieved by crosslinking homogeneous PPGda/PEGda blends. The results reported herein confirm that crosslinked polyether membranes are generally CO_2-selective due to their high CO_2 solubility, and that they constitute a versatile platform from which to develop novel materials with beneficial gas-separation properties.[47]

6.6. Acknowledgements

This work was supported by the U. S. Department of Energy under Contract No. DE-FG02-99ER14991 and the REU Program of the National Science Foundation.

6.7. References

1. Winter, U.; Weidner, H. *Fuel Cells* **2003**, *3*, 76.
2. Hefner, R. A. *Inter. J. Hydrog. Energy* **2002**, *27*, 1.
3. Ogden, J. M. *Phys. Today* **2002**, *55*, 69.
4. Young, S. *Nature* **2001**, *414*, 487.
5. *Chemical & Engineering News* **2002**, June 24, 61.
6. Kratz, W. C.; Rarig, D. L.; Pietratonio, J. M. *AIChE Symp. Ser.* **1988**, *84*, 36.
7. Kohl, A.; Nielson, R. *Gas Purification*; Gulf Publishing Co.: Houston, TX, 1997.
8. Tavolaro, A.: Drioli, E. *Adv. Mater.* **1999**, *11*, 975.
9. Petropoulos, J. H. *Mechanisms and Theories for Sorption and Diffusion of Gases in Polymers*; CRC Press: Boca Raton, 1994.
10. Aoki, T. *Prog. Polym. Sci.* **1999**, 24, 951.
11. Merkel, T. C.; Freeman, B. D.; Spontak, R. J.; He, Z.; Pinnau, I.; Meakin, P.; Hill, A. J. *Science* **2002**, *296*, 519.
12. Merkel, T. C.; Freeman, B. D.; Spontak, R. J.; He, Z.; Pinnau, I.; Meakin, P.; Hill, A. J. *Chem. Mater.* **2003**, *15*, 109.
13. Merkel, T. C.; He, Z. J.; Pinnau, I.; Freeman, B. D.; Meakin, P.; Hill, A. J. *Macromolecules* **2003**, *36*, 8406.
14. Okamoto, K. -I.; Fujii, M.; Okamyo, S.; Suzuki, H.; Tanaka, K.; Kita, H. *Macromolecules* **1995**, *28*, 6950.
15. Bondar, V. I.; Freeman, B. D.; Pinnau, I. *J. Polym. Sci. B: Polym. Phys.* **1999**, *37*, 2463.
16. Bondar, V. I.; Freeman, B. D.; Pinnau, I. *J. Polym. Sci. B: Polym. Phys.* **2000**, *38*, 2051.
17. Kim, J. H.; Seong, Y. H.; Lee, Y. M. *J. Membr. Sci.* **2001**, *190*, 179.
18. Patel, N. P.; Spontak, R. J. *Macromolecules* (in press).
19. Patel, N. P.; Spontak, R. J. *Macromolecules* (submitted).
20. Spontak, R. J.; Patel, N. P. In *Developments in Block Copolymer Science and Technology*; Hamley, I. W., Ed.; Wiley: New York, 2004, pp. 159-212.
21. Patel, N. P.; Miller, A. C.; Spontak, R. J. *Adv. Mater.* **2003**, *15*, 729.
22. Patel, N. P.; Miller, A. C.; Spontak, R. J. *Adv. Funct. Mater.* (submitted).
23. Petropoulos, J. H. *J. Polym. Sci. B: Polym. Phys.* **1985**, *23*, 1309.
24. Rothon, R. N. *Adv. Polym. Sci.* **1999**, *139*, 67.

25. Krishnamoorthi, R.; Vaia, R. A. (Eds.) *Polymer Nanocomposites: Synthesis, Characterization and Modeling*; American Chemical Society: Washington, D. C., 2002; Vol. 804.
26. O'Neill, M. L.; Cao, Q.; Fang, M.; Johnston, K. P.; Wilkinson, S. P.; Smith, C. D.; Kerschner, J. L.; Jureller, S. H. *Ind. Eng. Chem. Res.* **1998**, *37*, 3067.
27. Walls, H. J.; Riley, M. W.; Gupta, R. R.; Spontak, R. J.; Fedkiw, P. S.; Khan, S. A. *Adv. Funct. Mater.* **2003**, *13*, 710.
28. Subramanian, P. M.; Plotzker, I. G. In *Polymer Blends, Vol. 2*; Paul, D. R., Bucknall, C. B., Eds.; Wiley: New York, 2000; Chap. 30.
29. Weinkauf, D. H.; Paul, D. R. *J. Polym. Sci. B: Polym. Phys.* **1992**, 30, 817.
30. Burns, R. L.; Koros, W. J. *Macromolecules* **2003**, *36*, 2374.
31. Felder, R. M.; Huvard, G. S. *Permeation, Diffusion and Sorption of Gases and Vapors*; Fava, R., Ed.; Academic Press: New York, 1978; Vol. 16C, p. 315.
32. Macosko, C. W. *Rheology: Principles, Measurements and Applications*; VCH: New York, 1994.
33. Kavanagh, G. M.; Ross-Murphy, S. B. *Prog. Polym. Sci.* **1998**, *23*, 533.
34. Ghosal, K.; Freeman, B. D. *Polym. Adv. Technol.* **1994**, *5*, 673.
35. Graham, T. *Philos. Mag.* **1866**, *32*, 401.
36. Koros, W. J.; Hellums, M. W. ; In *Encyclopedia of Polymer Science and Engineering*; Kroschwitz, J. I., Ed.; Wiley: New York, 1989; Supplement volume, pp. 724-802.
37. Naito, Y.; Mizoguchi, K.; Terada, K.; Kamiya, Y. *J. Polym. Sci. B: Polym. Phys.* **1991**, *29*, 457.
38. Story, B. J.; Koros, W. J. *J. Membr. Sci.* **1992**, *67*, 191.
39. Ghosal, K.; Chern, R. T.; Freeman, B. D.; Savariar, R. *J. Polym. Sci. B: Polym. Phys.* **1995**, *33*, 657.
40. Garzon, B.; Lago, S.; Vega, C.; de Miguel, E.; Rull, L. F. *J. Chem. Phys.* **1994**, *101*, 4166.
41. Michaels, A. S.; Bixler, H. J. *J. Polym. Sci.* **1961**, *50*, 393.
42. Bharadwaj, R. K.; Mehrabi, A. R.; Hamilton, C.; Trujillo, C.; Murga, M.; Fan, R.; Chavira, A.; Thompson, A. K. *Polymer* **2002**, *43*, 3699.
43. Raghavan, S. R.; Hou, J.; Baker, G. L.; Khan, S. A. *Langmuir* **2000**, *16*, 1066.

44. Maxwell, C. *Treatise on Electricity and Magnetism*; Oxford University Press: London, 1873; Vol. 1.
45. Nielsen, L. W. *J. Macromol. Sci*. **1967**, *A1*, 929.
46. Eckert, S.; Meier, G.; Alig, I. *Phys. Chem. Chem. Phys.* **2002**, *4*, 3743.
47. Shiflett, M. B.; Foley, H. C. *Science* **1999**, *285*, 1902.

Table 6.1. Predictive capability assessment (ξ_i) values discerned for PPGda900 nanocomposites.[a]

Nanofiller	CO_2	H_2	O_2	N_2
FS	13.68	1.56	0.16	0.24
OC	7.80	1.32	0.55	0.79
OC[b]	3.14	0.49	—	—

[a] The parameter tabulated here is defined by eq.6. 8 and signifies greater accuracy of eq.6. 7 as it approaches zero.

[b] Parameters are determined on the basis of eq.6. 9 along with the values of β provided in the text.

List of symbols:

E = open circle

J = filled circle

C = open triangle

H = filled triangle

G = open square

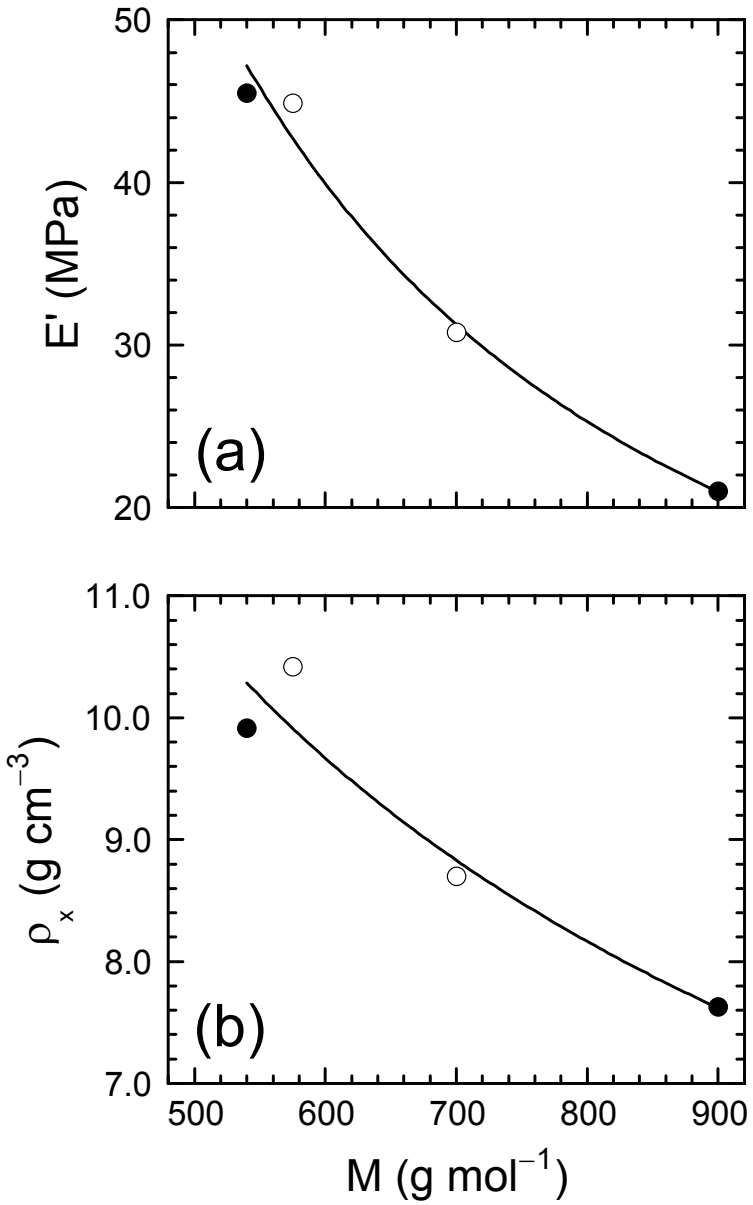

Figure 6.1. Dependence of (a) the dynamic elastic tensile modulus (E') and (b) the crosslink density (ρ_x) on the oligomer molecular weight (M) of crosslinked PPGda (J) and PEGda (E) membranes at ambient temperature. The solid line in (a) is a power-law fit to the data, whereas the solid line in (b) serves as a guide for the eye.

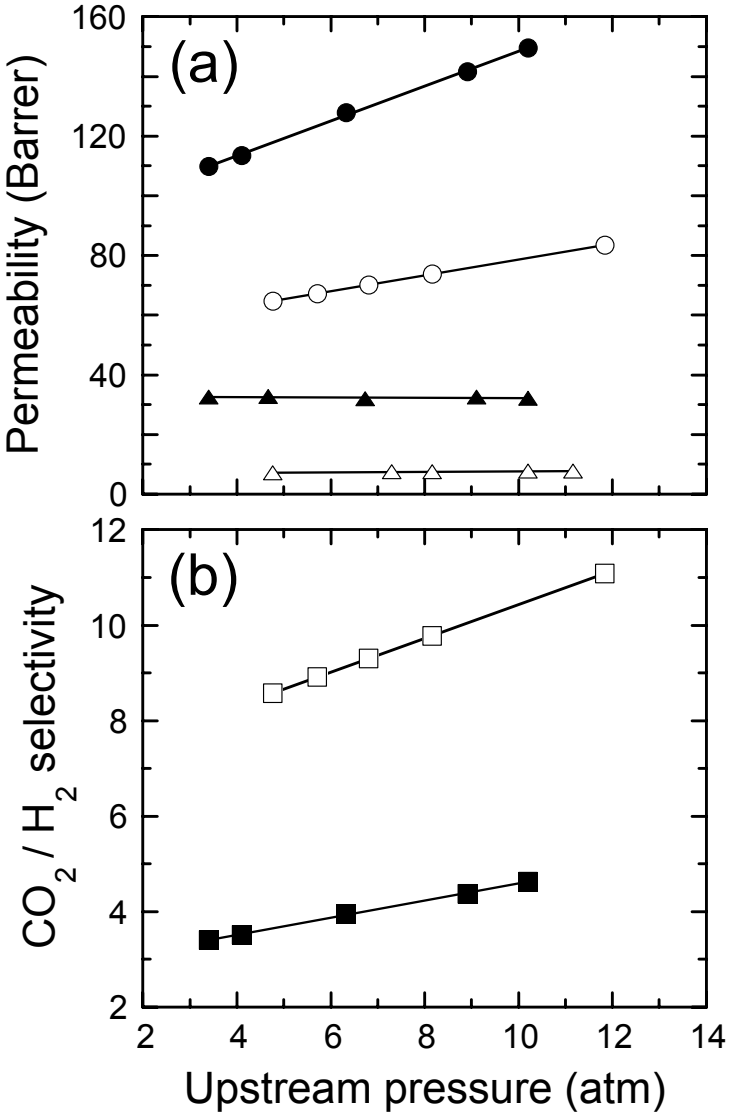

Figure 6.2. The (a) permeabilities of CO_2 (circles) and H_2 (triangles) and (b) CO_2/H_2 selectivity presented as functions of upstream (transmembrane) pressure in PPGda900 (filled symbols) and PEGda700 (open symbols) membranes at 23°C. The solid lines are linear regressions to the data.

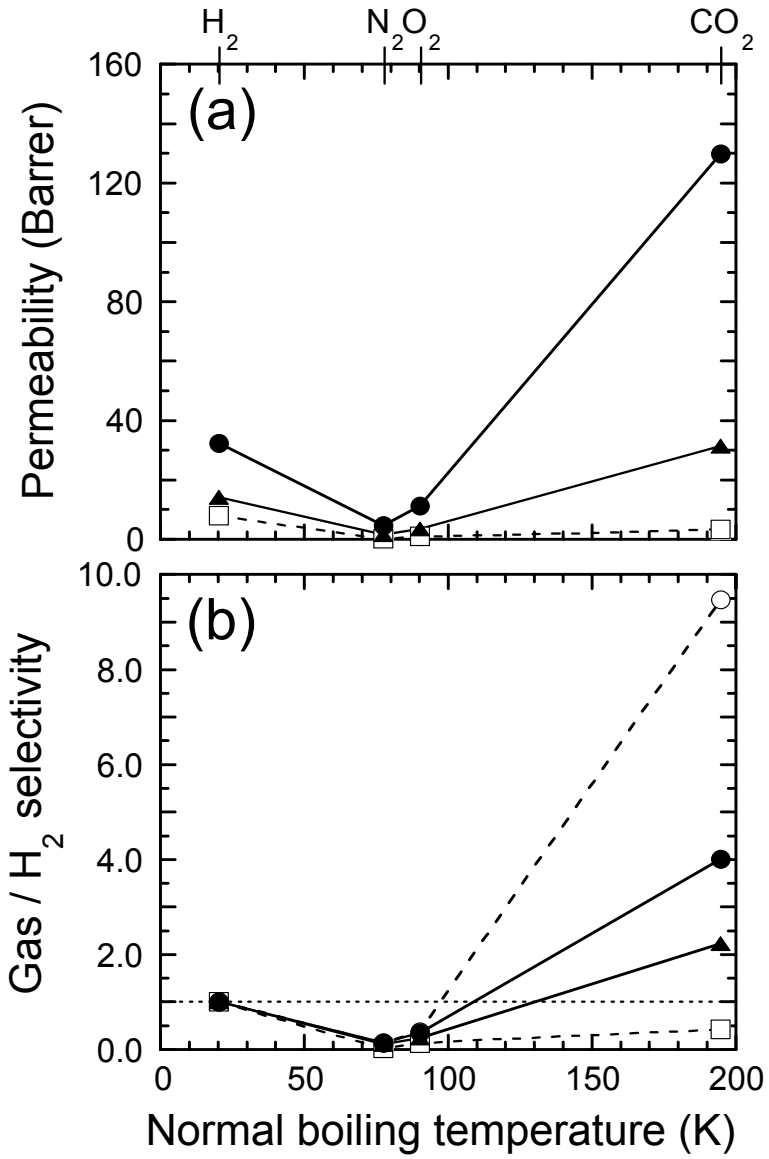

Figure 6.3. The (a) permeability and (b) gas/H_2 selectivity of H_2, N_2, O_2 and CO_2 (labeled) displayed as functions of the penetrant normal boiling point for PP with a reported[37] crystallinity of ~60% (G), PPGda540 (H) and PPGda900 (J) at 23°C. Included in (b) are data from the PEGda700 membrane (E). The solid and dashed lines connect the data, whereas the dotted line in (b) identifies unity gas/H_2 selectivity.

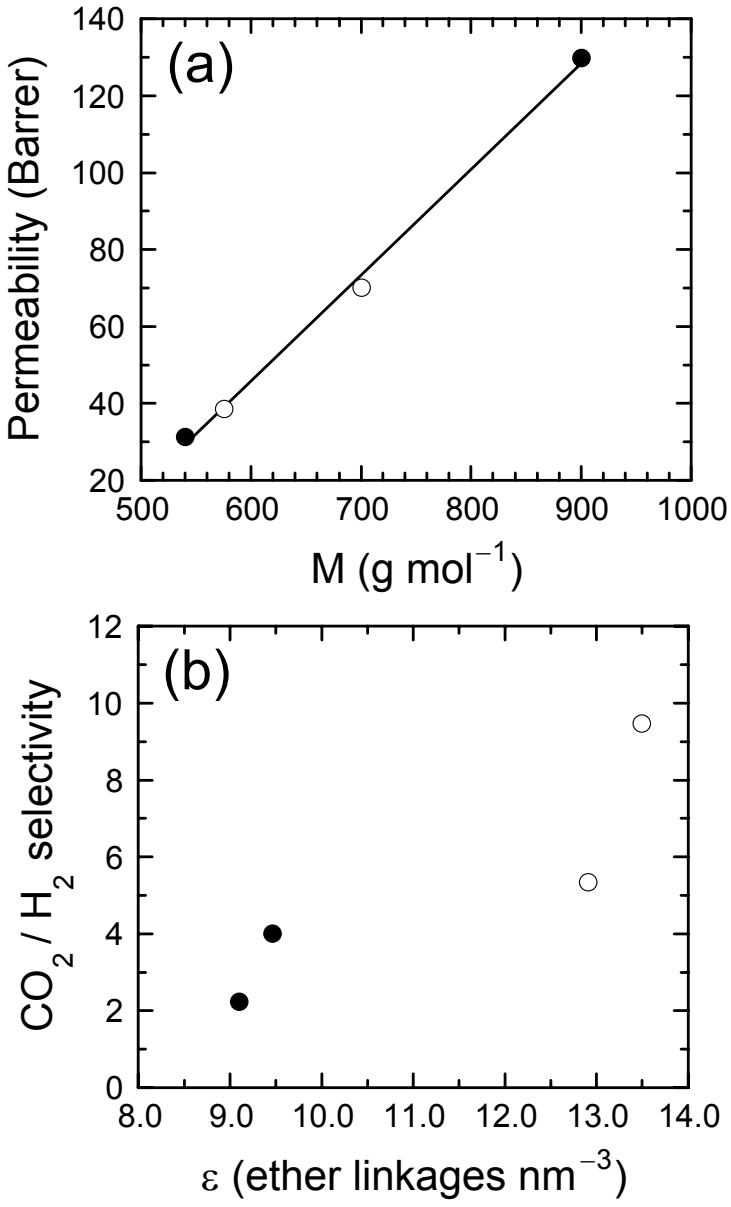

Figure 6.4. The dependence of (a) CO_2 permeability on polyether molecular weight and (b) CO_2/H_2 selectivity on ether linkage density (ε) in PPGda (J) and PEGda (E) membranes at 23°C. The solid line in (a) is a linear regression to the data.

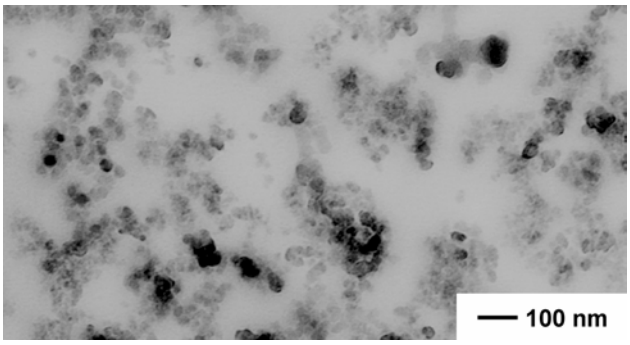

Figure 6.5. Zero-loss TEM image acquired from the 90/10 PPGda900/FS nanocomposite confirming the uniform distribution of FS nanoparticles within the membrane.

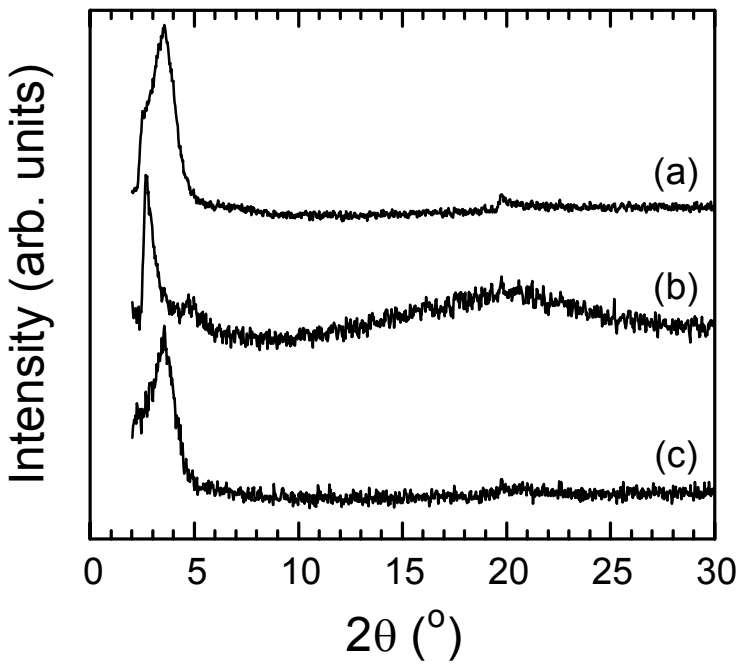

Figure 6.6. XRD patterns collected from (a) the neat OC nanofiller (Cloisite® 93A), (b) a 90/10 PPGda900/OC nanocomposite and (c) a 90/10 PEGda700/OC nanocomposite with Cu Kα radiation at ambient temperature. The data have been shifted vertically to facilitate examination of the data.

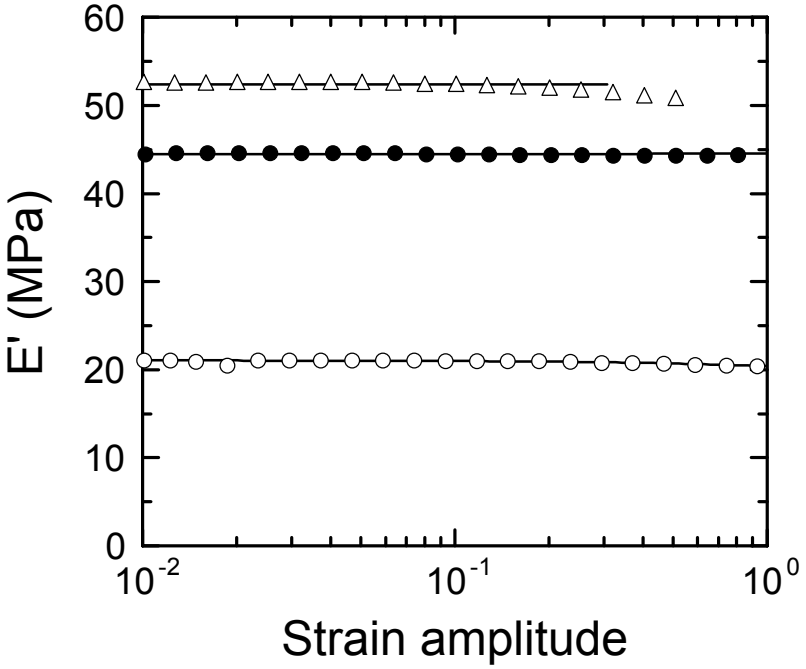

Figure 6.7. Dependence of E' on strain amplitude for the neat PPGda900 membrane (E), as well as the PPGda900/FS (J) and PPGda900/OC (C) nanocomposites with 10 wt% nanofiller, at ambient temperature. The solid lines are linear regressions to the data at low strains (< 0.1).

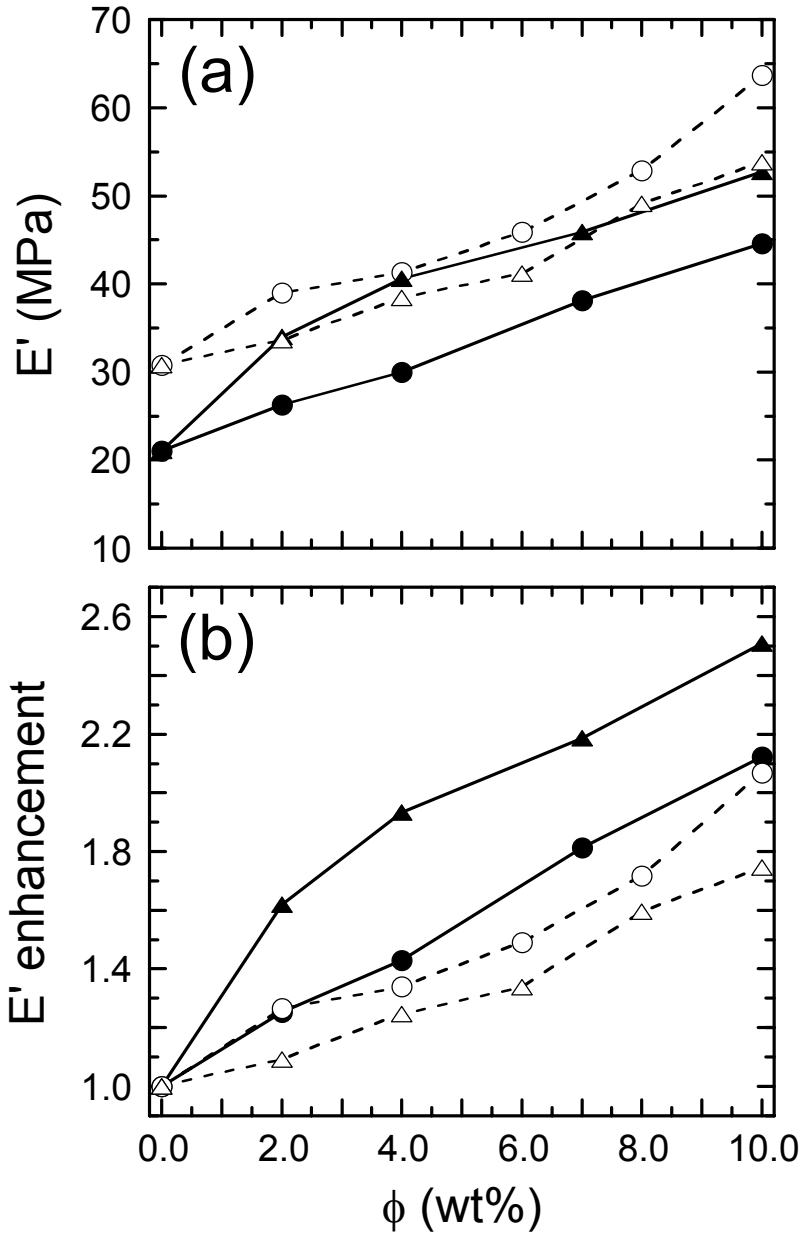

Figure 6.8. Dependence of (a) E' and (b) E' normalized with respect to E'(ϕ = 0) on nanofiller concentration (ϕ) for PPGda900 (filled symbols) and PEGda700 (open symbols) membranes containing FS (circles) and OC (triangles). The data have been collected at ambient temperature. The solid and dashed lines connect the data.

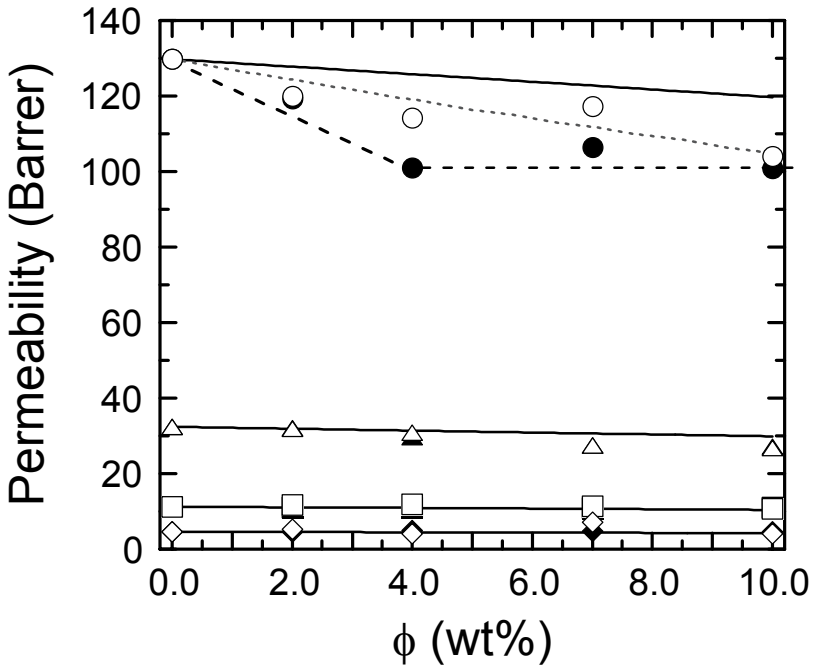

Figure 6.9. The permeabilities of CO_2 (circles), H_2 (triangles), O_2 (squares) and N_2 (diamonds) presented as functions of nanofiller concentration in PPGda900 nanocomposites containing FS (filled symbols) and OC (open symbols) at 23°C. The solid and dotted lines denote predictions obtained from Eqs. 6.7 and 6.9, respectively. The dashed line shows the general trend of the data.

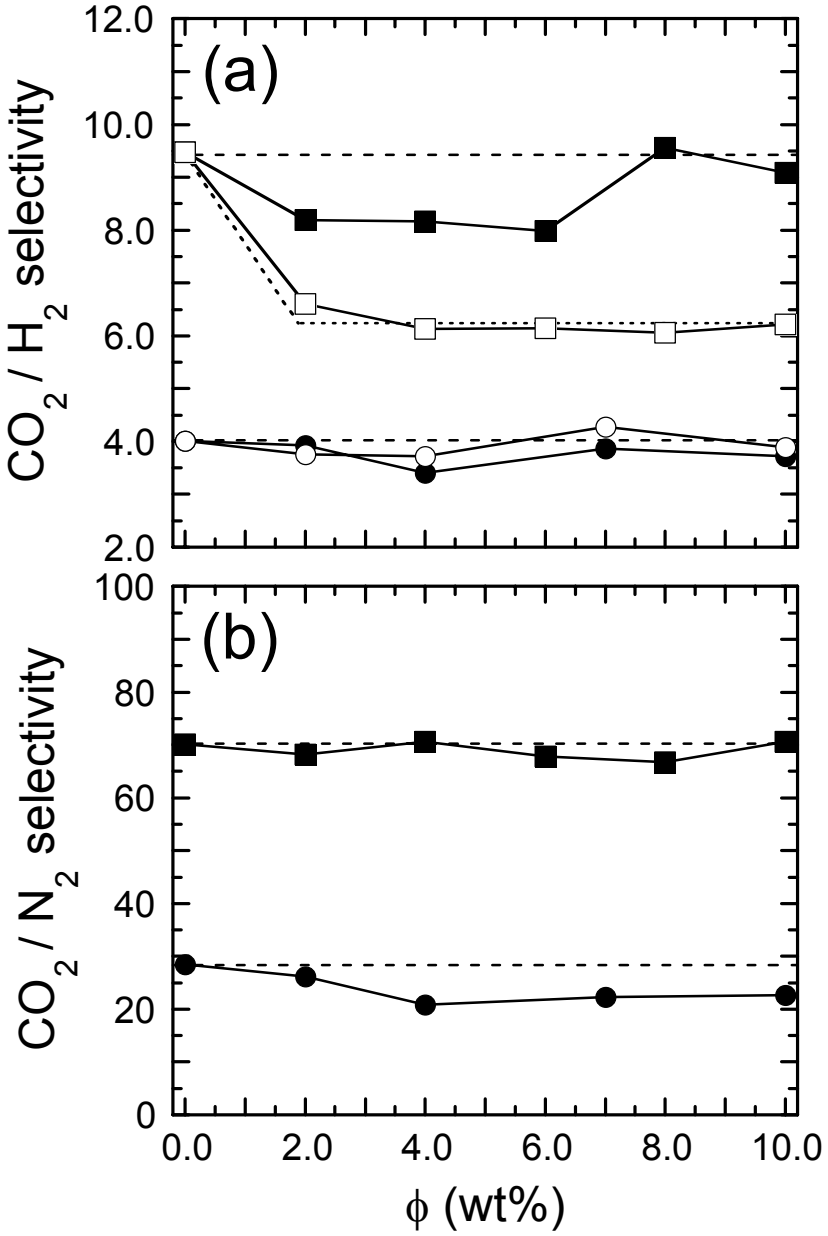

Figure 6.10. The composition dependence of (a) the CO_2/H_2 selectivity and (b) the CO_2/N_2 selectivity of PPGda900 (circles) and PEGda700 (squares) membranes containing FS (filled symbols) and OC (open symbols) at 23°C. The dashed lines identify the selectivity of the neat membrane (at $\phi = 0$), and the dotted line in (a) shows the general trend of the data.

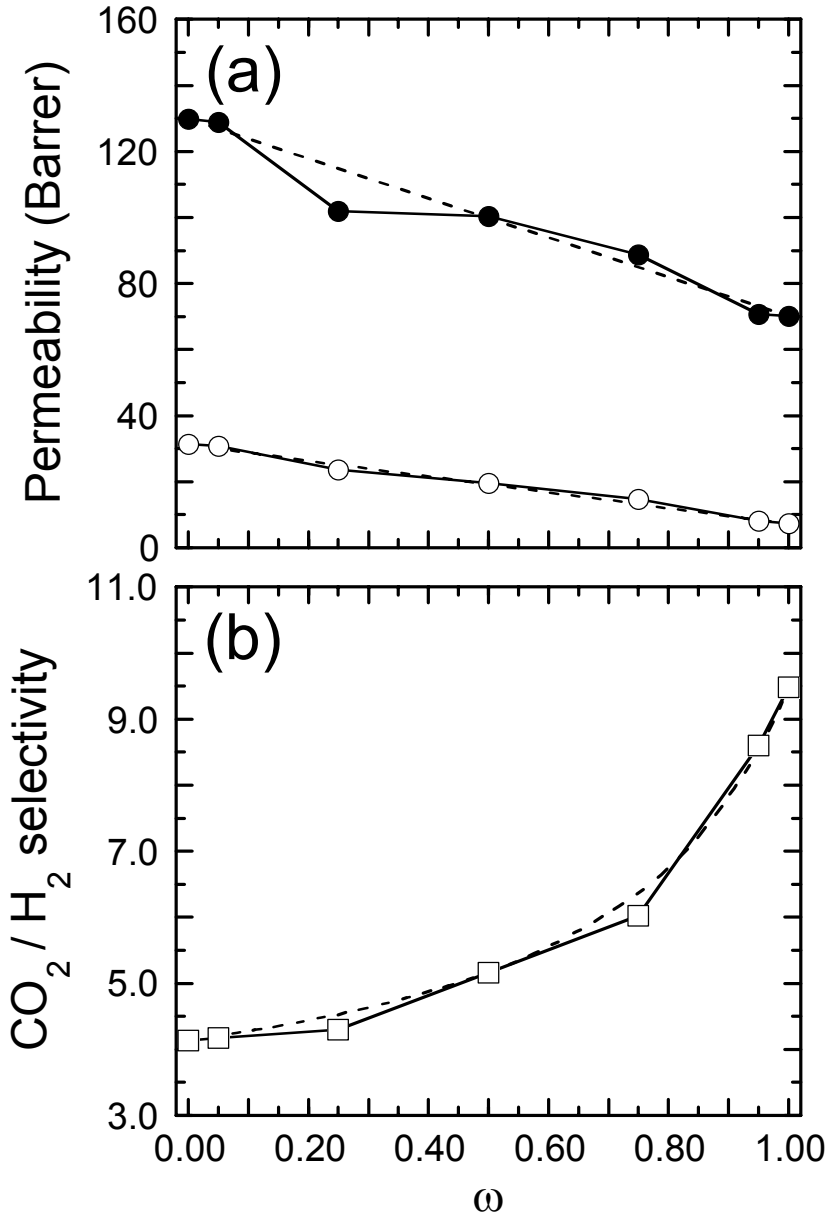

Figure 6.11. Variation of (a) CO_2 (J) and H_2 (E) permeabilities and (b) CO_2/H_2 selectivity with blend composition (ω) in crosslinked homogeneous blends of PPGda900 and PEGda700 at 23°C. The solid lines serve to connect the data, whereas the dashed lines are predictions from the linear rule of mixtures (eq.6.10) in conjunction with eq.6.5.

Chapter 7

Summary and Recommendations for Future Work

7.1. Summary

The thesis presented here explores the fundamental structure-gas transport relationships in polymeric materials designed to separate large acid-gas molecules selectively from mixtures with light gases. The measurement of gas permeation properties in the microphase-ordered SEOS copolymer and its blends with PEG homopolymers reveal several important results:

- Nonpolar gas selectivity relative to H_2 displays behavior that is similar to rubbery polymers. In marked contrast, CO_2 exhibits higher selectivity in all the copolymer-containing membranes developed during the course of this study due to specific interactions between the ether moiety in the (co)polymer and the quadrupolar moment of the CO_2 molecule. From these observations, the polyether microphase constitutes the main locus for molecular transport in these membranes, whereas the glassy styrenic block provides the membrane with satisfactory mechanical integrity.
- Addition of PEG to the SEOS copolymer results in generally improved membrane performance IF the added PEG is amorphous. Permeation problems associated with the presence of PEO crystals can be alleviated by melting the crystals at slightly elevated temperatures, at which the CO_2/nonpolar gas selectivity abruptly increases due to the increased availability of amorphous PEO for gas transport.

- A morphological transition in the SEOS copolymer can be achieved by adding an appropriate amount of PEG homopolymer. In this case, the PEG molecular weight and its distribution within the host microphase of the copolymer play important roles in determining the extent of homopolymer mixing within the copolymer. Gas transport properties are affected by the transition from alternating lamellae to a PEG-continuous matrix and, depending on factors such as the degree of crystallinity, exhibit sharp changes upon melting. The low-molecular-weight PEG is found to be more effective in transforming the copolymer morphology and concurrently improving CO_2 selectivity as well as permeability.
- Nonequilibrium, yet long-lived, morphologies can be generated by preparing mesoblends of the block copolymer and homopolymer. In this methodology, PEG homopolymer molecules dissolved in an EO-selective solvent diffuse into midblock microphase of the copolymer, which does not dissolve upon immersion in the solvent due to repulsive attractions between the copolymer hard block and solvent. The final morphology generated in this fashion is a complex function of solvent concentration, temperature and homopolymer molecular weight.
- The diffusion coefficient of PEG at constant molecular weight can be extracted from mass uptake data and is determined to be independent of solvent quality and solution concentration. The equilibrium solubility, on the other hand, changes significantly with both factors, in addition to PEG molecular weight. The existence of crystals in the midblock of the SEOS copolymer is responsible for the reduced homopolymer mobility relative to that in the AEG copolymer. Incorporation of PEG within the AEG copolymer enhances CO_2 permeability as well as CO_2/H_2 selectivity.

In the second part of this study, we have developed crosslinked PEG– and PPG–based polymer membranes and nanocomposite membranes containing different type of nanofillers such as fumed silica and nanoclay. Several important outcomes are listed as follows:

- The PEGda membranes are mechanically strong, optically clear and exhibit exceptionally high CO_2/H_2 selectivity coupled with relatively high CO_2 permeability. Due to the low molecular weight of the PEGda oligomers, these membranes are completely amorphous and therefore yield high penetrant permeabilities.
- The CO_2/H_2 selectivity, as well as CO_2 permeability, can be systematically tuned in these membranes by varying the oligomer molecular weight or, alternatively, the number of ether linkages per molecule. The elastic modulus, however, decreases gradually with increasing chain length.
- Increasing the upstream pressure does not affect the permeabilities of H_2 and other nonpolar gases. This process variable has a significant impact on CO_2 permeability, which increases almost linearly with increasing pressure. Such enhancement is due to improvement in CO_2/H_2 solubility selectivity.
- Gas transport properties show little variation upon addition of up to 10 wt% fumed silica in PEGda nanocomposites. The permeability of all the penetrants explored in these nanocomposites is accurately described by the Maxwell model. Addition of fumed silica serves to improve the elastic modulus, thereby indicating that such membranes can be strengthened without depreciating CO_2/H_2 selectivity. Incorporation of plate-like nanoclays, on the other hand, decreases CO_2 permeability abruptly since intercalated or

exfoliated clay is more effective in hindering the permeation of relatively large penetrant molecules.

- Temperature-dependent permeation of all the penetrants studied is found to exhibit Arrhenius behavior. Activation energies deduced for nonpolar gases from such investigation are dominated by the diffusive activation energy. Conversely, CO_2 permeation possesses a substantially negative heat of sorption due to its site-specific interactions with the ether linkages of PEG. Thus, the activation energy for permeation of CO_2 is markedly lower than the activation energy for all other gases in PEGda-based membranes.
- In comparison to PEG membranes, PPG nanocomposites generally exhibit significantly higher CO_2 permeability but lower CO_2/nonpolar gas selectivity. The presence of one additional methyl group in the PPG repeat unit affords higher chain mobility, resulting in increased gas permeation. However, the number of ether linkages per molecule, which is responsible for the high CO_2/nonpolar separation factor in PEG, is smaller in PPG at comparable oligomer molecular weights. Blending PPGda and PEGda prior to crosslinking yields membranes that exhibit intermediate transport properties described by the linear rule of mixtures.

7.2. Future Work and Recommendations

In regard to the SEOS/PEG blended membranes, we have demonstrated that an order-order transition from a polyether-confined to polyether-continuous morphology is essential for improved membrane performance. In-depth characterization of this transition, as well as other changes in morphology, must be performed by available analytical methods (e.g., TEM

and small-angle scattering) to establish more precisely the relationship between nanostructure and gas-transport properties. While the polyether constitutes the main locus of molecular transport in these blended membranes, the presence of styrenic blocks strongly compromises the net CO_2/H_2 selectivity of the membranes. In this regard, it may be possible to synthesize new block copolymer molecules in which the hard block is not only CO_2-selective but also sufficiently strong to impart the requisite mechanical properties. One such hard-block candidate is poly(1-trimethylsilyl-1-propyne) [PTMSP], which behaves as a nanoporous polymer glass. Moreover, it may be interesting to establish the effect of various copolymer architectures, such as linear and nonlinear, on gas-transport properties, since the architecture will have a strong impact on interfacial curvature and, hence, morphological development. Different transport models may need to be developed to explain the resultant gas permeation data and predict permeability and selectivity without performing additional experiments. Precise determination of morphologies will again play an important role in developing such models since morphology directly affects molecular transport through a nanostructured membrane.

Direct measurement of penetrant diffusion coefficient and solubility in PEGda membranes will be useful to determine the individual contributions of each to permeation. On the basis of the permeability values reported here, we contend that solubility selectivity of CO_2 over H_2 is responsible for exceptional CO_2/H_2 selectivity. This conclusion should be verified. In this same vein, the effect of nanofillers is presumed to affect the diffusion coefficient to a greater extent than solubility. This again should be confirmed, and tortuosity calculations can more precisely establish the role of nanofillers differing in geometry and size in molecular transport. Since attractive interactions between CO_2, an acid gas, and the

polyether are responsible for membrane efficacy, it would likewise be interesting to incorporate nanoscale fillers with functional surface groups to improve further transport properties. Different type of amines currently used as liquids in stripping CO_2 from mixed gas streams but incorporated into the PEGda network may be desirable for enhancing CO_2 solubility and, therefore, permeability. We have established that an increase in upstream pressure or a decrease in temperature enhances CO_2/H_2 selectivity. These results are clearly extendable to broader ranges than those investigated in this work. High-pressure sorption, for instance, should be performed to discern the roles of solubility and diffusivity at elevated pressures. All the gas permeation experiments performed here have been performed on the basis of pure gases. In industrial applications, however, membranes are routinely used in conjunction with mixed-gas streams. Therefore, it is recommended that measurements similar to those reported herein should be conducted with mixed gases of known composition to ascertain transport properties in the presence of co-permeating gases. The membranes developed here have been exclusively tested for CO_2/H_2 selectivity. Molecular transport of other acid gases, such as hydrogen sulfide and ammonia, obey the same principles upon which the PEGda membranes have been developed. Such membranes should therefore be tested for the removal of sulfur or acidic impurities present in natural gas streams or the purification of air in confined environments such as in submarines. Due to the optical clarity and rubbery nature of PEGda membranes, these materials may also be utilized in the preparation of diagnostic materials and sensors.

REFERENCES

(1999). Polymer Handbook. New York, Wiley.

(2002). "Facts and figures for the chemical industry." Chemical & Engineering News 80: 61-62.

Abetz, V. and T. Goldacker (2000). "Formation of superlattices via blending of block copolymers." Macromolecular Rapid Communications 21: 16-34.

Alexandridis, P. and R. J. Spontak (1999). "Solvent-regulated ordering in block copolymers." Current Opinion in Colloid & Interface Science 4: 130-139.

Amerongen, G. J. V. (1964). Rubber Chemistry and Technology 37: 1065.

Andrady, A. L. and M. D. Sefcik (1984). "Transport of hydrogen and carbon monoxide in highly crosslinked poly(propylene glycol) networks." Journal of Polymer Science: Part B, Polymer Physics 22: 237-243.

Baetzold, J. P., I. Gancaez , et al. (1994). "Mechanical property modification and morphology of poly(styrene-b-hydrogenated butadiene-b-styrene)/poly(hydrogenated butadiene) blends." Macromolecules 27: 5329-5340.

Bailey, F. E. and J. V. Koleske (1976). Poly(ethylene oxide). New York, Academic Press.

Baker, R. W. and J. G. Wijmans (1994). In Polymeric Gas Separation Membranes, Paul, D. R. and Yampol'skii, Y. P. Eds.; CRC Press: Boca Raton, pp.353-397.

Baker, R. W., N. Yoshioka, et al. (1987). "Separation of organic vapors from air." Journal of Membrane Science 31: 259-271.

Balasamo, V. and R. Stadler (1999). "Influence of the crystallization temperature on the microphase morphology of a semicrystalline ABC triblock copolymer." Macromolecules 32: 3994-3999.

Balik, C. M. (1996). "On the extraction of diffusion coefficients from gravimetric data for sorption of small molecules by polymer thin films." Macromolecules 29: 3025-3029.

Barrer, R. M. (1968). Diffusion and permeation in heterogeneous media. In Diffusion in Polymers. J. Crank and G. S. Park. Eds.; London and New York, Academic Press: p.165.

Bates, F. S. (1991). "Polymer-polymer phase behavior." Science 251: 898-905.

Bates, F. S. and G. H. Fredrickson (1999). "Block copolymers-designer soft materials." Physics Today 52: 32-38.

Bhide, B. D. and S. A. Stern (1993). "Membrane processes for the removal of acid gases from natural gas. 1. Process configurations and optimization of operating conditions." Journal of Membrane Science 81: 209-237.

Bhide, B. D. and S. A. Stern (1993). "Membrane processes for the removal of acid gases from natural gas. 2. Effects of operating conditions, economic parameters, and membrane properties." Journal of Membrane Science 93: 239-252.

Bondar, V. I., B. D. Freeman, et al. (1997). "Characterization and analysis of the sorption and pure-gas permeation properties of polyether-polyamide block copolymers." Proceedings of the American Chemical Society Division of Polymeric Materials 77: 311.

Bondar, V. I., B. D. Freeman, et al. (1999). "Gas sorption and characterization of poly(ether-b-amide) segmented block copolymers." Journal of Polymer Science Part-B Polymer Physics 37: 2463-2475.

Bondar, V. I., B. D. Freeman, et al. (2000). "Gas transport properties of poly(ether-b-amide) segmented block copolymers." Journal of Polymer Science Part-B Polymer Physics 38: 2051-2062.

Breck, D. W. (1974). Zeolite molecular sieves : structure, chemistry, and use. Florida, Krieger Publishing Company.

Bronstein, L. M. (2003). "Nanoparticles made in mesoporous solids." Topics in Current Chemistry 226: 55-89.

Chan, V. Z.-H., J. Hoffman, et al. (1999). "Ordered bicontinuous nanoporous and nanorelief ceramic films from self assembling polymer precursors." Science 286: 1716-1719.

Chatterjee, A. and T. Iwasaki (1999). "A novel approach using DFT to explain the selective permeation of small gaseous molecules through Y-type zeolite membrane." Journal of Physical Chemistry A 103: 9857-9863.

Cohen, R. E., A. Bellare, et al. (1994). "Spatial organization of polymer chains in a crystallizable diblock copolymer of polyethylene and polystyrene." Macromolecules 27: 2321-2323.

Cohen, R. E., P.-L. Cheng, et al. (1990). "Path-dependent morphologies of a diblock copolymer of polystyrene/hydrogenated poly butadiene." Macromolecules 23: 324-327.

Court, F. and T. Hashimoto (2002). "Morphological studies of binary mixtures of block copolymers. 2. Chain organization of long and short blocks in lamellar microdomains and its effect on domain size and stability." Macromolecules 32: 2566-2575.

Cox, J. K., A. Eisenberg, et al. (1999). "Patterned surfaces via self-assembly." Current Opinion in Colloid and Interface Science 4: 52-59.

Csernica, J., R. F. Baddour, et al. (1987). "Gas permeability of a polystyrene-polybutadiene block copolymer with oriented lamellar domains." Macromolecules 20: 2468-2471.

Davankov, V. A. and M. P. Tsyurupa (1990). "Structure and properties of hypercrosslinked polystyrene- The first representative of a new class of polymer networks." Reactive Polymers 13: 27-42.

de Vos, R. M. and H. Verweij (2002). "High-selectivity, high-flux silica membranes for gas separation." Science 279: 1710-1711.

Felder, R. M. and G. S. Huvard (1978). Permeation, diffusion and sorption of gases and vapors. Methods of Experimental Physics. R. Fava. New York, Academic Press. 16C: 315.

Figueiredo, P., S. Geppert, et al. (2001). "Ordering of cylindrical microdomains in thin films of hybrid isotropic/liquid crystalline triblock copolymers." Macromolecules 34: 171-180.

Folkes, M. J. and P. S. Hope, Eds. (1993). Polymer Blend and Alloys. London, Blackie Academic & Professional.

Fredrickson, G. H. and E. Helfand (1987). "Fluctuation effects in the theory of microphase separation in block copolymers." Journal of Chemical Physics 87: 697-705.

Freeman, B. D. (1999). "Basis of permeability/selectivity tradeoff relations in polymeric gas separation membranes." Macromolecules 32: 375-380.

Freeman, B. D. and I. Pinnau (1997). "Separation of gases using solubility-selective polymers." Trends in Polymer Science 5: 167.

Furgiuele, N., A. H. Lebovitz, et al. (1999). "Novel strategy for polymer blend compatibilization: Solid-state shear pulverization." Macromolecules 33: 225-228.

Ghosal, K., R. T. Chern, et al. (1995). "The effect of aryl nitration on gas sorption and permeation in polysulfone." Journal of Polymer Science Part-B Polymer Physics 33: 657-666.

Ghosal, K. and B. D. Freeman (1994). "Gas separation using polymer membranes: An overview." Polymers for Advanced Technologies 5: 673-697.

Glotzer, S. C., R. Bansil, et al. (1993). "Physical gels and microphase separation in multiblock copolymers." Physica A: Statistical and Theoretical Physics 201: 482-495.

Goldacker, T., V. Abetz, et al. (2000). "Blends of block copolymers." Macromolecular Symposia 149: 93-98.

Graham, T. (1866). Philos. Mag. 32: 401.

Guy, K. W. A. (2000). "The hydrogen economy." Process Safety and Environmental Protection 78(B4): 324-347.

Hadjichristidis, N., M. Ptsikalis, et al. (2001). "Polymers with complex architecture by living anionic polymerization." Chemical Reviews 101: 3747-3792.

Hajduk, D. A., P. E. Harper, et al. (1994). "The gyroid: A new equilibrium morphology in weakly segregated diblock copolymers." Macromolecules 27: 4063-4075.

Hajduk, D. A., H. Takenouchi, et al. (1997). "Stability of the perforated layer (PL) phase in diblock copolymer melts." Macromolecules 30: 3788-3795.

Hamley, I. W. (1998). The Physics of Block Copolymers. Oxford, Oxford University Press.

Hamley, I. W., J. P. A. Fairclough, et al. (1996). "Crystallization in oriented semicrystalline diblock copolymers." Macromolecules 29: 8835-8843.

Hardy, C. M., F. S. Bates, et al. (2002). "Model ABC triblock copolymers and blends near the order-disorder transition." Macromolecules 35: 3189-3197.

Hashimoto, T., H. Tanaka, et al. (1990). "Ordered structures in mixtures of a block copolymer and homopolymers. 2. Effects of molecular weights of homopolymers." Macromolecules 23: 4378-4386.

Hefner, R. A. (2002). "The age of energy gases." International Journal of Hydrogen Energy 27: 1-9.

Helfand, E. and Z. R. Wasserman (1976). "Block copolymer theory .4. Narrow interphase approximation." Macromolecules 9: 879-888.

Helfand, E. and Z. R. Wasserman (1978). "Block copolymer theory .5. Spherical domains." Macromolecules 11: 960-966.

Helfand, E. and Z. R. Wasserman (1980). "Block copolymer theory .6. Cylindrical domains." Macromolecules 13: 994-998.

Hirayama, Y., Y. Kase, et al. (1999). "Permeation properties to CO_2 and N_2 of poly(ethylene oxide)-containing and crosslinked polymer films." Journal of Membrane Science 160: 87-99.

Holden, G., N. R. Legge, et al. (1996). Thermoplastic Elastomer. Munich, Hanser.

Hong, K. M. and J. Noolandi (1981). "Theory of inhomogeneous multicomponent polymer systems." Macromolecules 14: 727-736.

Hong, S. U., J. H. Laurer, et al. (1998). "Morphological and isothermal diffusive probe analyses of low- molecular-weight diblock copolymers." Macromolecules 31: 2174-2184.

Hong, S. U., S. Stolken, et al. (1998). "Anomalous sorption in a poly(styrene-b-isoprene) diblock copolymer near the order-disorder transition." Macromolecules 31: 937-940.

Jacques, C. H. M. and H. B. Hopfenberg (1974). "Vapor and liquid equilibria in glassy polyblends of polystyrene and poly(2,6-dimethyl-1,4-phenylene oxide)." Polymer Engineering and Science 14: 441-448.

Kabanov, A. V., E. V. Batrakova, et al. (2002). "Pluronic block copolymers for overcoming drug resistance in cancer." Advanced Drug Delivery Reviews 54: 759-779.

Kane, L., D. A. Norman, et al. (2001). "Molecular, nanostructural and mechanical characteristics of lamellar triblock copolymer blends: effects of molecular weight and constraint." Macromolecular Rapid Communications 22: 281-296.

Khandpur, A. K., S. Forster, et al. (1995). "Polyisoprene-polystyrene diblock copolymer phase diagram near the order-disorder transition." Macromolecules 28: 8796-8806.

Kim, J. H., S. Y. Ha, et al. (2001). "Selective permeation of CO_2 through pore-filled polyacrylonitrile membrane with poly(ethylene glycol)." Journal of Membrane Science 186: 97-107.

Kim, J. H., Y. H. Seong, et al. (2001). "Gas permeation of poly(amide-6-b-ethylene oxide) copolymer." Journal of Membrane Science 190: 179-193.

Kimishima, K., T. Hashimoto, et al. (1995). "Spatial distribution of added homopolymer within the microdomains of a mixture consisting of an ABA-type triblock copolymer and a homopolymer." Macromolecules 28: 3842-3853.

Kimishima, K., T. Koga, et al. (2000). "Thermoreversible order-order transition between spherical and cylindrical microdomain structures of block copolymer." Scattering from Polymers. ACS Symposium Series. 739: 514-530.

King, M. R., S. A. White, et al. (1999). "Mesogel networks via selective midblock swelling of lamellar triblock copolymers." Langmuir 15: 7886-7889.

Kohl, A. and R. Nielson (1997). Gas Purification. Houston, TX, Gulf Publishing Co.

Koros, W. J. and R. T. Chern (1987). . Handbook of Separation Process Technology. R. W. Rousseau, John Wiley & Sons.

Koros, W. J. and M. W. Hellums (1989). In Encyclopedia of Polymer Science and Engineering. J. I. Kroschwitz. Ed.; New York, Wiley. Supp.: 724-802.

Kratz, W. C., D. L. Rarig, et al. (1988). "Hydrogen and carbon dioxide coproduction from steam methane reformer off gas by pressure swing adsorption." AIChE Symposium Series 84: 36.

Krishnamoorthi, R. and R. A. Vaia, Eds. (2002). Polymer Nanocomposites: Synthesis, Characterization and Modeling. ACS Symposium Series. Washington, DC, Oxford University Press.

Laurer, J. H., D. A. Hajduk, et al. (1998). "Bicontinous morphologies in homologous multiblock copolymers and their homopolymer blends." Macromolecules 31: 7546-7549.

Laurer, J. H., S. D. Smith, et al. (1998). "Interfacial modification as a route to novel bilayered morphologies in binary block copolymer/homopolymer blends." Macromolecules 31: 4975-4985.

Lee, S. H. and K. Char (1998). "SAXS and rheological studies on the order-disorder transition in mixtures of polystyrene-b-polyisoprene-b-polystyrene and low molecular weight polystyrene." Polymeric Materials Science and Engineering 74: 314-315.

Lee, S. H., J. T. Koberstein, et al. (1994). "Spatial Distribution of a Midblock-Associating Homopolymer Blended into a Triblock Copolymer." Macromolecules 27: 3199-3206.

Leibler, L. (1980). "Theory of microphase separation in block copolymers." Macromolecules 13: 1602-1617.

Leibler, L. (1988). "Emulsifying effects of block copolymers in incompatible polymer blends." Makromol. Chem. Macromol. Symp. 16: 1-17.

Li, J., S. Wang, et al. (1998). "Effect of polyethylene glycol (PEG) on gas permeabilities and permselectivities in its cellulose acetate blend membranes." Journal of Membrane Science 138: 143-152.

Lijia, A. N., H. E. Dayong, et al. (1997). "Effects of molecular weight and interaction parameter on the glass transition temperature of polystyrene mixtures and its blends with polystyrene/poly (2, 6-Dimethyl -p-phenylene oxide)." European Polymer Journal 33: 1523-1528.

Macosko, C. W. (1994). Rheology: Principles, Measurements and Applications. New York, VCH Publisher.

Matsen, M. W. (1995). "Stabilizing new morphologies by blending homopolymer with block copolymer." Physical Review Letters 74: 4225-4228.

Matsen, M. W. and F. S. Bates (1996). "Origins of complex self-assembly in block copolymer." Macromolecules 29: 7641-7644.

Matsen, M. W. and M. Schick (1994). "Stable and unstable phases of a diblock copolymer melt." Physical Review Letters 72: 2660-2663.

Maxwell, C. (1873). Treatise on Electricity and Magnetism. London, Oxford University Press.

Merkel, T. C., V. I. Bondar, et al. (2000). "Gas sorption, diffusion, and permeation in poly(dimethylsiloxane)." Journal of Polymer Science Part-B Polymer Physics 38: 415-434.

Merkel, T. C., B. D. Freeman, et al. (2002). "Ultrapermeable, reverse-selective nanocomposite membranes." Science 296: 519-522.

Merkel, T. C., B. D. Freeman, et al. (2003). "Sorption, transport and structural evidence for enhanced free volume in poly(4-methyl-2-pentyne)/fumed silica nanocomposite membranes." Chemistry of Materials 15: 109-123.

Michaels, A. S. and H. J. Bixler (1961). "Solubility of gases in polyethylene." Journal of Polymer Science 50: 393.

Miyata, T., S. Obata, et al. (1999). "Morphological effects of microphase separation on the permselectivity for aqueous ethanol solutions of block and graft copolymer membranes containing poly(dimethyl siloxane)." Macromolecules 32: 3712-3720.

Mogri, Z. and D. R. Paul (2001). "Gas sorption and transport in poly(alkyl(meth)acrylate)s." Polymer 42: 7765-7780.

Nojima, S., K. Kato, et al. (1992). "Crystallization of block copolymers. 1. Small-angle x-ray scattering study of an ε- caprolactone-butadiene Diblock copolymer." Macromolecules 25: 2237-2242.

Norman, D. A., L. Kane, et al. (1998). "Triblock copolymer/homopolymer blends: Conformational changes, microstructural transition and macrophase separation." Journal of Materials Science Letters 17: 545-549.

Nugay, N. and B. Erman (2001). "Hybrid reinforcement in nitrile rubber composites." Macromolecular Symposia 169: 269-274.

Okamoto, K.-I., M. Fujii, et al. (1995). "Gas permeation properties of poly(ether imide) segmented copolymers." Macromolecules 28: 6950-6956.

O'Neill, M. L., Q. Cao, et al. (1998). "Solubility of homopolymers and copolymers in carbon dioxide." Industrial & Engineering Chemistry Research 37: 3067-3079.

Park, C., W. H. Jo, et al. (2000). "Morphological effect of dispersed phase on gas permeation properties through heterophase polymer membrane: theoretical and experimental approaches." Polymer 41: 1765-1771.

Park, C., D. C. Rosa, et al. (2000). "Influence of an oriented glassy cylindrical microdomain structure on the morphology of crystallizing lamellae in a semicrystalline terpolymer." Macromolecules 33: 7931-7938.

Park, H. B., S. Y. Ha, et al. (2000). "Percolation behavior of gas permeability in rigid-flexible block copolymer membranes." Journal of Membrane Science 177: 143-152.

Patel, N. P., A. C. Miller, et al. "Highly CO_2-permeable and selective membranes derived from cross-linked poly(ethylene glycol) and its nanocomposites." Advanced Functional Materials Accepted.

Patel, N. P., A. C. Miller, et al. (2003). "Highly CO_2-permeable and selective polymer nanocomposite membranes." Advanced Materials 15: 729-733.

Patel, N. P. and R. J. Spontak "Gas permeation properties of a poly(styrene-*b*-ethylene oxide-*b*-styrene) triblock copolymer and its blends with poly(ethylene glycol)." Macromolecules In press.

Patras, G., G. G. Qiao, et al. (2000). "Characterization of the pore structure of aqueous three-dimensional polyacrylamide gels with a novel crosslinker." Electrophoresis 21: 3843-3850.

Paul, D. R. and C. B. Bucknall (2000). Polymer Blends. New York, John Wiley & Sons, Inc.

Petropoulos, J. H. (1985). "A comparative study of approaches applied to the permeability of binary composite polymeric membranes." Journal of Polymer Science Part-B Polymer Physics 23: 1309-1324.

Petropoulos, J. H. (1994). In Polymeric Gas Separation Membranes, Paul, D. R. and Yampol'skii, Y. P., Eds.; Boca Raton, CRS Press:17-81.

Premnath, V. (1996). "A model for the permeation of gases in block copolymer membranes with lamellar morphology." Journal of Membrane Science 110: 133-137.

Qi, S. and Z. Wang (1997). "Kinetics of phase transitions in weakly segregated block copolymers: Pseudo-stable and transient states." Physical Review E 55: 1682-1697.

Quan, X., I. Gancarz, et al. (1987). "Effect of homopolymer molecular weight on the morphology of block copolymer/homopolymer blends." Macromolecules 20: 1431-1434.

Quiram, D. J., R. A. Register, et al. (1997). "Crystallization of asymmetric diblock copolymers from microphase separated melts." Macromolecules 30: 4551-4558.

Quiram, D. J., R. A. Register, et al. (1997). "Dynamics of structure formation and crystallization in asymmetric diblock copolymers." Macromolecules 30: 8338-8343.

Raghavan, S. R., M. W. Riley, et al. (1998). "Composite polymer electrolytes based on poly(ethylene glycol) and hydrophobic fumed silica: dynamic rheology and microstructure." Chemistry of Materials 10: 244-251.

Rangrajan, P., R. A. Register, et al. (1993). "Morphology of semicrystalline block-copolymers of ethylene-(ethylene-alt-propylene)." Macromolecules 26: 4640-4645.

Reid, R. C., J. M. Prausnitz, et al. (1987). . The properties of gases and liquids. New York, McGraw-Hill: 741.

Roberge, R. L., N. P. Patel, et al. (2001). "Block copolymer/homopolymer mesoblends: Preparation and characterization." Macromolecules 35: 2268-2276.

Robeson, L. M. (1991). "Correlation of separation factor versus permeability for polymeric membranes." Journal of Membrane Science 62: 165-185.

Rothon, R. N. (1999). "Mineral fillers in thermoplastics: Filler manufacture and characterization." Advances in Polymer Science 139: 67-107.

Seguela, R. and J. Prud'homme (1989). "Structural and mechanical properties of a polyethylene-based thermoplastic elastomer." Polymer 30: 1446-1455.

Semenov, A. N. (1985). Soviet Physics JETP 61: 733.

Shonaike, G. O. and G. P. Simon (1999). Polymer Blends and Alloys. New York, Marcel Dekker, Inc.

Simon, P. F. W., R. Ulrich, et al. (2001). "Block copolymer-ceramic hybrid materials from organically modified ceramic precursors." Chemistry of Materials 13: 3464-3486.

Spontak, R. J. and P. Alexandridis (1999). "Advances in self-ordering macromolecules and nanostructure design." Current Opinion in Colloid & Interface Science 4: 140-146.

Spontak, R. J. and N. P. Patel (2000). "Thermoplastic elastomers: fundamentals and applications." Current Opinion in Colloid & Interface Science 5: 334-341.

Spontak, R. J. and N. P. Patel (2004). Phase behavior of Block Copolymer Blends, In Developments in Block Copolymer Science and Technology, Hamley, I. W., Ed.; John Wiley & Sons, Inc., pp.159-212.

Spontak, R. J. and S. D. Smith (2001). "Perfectly-alternating linear (AB)(n) multiblock copolymers: Effect of molecular design on morphology and properties." Journal of Polymer Science Part B Polymer Physics 39: 947-955.

Stern, S. A. (1994). "Polymers for gas separations: the next decade." Journal of Membrane Science 94: 1-65.

Stevens, J. E., W. Thongruang, et al. (2003). "Solvent-facilitated homopolymer sorption in swollen block copolymer matrices." Macromolecules 36: 3206-3209.

Story, B. J. and W. J. Koros (1992). "Sorption and transport of CO_2 and CH_4 in chemically modified poly(phenyl oxide)." Journal of Membrane Science 67: 191-210.

Tavolaro, A. and E. Drioli (1999). "Zeolite Membranes." Advanced Materials 11: 975-996.

Thomas, E. L., D. B. Alward, et al. (1986). "Ordered Bicontinuous Double-Diamond Structure of Star Block Copolymers: A New Equilibrium Microdomain Morphology." Macromolecules 19: 2197-2202.

Toy, L. G., B. D. Freeman, et al. (1997). "Gas permeability and phase morphology of poly(1-trimethylsilyl)-1-propyne)/poly(1-phenyl-1-propyne) blends." Macromolecules 30: 4766-4769.

Tsyurupa, M. P., Y. V. Oslonovich, et al. (1995). "Phase separation in the synthesis of hyper-cross-linked polystyrene networks in cyclohexane." Chemical Transformations 37: 964-968.

Utracki, L. A. (1990). Polymer Alloys and Blends: Thermodynamic and Rheology. New York, Oxford University Press.

Walls, H. J., M. W. Riley, et al. (2003). "Nanocomposite electrolytes derived from fumed silica and hectrorites: Passive vs. active fillers." Advanced Functional Materials 13: 710-717.

Walls, H. J., J. Zhou, et al. (2000). "Fumed silica-based composite polymer electrolytes: synthesis, rheology and electrochemistry." Journal of Power Sources 89: 156-162.

Weinkauf, D. H. and D. R. Paul (1990). . Barrier Polymers and Barrier Structures. W. J. Koros. Washington, D. C., American Chemical Society: 60-91.

Wijmans, J. G. and R. W. Baker (1995). "The solution-diffusion model- A review." Journal of Membrane Science 107: 1-21.

Winebrake, J. J. and B. P. Creswick (2003). "The future of hydrogen fueling systems for transportation: An application of perspective-based scenario analysis using the analytic hierarchy process." Technological Forecasting and Social Change 70: 359-384.

Winey, K. I., E. L. Thomas, et al. (1991). "Ordered morphologies in binary blends of diblock copolymer and homopolymer and characterization of their intermaterial dividing surfaces." Journal of Chemical Physics 95: 9367-9375.

Winey, K. I., E. L. Thomas, et al. (1992). "Isothermal morphology diagrams for binary blends of diblock copolymer and homopolymer." Macromolecules 25: 2645-2650.

Yeh, J. T., H. W. Pennline, et al. (2001). "Study of CO_2 absorption and desorption in a packed column." Energy & Fuels 15: 274-278.

Young, R. J. and P. Lovell (1991). Introduction to Polymers. New York, Chapman and Hall.

Zhu, L., S. Z. D. Cheng, et al. (2000). "Crystallization temperature dependent crystal orientations within nanoscale confined lamellae of a self-assembled crystalline-amorphous diblock copolymer." Journal of the American Chemical Society 122: 5957-5967.

Zhulina, E. B. and A. Halperin (1992). "Lamellar mesogels and mesophases: a self-consistent-field theory." Macromolecules 25: 5730-5741.

Zilg, C., C. Dietsche, et al. (2001). "Nanofillers based upon organophillic layered silicates." Macromolecular symposia 169 (Fillers and filler polymers): 65-77.